AD-A110 198 NAVAL AIR TEST CENTER PATUXENT RIVER MD F/G 1/3
AL6-164 POD/AV-8C ENVIRONMENTAL EVALUATION FLIGHT TEST.(U)
DEC 81 L J MERTAUGH
UNCLASSIFIED NATC-TM-81-109-SY NL

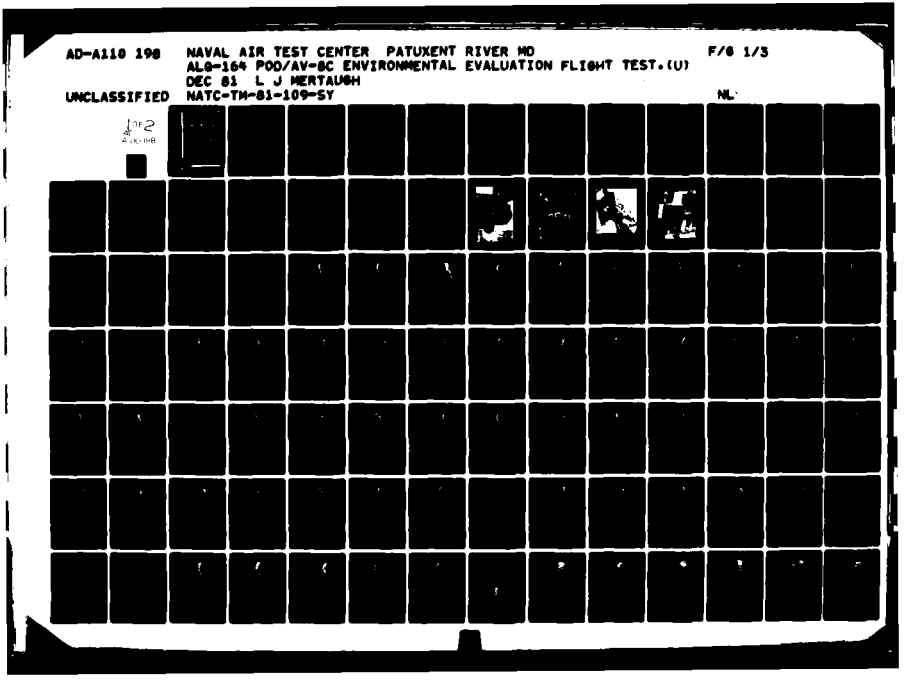

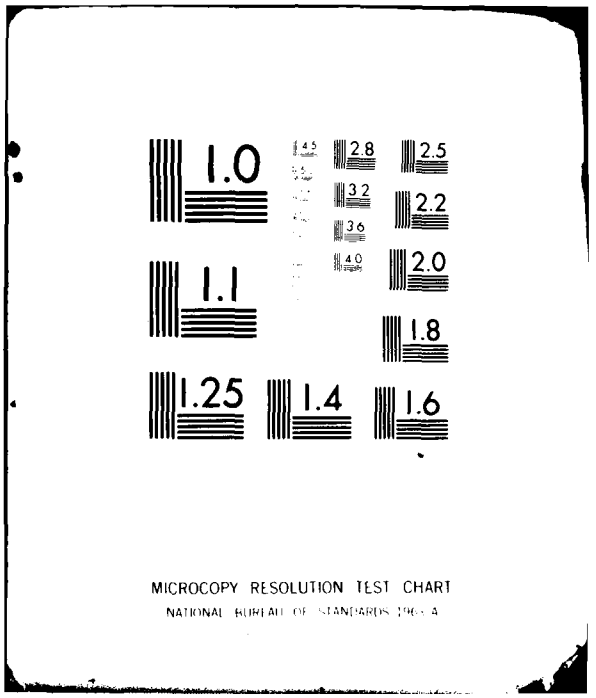
1.0
1.1
1.25
1.4
1.6
1.8
2.0
2.2
2.5
2.8
3.2
3.6
4.0
MICROCOPY RESOLUTION TEST CHART
NATIONAL BUREAU OF STANDARDS 1963-A

LEVEL II 12

TM 81-109 SY

Technical Memorandum

ALQ-164 POD/AV-8C ENVIRONMENTAL EVALUATION FLIGHT TEST

Dr. Lawrence J. Mertaugh

Systems Engineering Test Directorate

11 December 1981

NAVAL AIR TEST CENTER
PATUXENT RIVER, MARYLAND

UNCLASSIFIED

SECURITY CLASSIFICATION OF THIS PAGE (When Data Entered)

REPORT DOCUMENTATION PAGE		READ INSTRUCTIONS BEFORE COMPLETING FORM
1. REPORT NUMBER TM 81-109 SY	2. GOVT ACCESSION NO. AD A110 198	3. RECIPIENT'S CATALOG NUMBER
4. TITLE (and Subtitle) ALQ-164 POD/AV-8C ENVIRONMENTAL EVALUATION FLIGHT TEST		5. TYPE OF REPORT & PERIOD COVERED TECHNICAL MEMORANDUM
		6. PERFORMING ORG. REPORT NUMBER
7. AUTHOR(s) DR. LAWRENCE J. MERTAUGH		8. CONTRACT OR GRANT NUMBER(s)
9. PERFORMING ORGANIZATION NAME AND ADDRESS SYSTEMS ENGINEERING TEST DIRECTORATE NAVAL AIR TEST CENTER PATUXENT RIVER, MARYLAND 20670		10. PROGRAM ELEMENT, PROJECT, TASK AREA & WORK UNIT NUMBERS
11. CONTROLLING OFFICE NAME AND ADDRESS NAVAL AIR TEST CENTER NAVAL AIR STATION PATUXENT RIVER, MARYLAND 20670		12. REPORT DATE 11 DECEMBER 1981 13. NUMBER OF PAGES 153
14. MONITORING AGENCY NAME & ADDRESS(if different from Controlling Office)		15. SECURITY CLASS. (of this report) UNCLASSIFIED 15a. DECLASSIFICATION DOWNGRADING SCHEDULE

16. DISTRIBUTION STATEMENT (of this Report)

APPROVED FOR PUBLIC RELEASE; DISTRIBUTION UNLIMITED.

17. DISTRIBUTION STATEMENT (of the abstract entered in Block 20, if different from Report)

18. SUPPLEMENTARY NOTES

19. KEY WORDS (Continue on reverse side if necessary and identify by block number)

FLIGHT TEST
VIBRATION
RAM AIR COOLING
TEMPERATURE
INSTRUMENTATION

20. ABSTRACT (Continue on reverse side if necessary and identify by block number)

This report provides the test results of a flight test program conducted to evaluate the environmental conditions to which the ALQ-164 pod is exposed when carried on the AV-8C aircraft. Descriptions are provided of the test program, test equipment, instrumentation, and methods of analysis. The test results include cooling-air mass flow and temperature, vibration levels measured on the pod structure and on the isolator mounted equipment support structure, and pod skin temperature. Test conditions include steady-state conditions throughout the available pod/aircraft flight envelope as well as various vertical takeoff and landing, short takeoff and landing, and gun fire operations.

DD FORM 1 JAN 73 1473 EDITION OF 1 NOV 65 IS OBSOLETE

UNCLASSIFIED 270 1

SECURITY CLASSIFICATION OF THIS PAGE (When Data Entered)

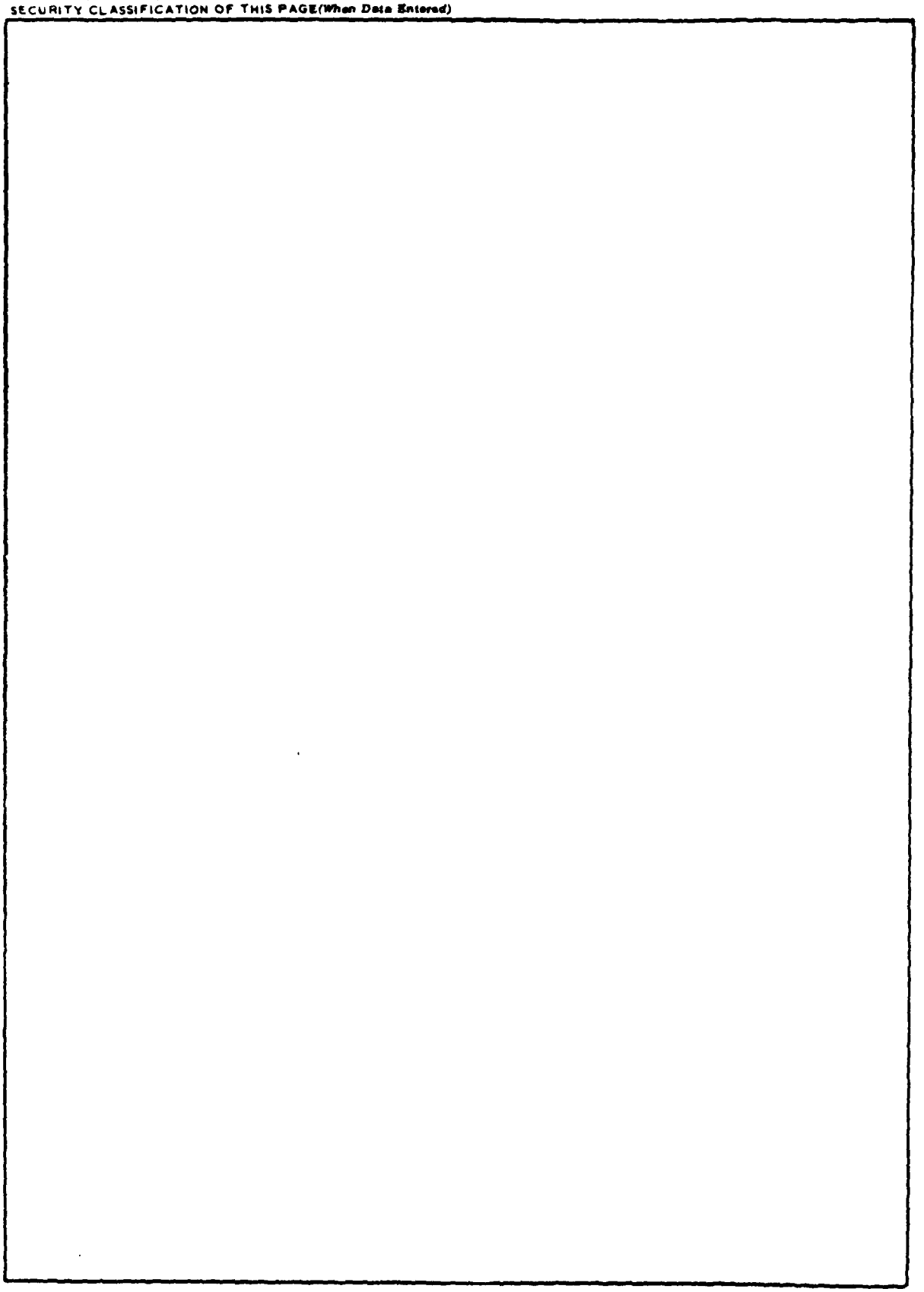

PREFACE

This Technical Memorandum presents the discussion and test results of a flight test program that was conducted to evaluate the environment of equipment carried in the AN/ALQ-164 DECM pod. This pod is carried on the AV-8C aircraft. Test information included cooling flow rates, vibration measurements, and temperature data.

The initial discussions pertaining to this portion of the DECM pod flight test program were held between NAVAIRTESTCEN and NAVAIRSYSCOM in September 1979. An AIRTASK was issued in May 1980 and the test flights were accomplished in September and October 1980. The test pod was a mass-model unit that provided appropriate cooling flow impedance characteristics and equipment mass distribution but was not electrically operable. This test program was conducted under AIRTASK No. A5495492, Work Unit No. 54921B-2. The NAVAIRTESTCEN project engineer was Mr. J. Boyd (Code SY91B) and the project was monitored by Mr. J. E. Cronin (AIR-54921B).

APPROVED FOR RELEASE

J. E. WISSLER, RADM, USN
Commander, Naval Air Test Center

TABLE OF CONTENTS

LIST OF ILLUSTRATIONS

INTRODUCTION

1. The ALQ-164 pod is designed to be carried on the centerline station of the AV-8C aircraft. This pod contains electronic equipment which is cooled by ram air and which is intended to operate over that portion of the aircraft flight envelope represented by flight speeds greater than 200 kt. This report describes the flight test program and the test results of the test program which were conducted to evaluate the adequacy of the ram air cooling system and to define the vibration environment of the pod equipment. Definition of pod skin temperatures was also an objective of this test program.

2. This test program was conducted with a nonoperating mass pod. The pod was a prototype unit that was originally used for structural testing. The pod equipment was represented by either actual equipment units or mass models of the units. The actual production cooling flow path was duplicated in this pod. Some of the mass models of pod equipment were replaced by combinations of flight test instrumentation and ballast. The flight test instrumentation included pressure transducers to allow determination of cooling air flow rate and to measure the available total pressure at the pod inlets, thermocouples to measure cooling flow inlet temperature and the pod surface temperatures, and accelerometers for vibration measurements on the pod structure and the isolator-mounted pod equipment support structure. The flight test data were telemetered to a ground station for storage and later analysis.

3. While the objective was to test the pod throughout the aircraft flight envelope, flight restrictions were imposed on the pod due to previous exposure to excessive loads during structural test. The flight clearance for carrying the pod on the AV-8C aircraft restricted operations to less than 450 KIAS, ± 2 g's normal acceleration, and symmetric maneuvers. These restrictions prevented verification of the available cooling flow and the vibration levels at the maximum speed of the aircraft. The cooling flow data obtained during this test program, however, do allow easy extrapolation to these flight conditions. Analysis of the vibration data presented in this report also indicates that extrapolation of the vibration data to the higher flight velocities is valid.

4. It should be noted that the concept of using the mass pod, rather than an all-up operational pod, to evaluate cooling adequacy is based on also having a full laboratory environmental test program for the pod. Verification of predicted cooling mass flows in flight in conjunction with demonstrated cooling of the operating equipment with these same predicted flow rates in the laboratory provides high confidence in the pod thermal design.

5. The test results presented in this report include measured temperatures and cooling flow rates as a function of altitude and Mach number and power spectral density (PSD) and time history (TH) vibration data. Composite PSD plots are also provided for all of the vibration data.

TEST CONFIGURATION AND DATA REDUCTION

POD CONFIGURATION

6. The ALQ-164 pod is a semimonocoque structure with removable reinforced-plastic nose and tail cones. The overall length of the pod is 85 in. and the pod diameter is 16 in. Pod mounting lugs use a 14-in. spacing and the pod mounts to the fuselage station on the AV-8C aircraft. As tested, the pod weight was 317 lb with the cg located 8.5 in. aft of the forward lug. A photograph of the pod is shown in figure 1.

7. The design of the pod provides an isolator-mounted vertical plate that serves as the cold-plate for cooling the electronic equipment and the mounting structure for the pod equipment. Antennae, housed within the nose and tail of the pod, are also attached to this cold-plate. The equipment cooling air is picked up through two ram-air scoops mounted on the forward upper portion of the cylindrical section of the pod. The ram air is ducted to the forward plenum of the cold-plate, through the cold-plate to a rear plenum, and out through two exit ports in the aft portion of the cylindrical section of the pod. Eight isolators, four on the top and four on the bottom, are used to mount the cold-plate to the pod structure. The design natural frequency of the cold-plate mounting is 25 Hz. Fins are provided within the cold-plate to increase the cooling air contact area with the plate. A moisture drain is provided in the bottom of the rear plenum. All ducting to the cold-plate are flexible rubber tubes. Electromagnetic gaskets are used between the cold-plate and the pod structure at both ends of the cold-plate.

8. The prototype cold-plate used in this test program differed from the production units in that all of the bosses, used to provide equipment mounting bolt holes without penetrating the air flow passage, were not provided in the test plate. This resulted in slightly greater cooling-flow cross sectional area and some cooling-flow leakage out of the cold-plate. All detected leakage was sealed with gasket or putty material. The slight difference in duct area is not considered to be significant.

POD INSTRUMENTATION

9. The pod test instrumentation consisted of pressure transducers and thermocouples to allow evaluation of the flow capability of the cold-plate, accelerometers to determine the vibration levels to which the pod and its equipment are exposed, and additional thermocouples to measure the pod skin temperature. The test data were telemetered directly to the ground station from an antenna mounted to the bottom of the pod. All instrumentation was located within the pod with only electrical power, instrumentation control signals, and an event marker signal coming from the test aircraft. The ground station recorded the telemetered data as well as a time code and the test pilots voice transmissions.

10. Further details of the instrumentation system, calibration data, and additional installation photographs are found in NAVAIRTESTCEN Technical Support Directorate Instrumentation Report TSD 01-05-122; subject, AV-8C (BuNo 158706) ALQ-164 Mass Model Pod of 22 January 1981, by Dale Rebarchick. It should be noted that both proportional bandwidth (PBW) and constant bandwidth (CBW) voltage controlled oscillators were used in multiplexing the test data. With the discriminator output filter used in processing the vibration test data, the deviation ratio for the CBW data was only two. While this value is less than the recommended value of five, this value of two has provided reasonable data accuracy in past test projects.

FLOW MEASUREMENT

11. The cooling flow test data included the differential pressure between the total pressure measured at the inlet scoops and the static pressure in the cold-plate forward plenum, the absolute static pressure in the forward plenum, and the differential static pressure between the cold-plate forward and aft plenums. The static temperature in the forward plenum was also measured. The total pressure probes that were installed in the inlet scoops are shown in figure 2.

VIBRATION MEASUREMENT

12. A total of eight piezoelectric accelerometers was mounted to the cold-plate and the pod structure. Six of these accelerometers were attached to the starboard side of the cold-plate. Four of these plate-mounted accelerometers were aligned with the pod lateral axis and were located near the top and bottom of the plate (adjacent to the second isolator - counting forward from the rear) and just aft of the forward plenum flange and just forward of the aft plenum flange (at about midheight). The two other plate-mounted accelerometers were aligned with the longitudinal and vertical axis of the pod and, with the bottom (lateral) plate accelerometer, actually were an integral triaxial accelerometer block. The remaining two accelerometers were mounted to the pod structure (also referred to as the housing) and were aligned with the pod lateral axis. These accelerometers were located adjacent to the top and bottom plate-mounted accelerometers. The accelerometers were mounted to mounting blocks that were secured to the pod or plate with machine screws. The single axis accelerometers attached to the mounting blocks with studs. The triaxial accelerometer mounted to the block with insulated machine screws. A typical accelerometer installation is shown in figure 3. This figure shows the bottom plate-mounted triaxial accelerometer and the housing-mounted single axis accelerometer.

TEMPERATURE MEASUREMENT

13. The three pod skin temperature thermocouples were mounted along a line representing the intersection of the lower surface of the pod and the vertical plane of symmetry of the pod. One was mounted in the nose cone back from the tip of the cone a distance that yielded a surface slope at approximately 45 deg to the longitudinal axis of the pod. The tail cone thermocouple was located at a similar point on the tail cone. The thermocouple mounted to the center section of the pod was mounted at about the middle of the pod. The thermocouples were mounted to the pod by securing the wire within a hole, drilled through the pod skin, with an epoxy adhesive. The objective of this thermocouple installation was to have the thermocouple junction protrude slightly beyond the pod surface contours so as to be exposed to the external air flow temperature rather than the skin temperature. Unfortunately, the realized thermocouple installation did not provide the intended junction placement. The tail-cone and center-body thermocouple junctions were submerged within the epoxy adhesive and did not extend to the outer surface of the skin. Considering the small mounting hole diameter (0.0625 in. ID), the temperatures measured by these thermocouples are considered to be representative of a pod local midthickness skin temperature. The nose cone thermocouple junction was also within the mounting hole (about one-half of the 0.0625 in. ID below the pod surface) but the junction was not submerged within the epoxy adhesive. As a result of this mounting configuration, the data from this thermoc ,le are considered to be mainly a measure of skin temperature during conventional flight. Under hover conditions, however, where engine exhaust can impinge on the surface of the pod and the external flow is highly turbulent, some measure of external flow temperature is being provided.

CALIBRATION AND ANALYSIS

14. All instrumentation transducers were calibrated prior to installation into the pod. Calibration of the cooling flow impedance characteristics of the cold-plate was accomplished with a calibrated laminar-flow flowmeter. Pressure measurements made during the plate calibration utilized the flight test instrumentation pressure transducers and a DVM. Ground analysis of the low-frequency test data was accomplished through the use of strip chart analog recorders. A dual-channel Fast-Fourier-Transform (FFT) analyzer and a digital memory scope were used to provide the analysis of the vibration data. All vibration data were filtered above 2000 Hz, and normal calibration procedures were followed during the playback of the test data.

TEST PROCEDURES

COLD-PLATE CALIBRATION

15. The calibration of the flow characteristics of the cold-plate was conducted using equipment similar to that used in various environmental tests by the pod contractor. The test setup is shown in figure 4. The controlled air flow was provided by the local environmental test facility and passed through a laminar-flow flowmeter before entering a plenum box. The airflow passed from the plenum box to each of the two pod inlet hoses that normally connect the inlet scoops to the forward plenum of the cold-plate. The calibration tests were conducted at two cooling flow temperatures, 14°C (57°F) and 70°C (158°F), and to a maximum facility mass flow capacity of 15 lb/min. The static pressure difference between the forward and aft plenums of the cold-plate and the flow temperature and density (as measured in the forward plenum) are used to correlate the mass flow data. The calibration data are shown in figure 6. The pressure parameter used in the calibration data was derived to provide a linear relationship and to collapse all flow data onto one calibration line. This presentation is based on the assumption of turbulent flow within the cold-plate, and extrapolation of the calibration data to much greater mass flows than provided by this calibration should be valid.

ATMOSPHERIC DATA

16. OAT data were not obtained during the test flights of this program. The ambient air temperature used in the analysis of the test data is based on meteorological data acquired near the time of the test flights in the general geographic area of the tests. Due to the time and geographic differences between the acquisition of the flight and the meteorologic data, it is possible that the assumed values of ambient temperature could be off by as much as $\pm 5^{\circ}$F. The ambient temperatures used in the reduction of the test data are shown in figure 5 for the two test flights.

GROUND TEST

17. Part of the ground checkout of the flight test instrumentation involved ground "raps" of the accelerometer mounting structure. This procedure was intended to verify the functional operation of the equipment and, in the case of the vibration measurement installations, to identify resonant frequencies that may be peculiar to the accelerometer mounting and not representative of the motion of the cg of the equipment to which the accelerometer was attached or which may later be located at the same location. Although it is not always possible to discount such a resonance as something that would not be sensed by a piece of equipment, these data do allow some additional insight into the interpretation of the flight test results.

18. In general, all plate-mounted accelerometers displayed a fairly well-defined resonance at about 1600 Hz. Some of these outputs also showed oscillations at frequencies above the 2000 Hz cutoff frequency used in the ground analysis of the flight test data, but these components were not consistent and were more difficult to identify. The apparent frequencies seen with the pod-housing mounted accelerometers were greater than the 2000 Hz cutoff frequency. It was not possible to excite the design resonant frequency of the cold-plate mounting (about 25 Hz) with the available equipment. It would appear that the 1600 Hz frequency on the plate must be inherent to the plate as it was seen with different types of accelerometers and mounting techniques (i.e., single-axis, stud-mounted accelerometers, and the machine-screw mounted triaxial accelerometers).

altitude. These values are considered to be midthickness skin temperatures and probably do not represent stabilized skin temperatures for these flight conditions. It should be noted that the test profile consisted of obtaining the cruise test data in a sequence of increasing altitudes. For the 500 and 20,000 ft altitudes, the lower speed data were obtained first. The higher speed data point was obtained first at 40,000 ft. The measured temperatures represent, therefore, the combined effects of the ambient temperature changes with altitude, the increase in stagnation temperature with airspeed, and the thermal inertia of the pod structure.

Table I

Pod Skin Incremental Temperature Above Ambient for Cruising Flight

Altitude (ft)	Mach No.	Incremental Temperature Above Ambient (°F)		
		Nose Cone	Center Body	Tail Cone
500	0.31	7.9	4.4	15.1
500	0.69	35.7	21.4	24.5
500	0.68	35.3	25.1	26.4
20,000	0.35	35.5	35.8	53.1
20,000	0.34	37.6	41.8	56.2
20,000	0.73	35.5	29.2	43.6
20,000	0.73	35.4	34.2	42.1
40,000	0.64	32.0	37.0	50.6
40,000	0.79	37.1	42.7	55.2

23. The incremental temperatures measured by the pod thermocouples during takeoffs and landings are shown in figures 9 and 10. These data are presented as a function of time and reflect the short duration of time in which these maneuvers are accomplished. There was no apparent charring of the pod surface paint during this test program.

VIBRATION DATA

24. The primary method of analysis for the vibration data obtained in this program was through the use of a digital FFT analyzer to produce PSD distributions of the outputs of the various accelerometers mounted in the pod. A limited number of TH plots are also shown in this report to provide better insight into the character of the data. Because of the large number of PSD plots presented, the annotations added to the machine-generated plots have been minimized. To ensure complete understanding of the annotations used on the plots, figure 11 provides an explanation of the various notes used. The horizontal scale (frequency) is common for all of the PSD plots (5 to 2000 Hz). The vertical scale (g^2/Hz) does vary in magnitude between plots with the maximum value shown near the top of the plot (note 2). Log-log scales are used for all of the PSD plots. A broadband RMS value of the measured acceleration is shown on most of the PSD plots. These values represent the contribution of all of the frequency data from 5 to 2000 Hz.

25. The presentation of the vibration data is organized so as to present the steady-state cruise data first. Following the cruise data are the extrapolated vibration data that are intended to provide some measure of the vibration levels that are expected at a flight condition corresponding to the maximum dynamic pressure the AV-8C aircraft is expected to see. The transient data, i.e., takeoffs, landings, and gun fire, are shown next. Finally, composite summary plots are shown that envelope all of the test (or extrapolated) data for each flight condition.

FLIGHT TEST

19. The flight test program consisted of two flights with the mass pod being carried on AV-8C aircraft, BuNo 158706. The first flight was conducted on 29 September 1980 and was discontinued soon after takeoff due to equipment problems. Data for four of the desired test conditions were obtained prior to stopping this first flight. The second test flight took place on 15 October 1980 and provided a complete test profile. Due to the previous exposure of the test pod to excessive structural loads, flight restrictions were imposed on the test aircraft when carrying this pod. Flight operations were restricted to symmetric flight, indicated airspeed not to exceed 450 kt and normal accelerations within a range of ± 2 g.

20. The flight-test test points were defined to provide an array of test conditions throughout the available flight envelope. Vectored-thrust takeoff and landings were performed as well as gun fire. The test conditions were as follows:

500 ft altitude, 199 and 448 kt
20,000 ft altitude, 155 and 340 kt
40,000 ft altitude, 190 and 238 kt
Gun fire, both guns, about 2,000 ft altitude and 440 kt
Short landing with nozzle braking
Short takeoff (wet)
Vertical takeoff
Vertical landing

Limited gunfire data were also obtained for single gun operation as one gun expended its available ammunition prior to the other gun during the gun-fire run. Except for the takeoff, landing, and gun fire operations, all test conditions were stabilized with at least 10 sec of data recorded.

DISCUSSION AND TEST RESULTS

COOLING FLOW DATA

21. The cooling flow flight test data measured the mass flow of cooling air that the pod scoops delivered to the cold-plate and the inlet temperature of the cooling air. These data are presented as a function of flight Mach number and pressure altitude in figures 7 and 8. The Mach numbers used in this report were computed with the assumed atmospheric temperature data (figure 5) and a true airspeed computed from the pilots indicated airspeed and neglecting possible instrument and aircraft position errors. The solid curves shown in figure 7 represent the pod contractor's predicted cooling flow. The test data show close agreement with the predicted values and indicate that environmental tests utilizing these mass flows should be realistic. The incremental temperature of the cooling air, as measured in the forward plenum of the cold-plate, above the assumed ambient air temperature is shown as a function of altitude and Mach number in figure 8. The solid curves in this figure represent a manually-faired second-order curve through the test data. Considering the assumed accuracy of the ambient atmospheric temperature data ($\pm 5^{\circ}$F), these measured temperatures are reasonably consistent with the flight conditions and an assumed effective plenum duct area of 4 sq. in.

POD SURFACE TEMPERATURE DATA

22. The measured data obtained with the pod skin thermocouples are shown in table I for cruising flight at the test altitudes of 500, 20,000 and 40,000 ft. These temperatures are presented as incremental temperatures above the estimated ambient temperature for each

altitude. These values are considered to be midthickness skin temperatures and probably do not represent stabilized skin temperatures for these flight conditions. It should be noted that the test profile consisted of obtaining the cruise test data in a sequence of increasing altitudes. For the 500 and 20,000 ft altitudes, the lower speed data were obtained first. The higher speed data point was obtained first at 40,000 ft. The measured temperatures represent, therefore, the combined effects of the ambient temperature changes with altitude, the increase in stagnation temperature with airspeed, and the thermal inertia of the pod structure.

Table I

Pod Skin Incremental Temperature Above Ambient for Cruising Flight

Altitude (ft)	Mach No.	Incremental Temperature Above Ambient (°F)		
		Nose Cone	Center Body	Tail Cone
500	0.31	7.9	4.4	15.1
500	0.69	35.7	21.4	24.5
500	0.68	35.3	25.1	26.4
20,000	0.35	35.5	35.8	53.1
20,000	0.34	37.6	41.8	56.2
20,000	0.73	35.5	29.2	43.6
20,000	0.73	35.4	34.2	42.1
40,000	0.64	32.0	37.0	50.6
40,000	0.79	37.1	42.7	55.2

23. The incremental temperatures measured by the pod thermocouples during takeoffs and landings are shown in figures 9 and 10. These data are presented as a function of time and reflect the short duration of time in which these maneuvers are accomplished. There was no apparent charring of the pod surface paint during this test program.

VIBRATION DATA

24. The primary method of analysis for the vibration data obtained in this program was through the use of a digital FFT analyzer to produce PSD distributions of the outputs of the various accelerometers mounted in the pod. A limited number of TH plots are also shown in this report to provide better insight into the character of the data. Because of the large number of PSD plots presented, the annotations added to the machine-generated plots have been minimized. To ensure complete understanding of the annotations used on the plots, figure 11 provides an explanation of the various notes used. The horizontal scale (frequency) is common for all of the PSD plots (5 to 2000 Hz). The vertical scale (g^2/Hz) does vary in magnitude between plots with the maximum value shown near the top of the plot (note 2). Log-log scales are used for all of the PSD plots. A broadband RMS value of the measured acceleration is shown on most of the PSD plots. These values represent the contribution of all of the frequency data from 5 to 2000 Hz.

25. The presentation of the vibration data is organized so as to present the steady-state cruise data first. Following the cruise data are the extrapolated vibration data that are intended to provide some measure of the vibration levels that are expected at a flight condition corresponding to the maximum dynamic pressure the AV-8C aircraft is expected to see. The transient data, i.e., takeoffs, landings, and gun fire, are shown next. Finally, composite summary plots are shown that envelope all of the test (or extrapolated) data for each flight condition.

26. Where possible, sufficient test data have been used to provide statistically significant random vibration plots. For those flight conditions that produced essentially stationary data, the PSD plots represent the average of eight samples of data (indicated by note 11 in figure 11). In the case of nonstationary data, only one sample of the test data was used so that a measure of the maximum level of vibration could be provided. The "time window" for the analyzer, when on the 2000 Hz range setting, is 0.2 sec for one sample of data. It should be noted that, where duplicate vibration data are shown for a given flight condition and accelerometer (i.e., data from both the 9/29/80 and the 10/15/80 test flights), the data obtained on the 10/15/80 test flight display lower levels of vibration - particularly at the higher frequencies. This reduction is most noticeable for the plate data, but the trend is also seen in the housing data. No specific discrepancy was found in either the instrumentation, the data playback equipment, or the internal pod configuration, and there was nothing to indicate that the flight conditions were not the same. No explanation can be offered for this difference in measured vibration.

CRUISING FLIGHT

27. The PSD data for a low and high-speed flight condition at pressure altitudes of 500, 20,000 and 40,000 ft are shown in figures 12 through 17. The lower speed at each altitude represents the anticipated minimum speed for well-controlled flight. The high-speed corresponds to either the maximum speed defined in the pod flight clearance or the maximum stabilized straight-and-level speed obtainable by the aircraft-pod configuration. In general, data from all accelerometers are shown for the high-speed flight condition at each altitude. All data are not shown for the low-speed flight conditions because they were not considered to provide needed data, and the corresponding PSD plots were never generated.

28. Although these vibration data plots are rather self-explanatory, there are some characteristics that should be noted. While the cold-plate isolators were selected to give a damped natural frequency of about 25 Hz, the test data would seem to indicate a somewhat higher resonant frequency for the test installation. A comparison between the housing data and the plate data indicates that the plate data tends to show no attenuation of the vibration energy content below about 70 Hz. Based on generalized isolator data, this would seem to indicate a resonant frequency of the order of 50 Hz. Also, the increase in isolator attenuation with frequency seems to stop at around 200 Hz. Above that frequency, the vibration level measured on the plate either remain at about the same level below the vibration seen on the housing or tends to increase to the housing level. This characteristic may be an indication that the vibration seen at the higher frequencies is due to acoustic sources rather than mechanical vibration being transmitted through the isolators. The increase in vibration level seen on the plate also reflects the 1600 Hz resonance found on the plate during the ground checks (see GROUND TESTS under TEST PROCEDURES).

VIBRATION DATA EXTRAPOLATION

29. Because of the flight restrictions that were imposed on the test aircraft when carrying this test pod (see FLIGHT TEST under TEST PROCEDURES), it was not possible to obtain pod vibration data at the maximum dynamic pressure that may be developed with a production pod. This limitation made it desirable to determine the feasibility of extrapolating the test data in order that some measure of the vibration that will be developed at maximum dynamic pressure can be obtained. To this end, the vibration data were analyzed to identify possible trends with dynamic pressure. Dynamic pressure was a logical flight parameter as it is a measure of required engine power and thrust and provides an indication of the available energy level in the external flow passing over the pod. The broadband RMS

values obtained from the accelerometer outputs were used as the initial measure of vibration. Figure 18 shows the correlation between RMS vibration for the upper and lower housing-mounted accelerometers and the free stream dynamic pressure. Although it was not expected that a linear relationship would be found, the best fit for the data does seem to be a straight line. The deviation from a linear fit at the lower values of dynamic pressure are assumed to reflect the induced drag increases associated with lower flight velocities and the corresponding increased contribution of the aircraft power plant to the sensed vibration levels. In general, the agreement between the test data and a straight line is considered to be good. It should be noted that, at the higher flight velocities, Mach number must also be a significant factor (i.e., power increases associated with drag divergence), but sustained flight in this region is unlikely and there are inadequate test data to evaluate this Mach number effect.

30. The variation of the broadband RMS vibration seen on the isolated plate is shown as a function of dynamic pressure in figures 19 and 20. The data for the top and bottom lateral axes are seen in figure 19 and those for the bottom vertical axis are shown in figure 20. Although there does seem to be a slight increase in vertical axis vibration with dynamic pressure, the low slope and data scatter make extrapolation questionable. Based on these data, it is concluded that the maximum vibration levels obtained on the plate during the flight test program are representative of the levels that will be found at higher dynamic pressures. Extrapolation of the housing data does seem to be a valid approach.

31. While the housing RMS data seems to correlate fairly well with dynamic pressure, it is not obvious that the PSD distribution with frequency will also scale in a reasonable fashion. To check on this scaling, the test data for a midvalue of dynamic pressure was scaled up and down to match the data obtained at other values of dynamic pressure. These comparisons of the PSD data are shown in figure 21. These data are for the housing bottom lateral accelerometer with the dashed curve representing the scaled results. The magnitude of the scaling is indicated by the scale factor (SF) shown above the graph. The scaling was accomplished through the calibration software built into the FFT analyzer. The accelerometer output was scaled in direct proportion to the ratio of the dynamic pressures of the flight conditions being used for comparison. Considering the repeatability of the vibration data in general and PSD results in particular, the agreement is reasonable and justifies extrapolation of the test data.

32. Scaled vibration data for the lateral axis, top and bottom positions on the pod housing, are shown in figure 22. These data are intended to represent a dynamic pressure of 1710 psf and are scaled from flight data obtained at a dynamic pressure of 775 psf. The 1710 psf dynamic pressure was given as a maximum design value for the AV-8C aircraft and is apparently in excess of any sustained flight condition that will be seen with this aircraft/pod configuration. A maximum dynamic pressure of 1370 is considered to be more realistic. Considering the uncertainties associated with extrapolating vibration data, the results shown in figure 22 are still considered to be useful for qualifying pod equipment.

NONSTATIONARY FLIGHT

33. While the cruise flight test conditions allow the acquisition of test data that can be considered to be stationary, there are a number of aircraft operating conditions that provide a rather severe vibration environment but are of short duration and often do not lend themselves to multiple sampling and averaging. Included in this category of operations are the various takeoff and landing modes and the firing of the automatic cannons. The test data for these flight conditions are presented in terms of accelerometer output TH's and single-sample PSD results for the most severe portion of the TH. For some portions of some of these flight conditions it is still possible to present meaningful averaged multiple-sample PSD data. These plots are suitably annotated (note 11, figure 11) and the use of multiple samples is pointed out in the discussion of the figures.

Short Takeoff and Landing Data

34. The TH data for the wet, short takeoff are shown in figure 23. Only the TH data for the bottom lateral axis accelerometer are shown for both the housing and the plate as these data are representative of all of the accelerometer data for this maneuver. The vertical lines on the plot denote 1-sec time intervals. The appropriate start times for the corresponding PSD plots are also shown on this TH figure.

35. The PSD plots for all of the accelerometers for the maximum amplitude portion of the TH data (start time of 12:38:09) are shown in figure 24. These plots represent one sample of test data and correspond to a time interval of 0.2 sec. The PSD data for an average of eight samples of the initial portion of the takeoff maneuver (start time of 12:38:07) are shown in figure 25. The time interval corresponding to the eight samples of data is somewhat less than 2 sec.

36. The TH data for a short landing, with nozzle braking, are shown for the bottom lateral accelerometers in figure 26. The corresponding PSD data for the last portion of this maneuver (start time 12:20:33) are shown in figure 27 for all of the accelerometers. Because of the relatively constant amplitude of the TH data, these PSD plots represent an average of eight samples of the landing test data.

Vertical Takeoff and Landing Data

37. The TH data for the two bottom lateral accelerometers are presented for a vertical takeoff maneuver in figure 28. The single-sample PSD results for all of the accelerometers are presented in figure 29.

38. The TH data for the two bottom accelerometers are shown for a vertical landing in figure 30. No PSD data are shown for the landing because these data add no additional information to that shown by the takeoff data.

Gun Fire Data

39. The gun fire vibration data are presented as TH plots of the two housing accelerometers and the forward and aft plate-mounted accelerometers and PSD plots for all of the accelerometers. The data are presented for both guns firing and for a single gun firing. The data were obtained on a single flight with the single-gun data resulting from one gun depleting its supply of ammunition before the other gun. Adequate data duration was obtained for the both-gun firing to allow eight-sample PSD plots to be generated. Only about 1 sec of single-gun data were obtained and only single-sample PSD plots are shown. Since the guns are not synchronized with each other, the two-gun firing data tend to be more random in character than the single-gun data. Although the single-gun data provide better definition of the harmonics of the gun firing rate, the data are still considered to be random and do not lend themselves to the type of nonnormalized analysis that is normally used with harmonic data (i.e., the frequency distribution of RMS acceleration content).

40. The TH data for the two-gun firing operation are shown in figure 31. It should be noted that the amplitude scales are different for the housing and the plate data. The nominal firing rate for each gun is 1142 rounds per minute (19 rounds per second), although this is difficult to identify on these two-gun plots. The PSD data for the two-gun operation are presented in figure 32. The harmonics of the firing rate are discernible (above the third harmonic), but their distinct amplitudes are within the normal variations found in data considered to be random. The lack of definition of the first two harmonics of the gun fire rate is apparently associated with the varying relative phasing between the firing of the two guns.

41. The TH data for single-gun firing are shown in figure 33. Here the firing rate is well-defined. It is interesting to note that successive rounds do not display a consistent response from a single accelerometer. This has been observed from accelerometer data obtained on other aircraft installations during gun fire and could be associated with varying round charges and possibly variations in the gun operation. The PSD data for the single-gun operation are shown in figure 34. Data duration required single-sample analysis. The better definition of the firing rate and, to some extent, the use of a single sample of the test data results in better definition of the primary frequency and the lower harmonics of the firing rate. Even with this mode of operation, the data are considered to lend themselves to random data analysis.

SUMMARY DATA

42. Composite PSD plots of the vertical takeoff, short takeoff and landing, gun fire, and cruise are presented in figure 35. Both housing and plate lateral vibration as well as plate longitudinal and vertical vibration data are shown. These composite data represent the envelope distribution of vibration energy within which all of the test data and scaled data fit (i.e., all PSD plots shown in this report will be within the corresponding composite plot).

43. Some license has been taken in constructing these composite plots to provide 6, 12 or 20 dB/octave slopes and to keep the number of slope changes to a reasonable number. The notation used on the composite plots is consistent with that of figure 11.

CONCLUSIONS

44. The predicted pod cooling airflow provided by the pod contractor is an accurate measure of the airflow measured during this test program.

45. While the skin temperature instrumentation did not provide all of the desired temperature data, the test data do indicate that the normal maneuver durations along with the thermal inertia of the pod structure do keep realized skin temperatures within reasonable limits.

46. Extrapolation of the pod vibration test data as a function of flight dynamic pressure does appear to be valid for cruising flight conditions above the lower operational flight velocities.

47. The vibration isolators used on the pod cold-plate tend to amplify the vibration levels seen by the pod at frequencies below 70 Hz. Attenuation of the vibration at frequencies above 70 Hz is realized up to about 200 Hz. Above 200 Hz, the apparent attenuation remains constant or is reduced as the frequency is further increased. This reduced isolator effectiveness at the higher frequencies may just reflect the changing character of the vibration excitation at these higher frequencies.

48. Barring local resonances, the composite PSD data should represent the maximum vibration levels that the plate-mounted pod equipment will see for the flight conditions tested and for the extended cruising flight condition.

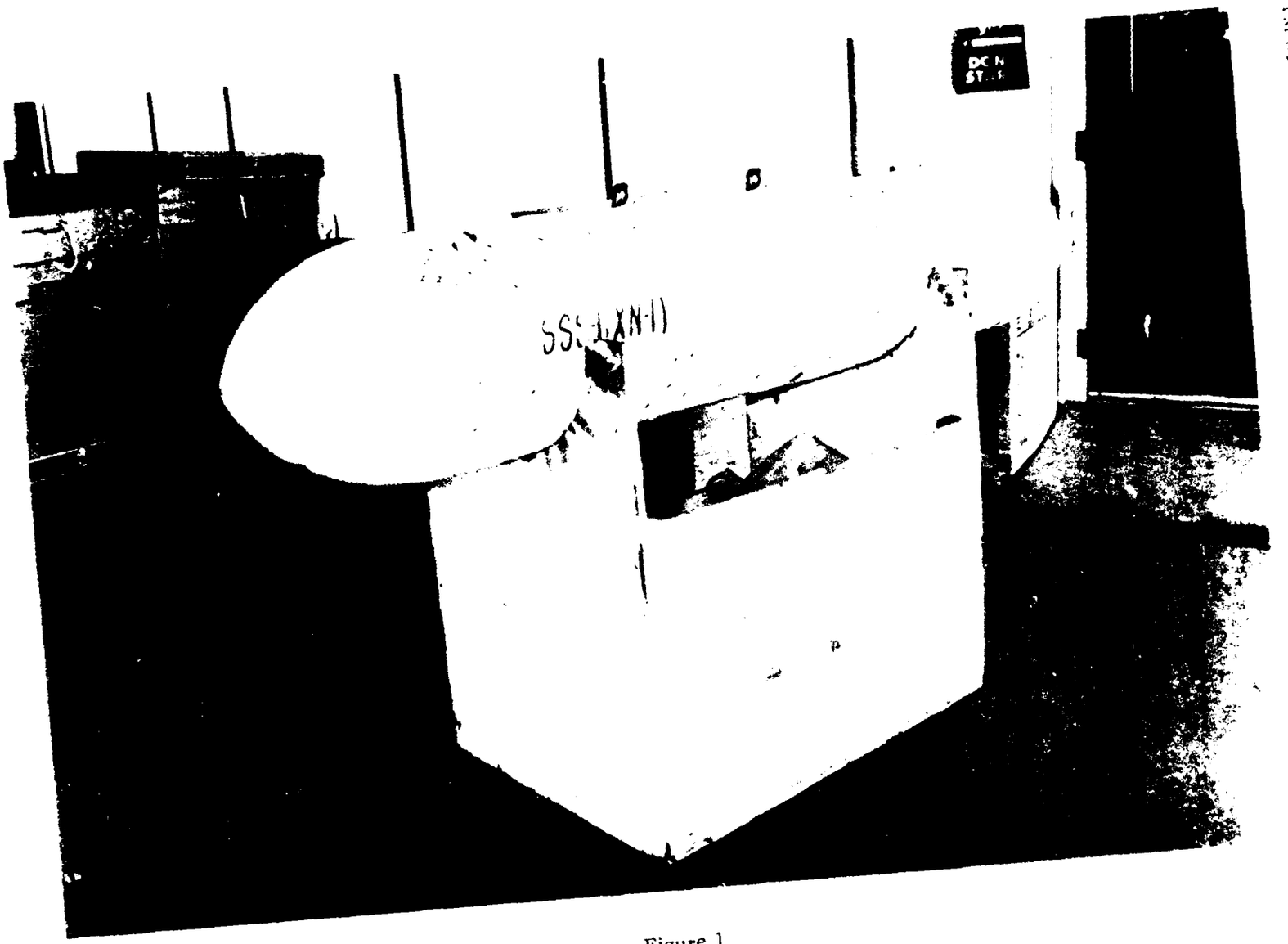

Figure 1
Pod Photograph

Figure 2
Total Pressure Probe Installation

Figure 3
Accelerometer Installation, Bottom Position,
Plate and Housing Transducers

Figure 4
Cold-Plate Calibration Setup

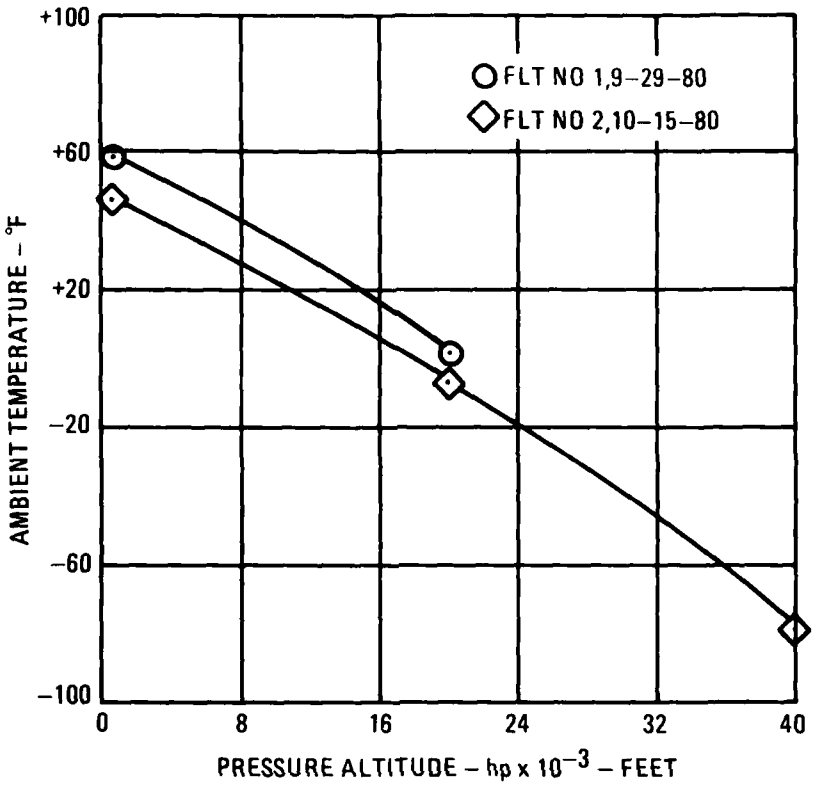

Figure 5
Atmospheric Ambient Temperature Variation with Altitude

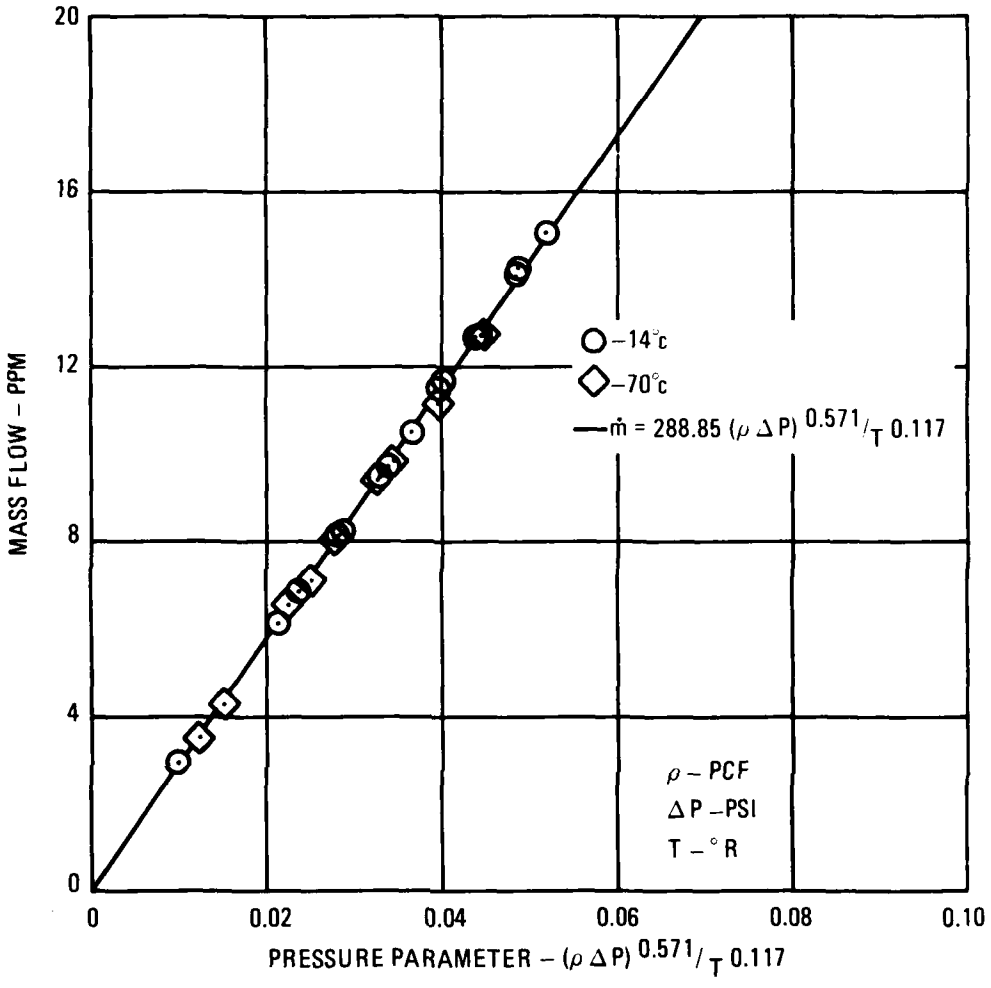

Figure 6
Cold-Plate Mass-Flow Calibration

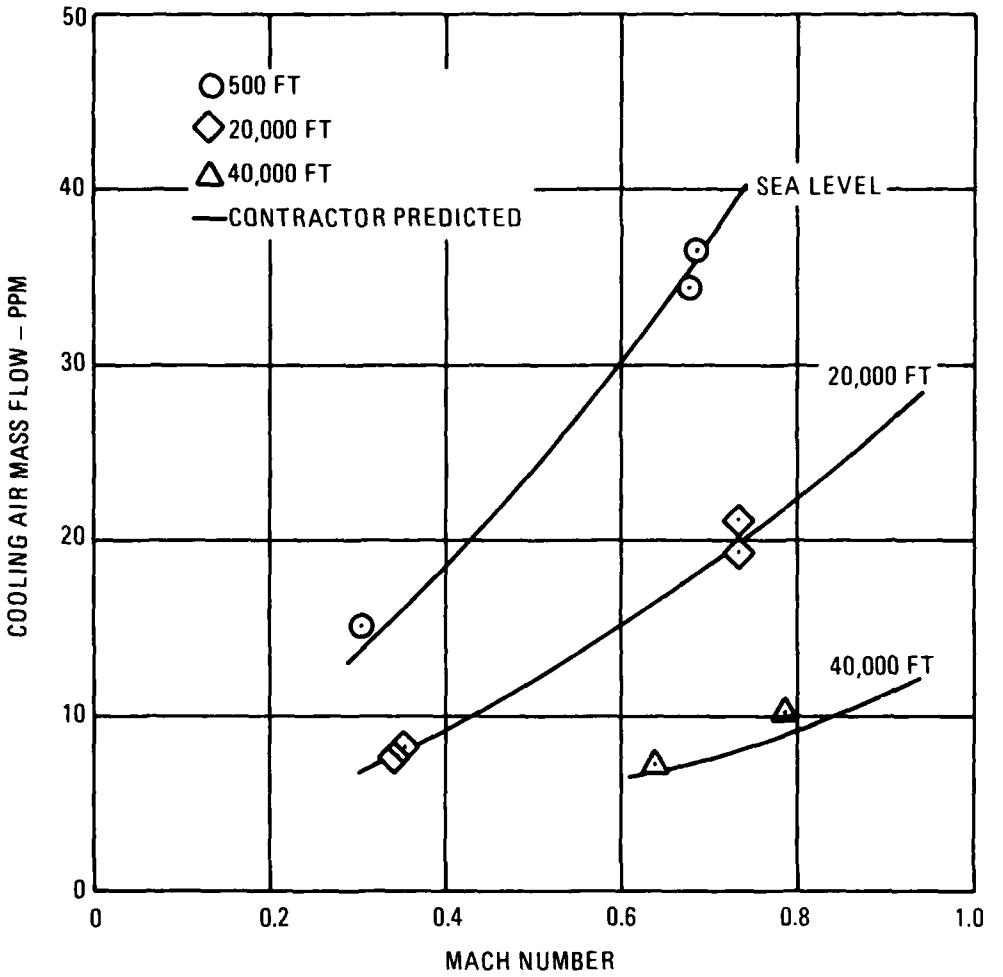

Figure 7
Cold-Plate Mass Flow

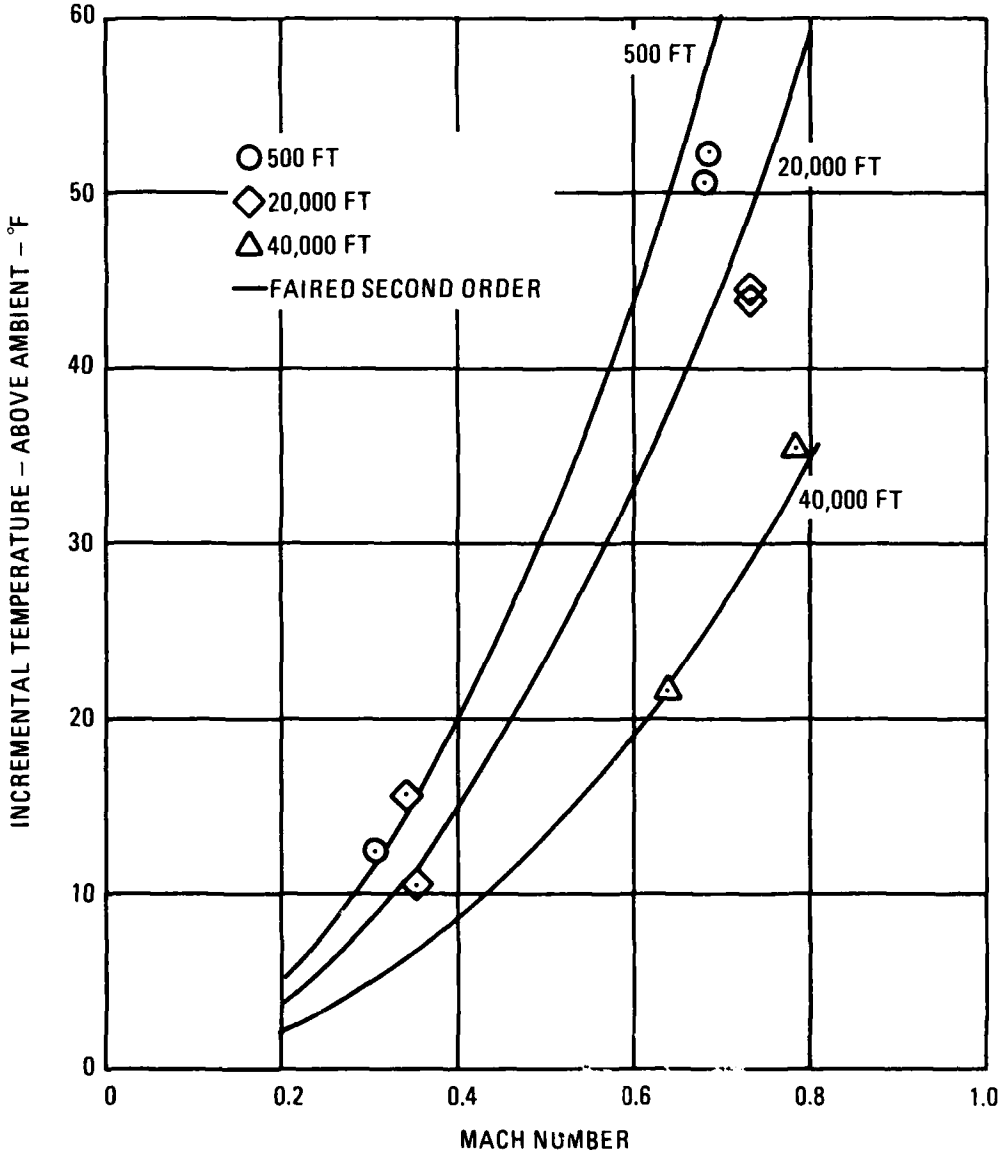

Figure 8
Cold-Plate Forward Plenum Temperature

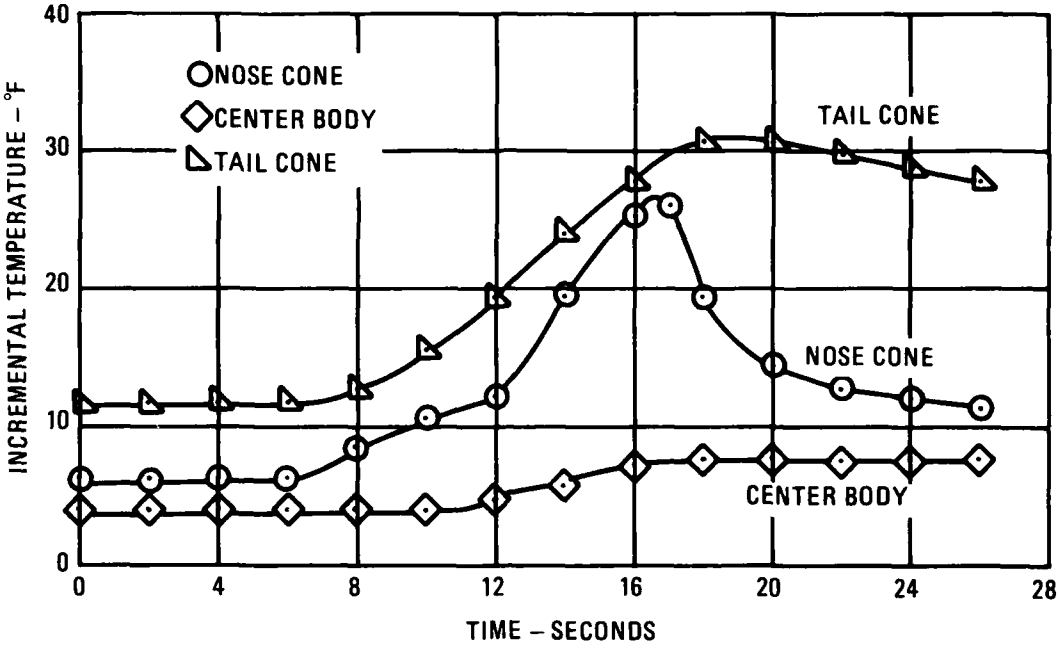

Figure 9
Incremental Temperature of the Pod Skin above Ambient Temperature during a Short Landing Using Nozzle Braking

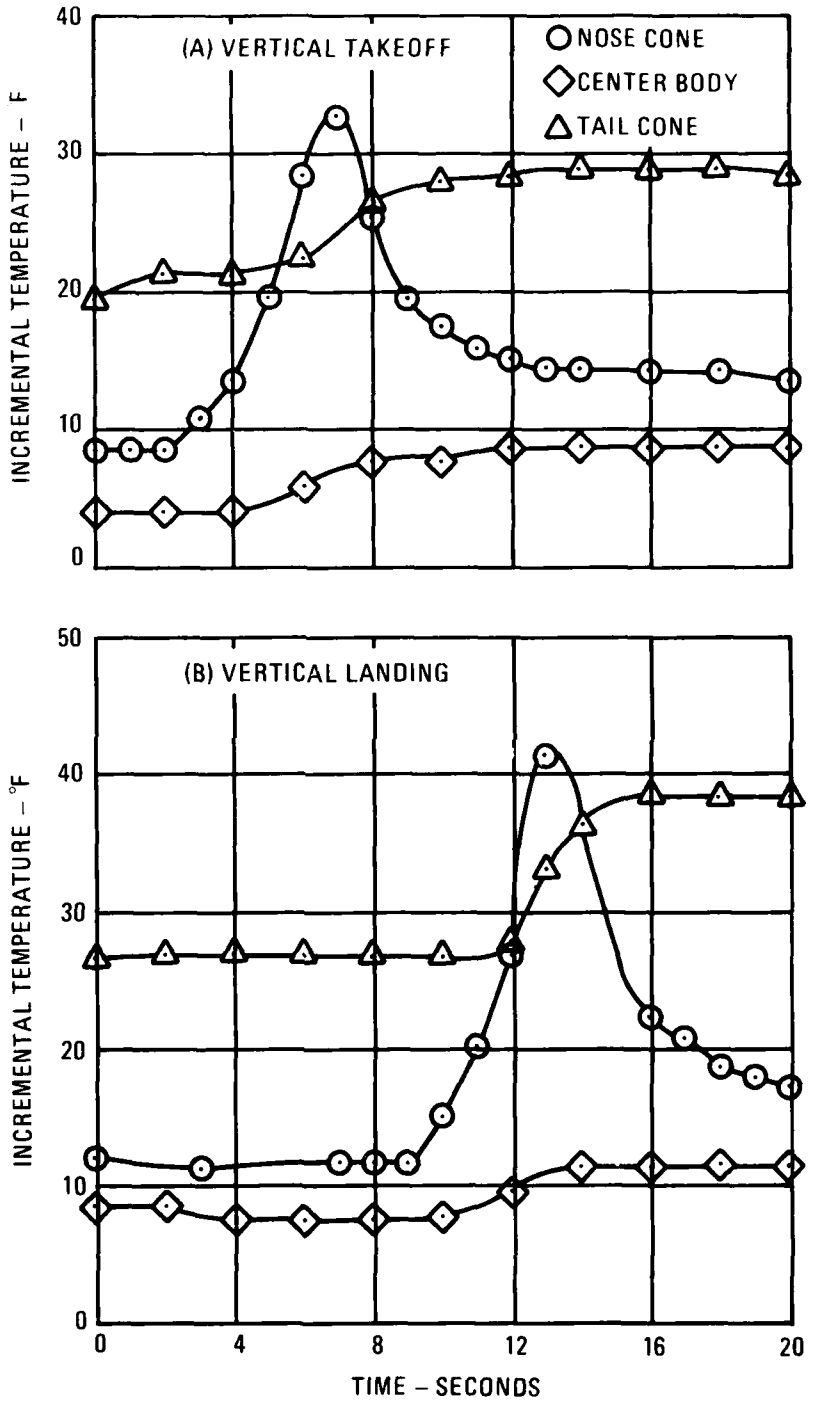

Figure 10
Incremental Temperature of the Pod Skin
above Ambient Temperature during Vertical Takeoff and Landing

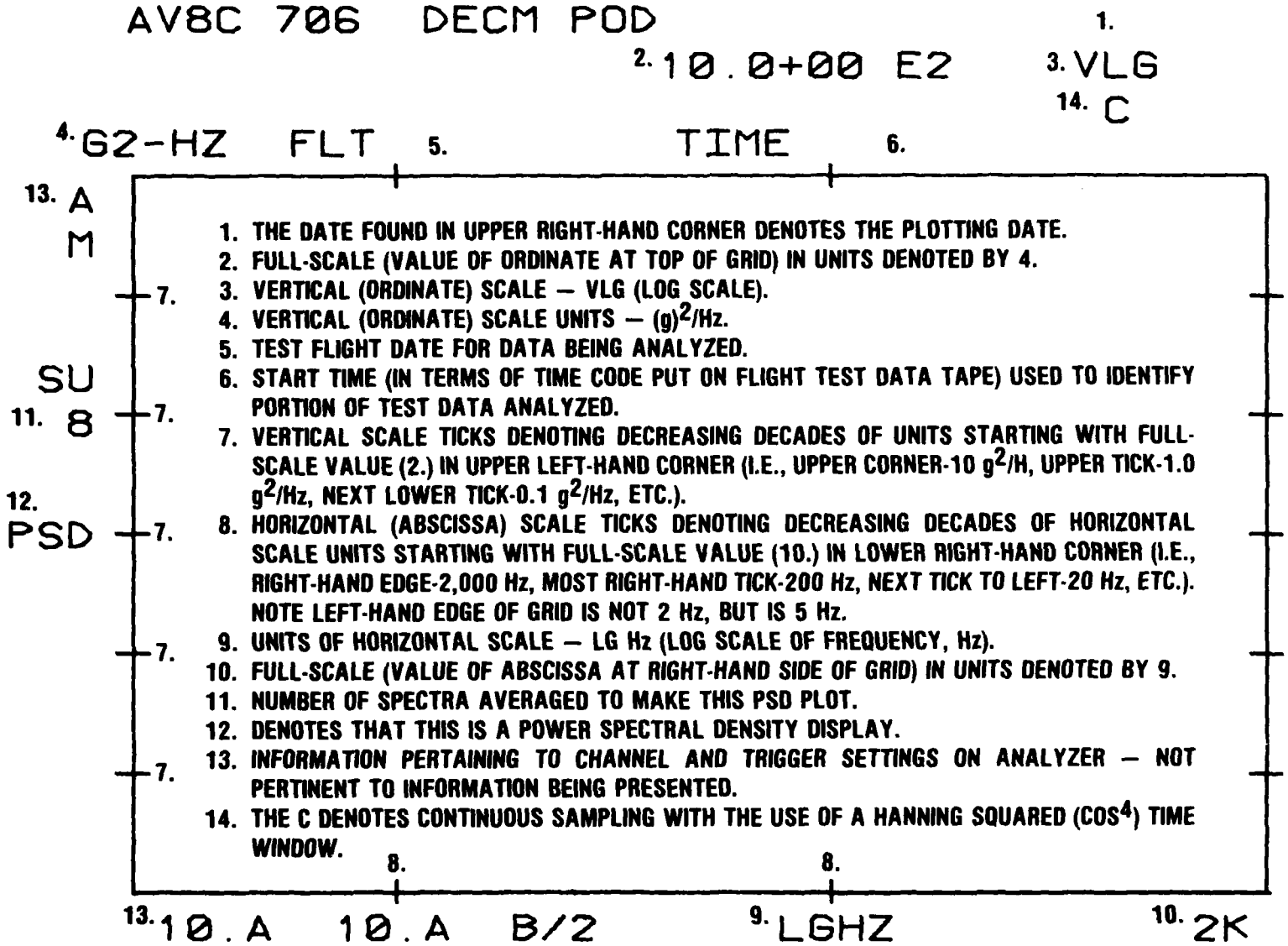

Figure 11
PSD Plot Notation

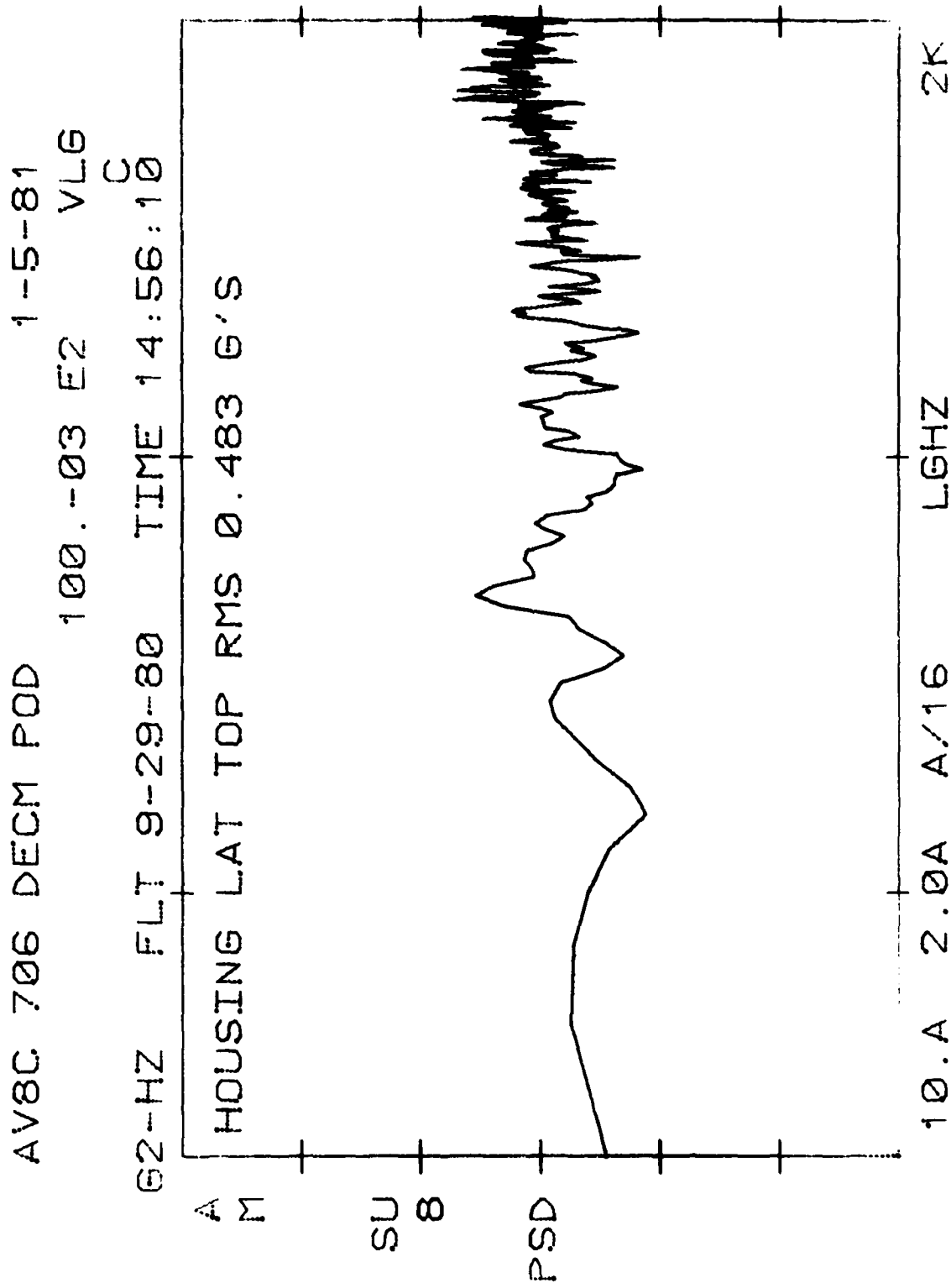

Figure 12
Cruise Flight, 500 ft Altitude and 200 KIAS, PSD

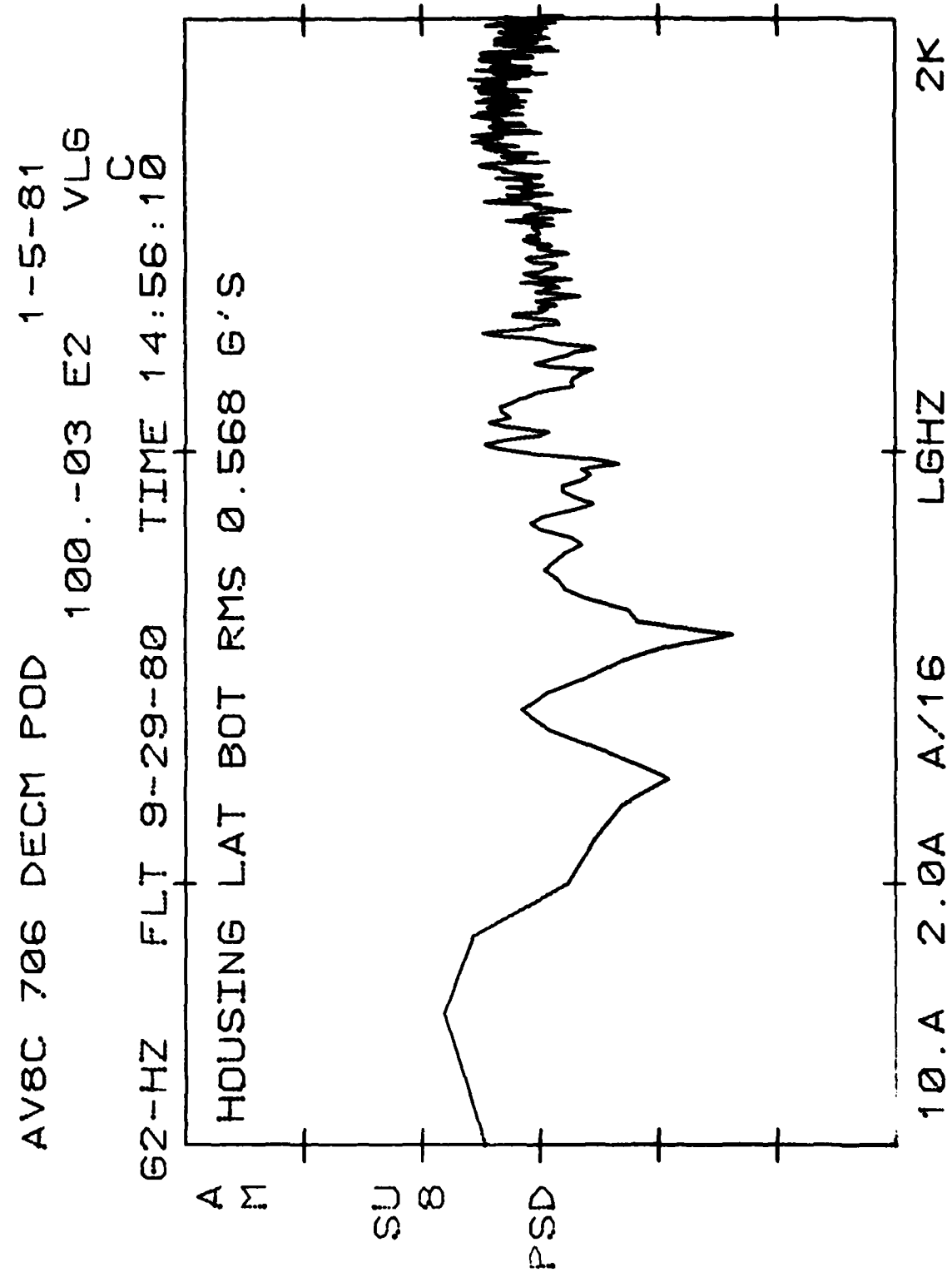

Figure 12 (Cont'd)

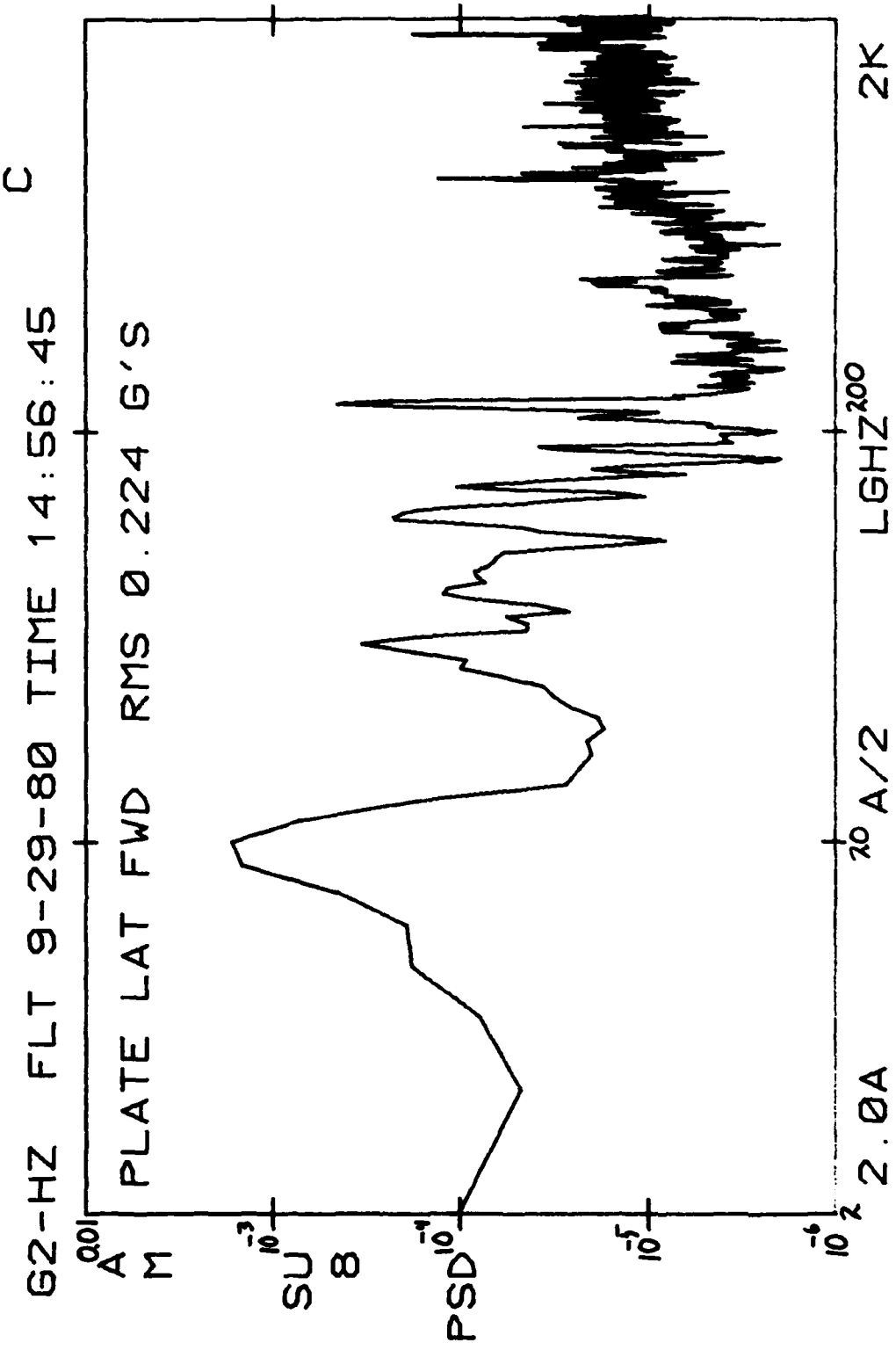

Figure 12 (Cont'd)

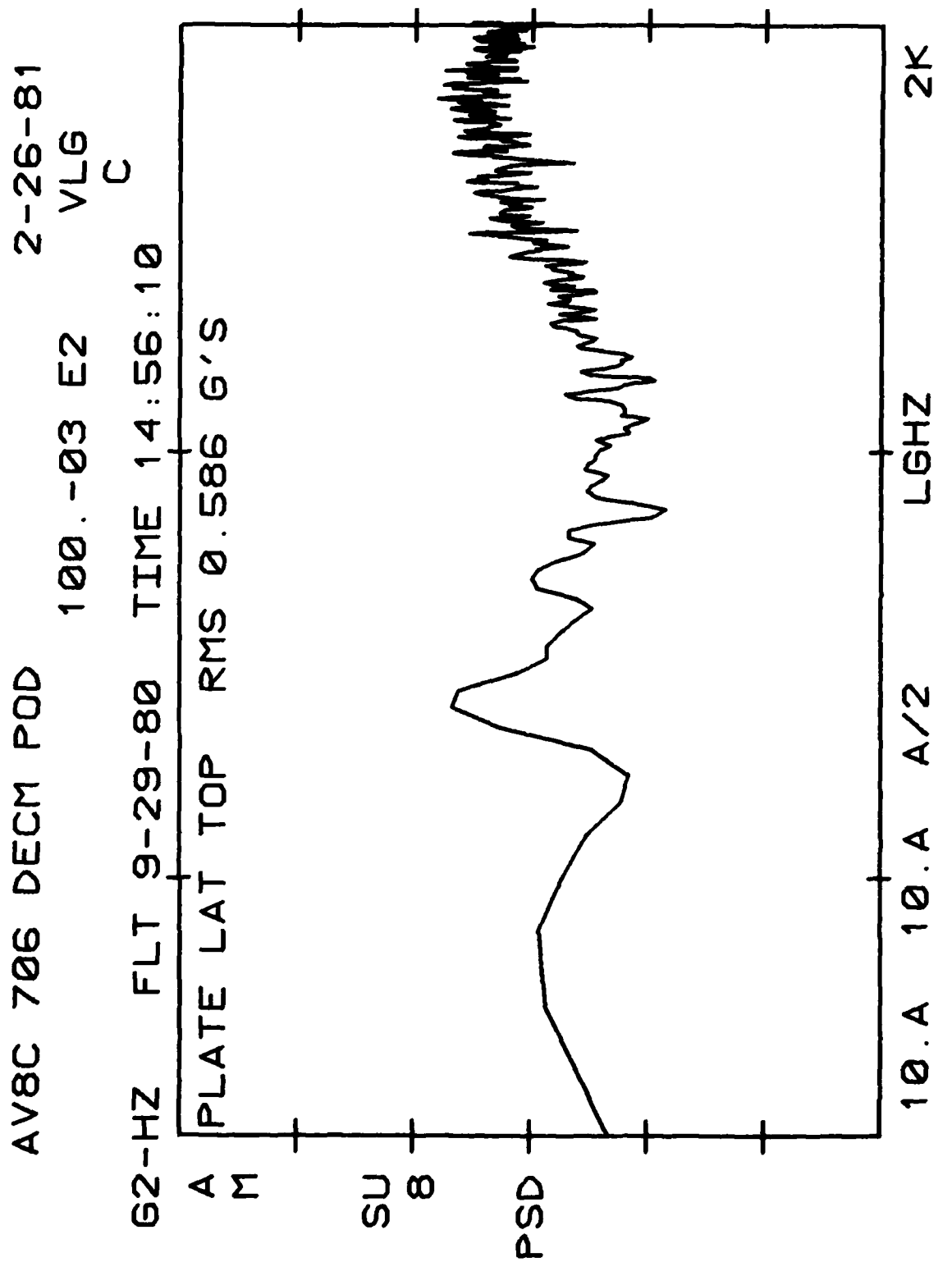

Figure 12 (Cont'd)

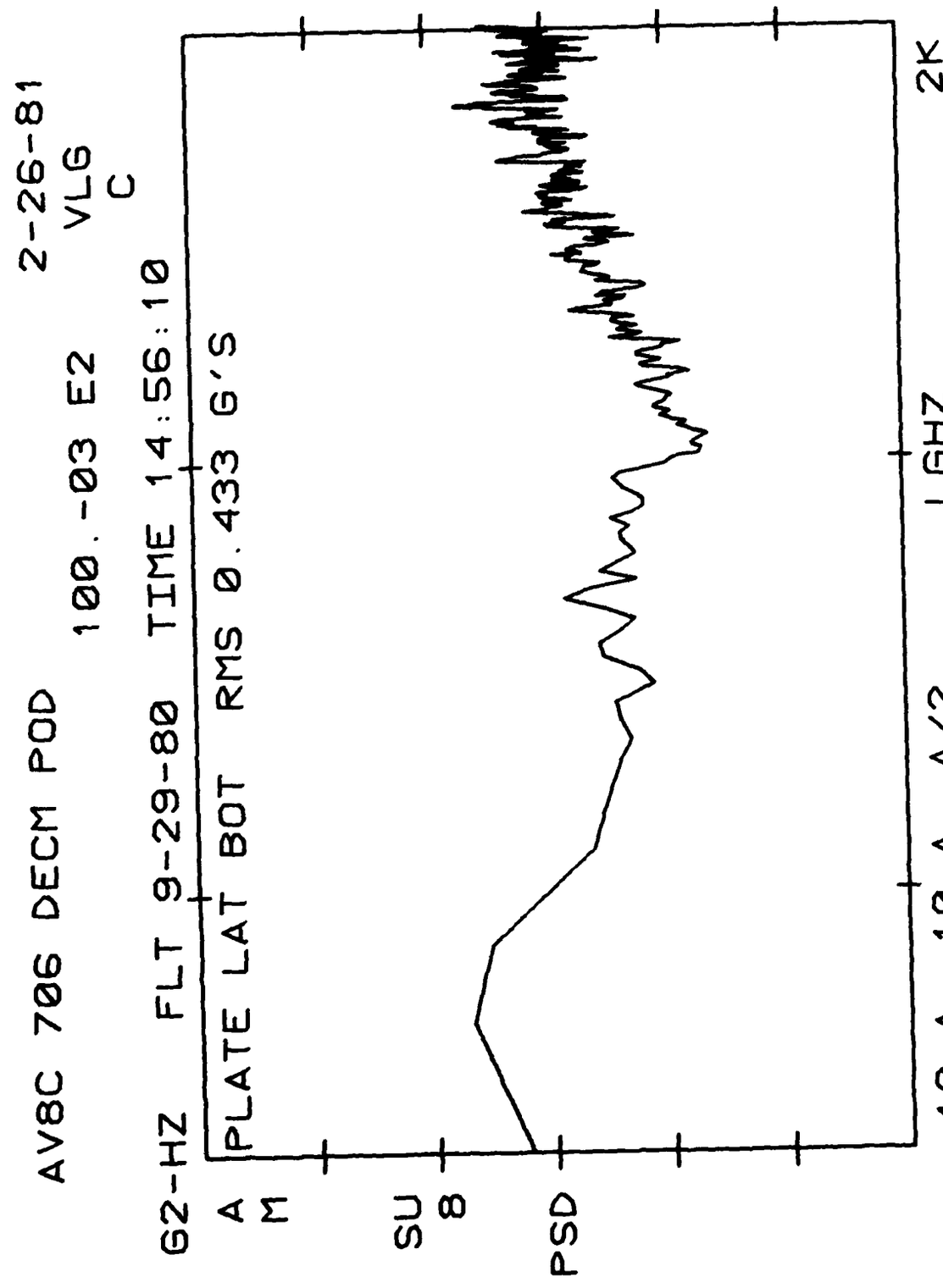

Figure 12 (Cont'd)

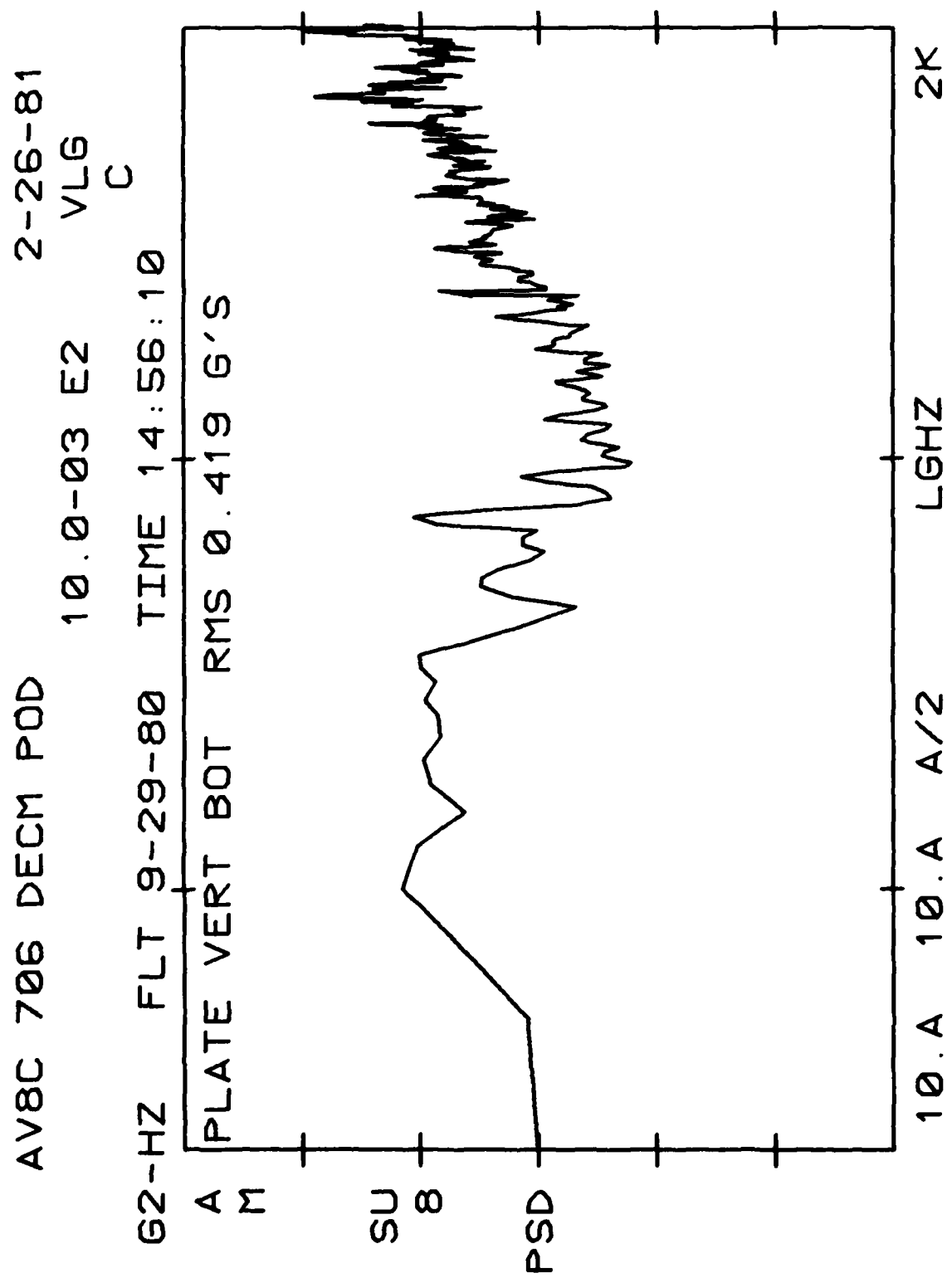

Figure 12 (Cont'd)

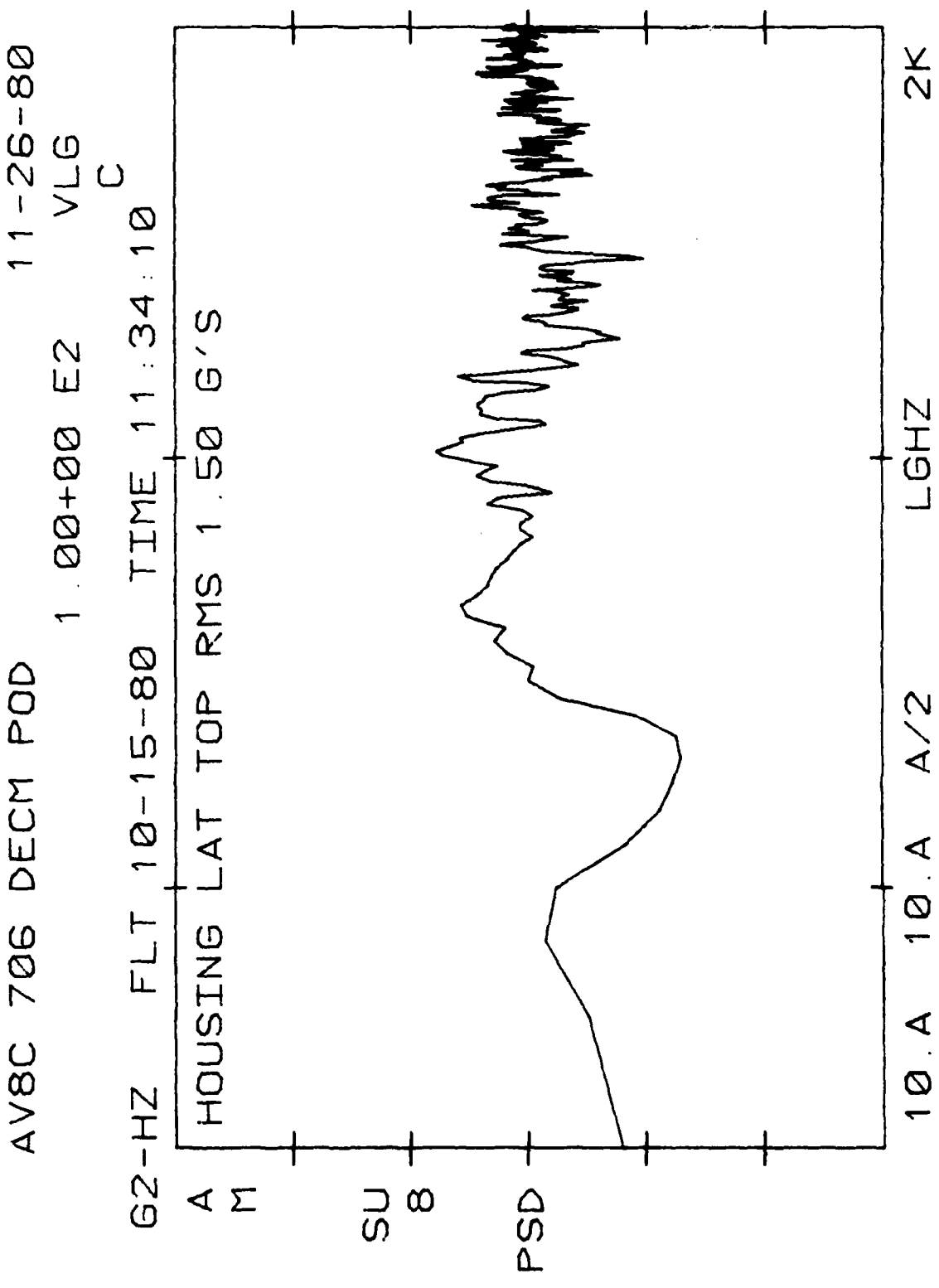

Figure 13
Cruise Flight, 500 ft Altitude and 448 KIAS, PSD

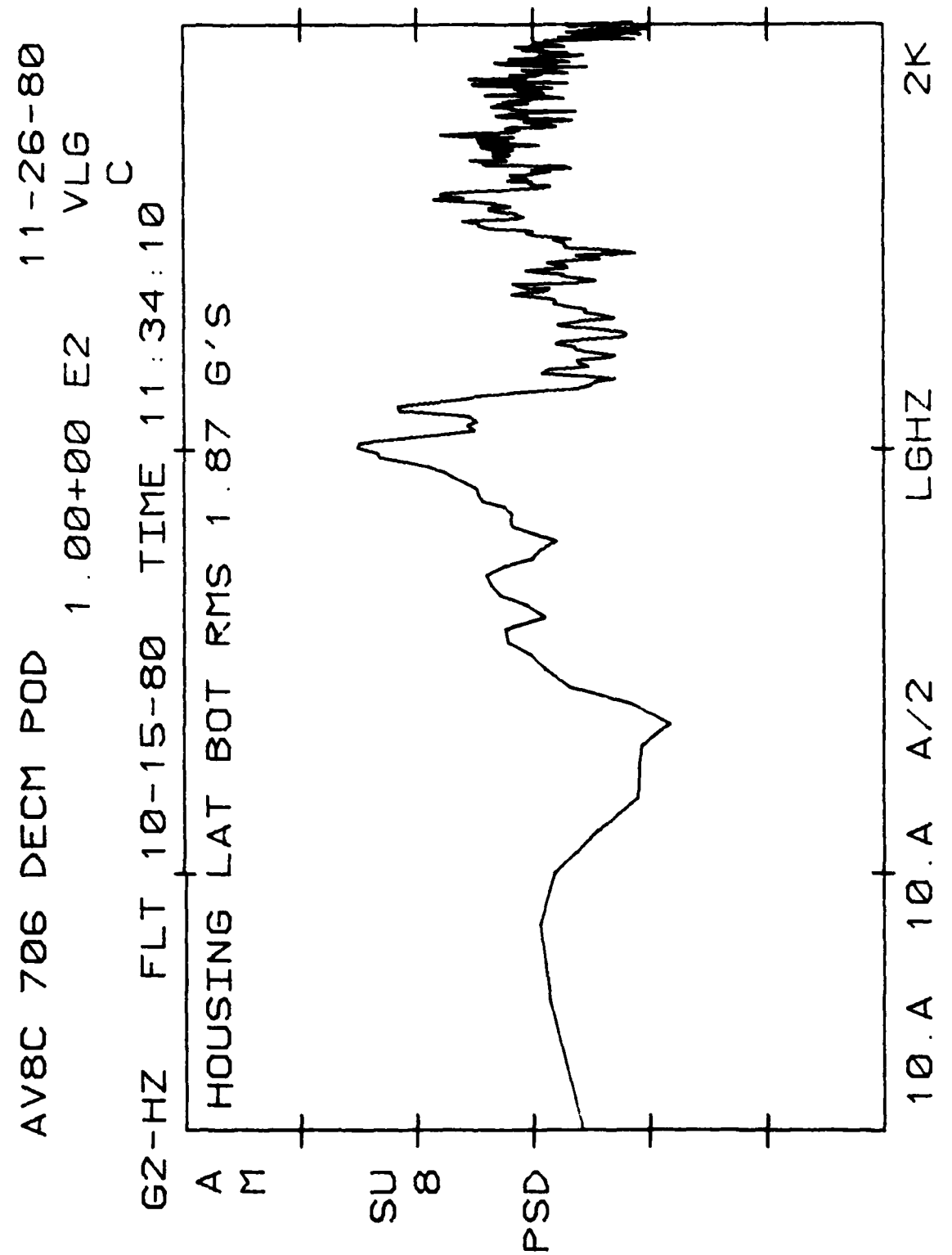

Figure 13 (Cont'd)

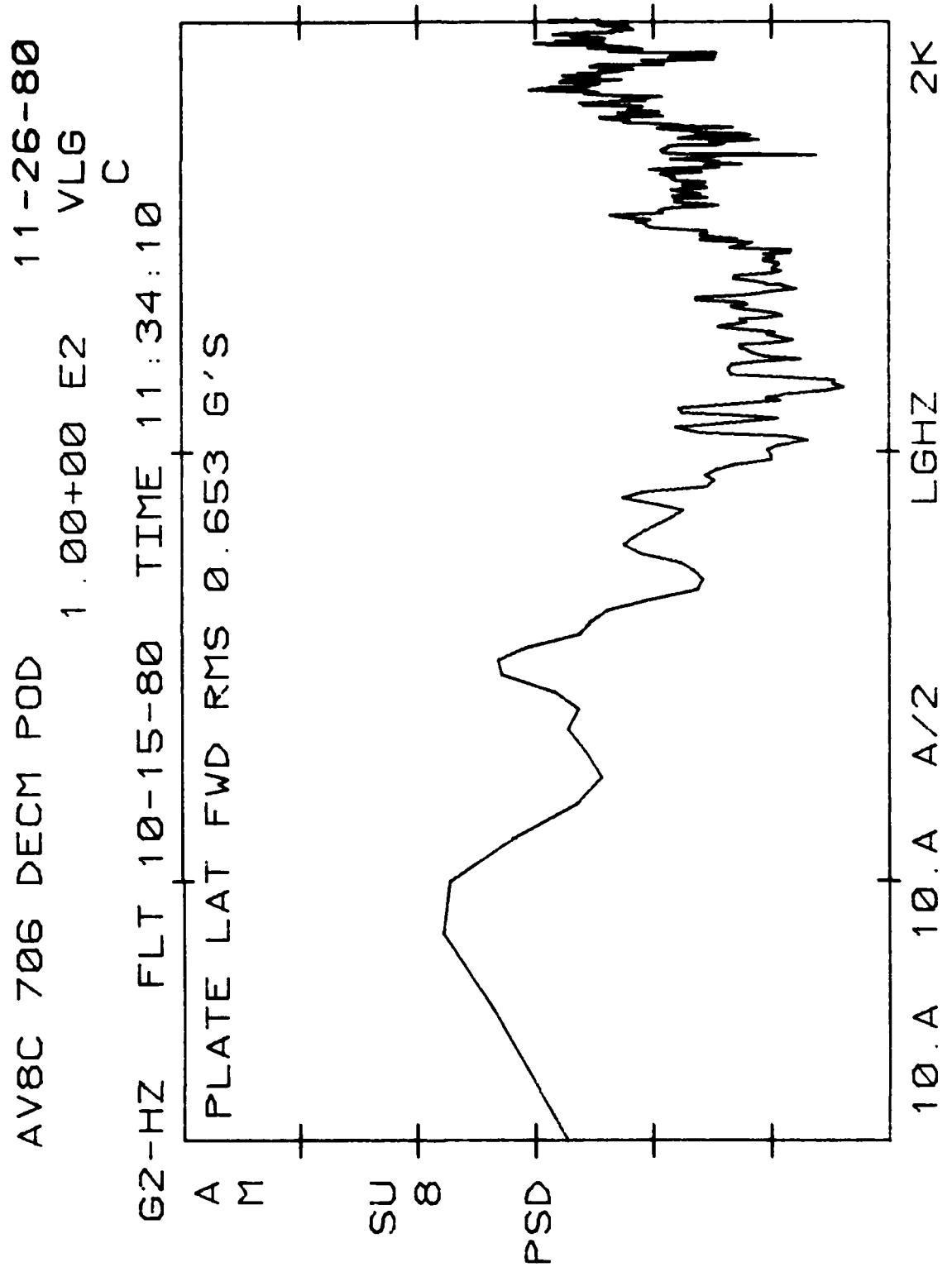

Figure 13 (Cont'd)

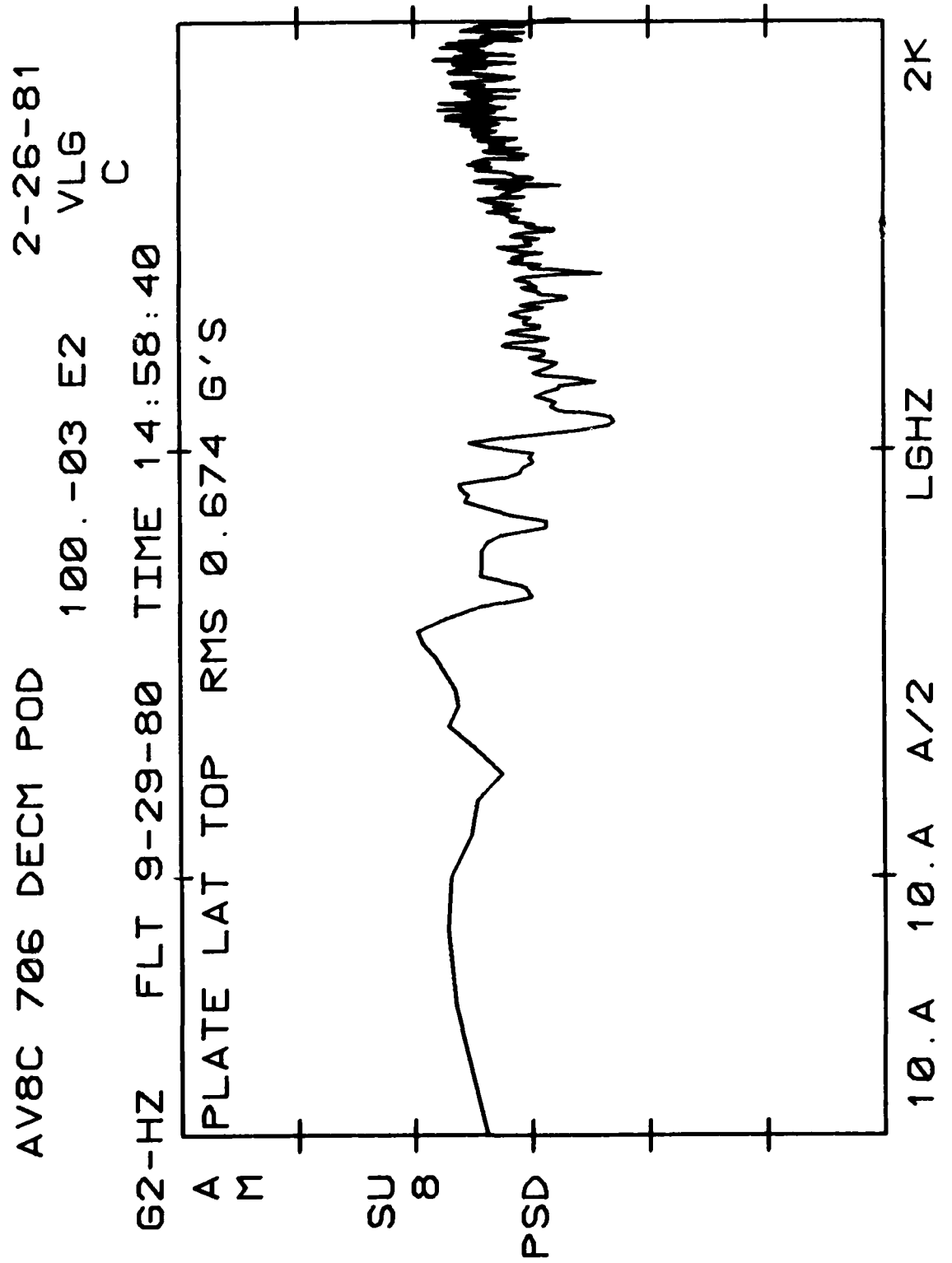

Figure 13 (Cont'd)

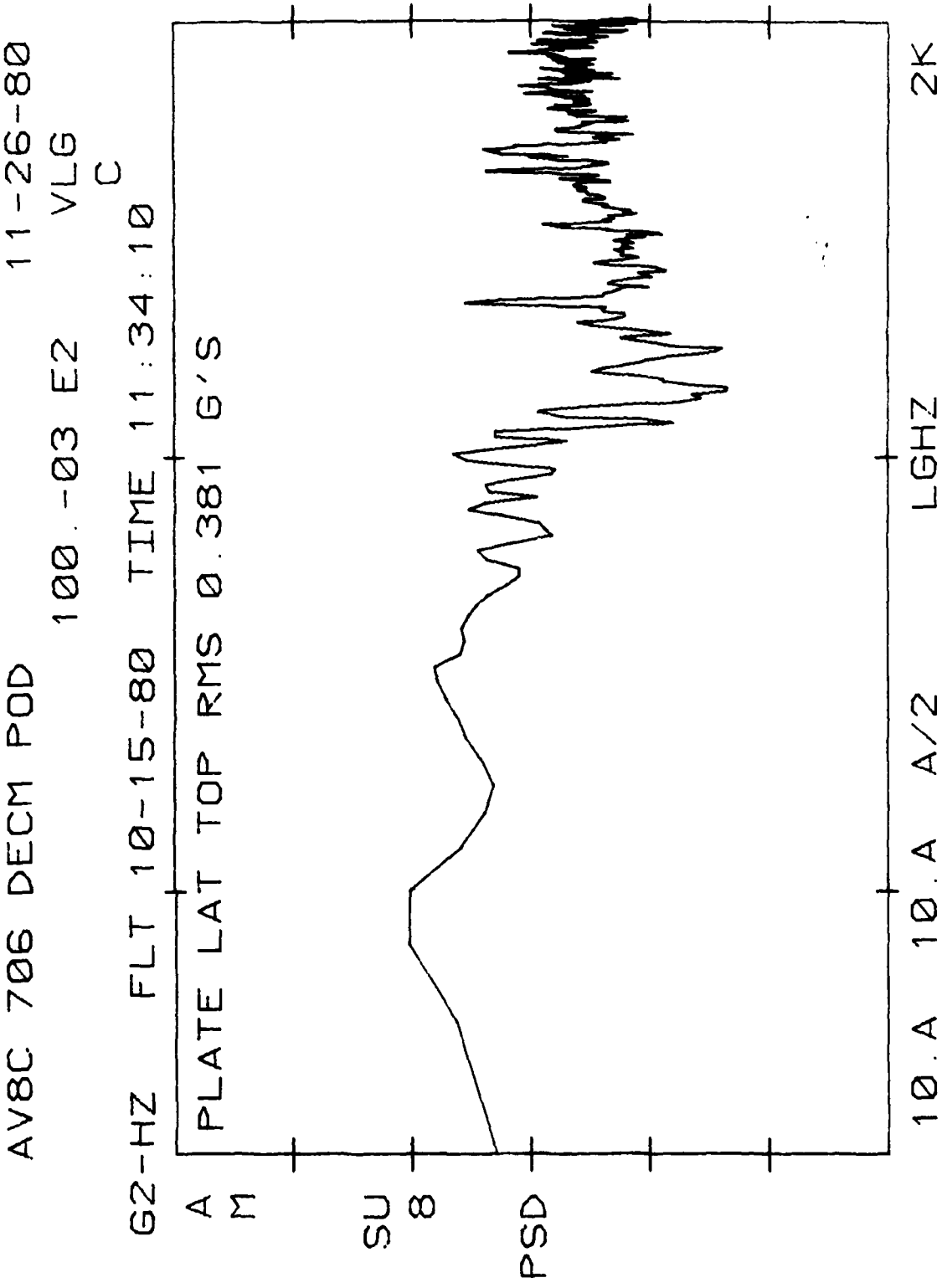

Figure 13 (Cont'd)

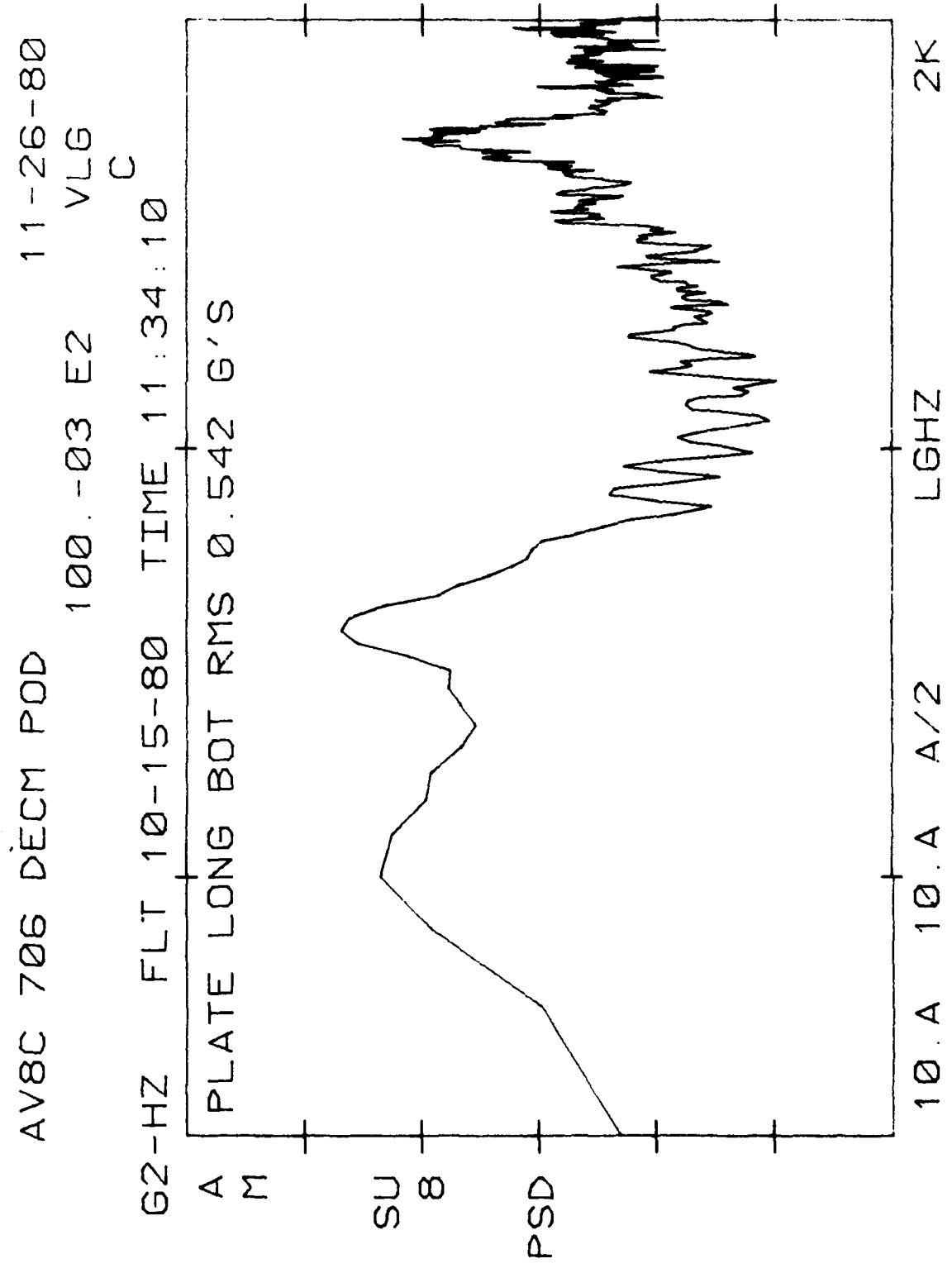

Figure 13 (Cont'd)

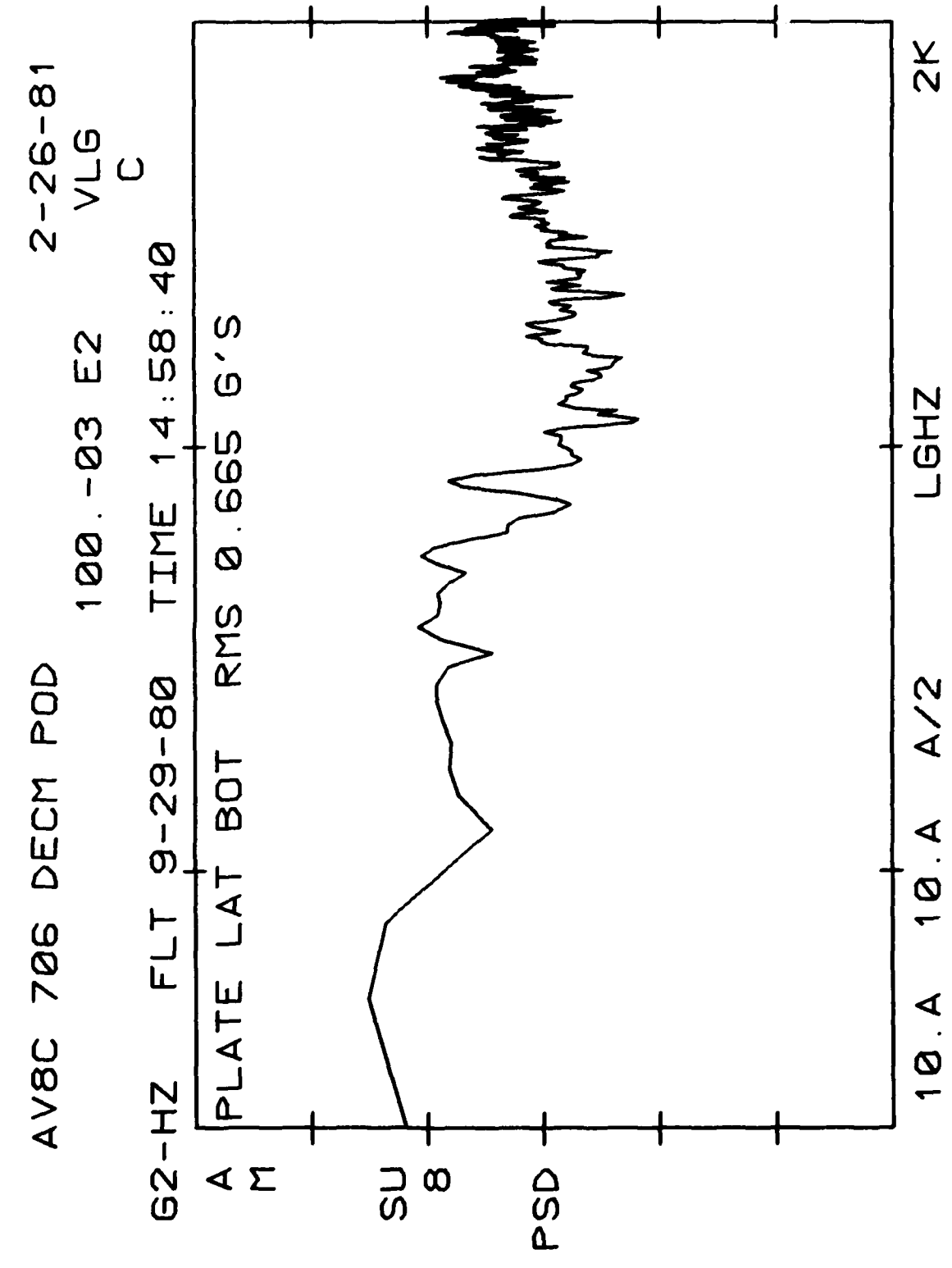

Figure 13 (Cont'd)

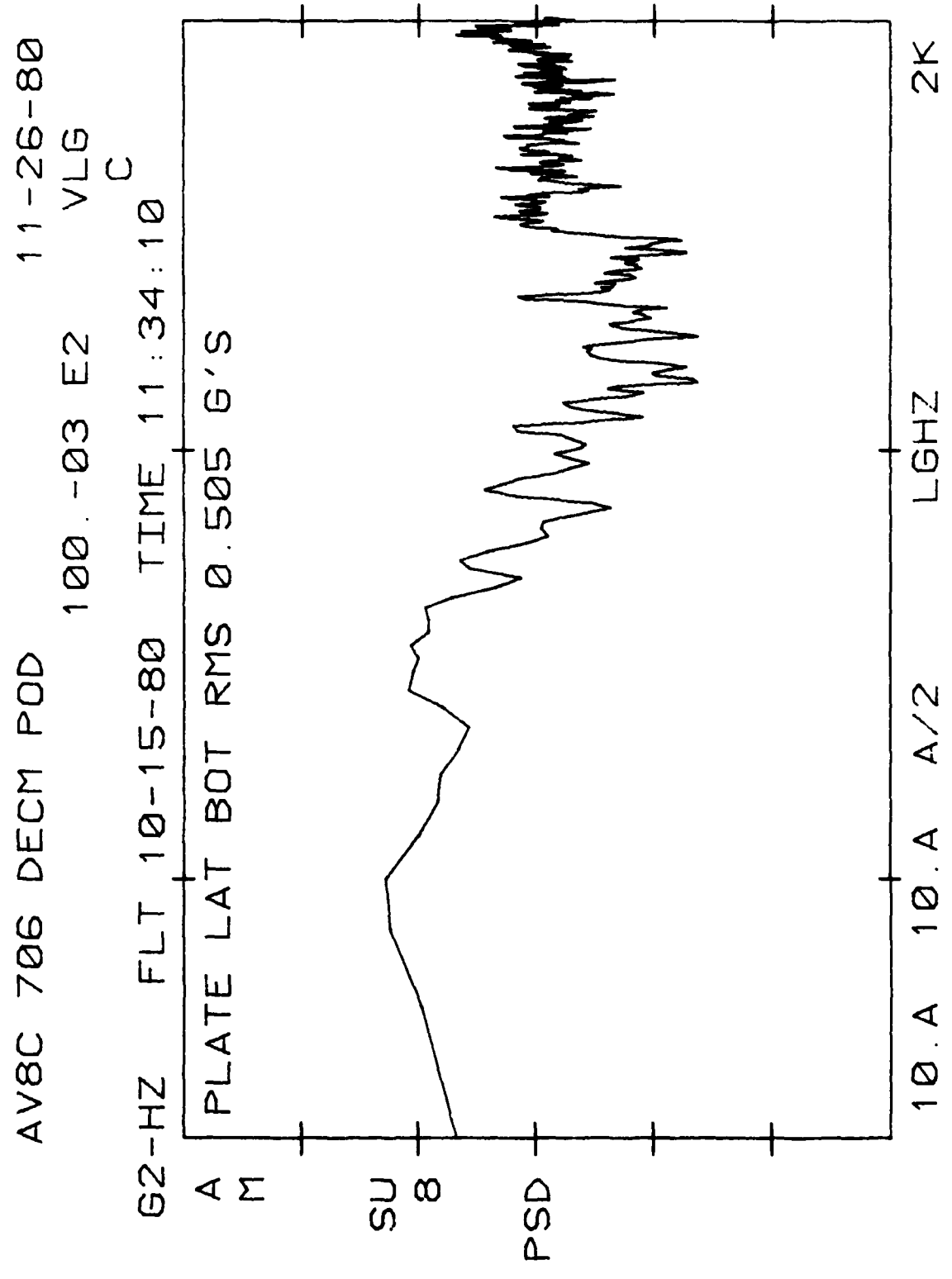

Figure 13 (Cont'd)

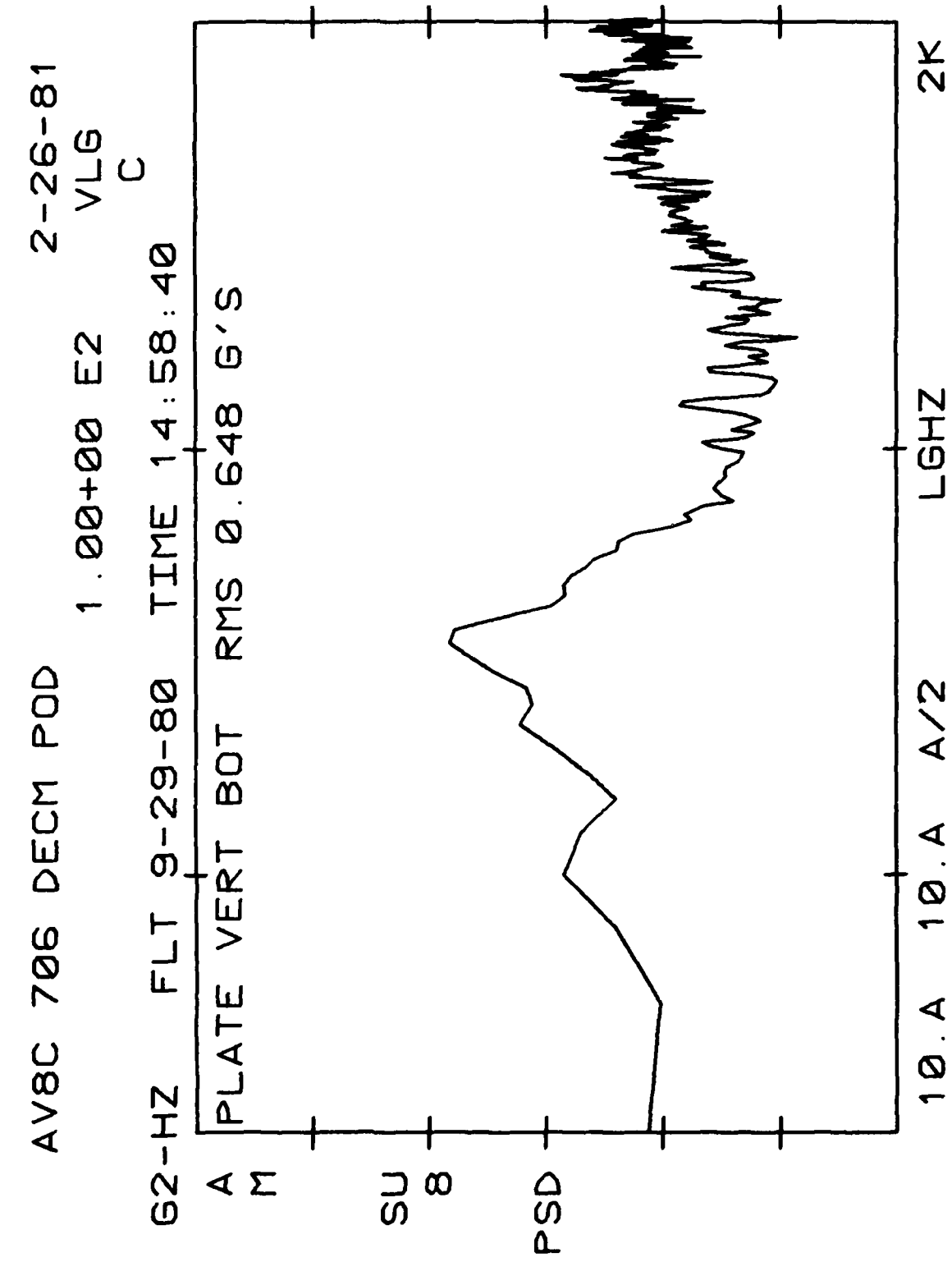

Figure 13 (Cont'd)

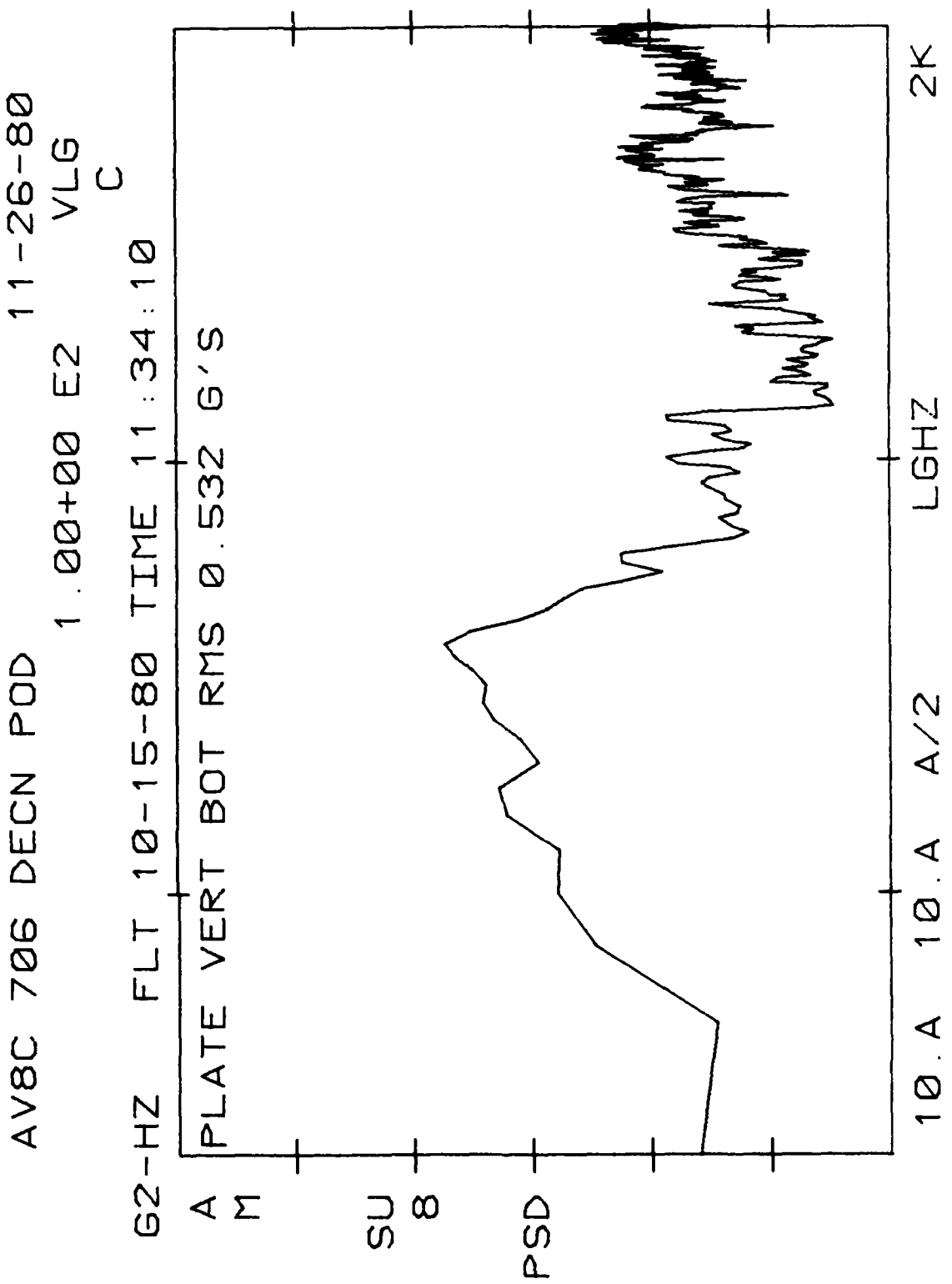

Figure 13 (Cont'd)

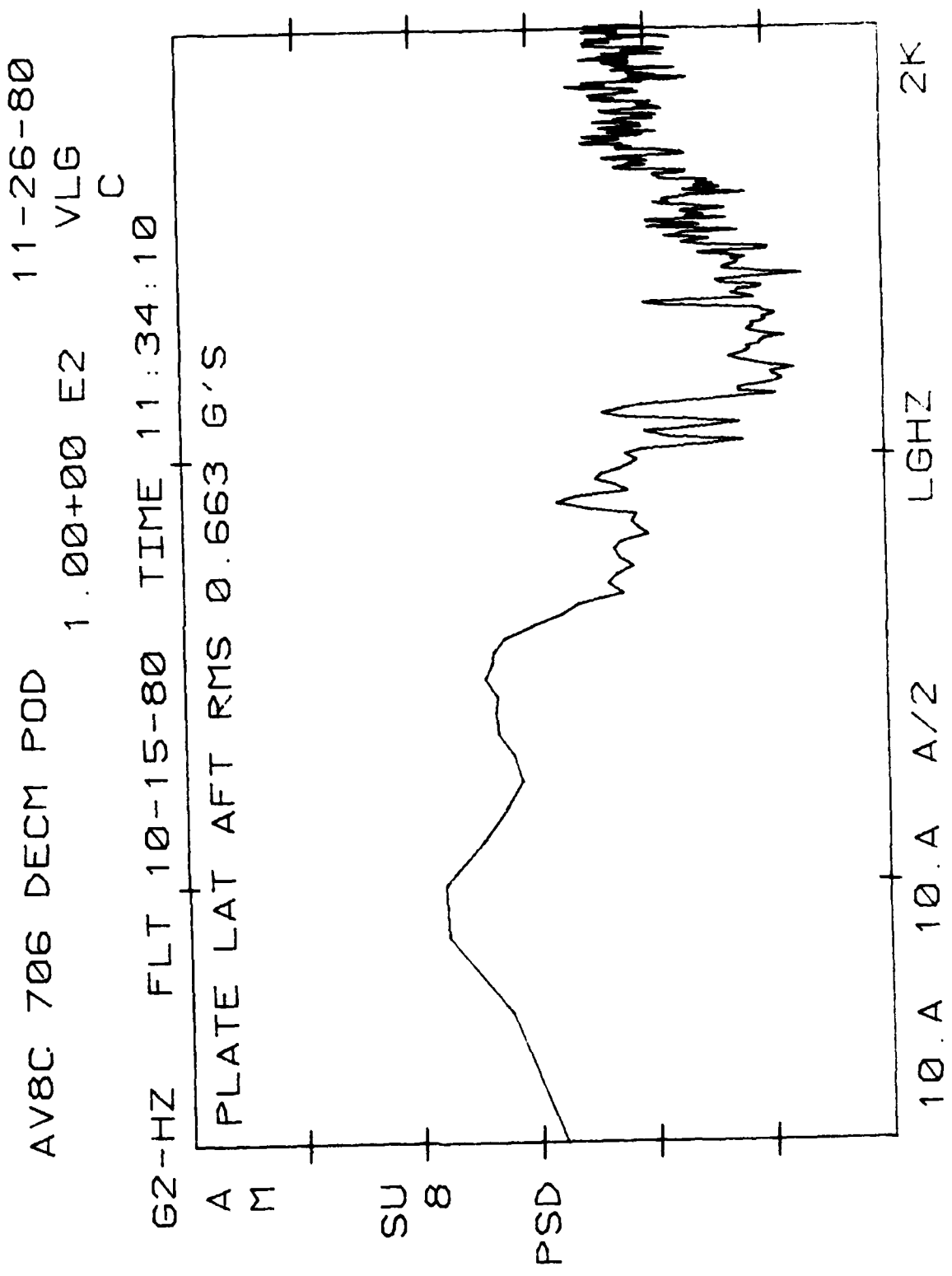

Figure 13 (Cont'd)

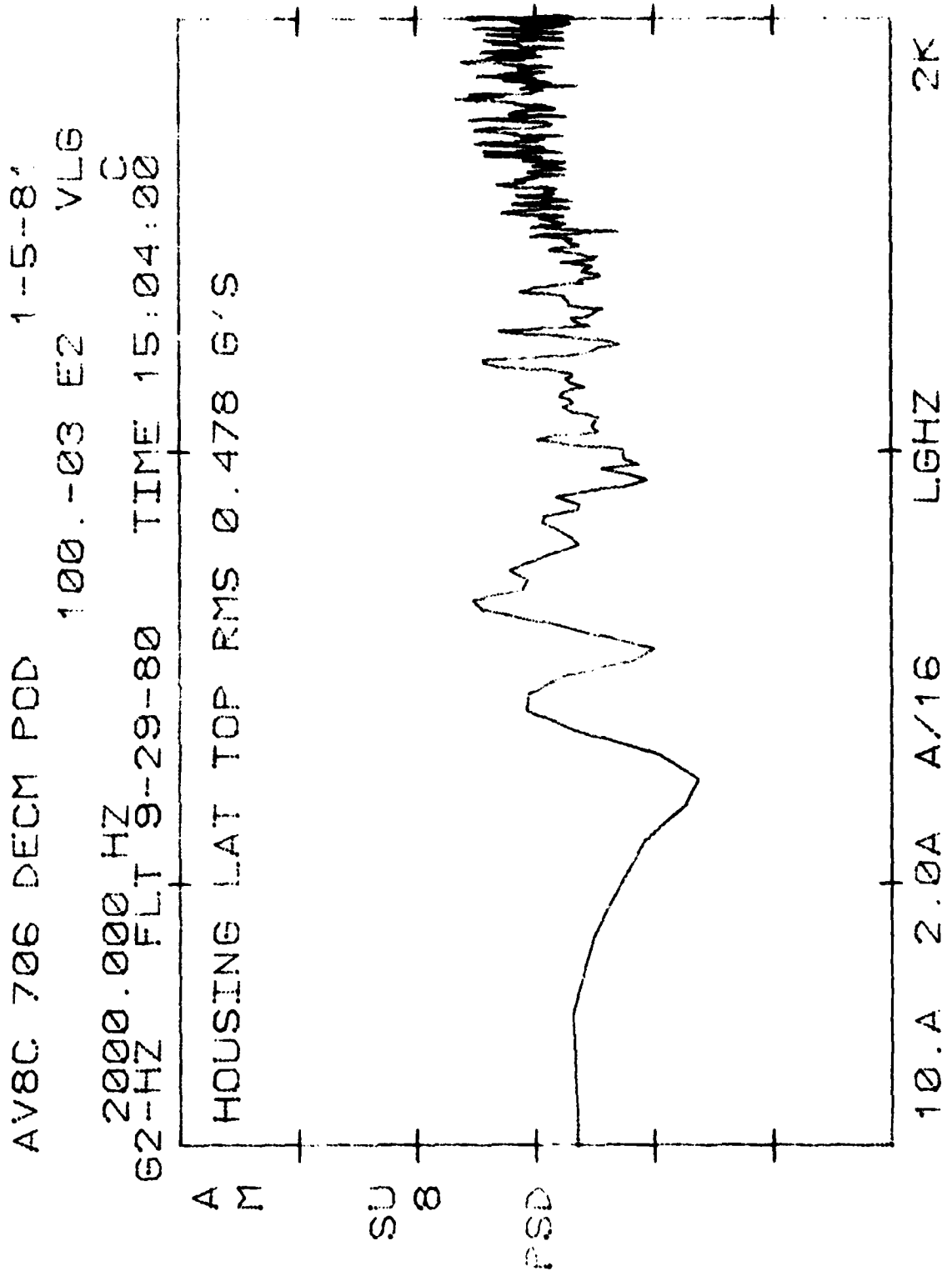

Figure 14
Cruise Flight, 20,000 ft Altitude and 155 KIAS, PSD

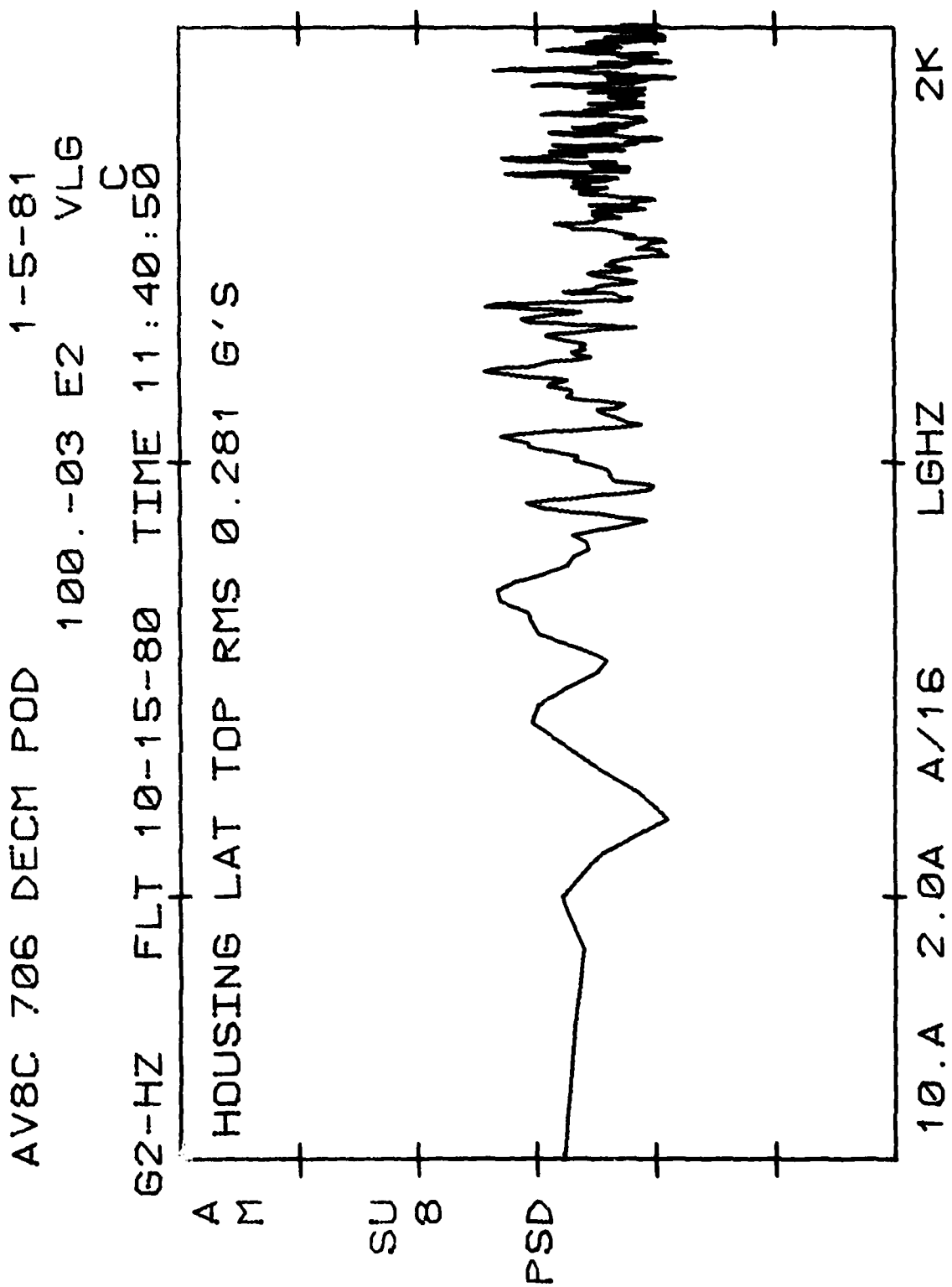

Figure 14 (Cont'd)

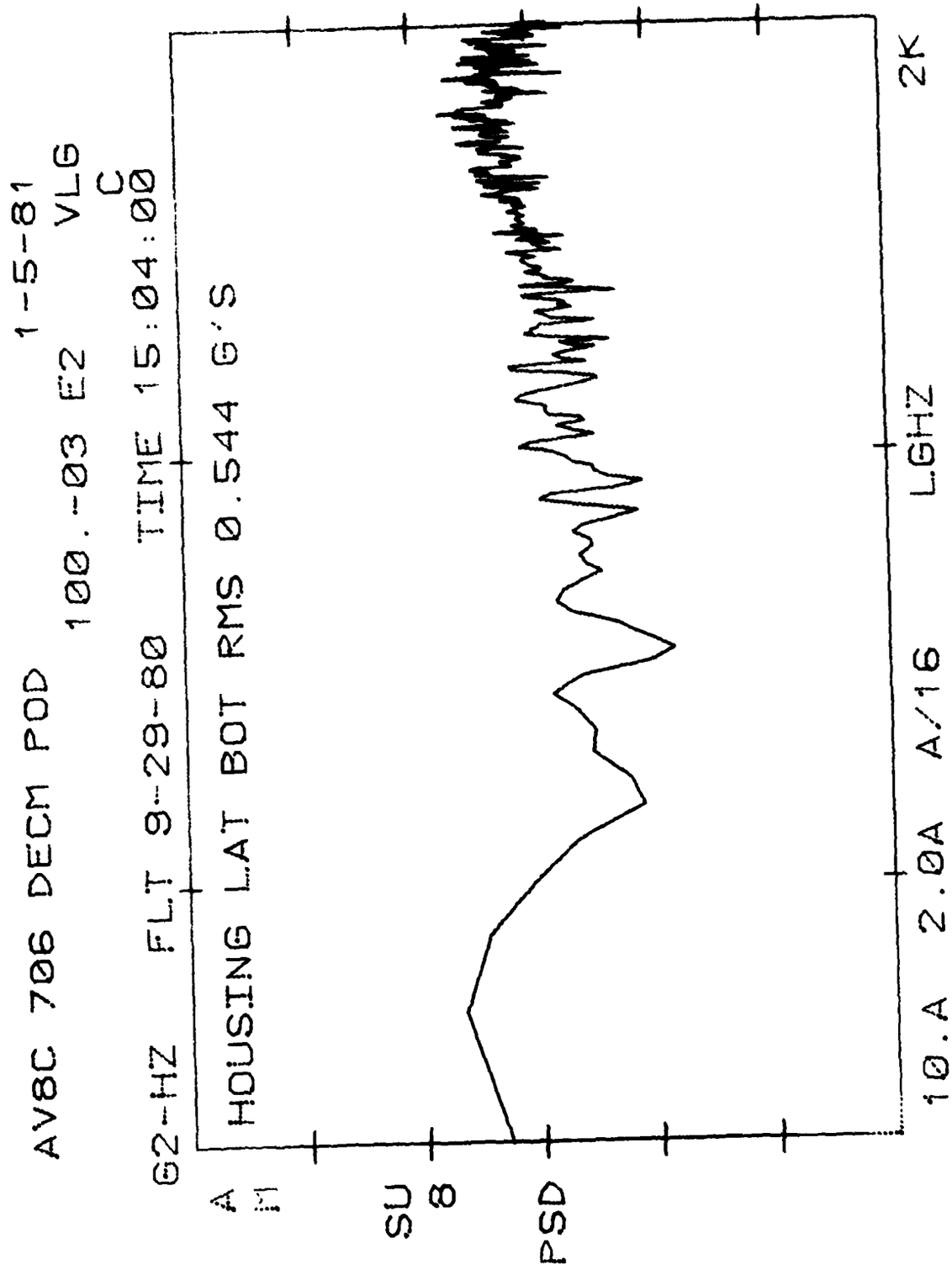

Figure 14 (Cont'd)

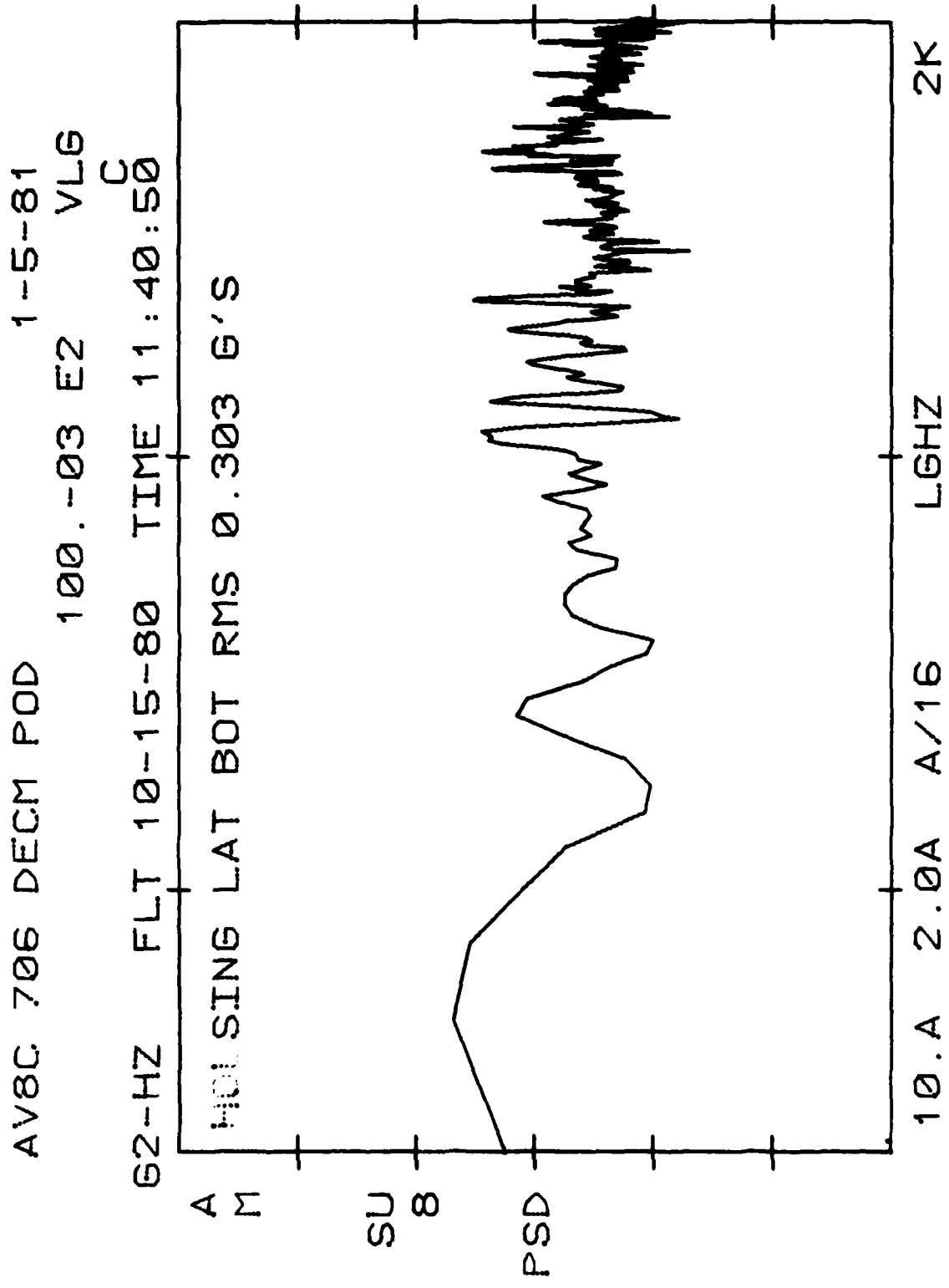

Figure 14 (Cont'd)

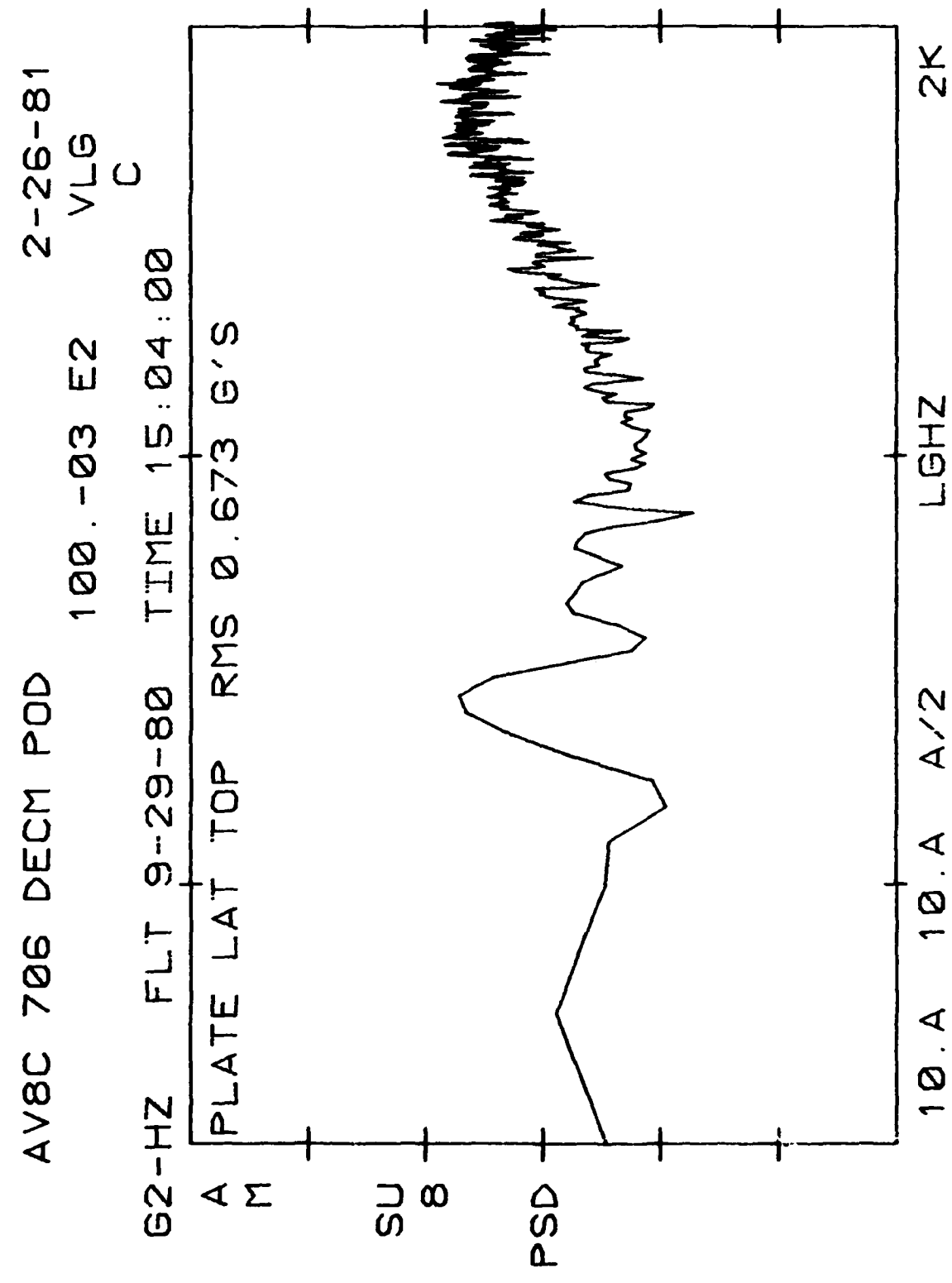

Figure 14 (Cont'd)

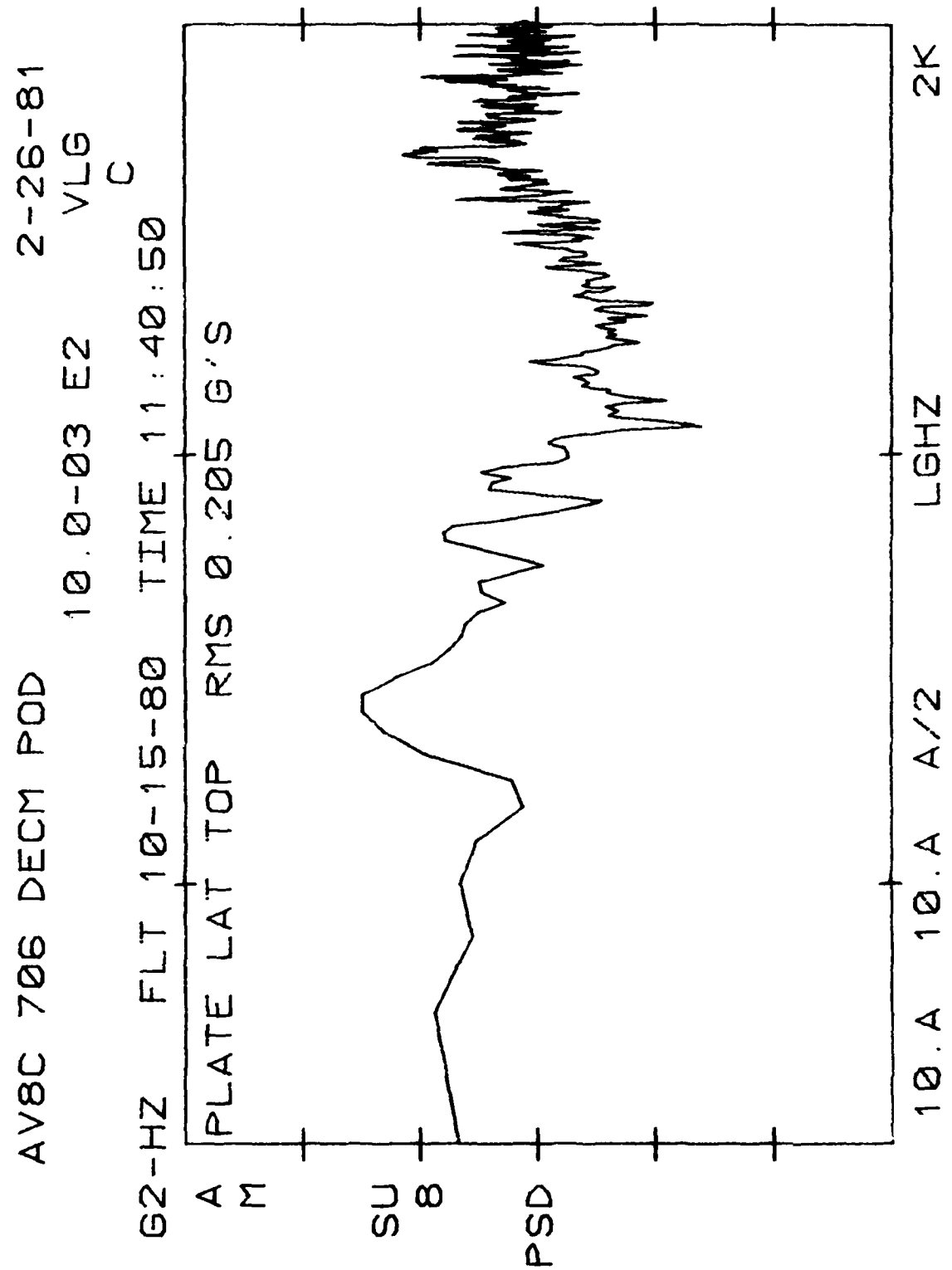

Figure 14 (Cont'd)

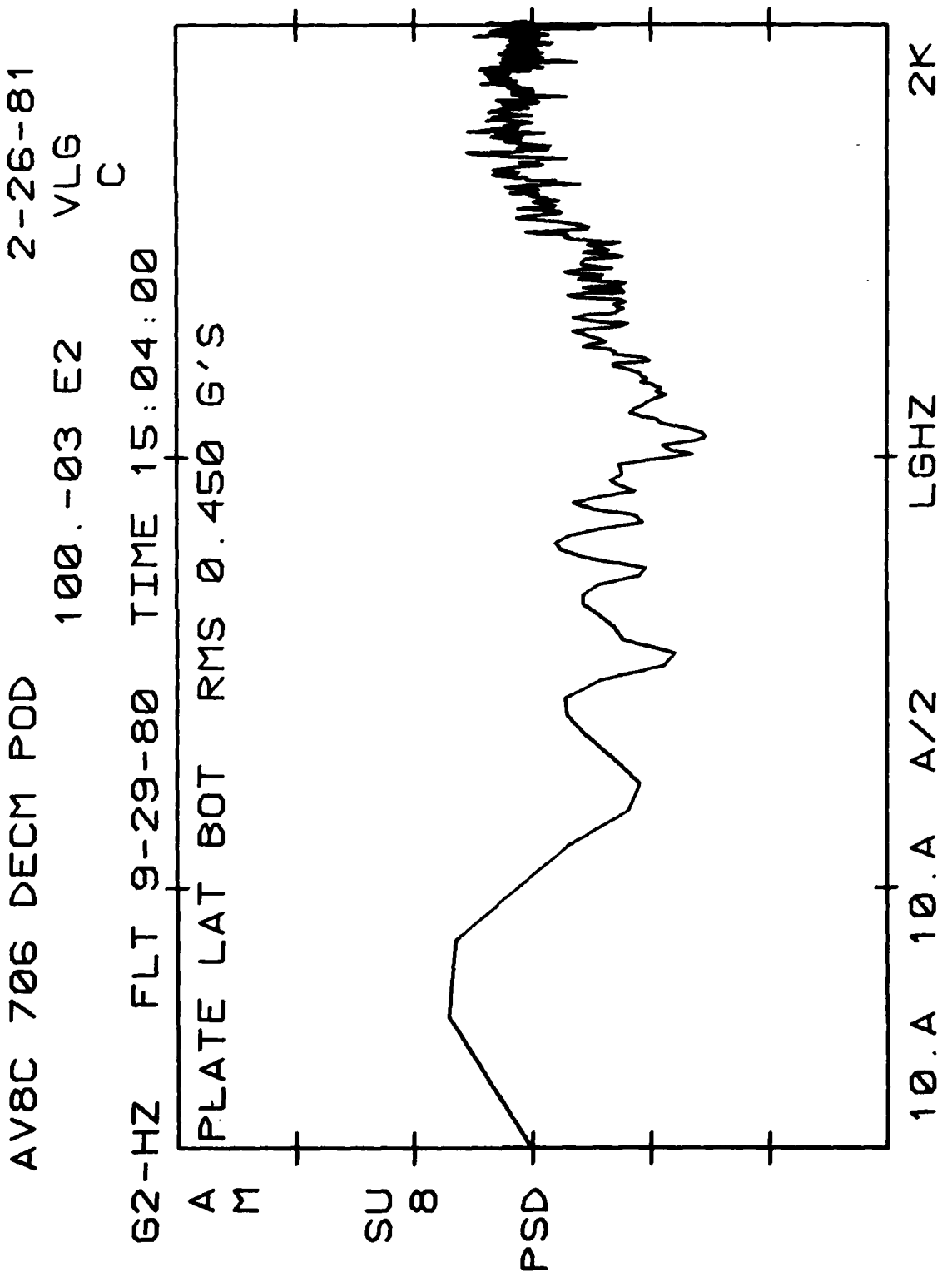

Figure 14 (Cont'd)

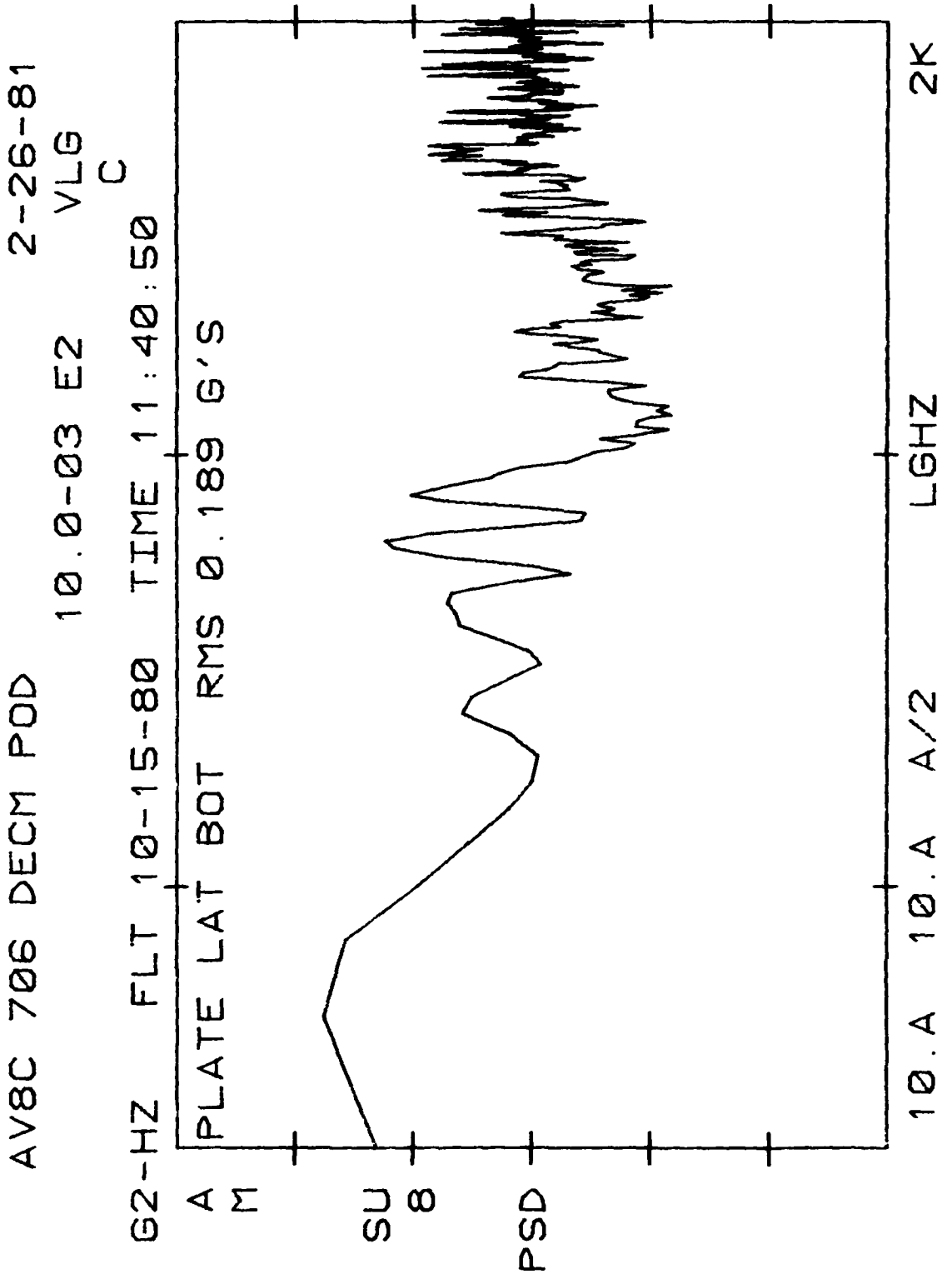

Figure 14 (Cont'd)

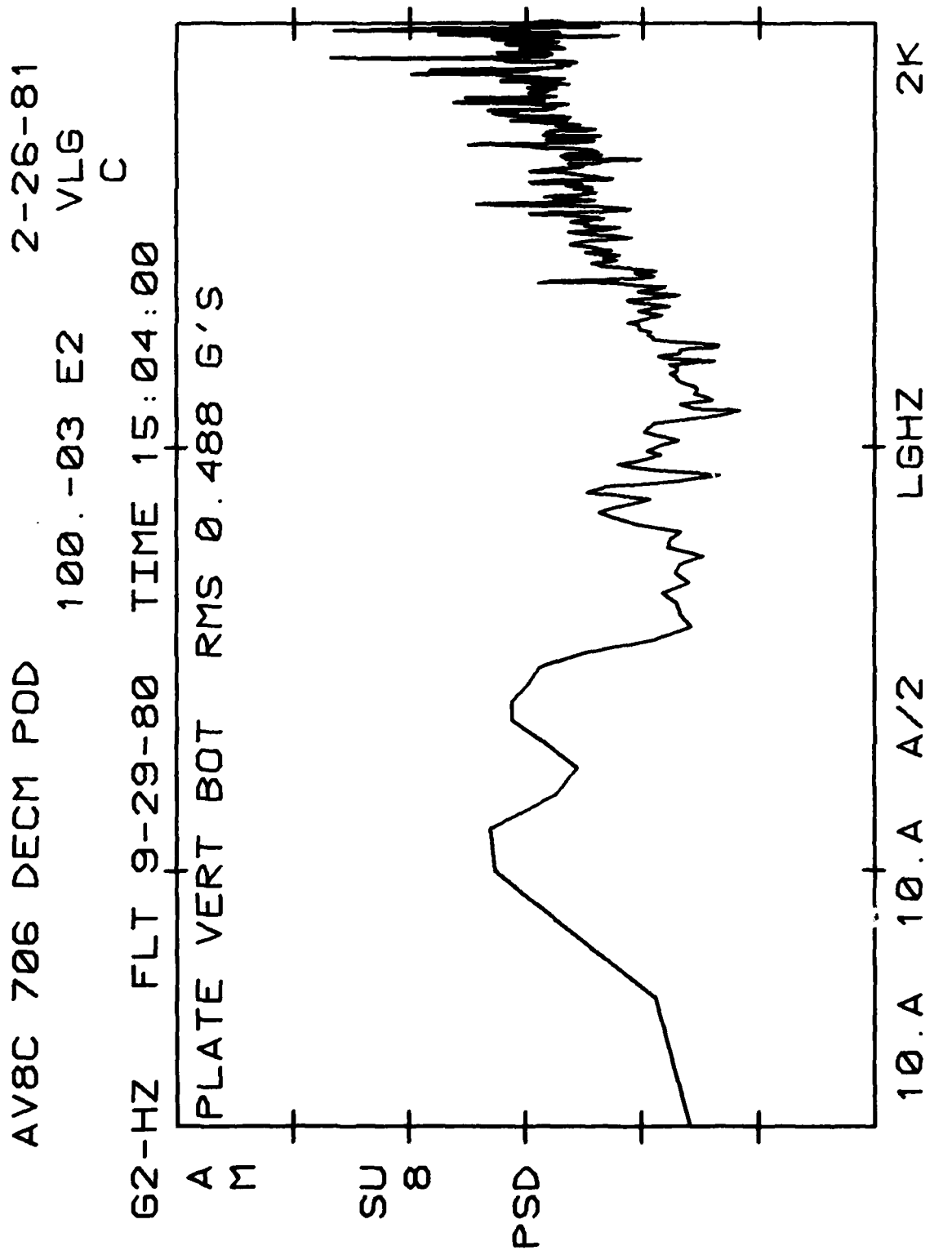

Figure 14 (Cont'd)

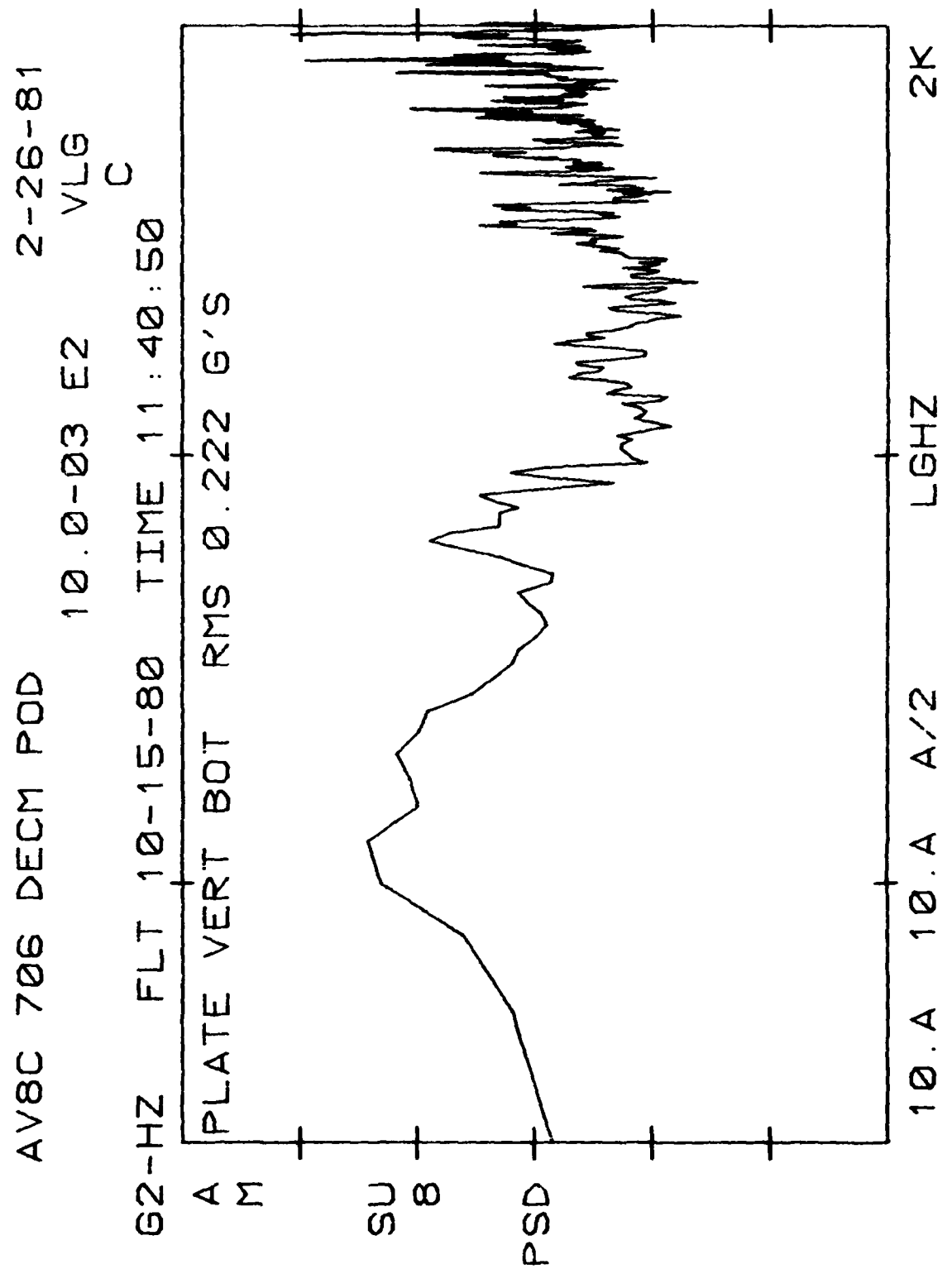

Figure 14 (Cont'd)

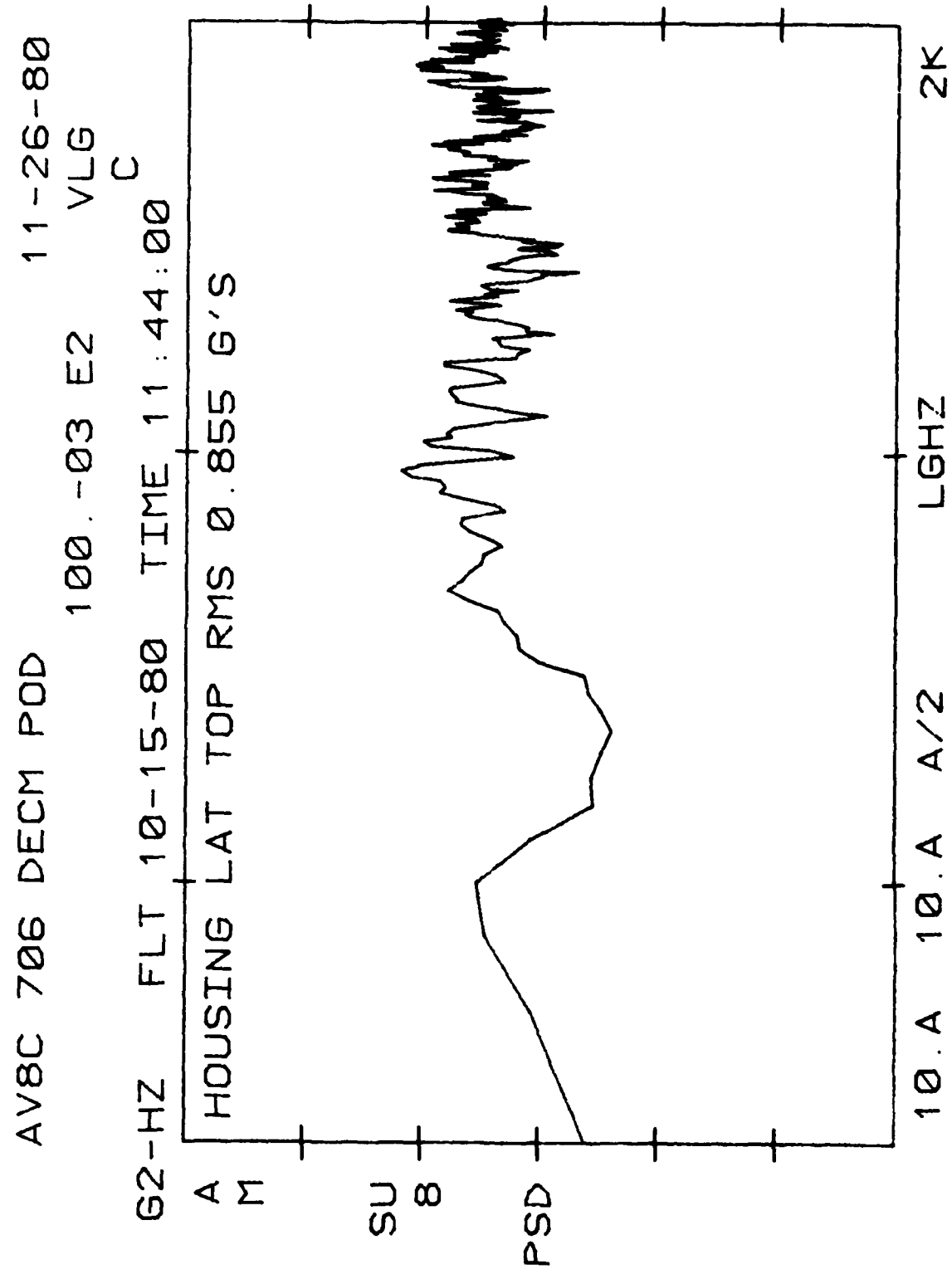

Figure 15
Cruise Flight, 20,000 ft Altitude and 340 KIAS, PSD

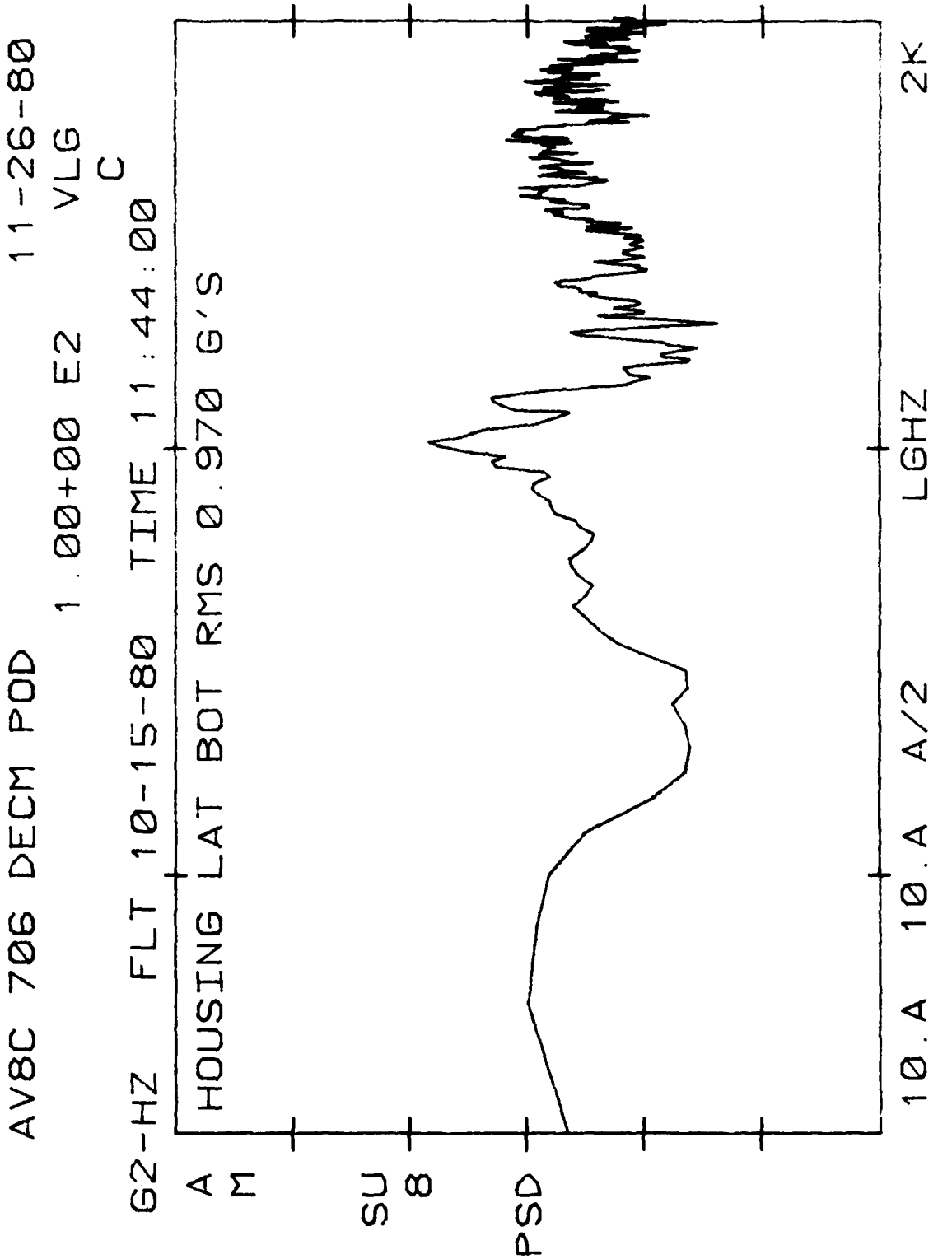

Figure 15 (Cont'd)

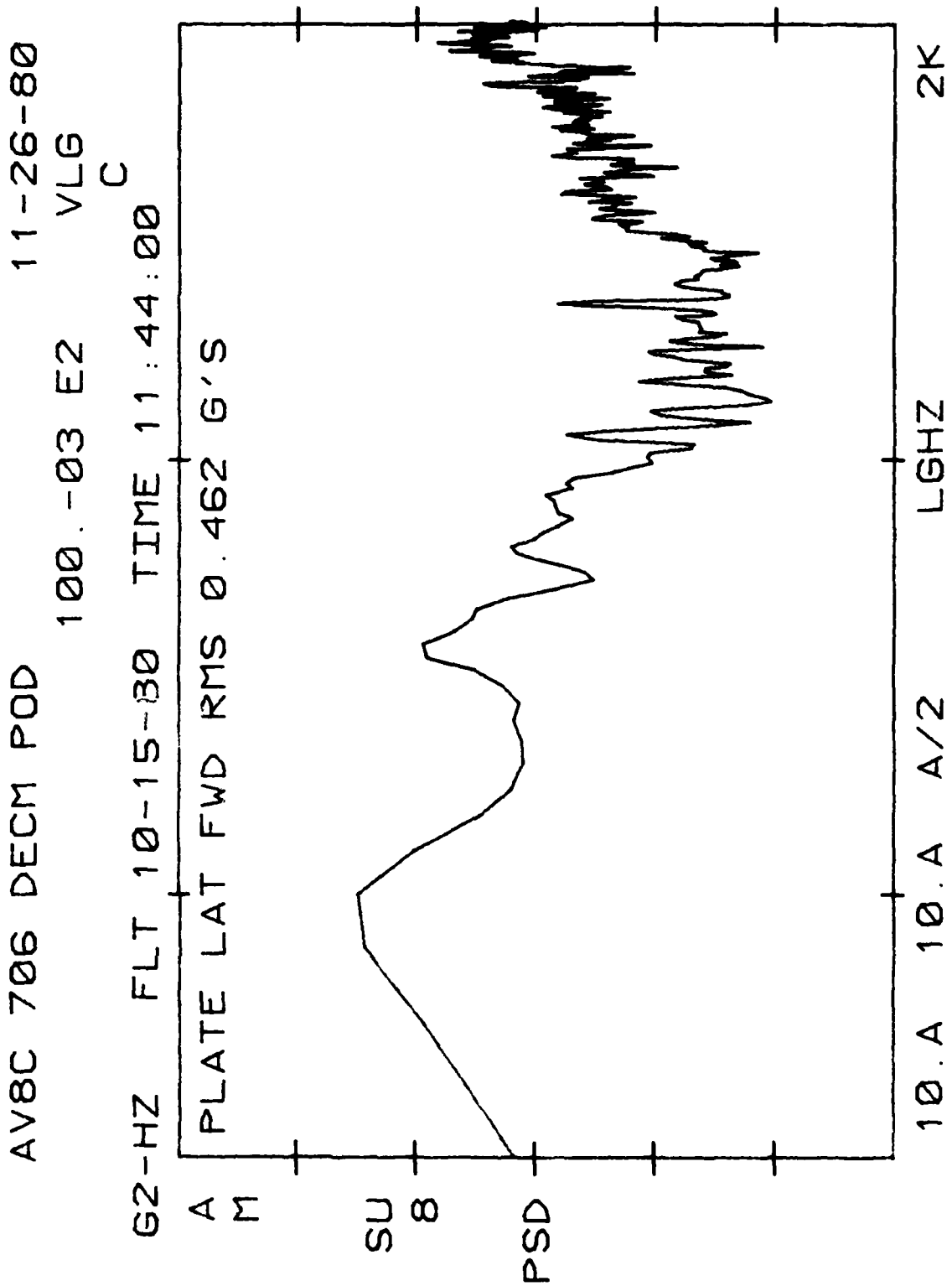

Figure 15 (Cont'd)

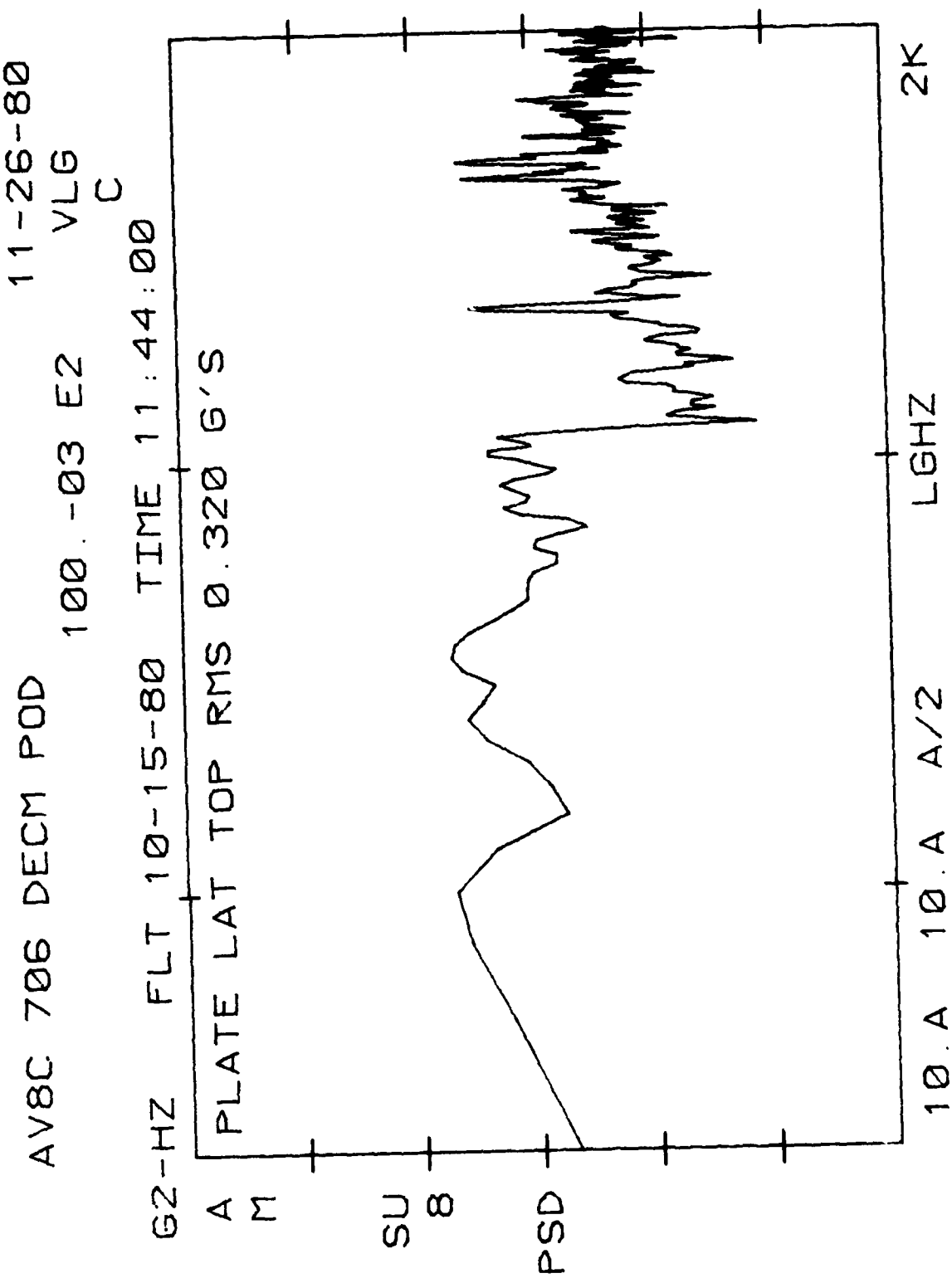

Figure 15 (Cont'd)

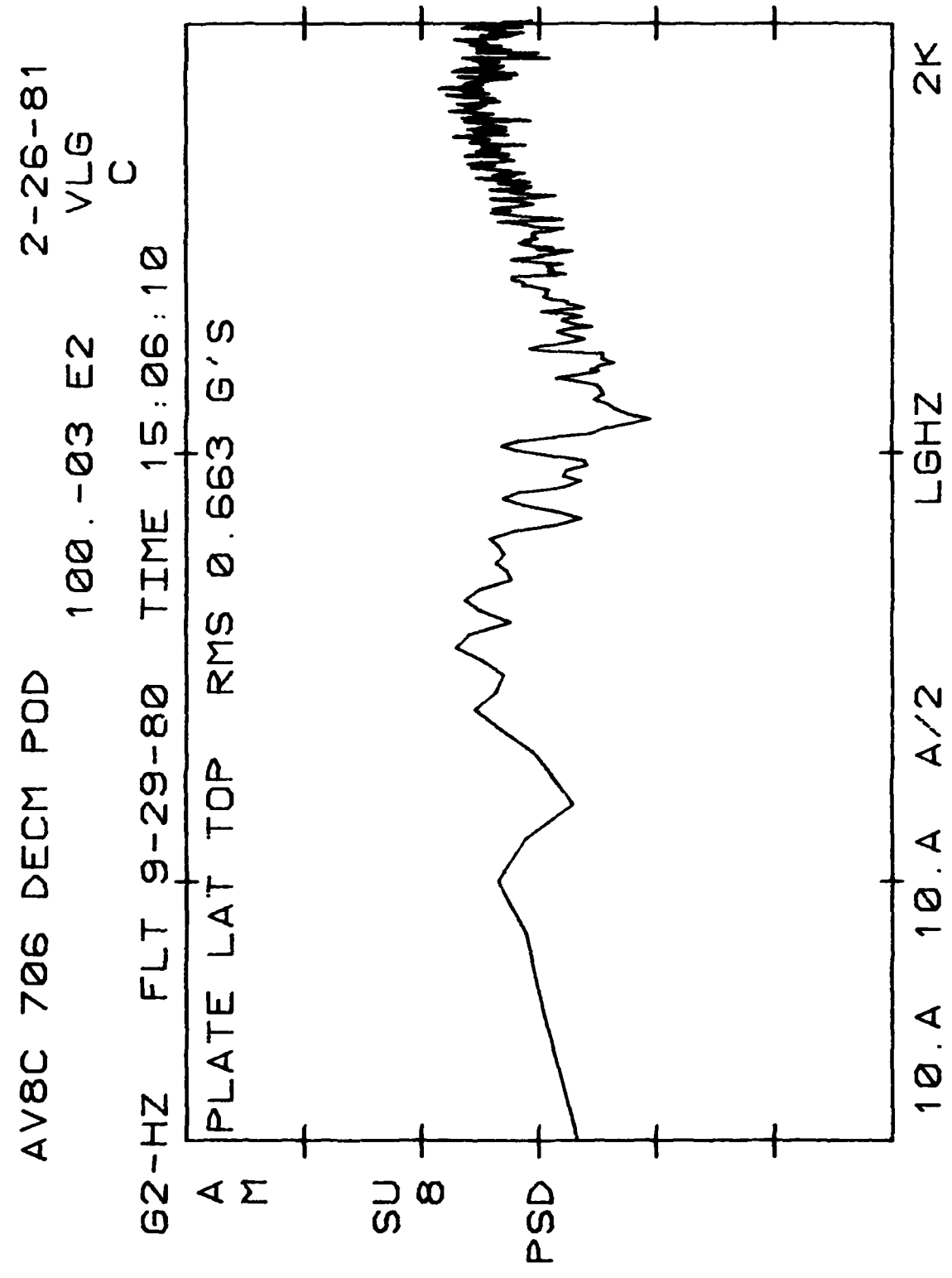

Figure 15 (Cont'd)

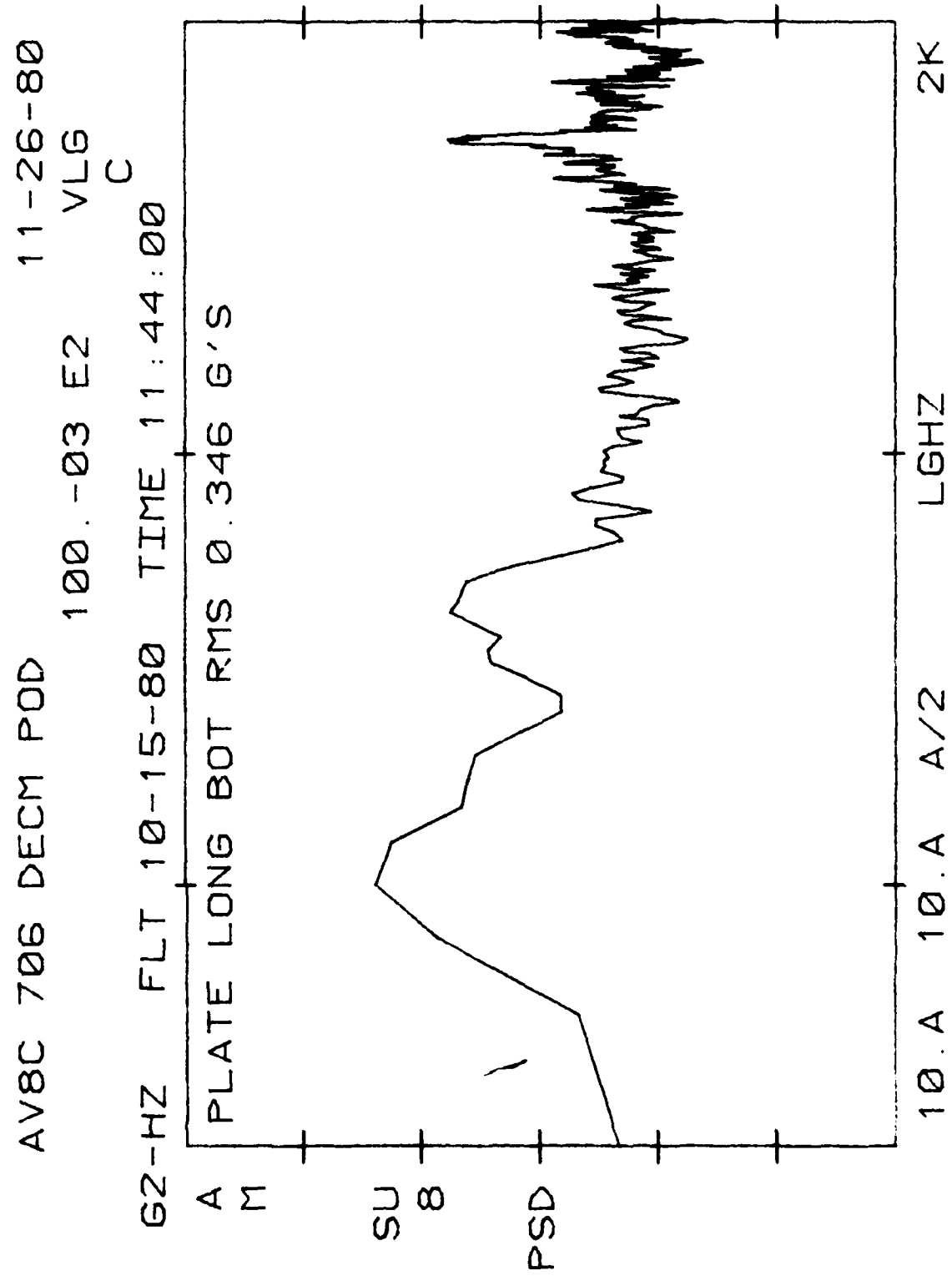

Figure 15 (Cont'd)

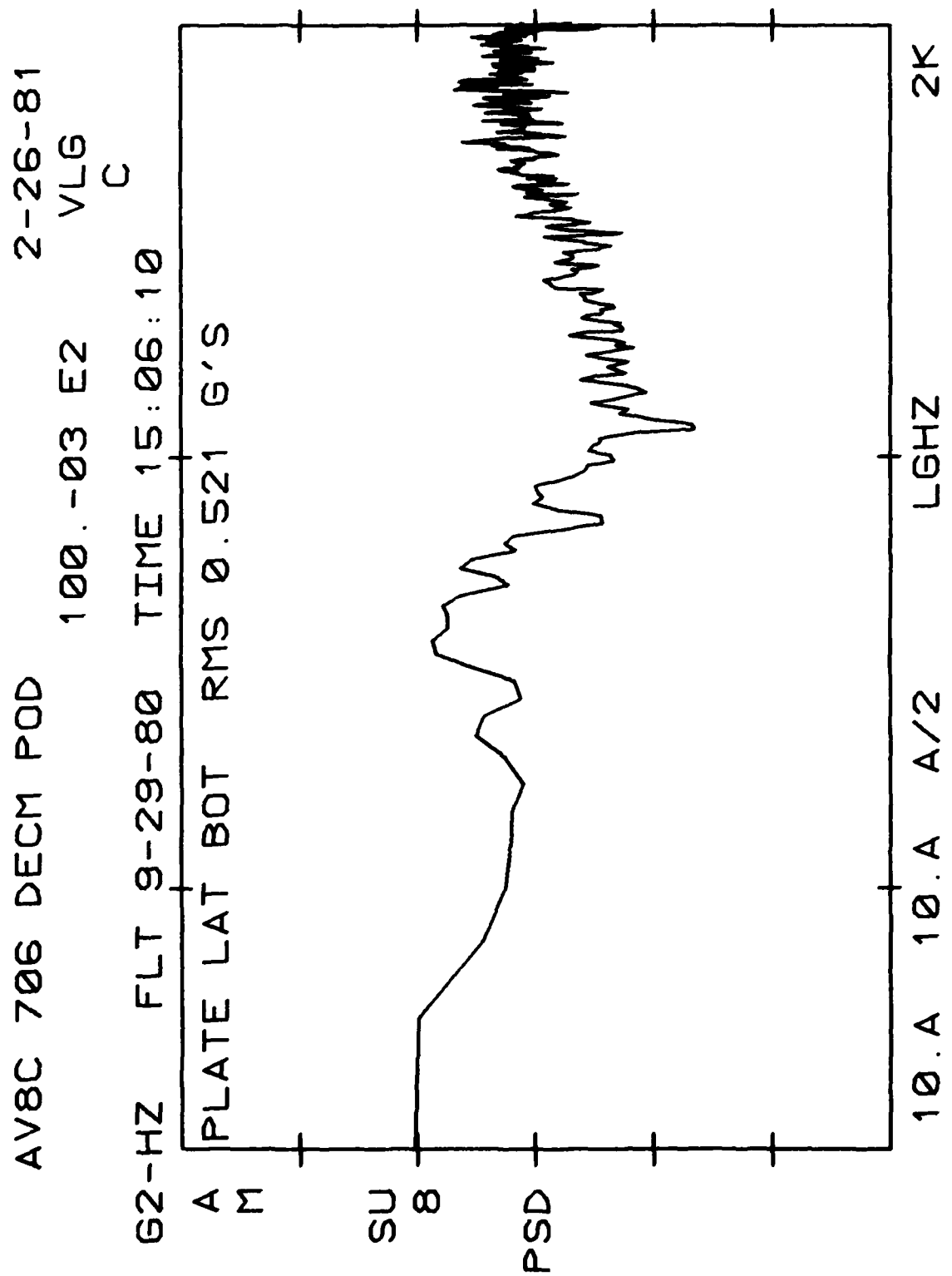

Figure 15 (Cont'd)

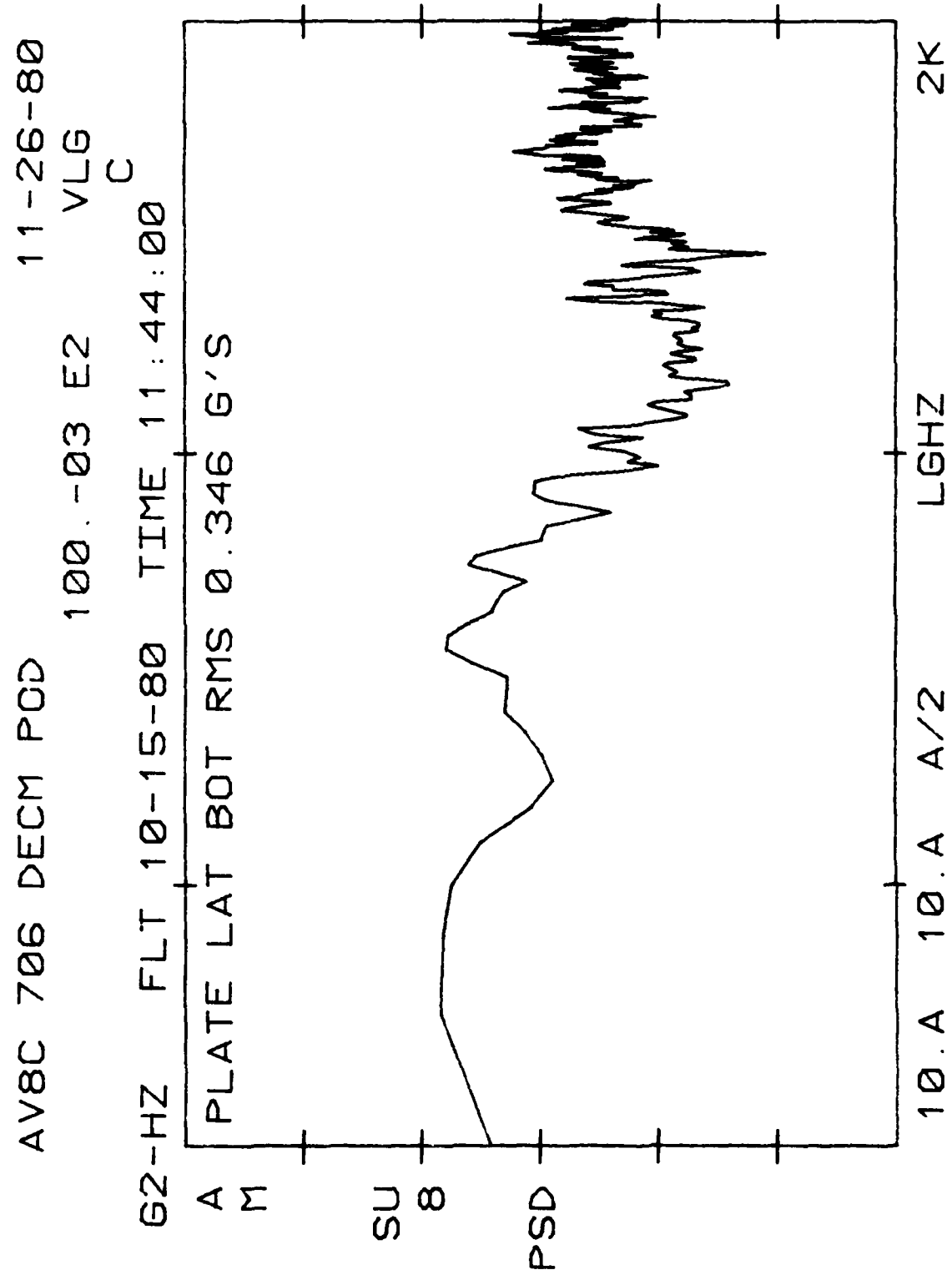

Figure 15 (Cont'd)

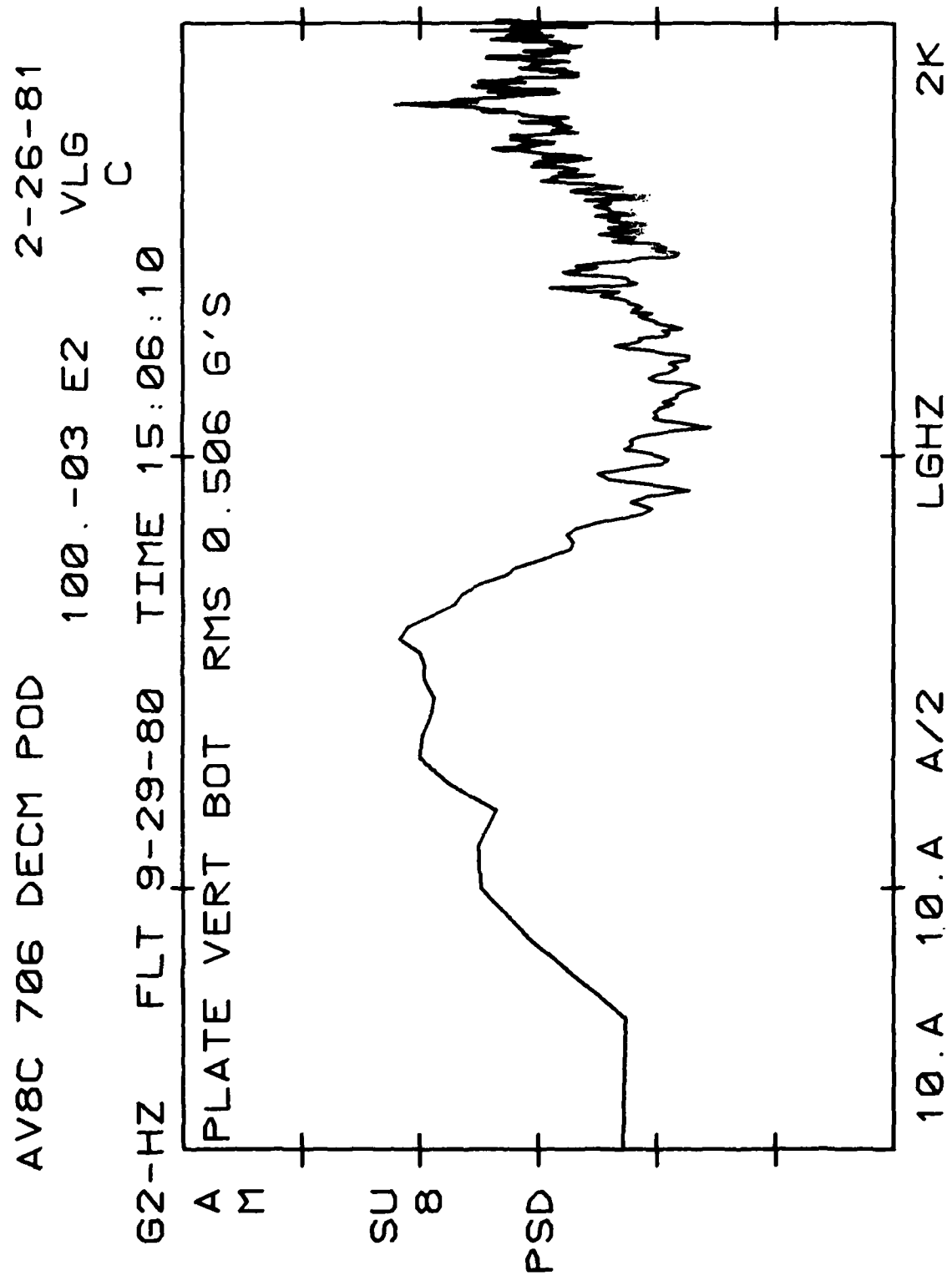

Figure 15 (Cont'd)

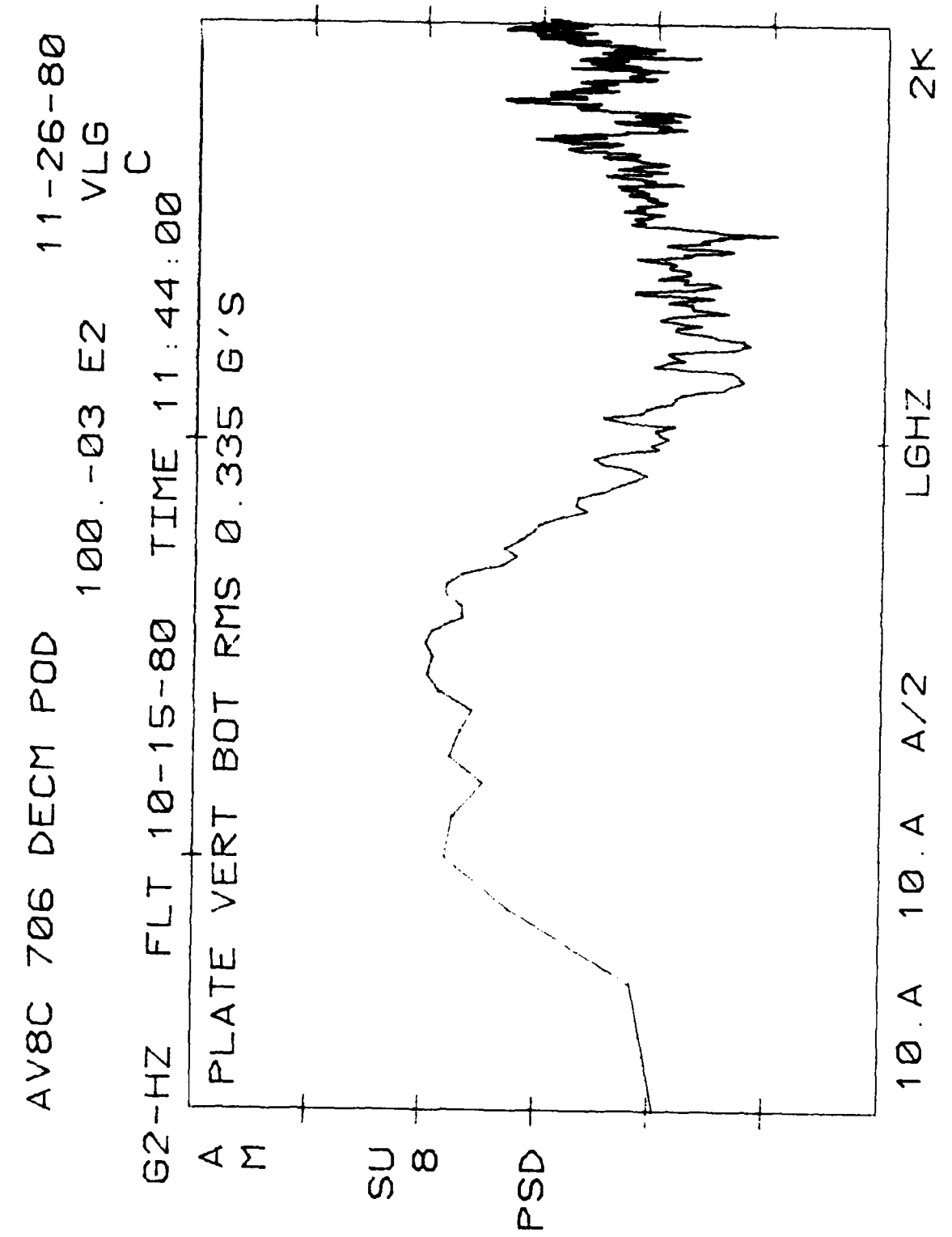

Figure 15 (Cont'd)

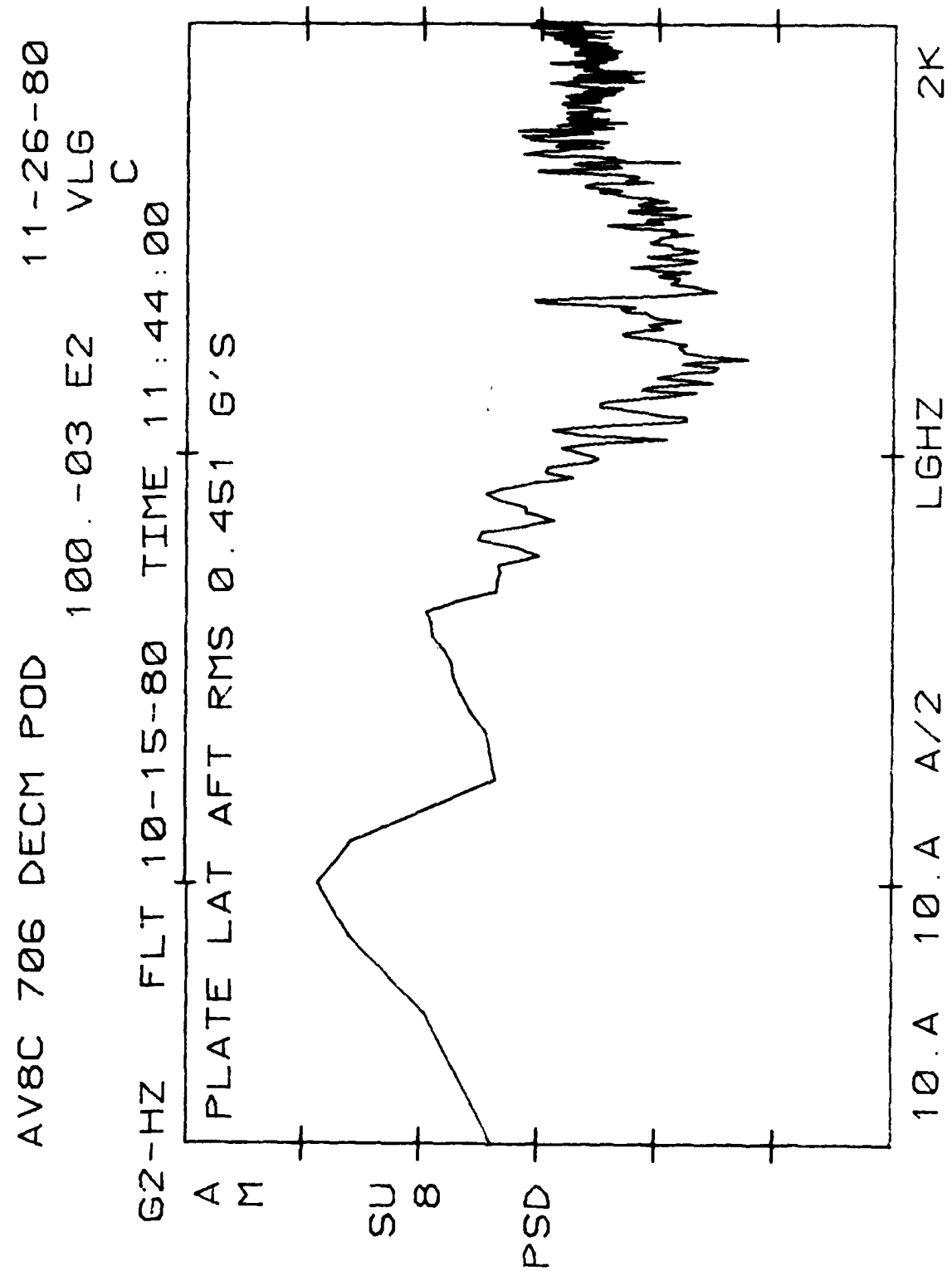

Figure 15 (Cont'd)

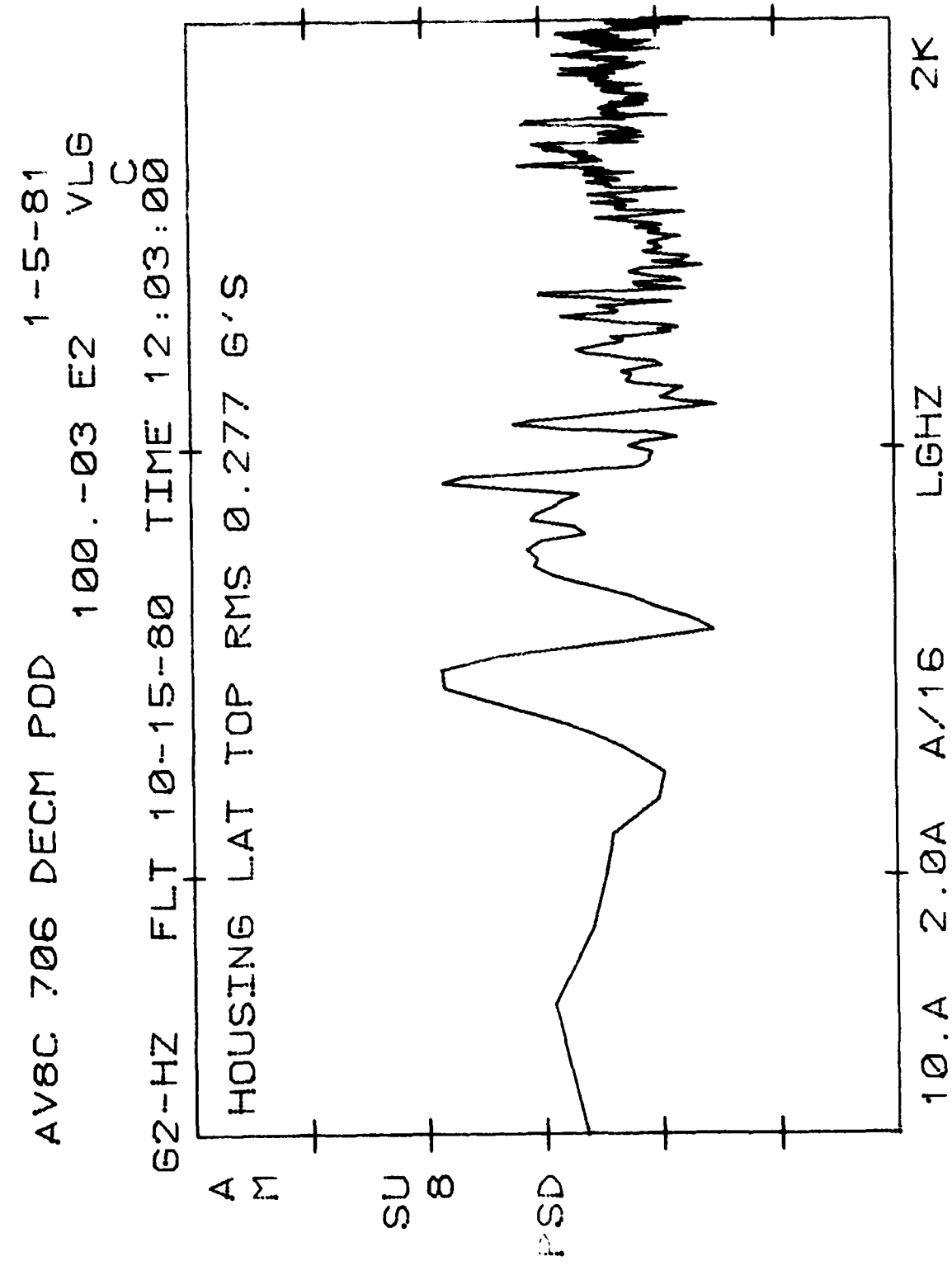

Figure 16
Cruise Flight, 40,000 ft Altitude and 190 KIAS, PSD

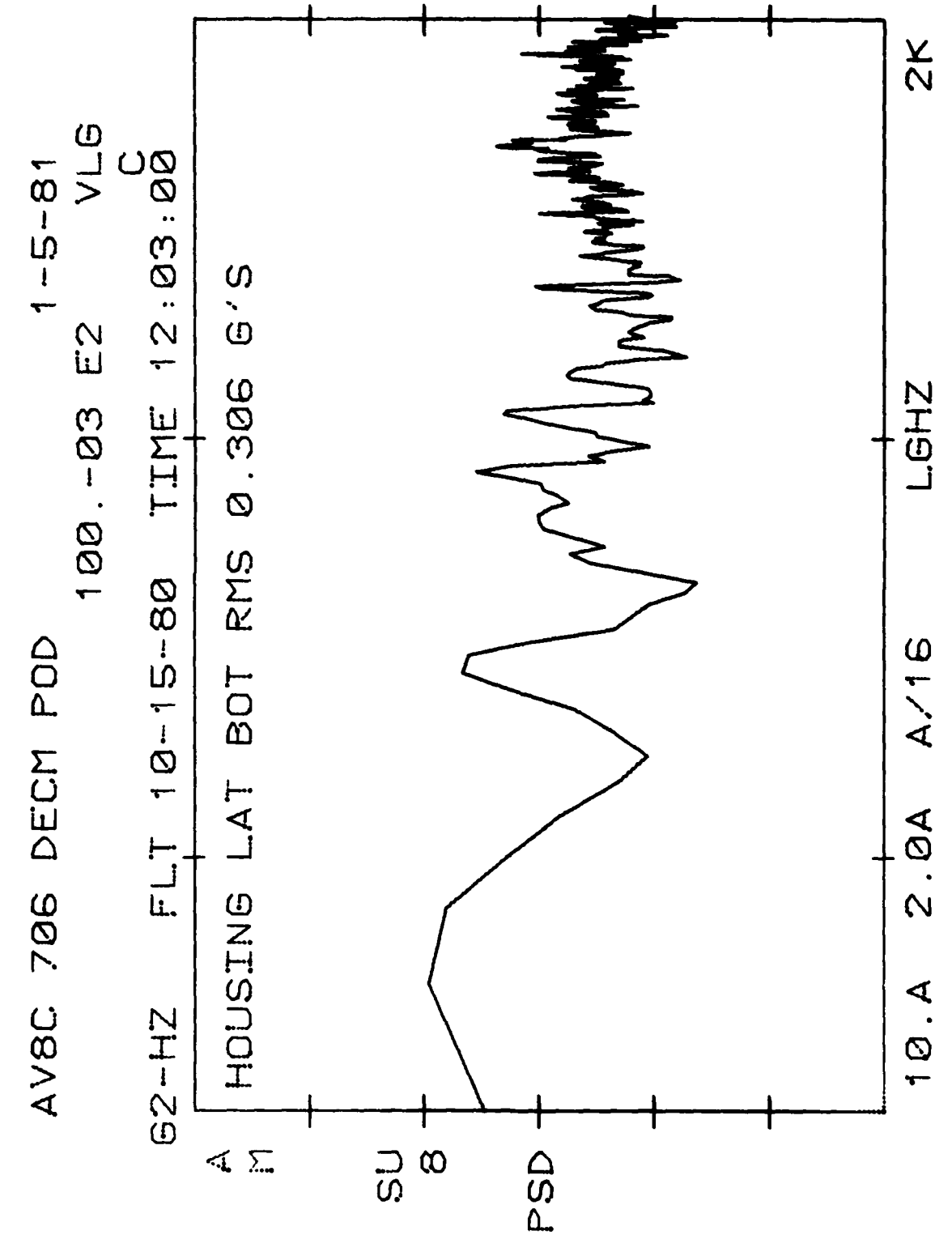

Figure 16 (Cont'd)

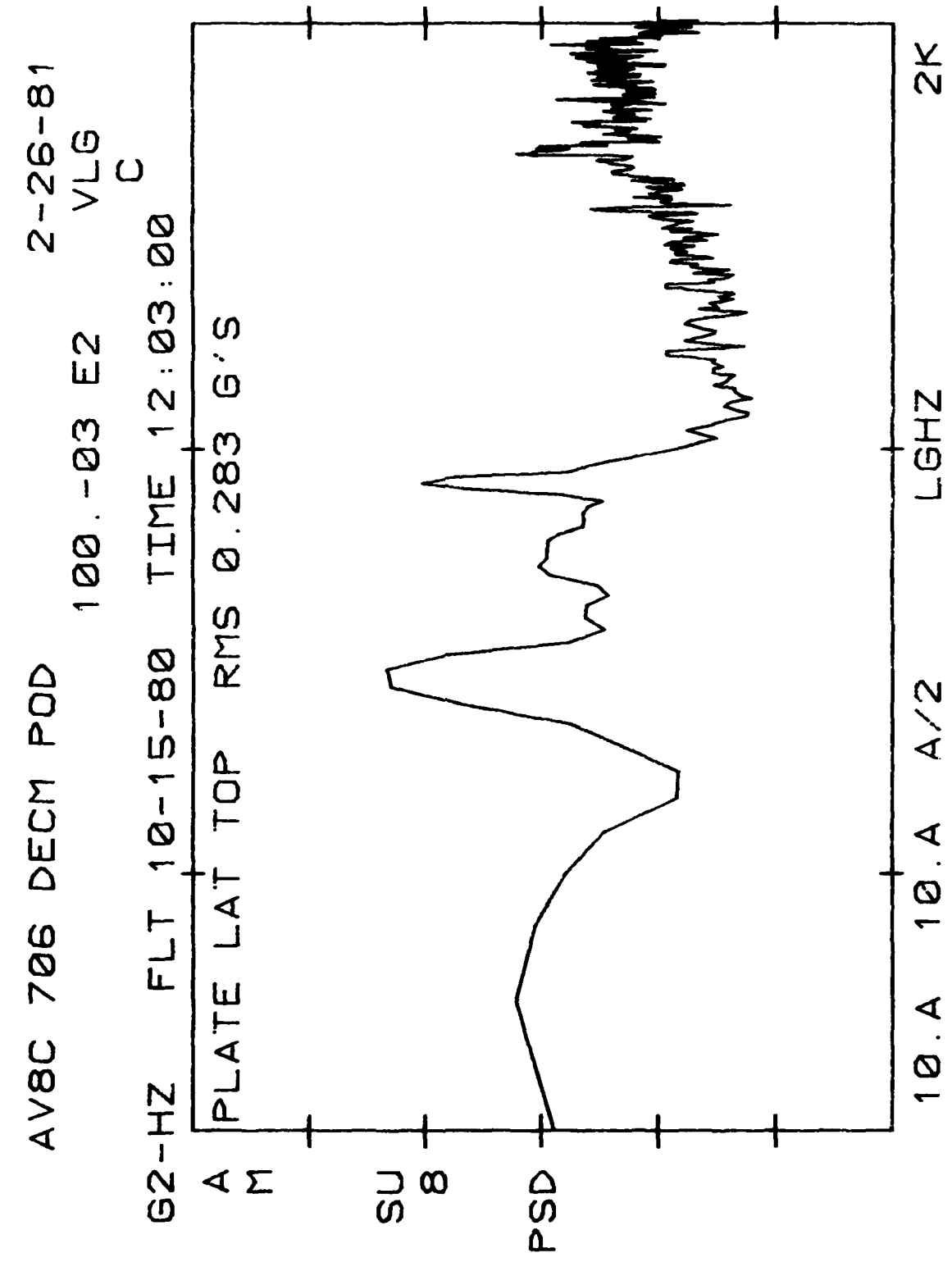

Figure 16 (Cont'd)

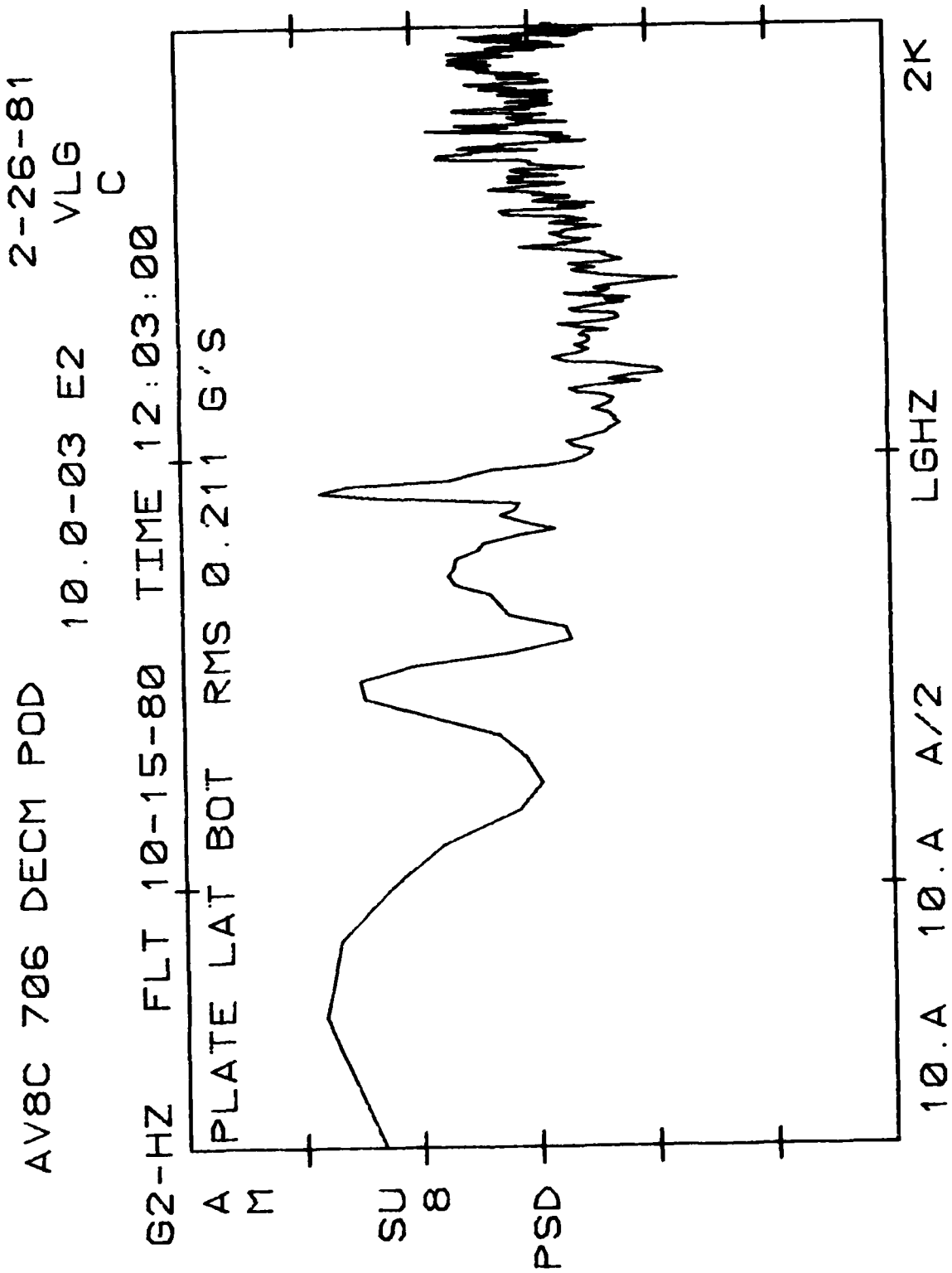

Figure 16 (Cont'd)

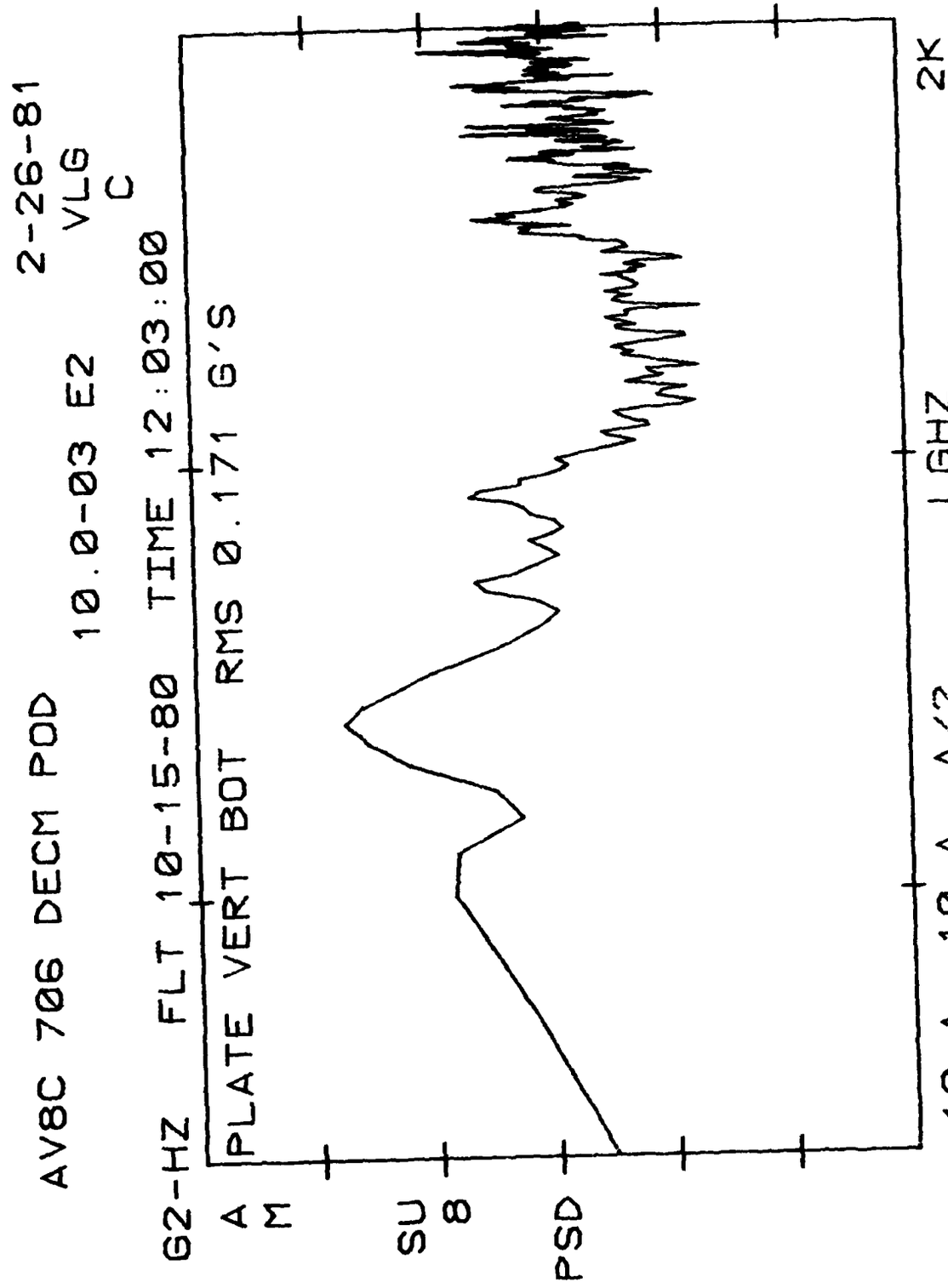

Figure 16 (Cont'd)

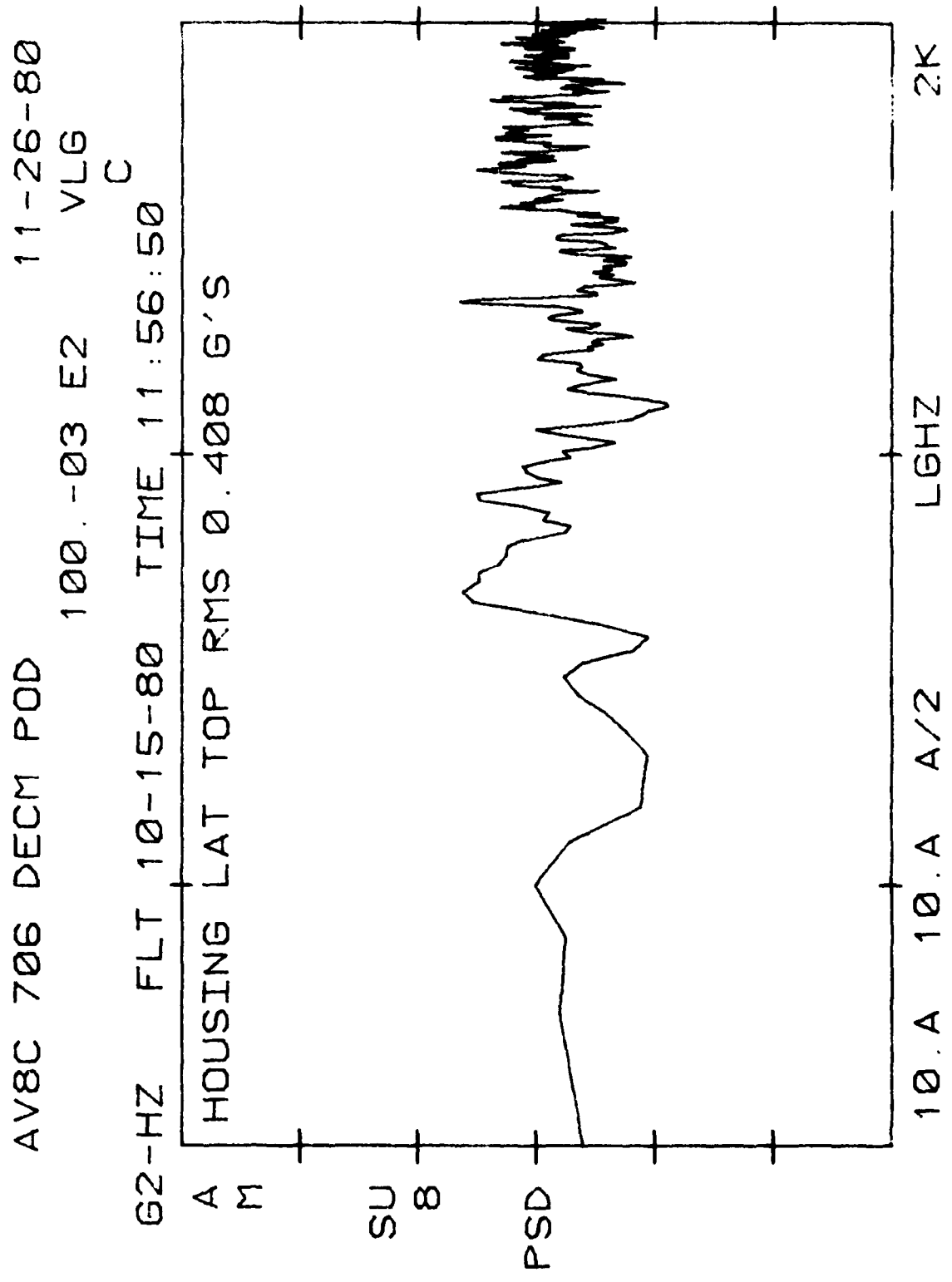

Figure 17
Cruise Flight, 40,000 ft Altitude and 238 KIAS, PSD

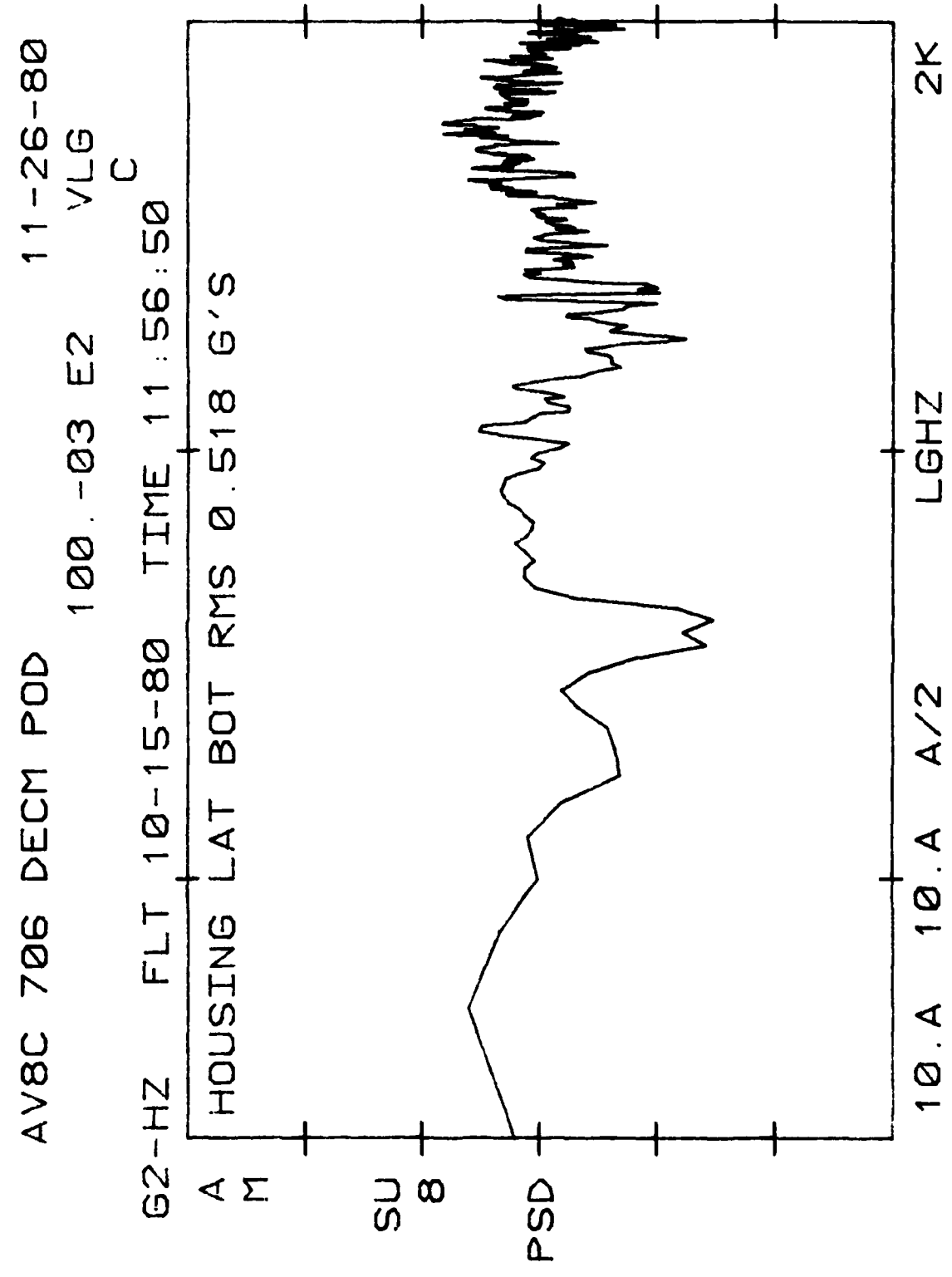

Figure 17 (Cont'd)

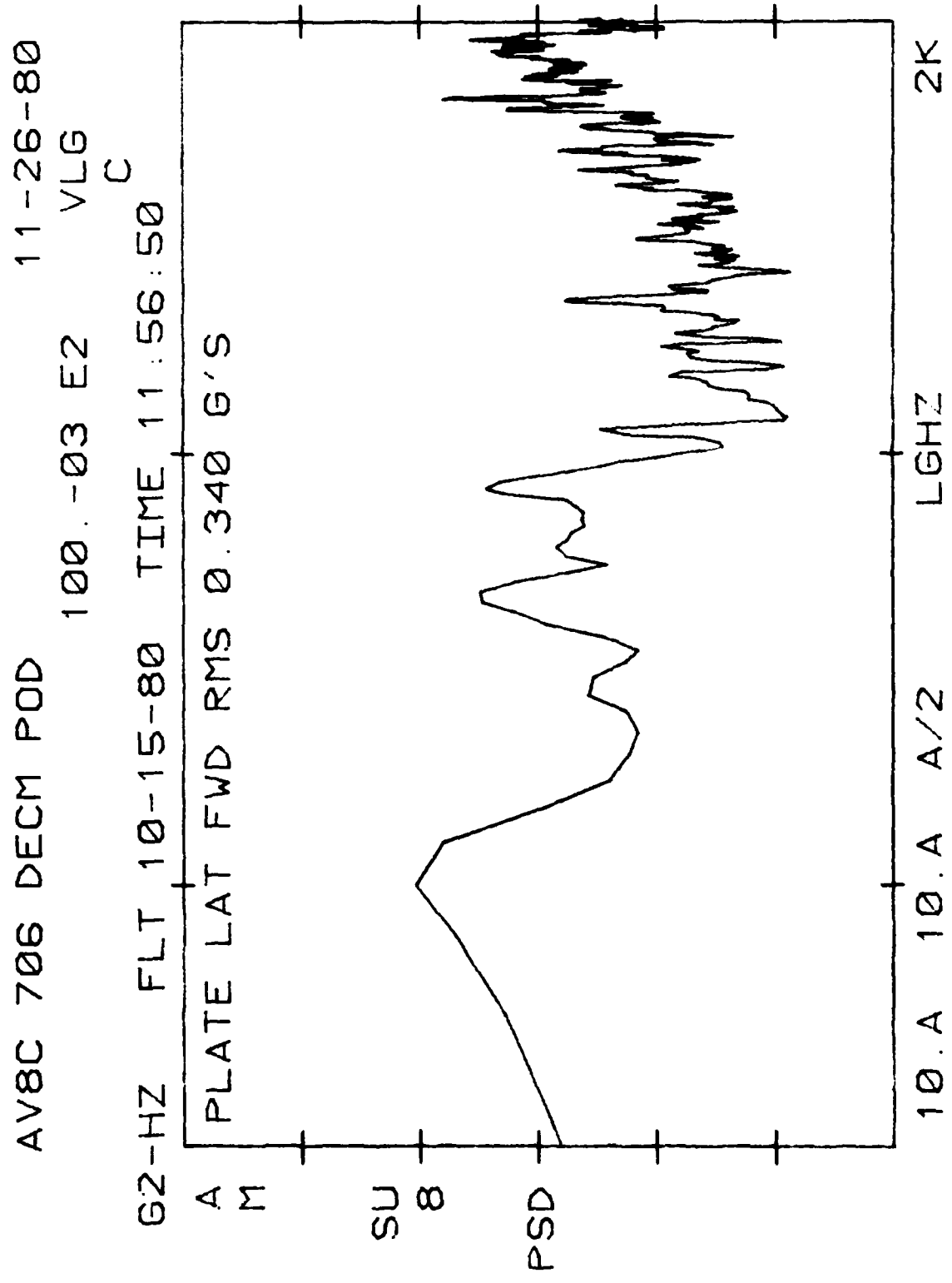

Figure 17 (Cont'd)

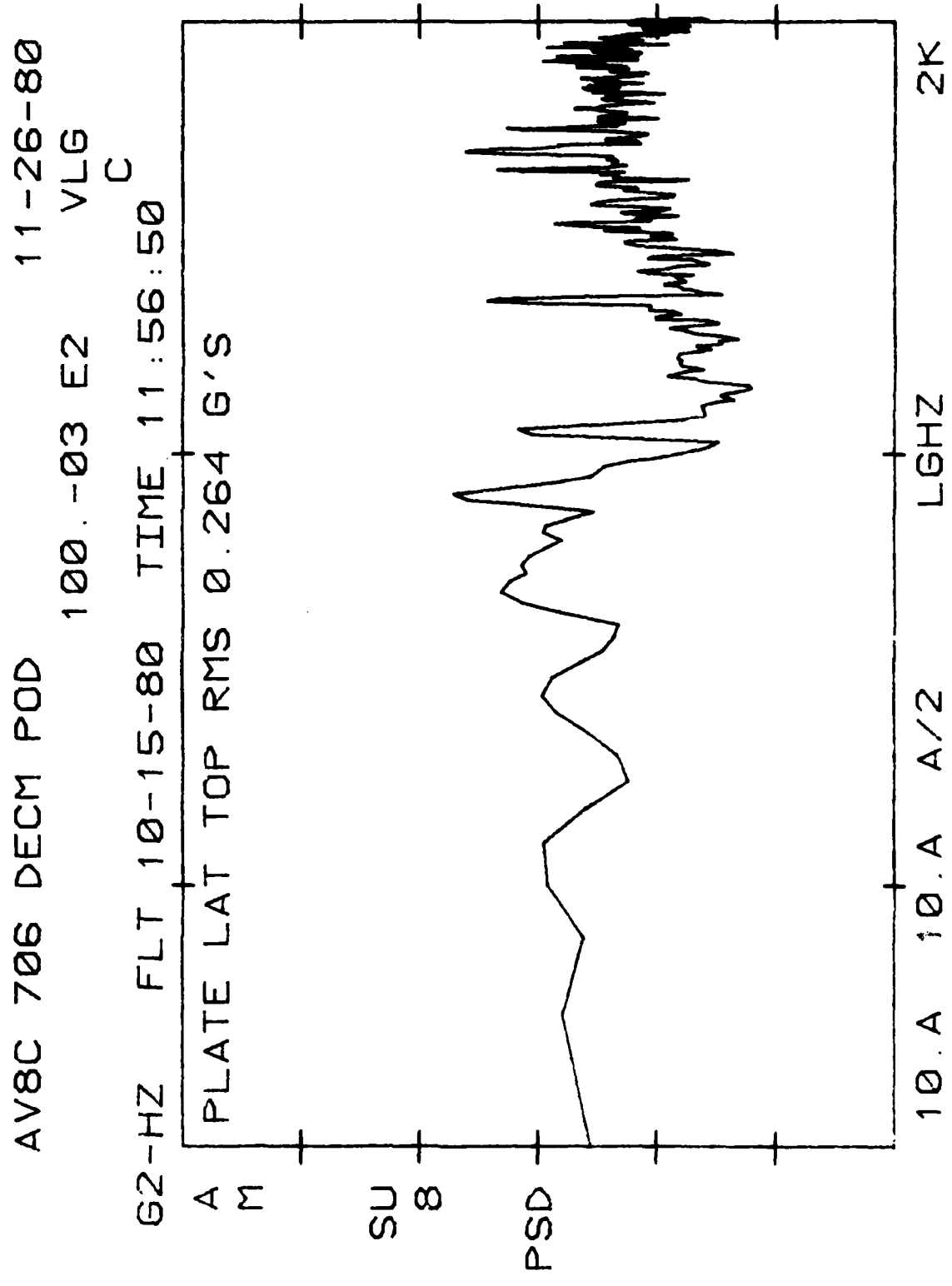

Figure 17 (Cont'd)

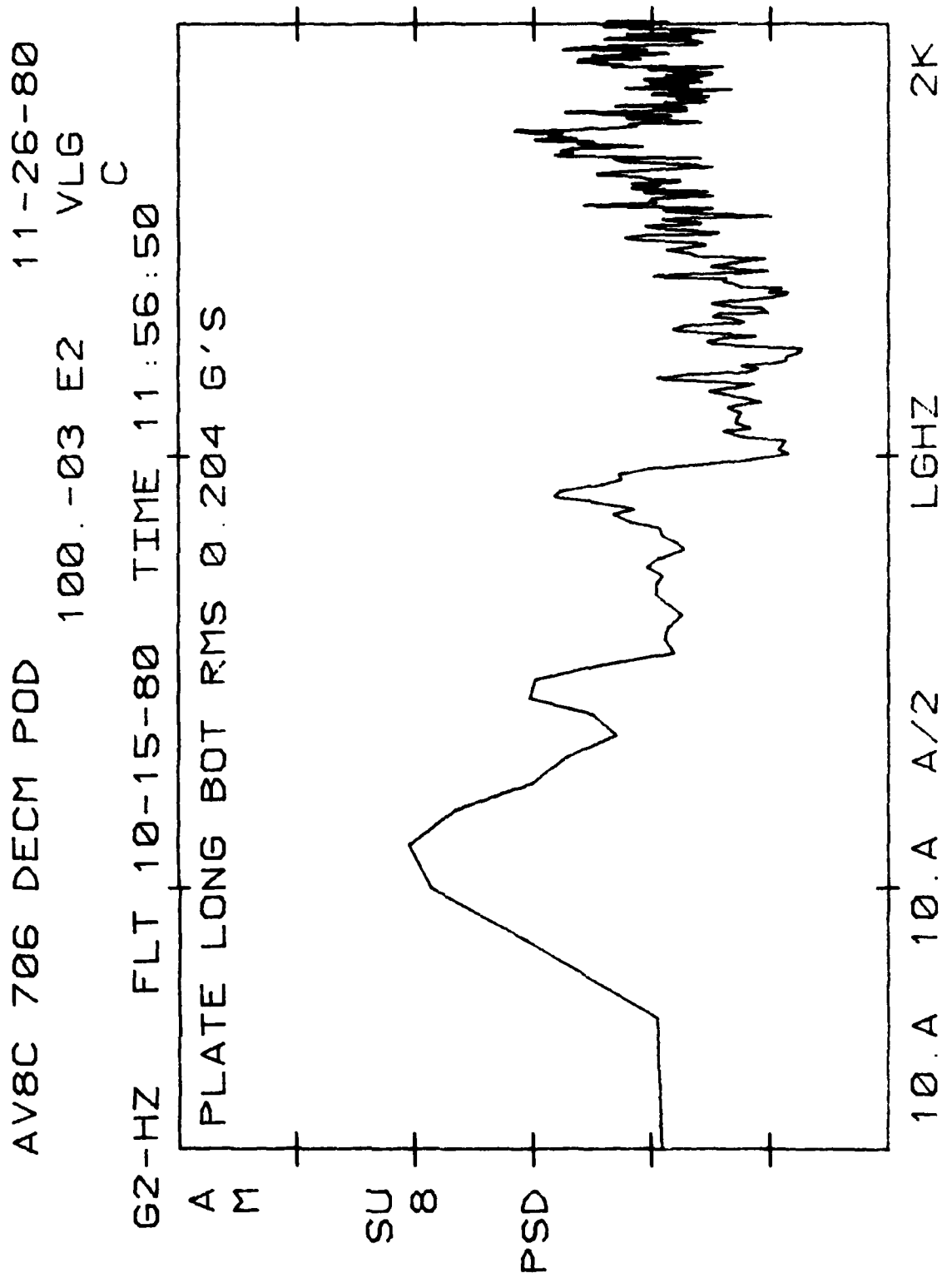

Figure 17 (Cont'd)

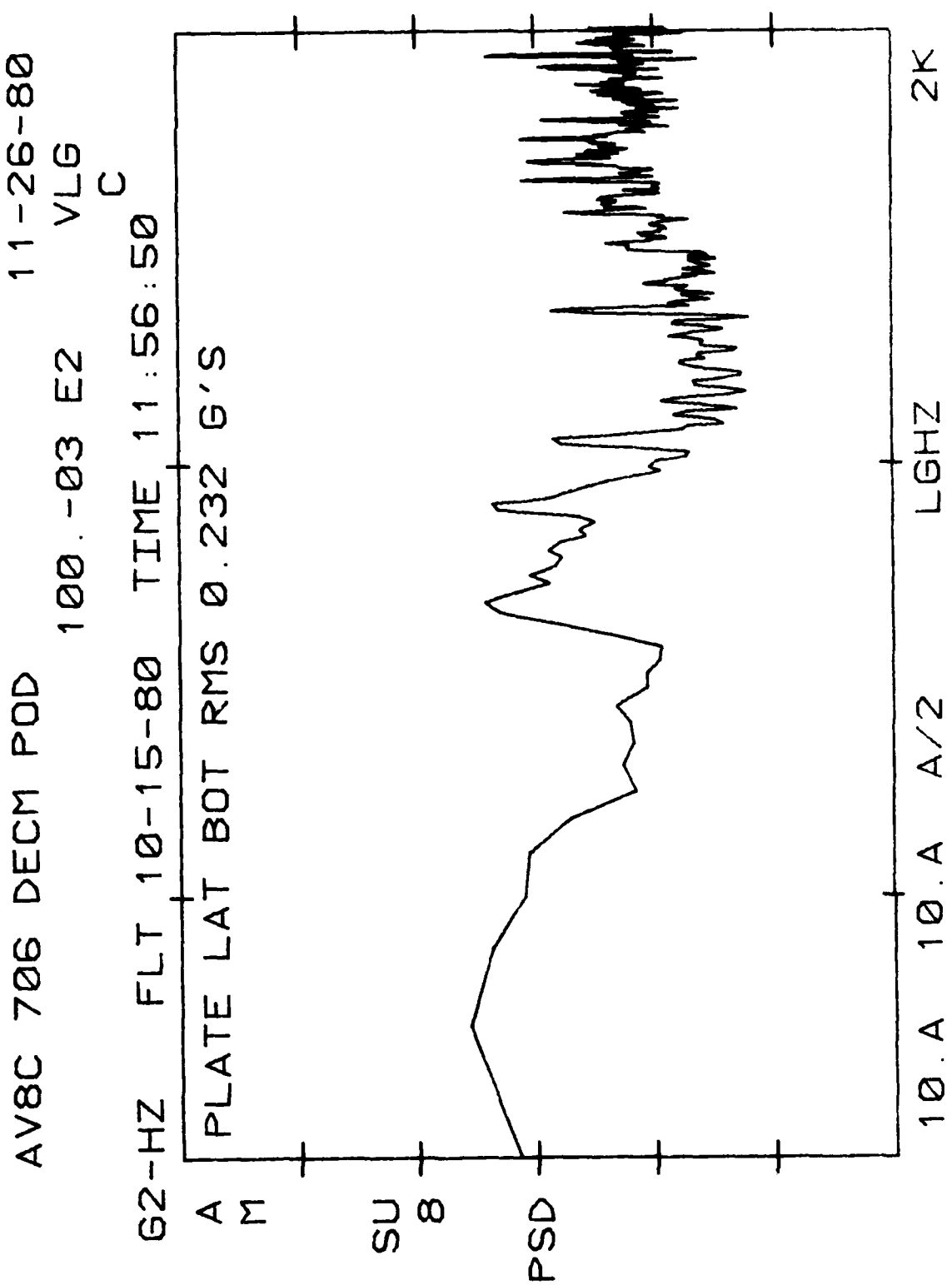

Figure 17 (Cont'd)

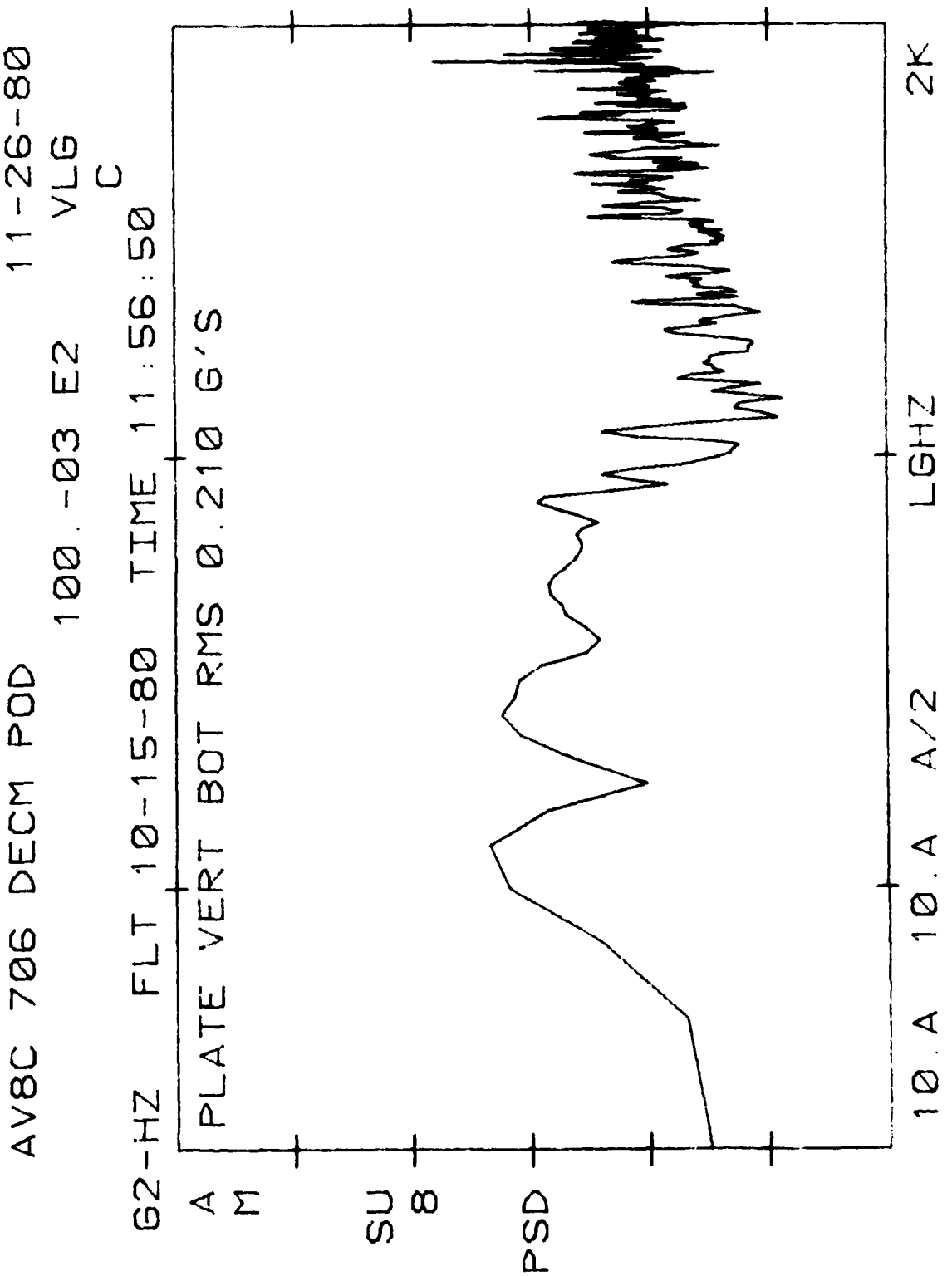

Figure 17 (Cont'd)

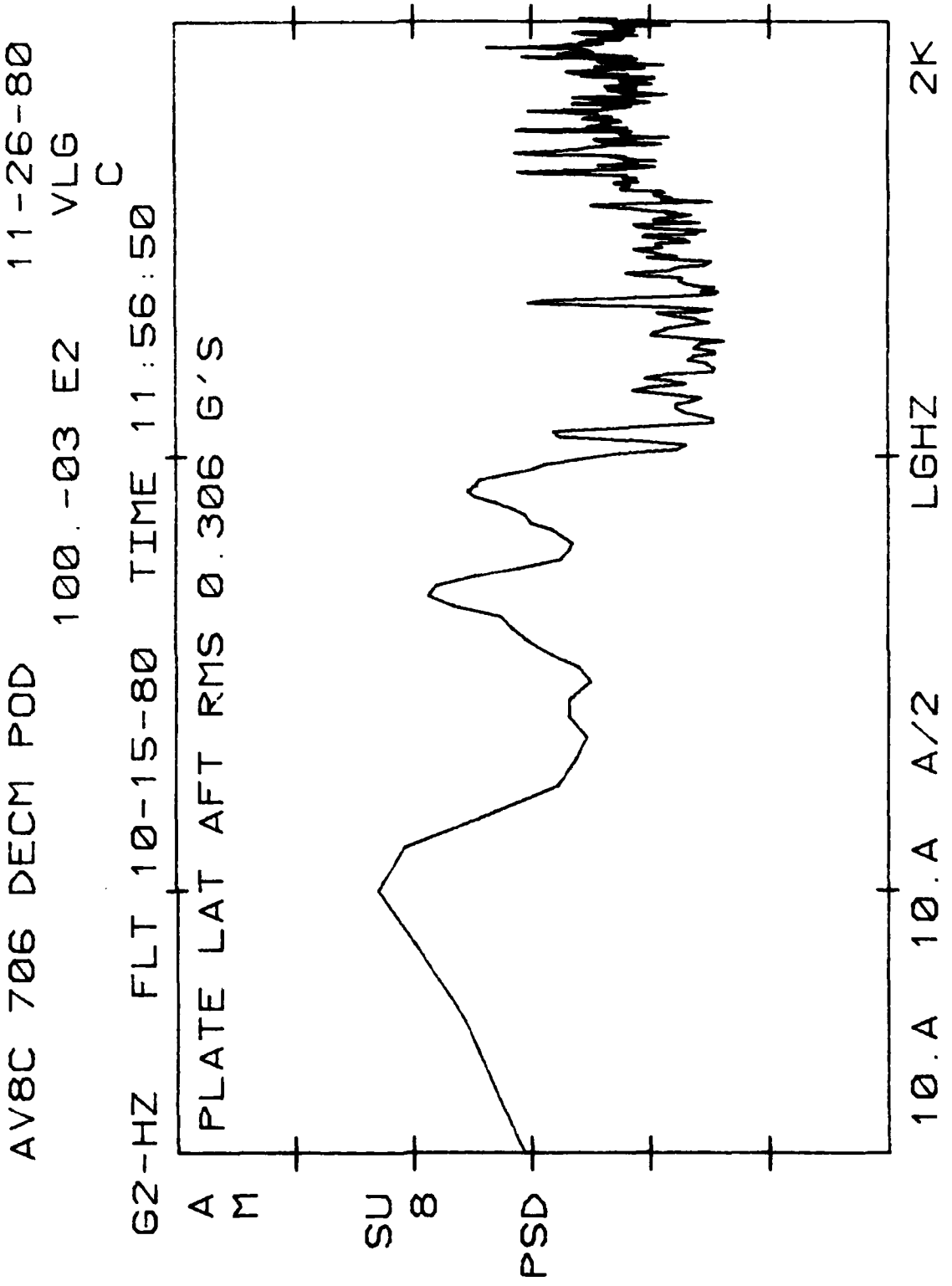

Figure 17 (Cont'd)

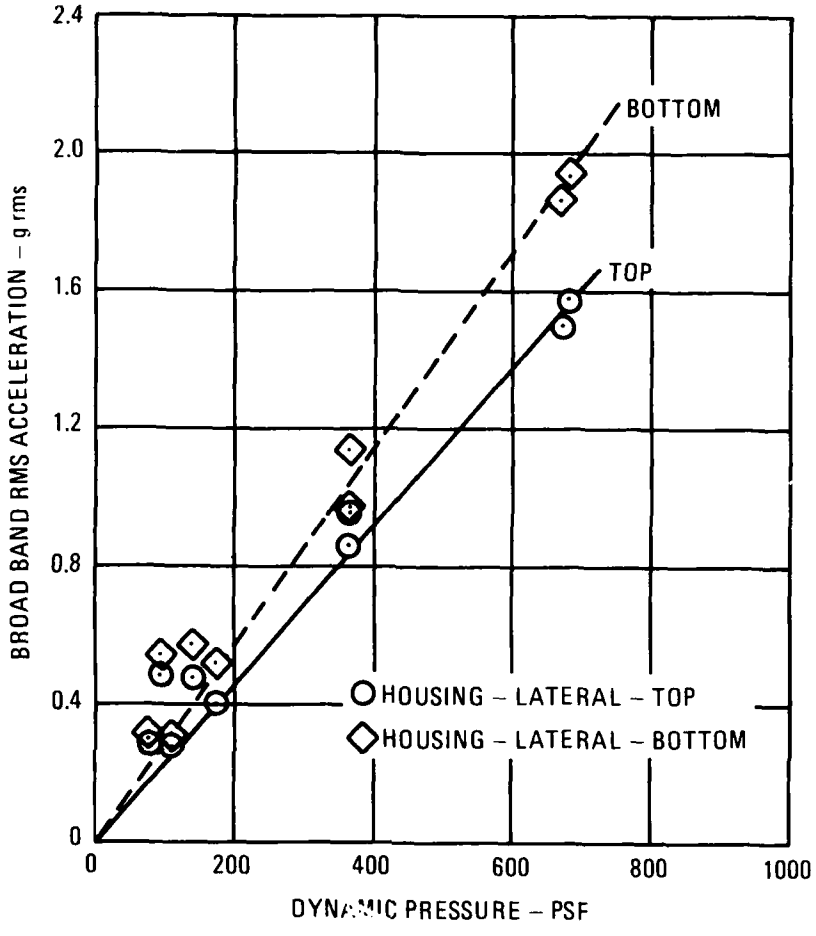

Figure 18
Variation of Housing Lateral Vibration with Dynamic Pressure

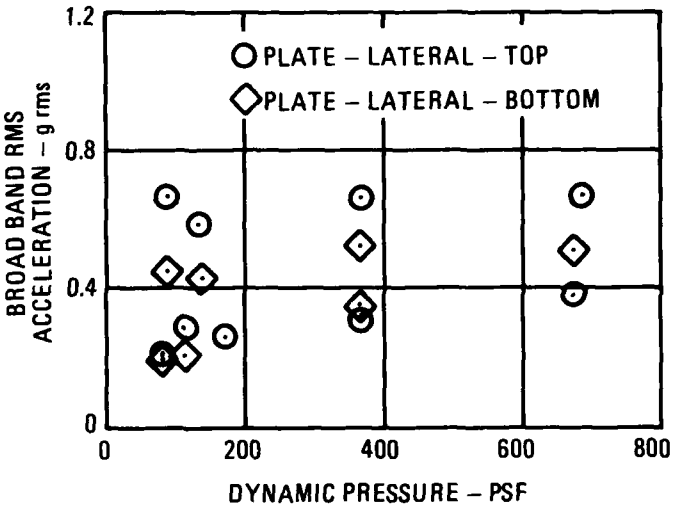

Figure 19
Variation of Plate Lateral Vibration with Dynamic Pressure

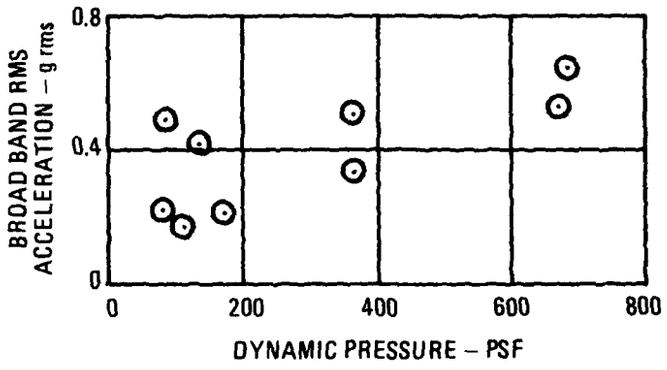

Figure 20
Variation of Plate Vertical Vibration with
Dynamic Pressure

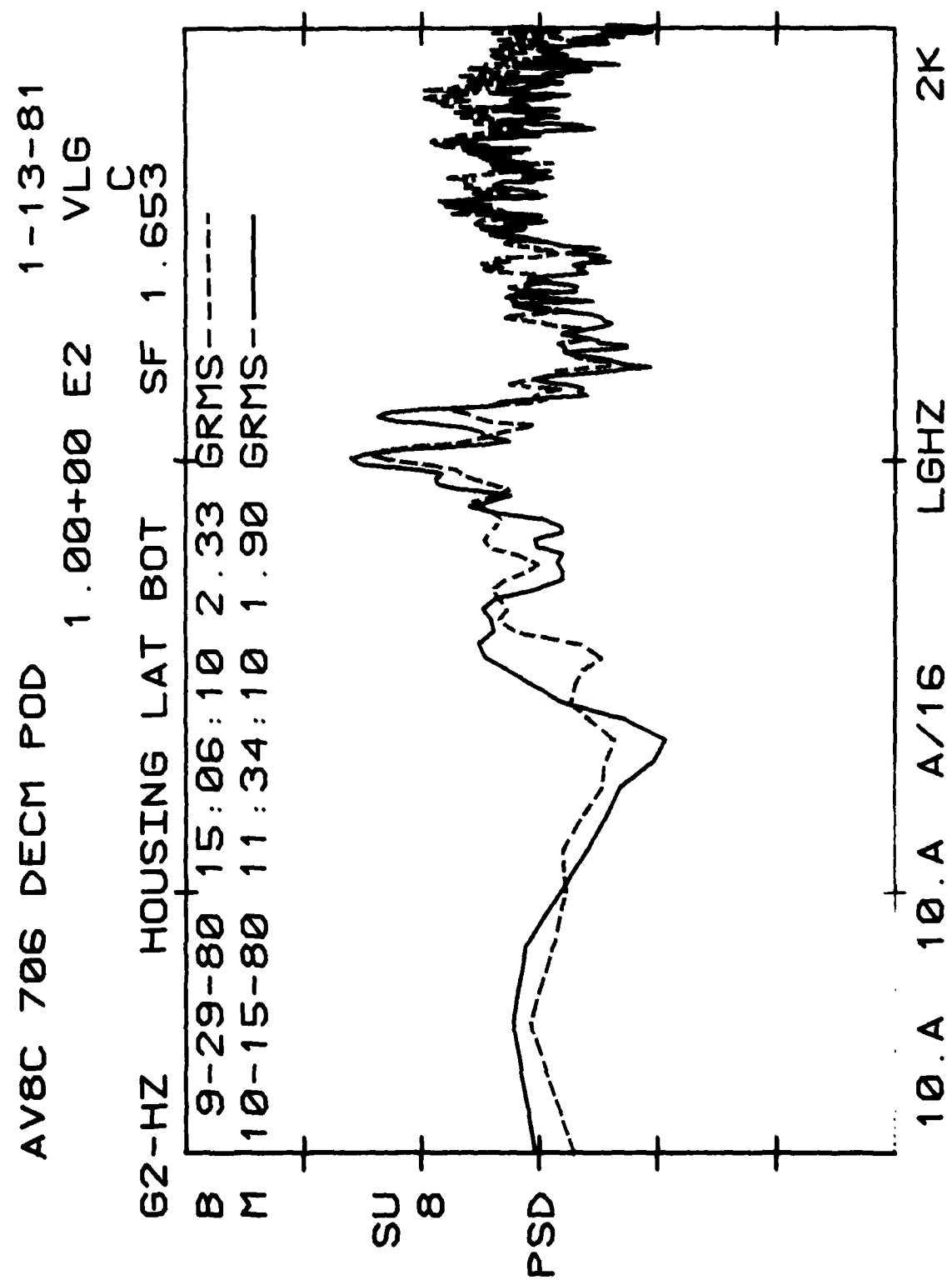

Figure 21
Comparison of Scaled Vibration Data, Housing, Lateral Axis, PSD

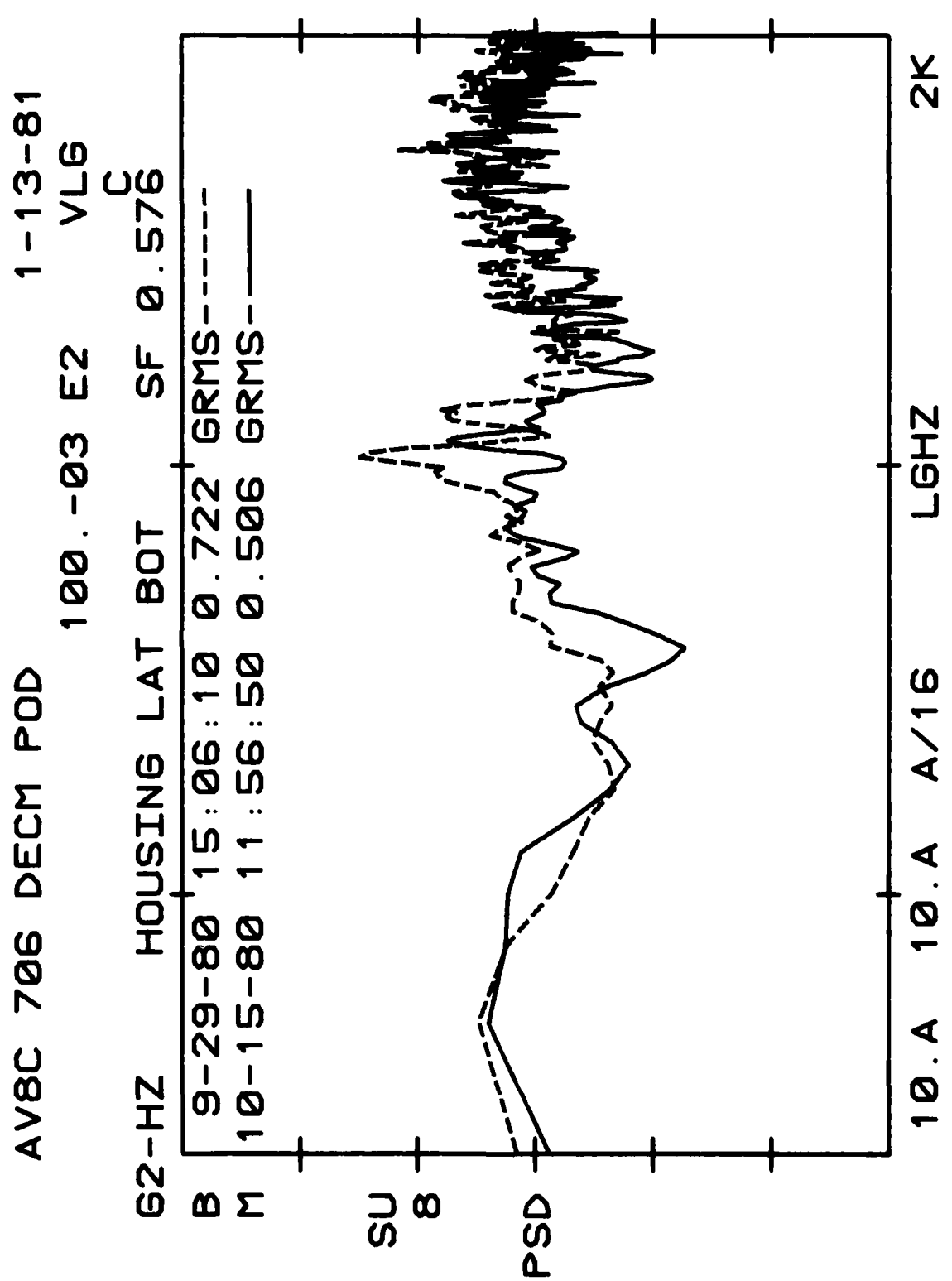

Figure 21 (Cont'd)

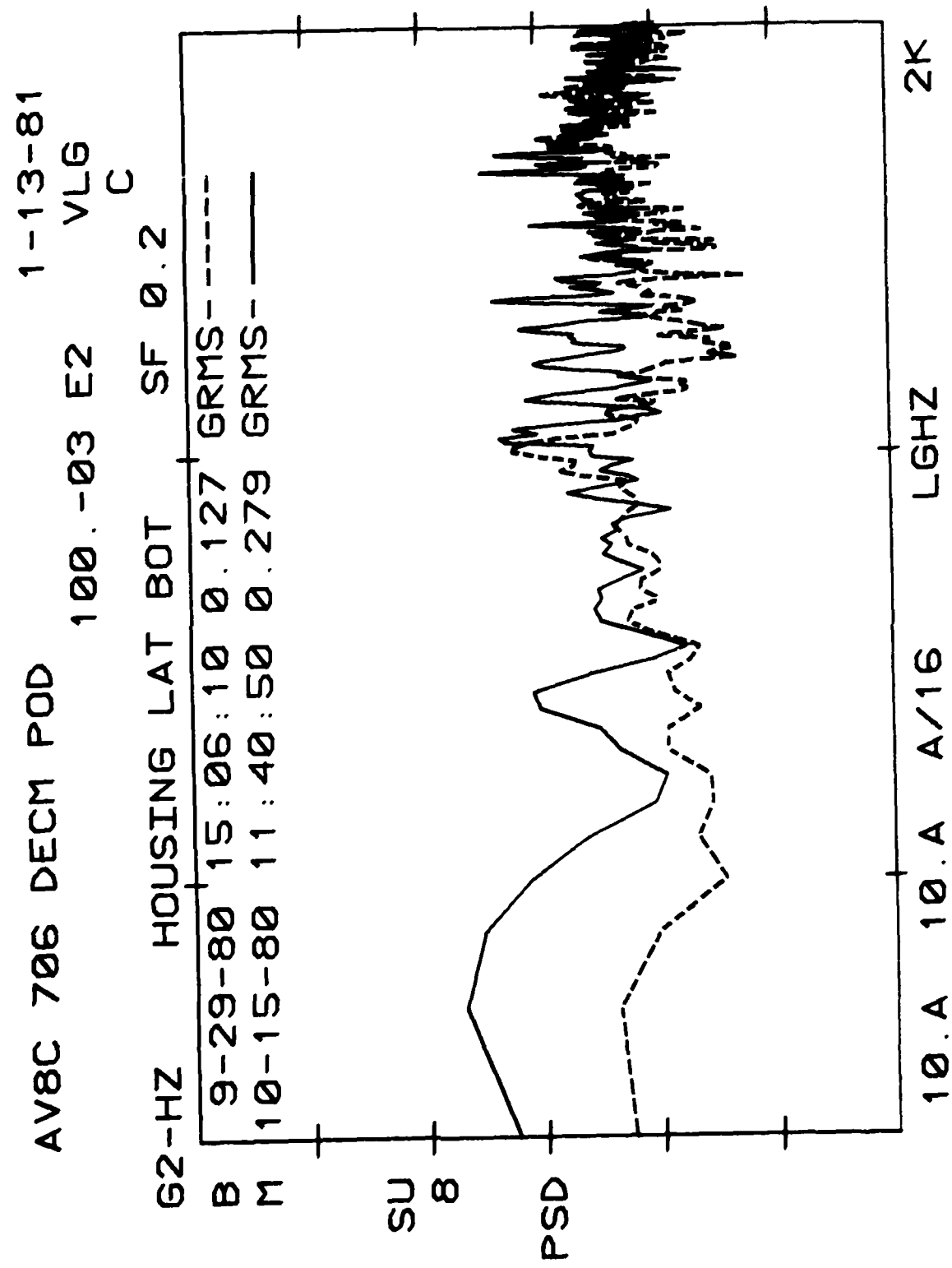

Figure 21 (Cont'd)

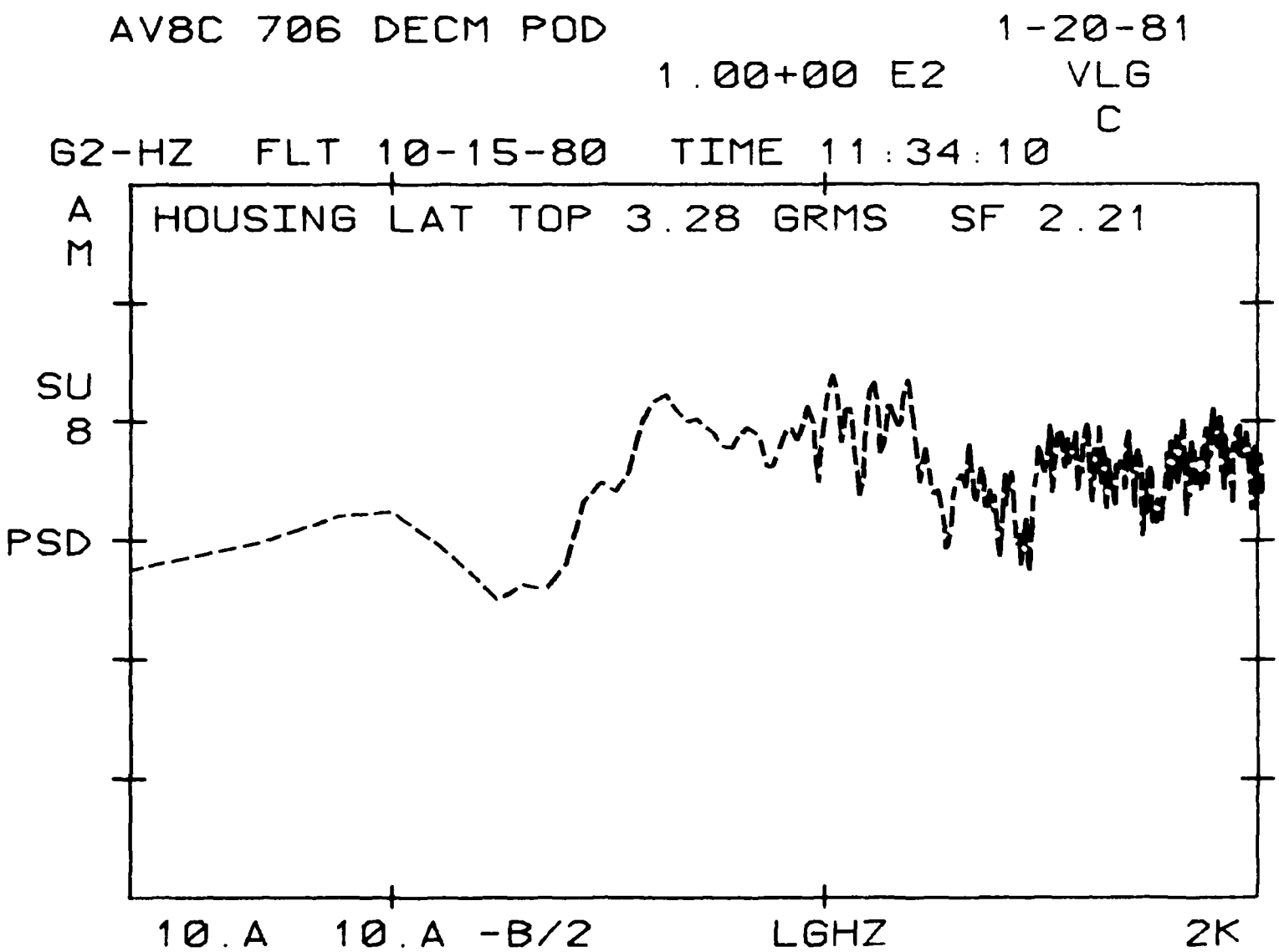

Figure 22
Scaled Vibration Data, Housing, Lateral Axis, PSD

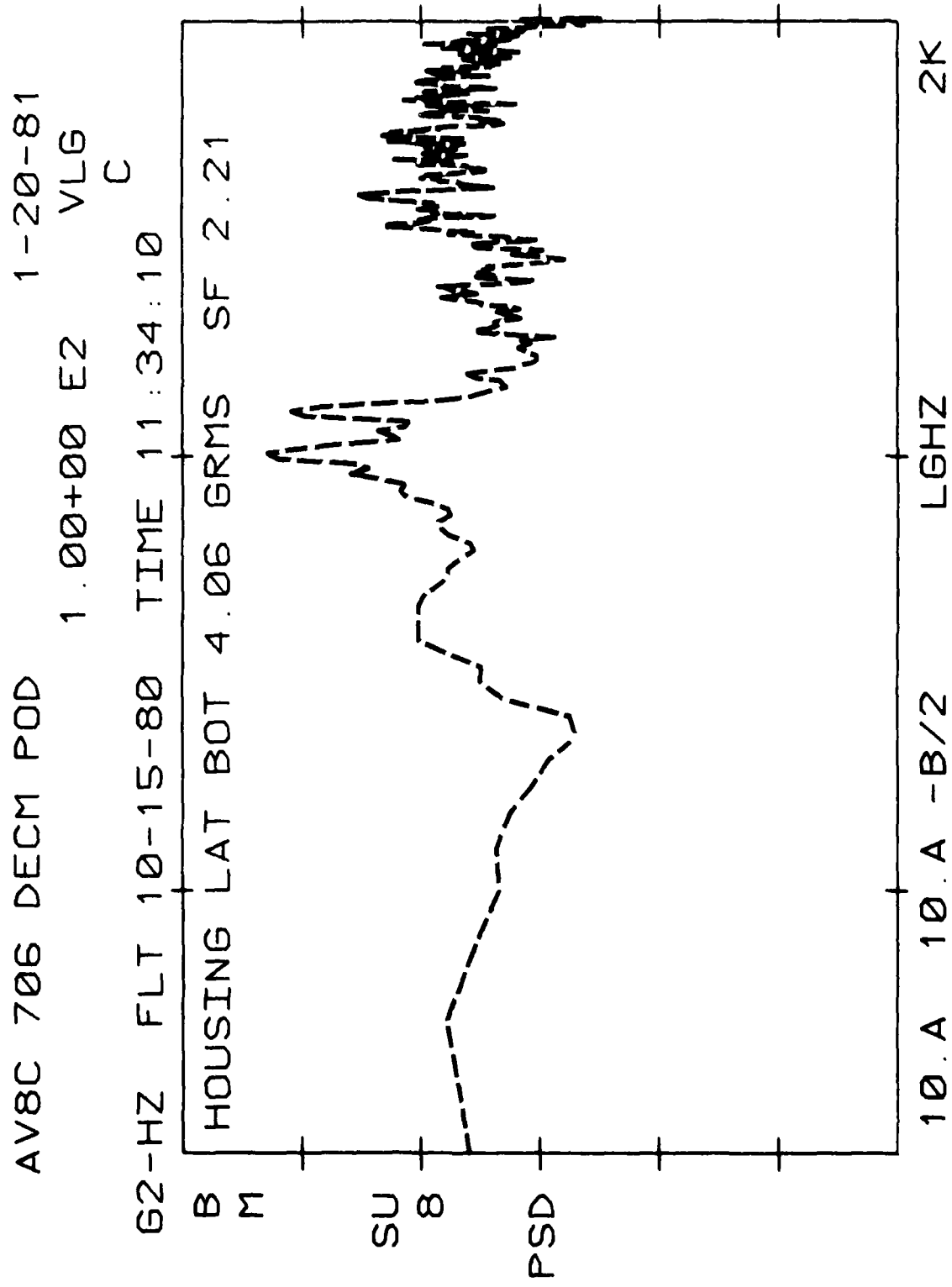

Figure 22 (Cont'd)

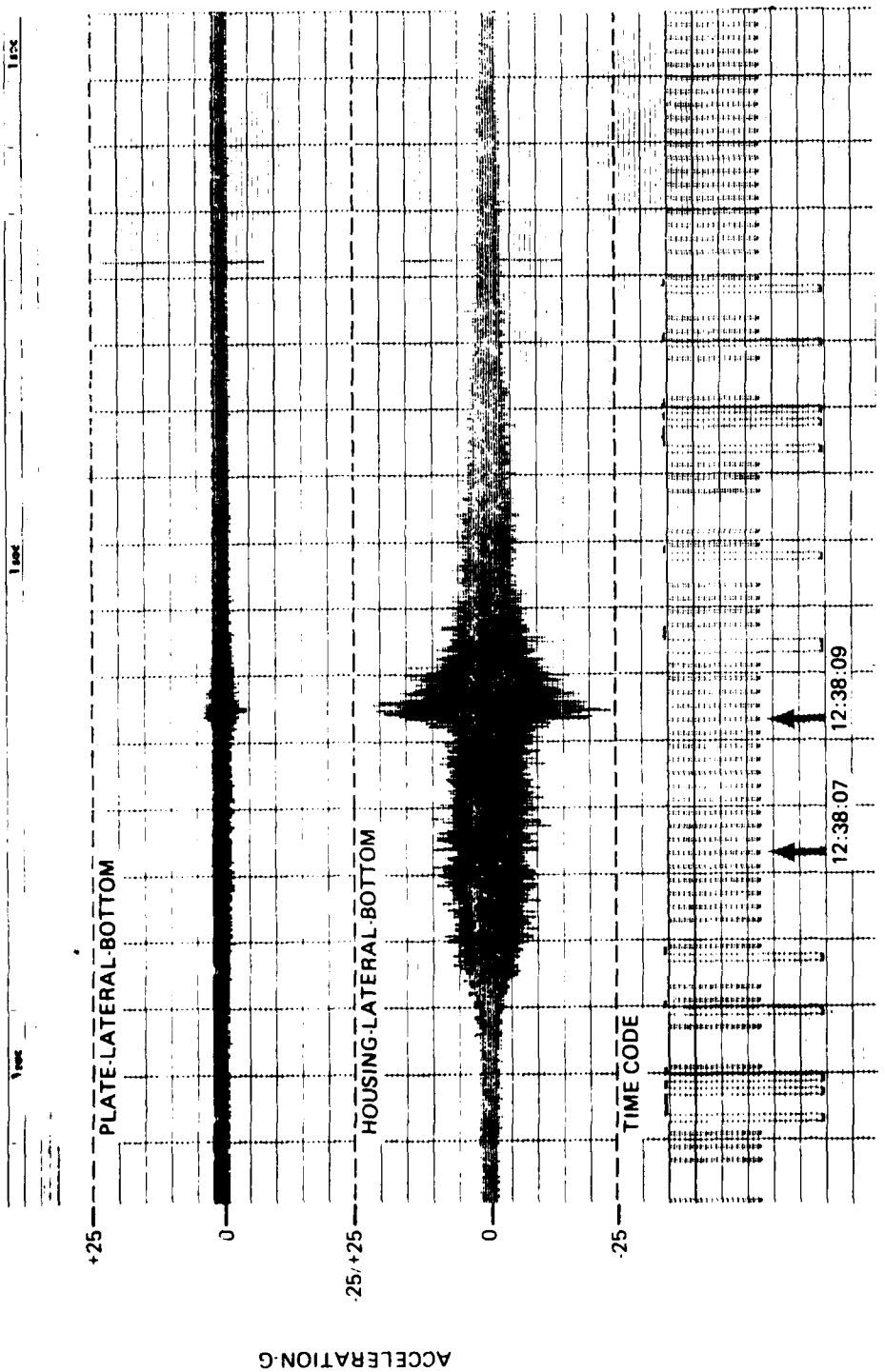

Figure 23
Short Takeoff (Wet) Time History

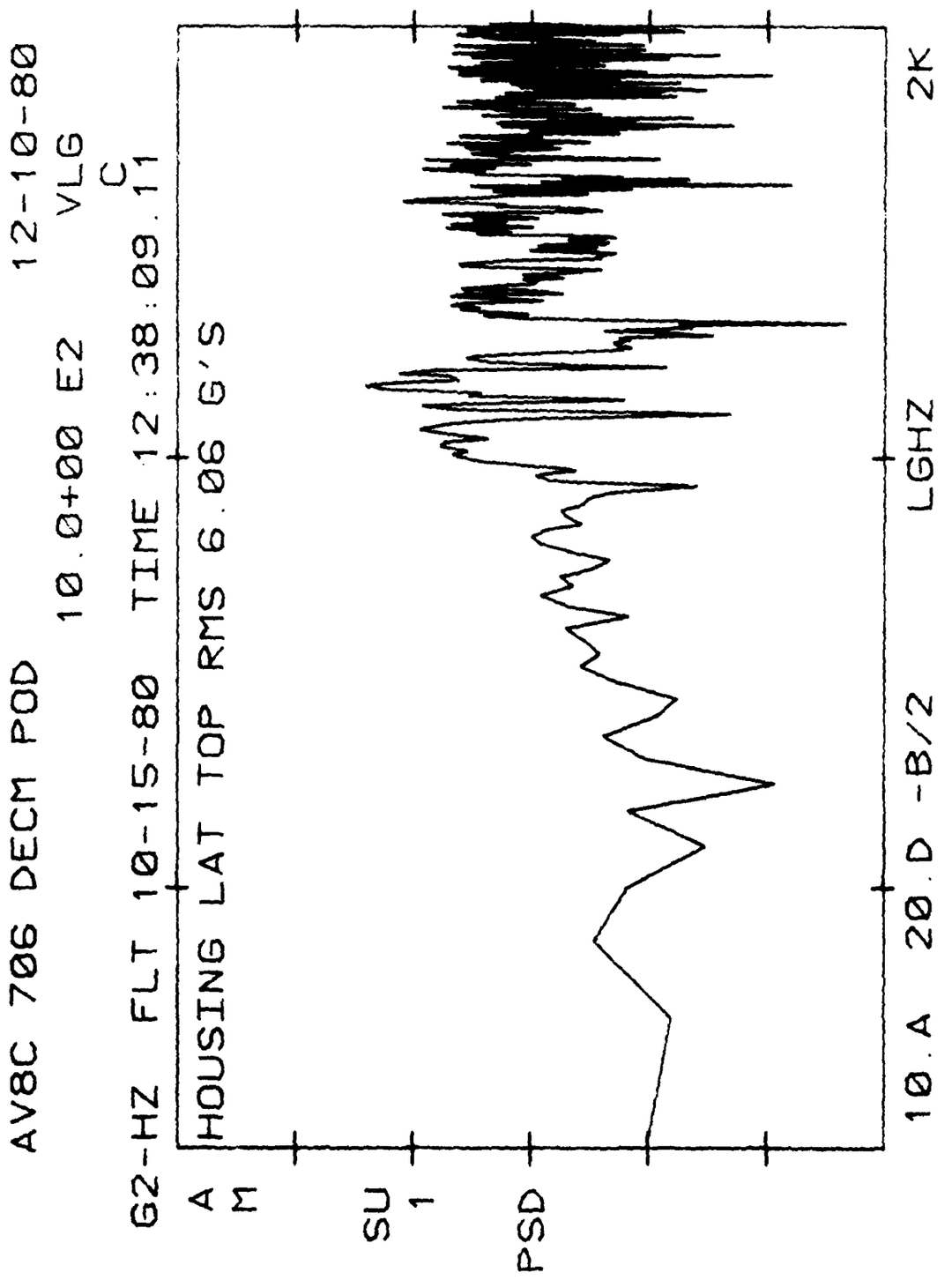

Figure 24
Short Takeoff (Wet), Maximum Vibration, PSD

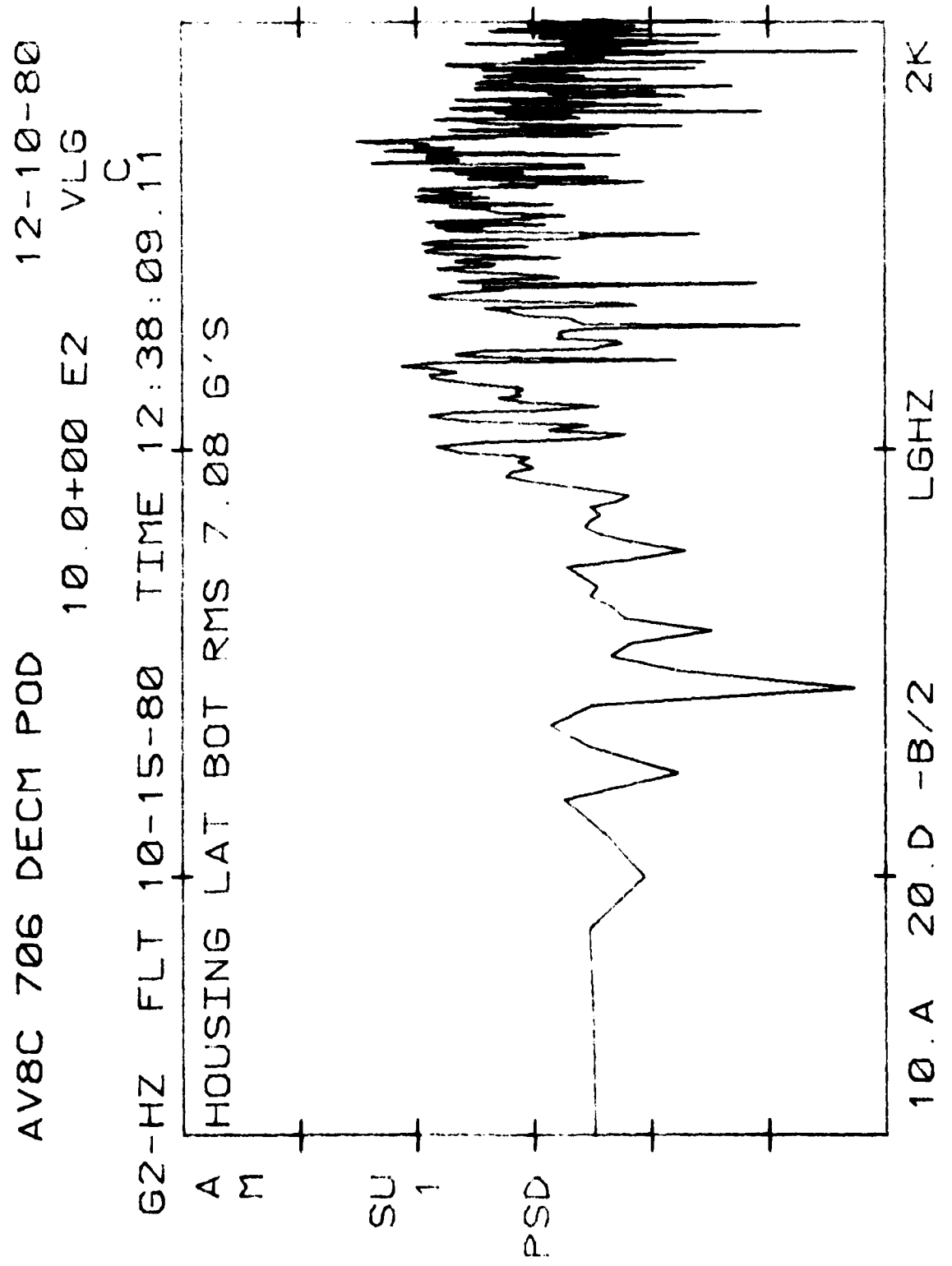

Figure 24 (Cont'd)

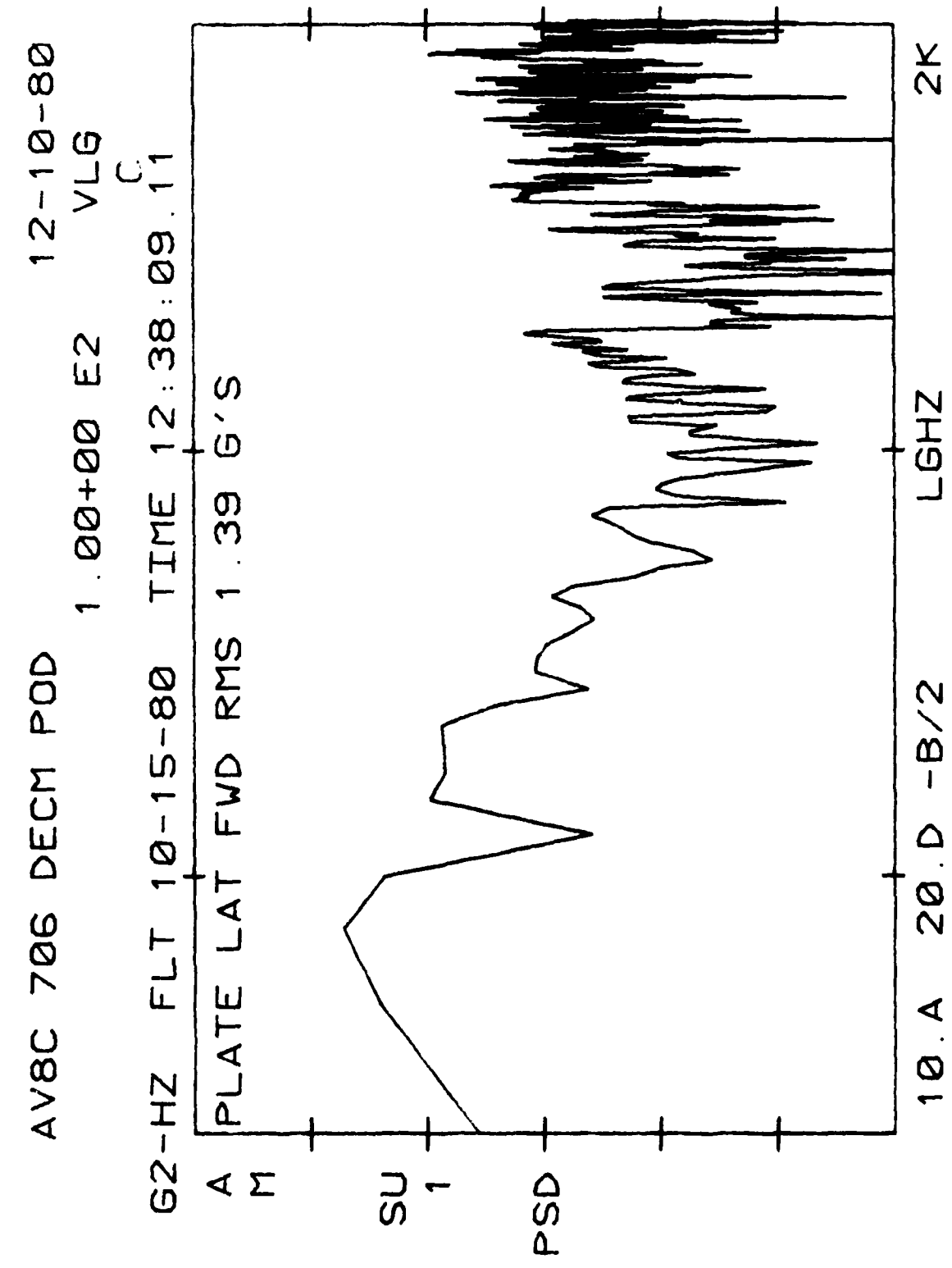

Figure 24 (Cont'd)

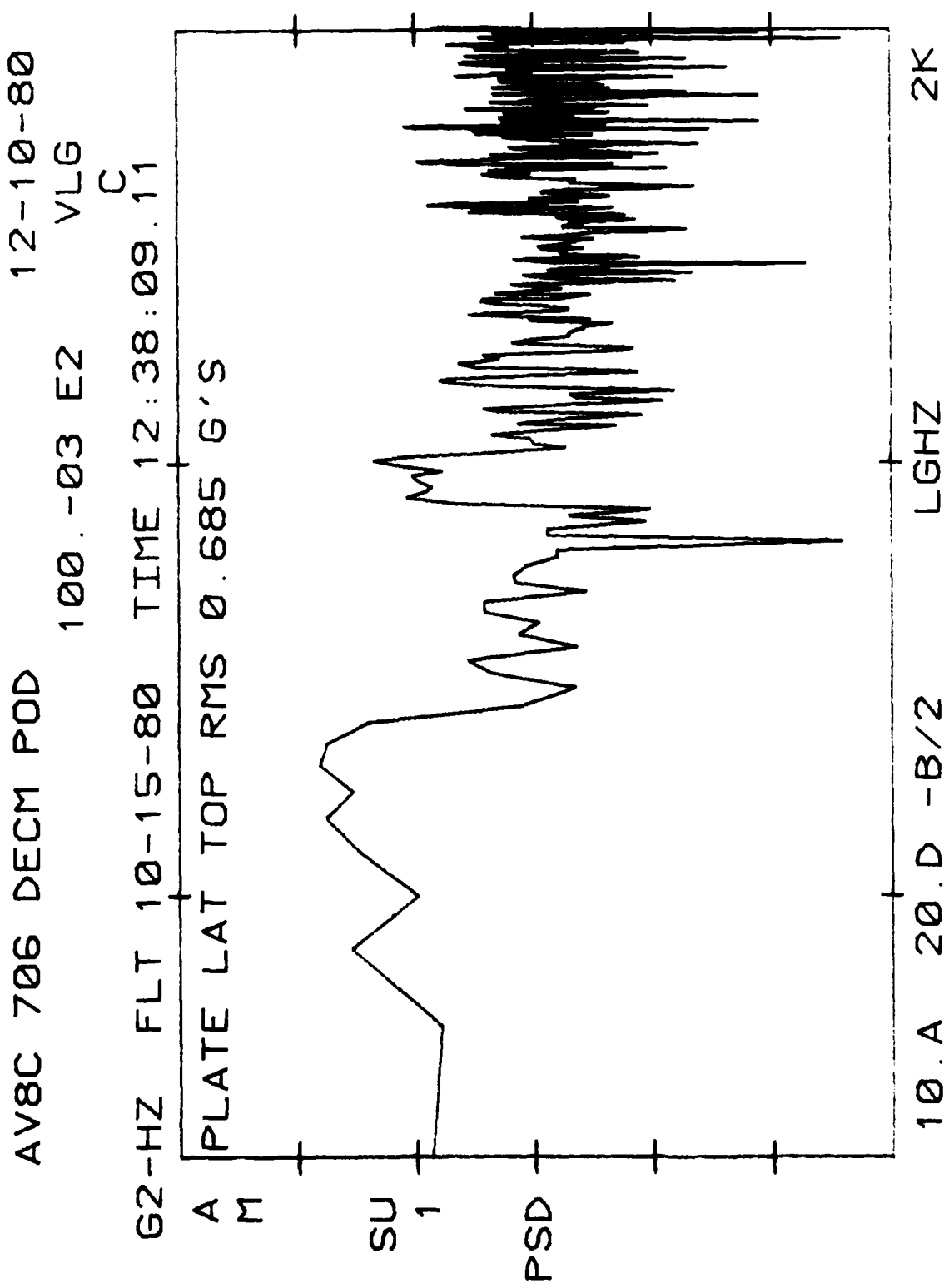

Figure 24 (Cont'd)

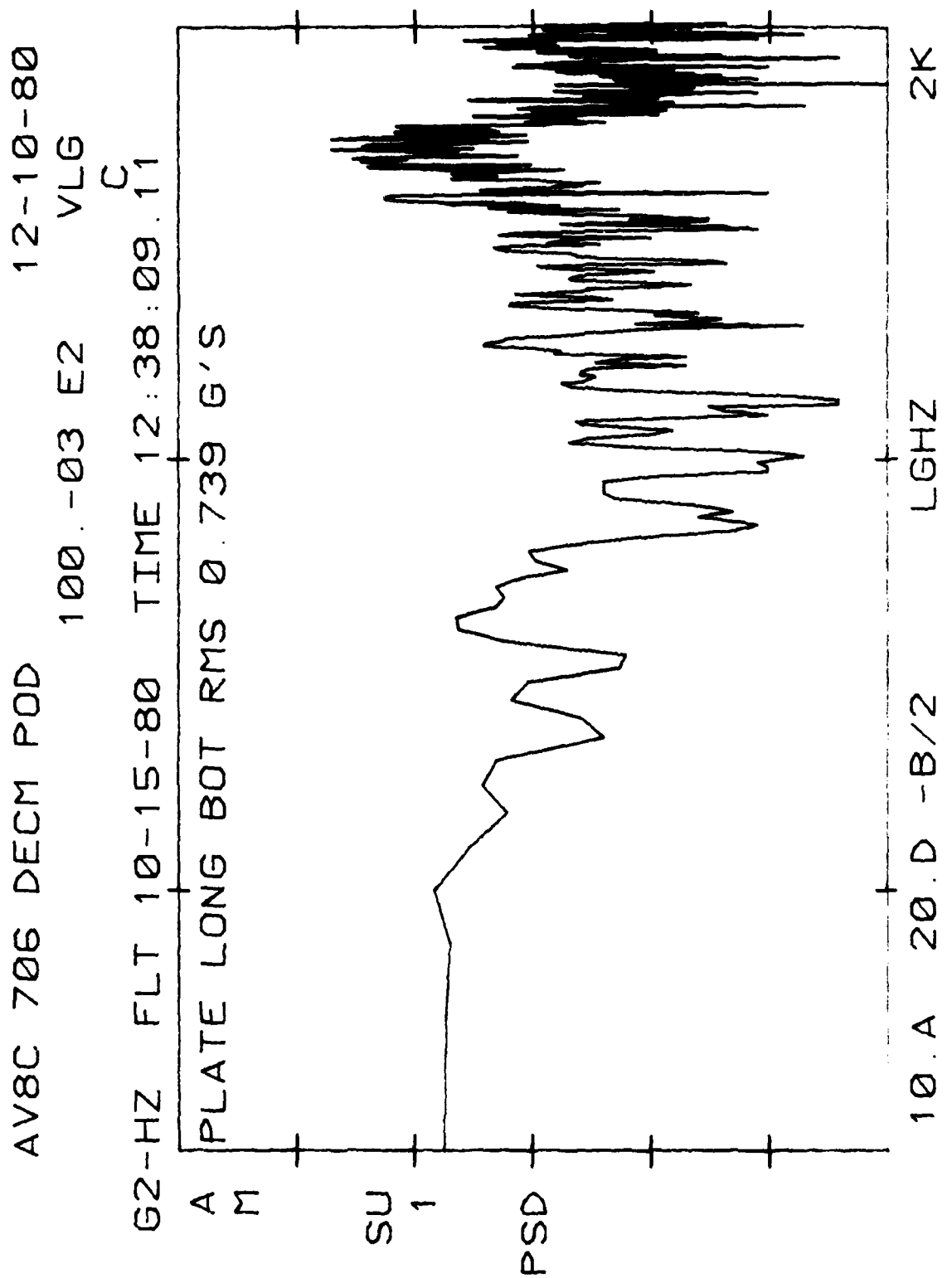

Figure 24 (Cont'd)

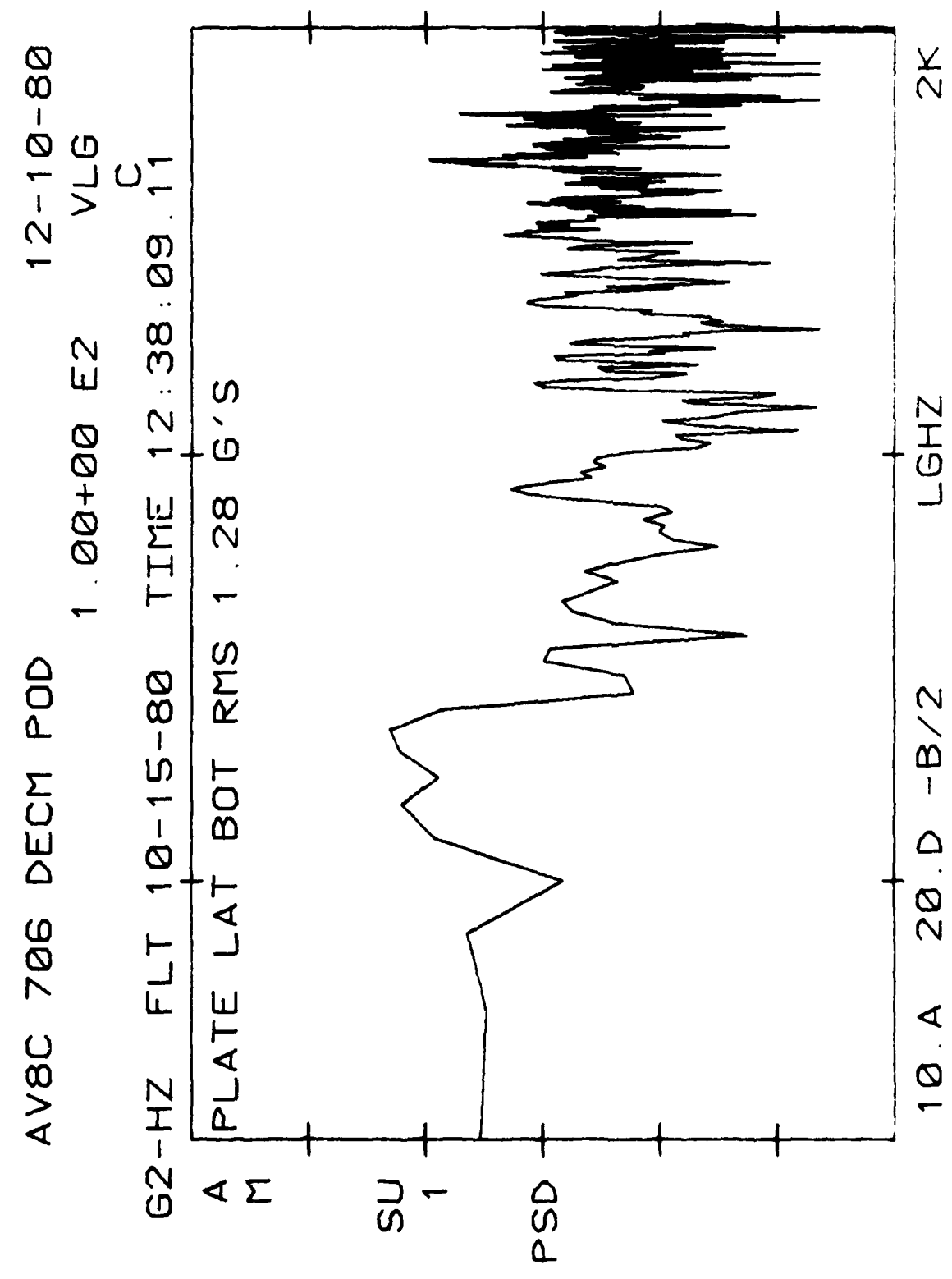

Figure 24 (Cont'd)

AD-A110 198 NAVAL AIR TEST CENTER PATUXENT RIVER MD F/G 1/3
AL8-164 POD/AV-8C ENVIRONMENTAL EVALUATION FLIGHT TEST.(U)
DEC 81 L J MERTAUGH
UNCLASSIFIED NATC-TM-81-109-SY NL

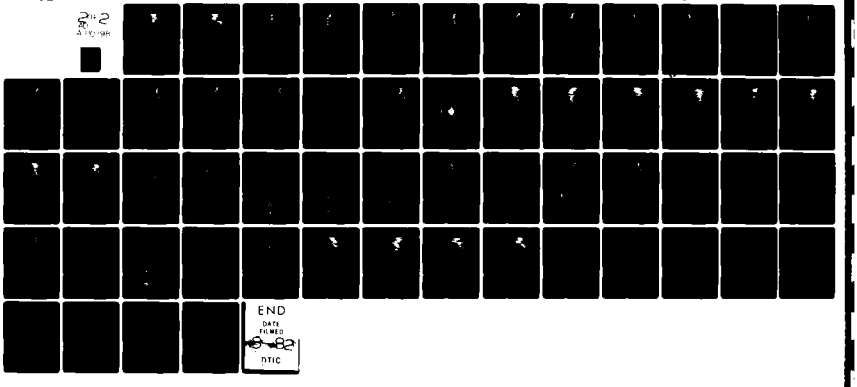

END
DATE FILMED
-82
DTIC

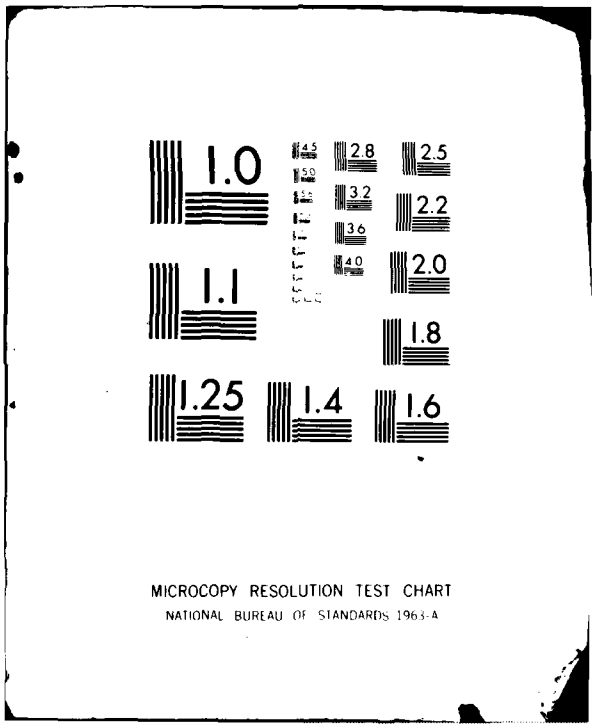
1.0
1.1
1.25
1.4
1.6
1.8
2.0
2.2
2.5
2.8
3.2
3.6
4.0
4.5
5.0
MICROCOPY RESOLUTION TEST CHART
NATIONAL BUREAU OF STANDARDS 1963-A

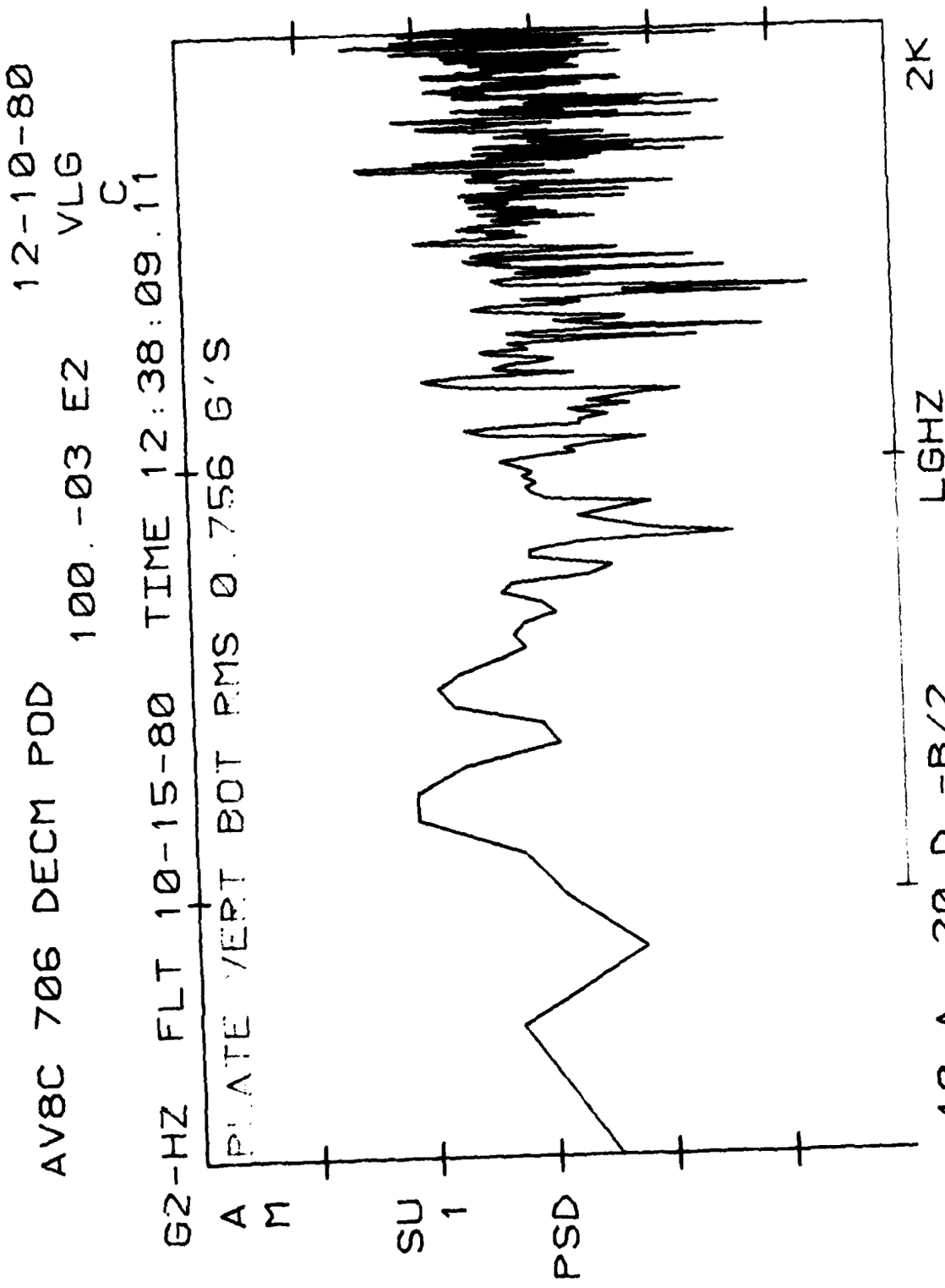

Figure 24 (Cont'd)

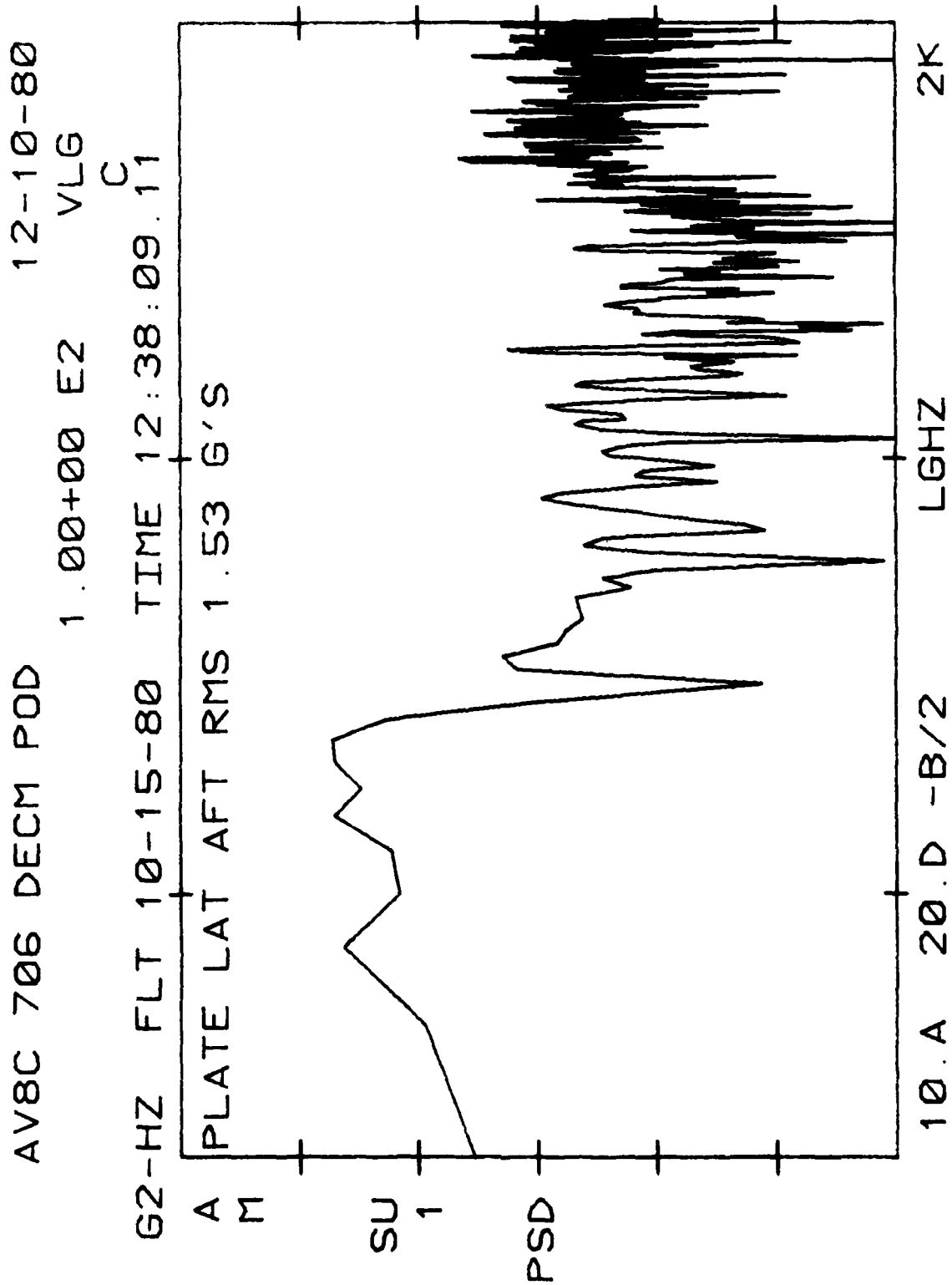

Figure 24 (Cont'd)

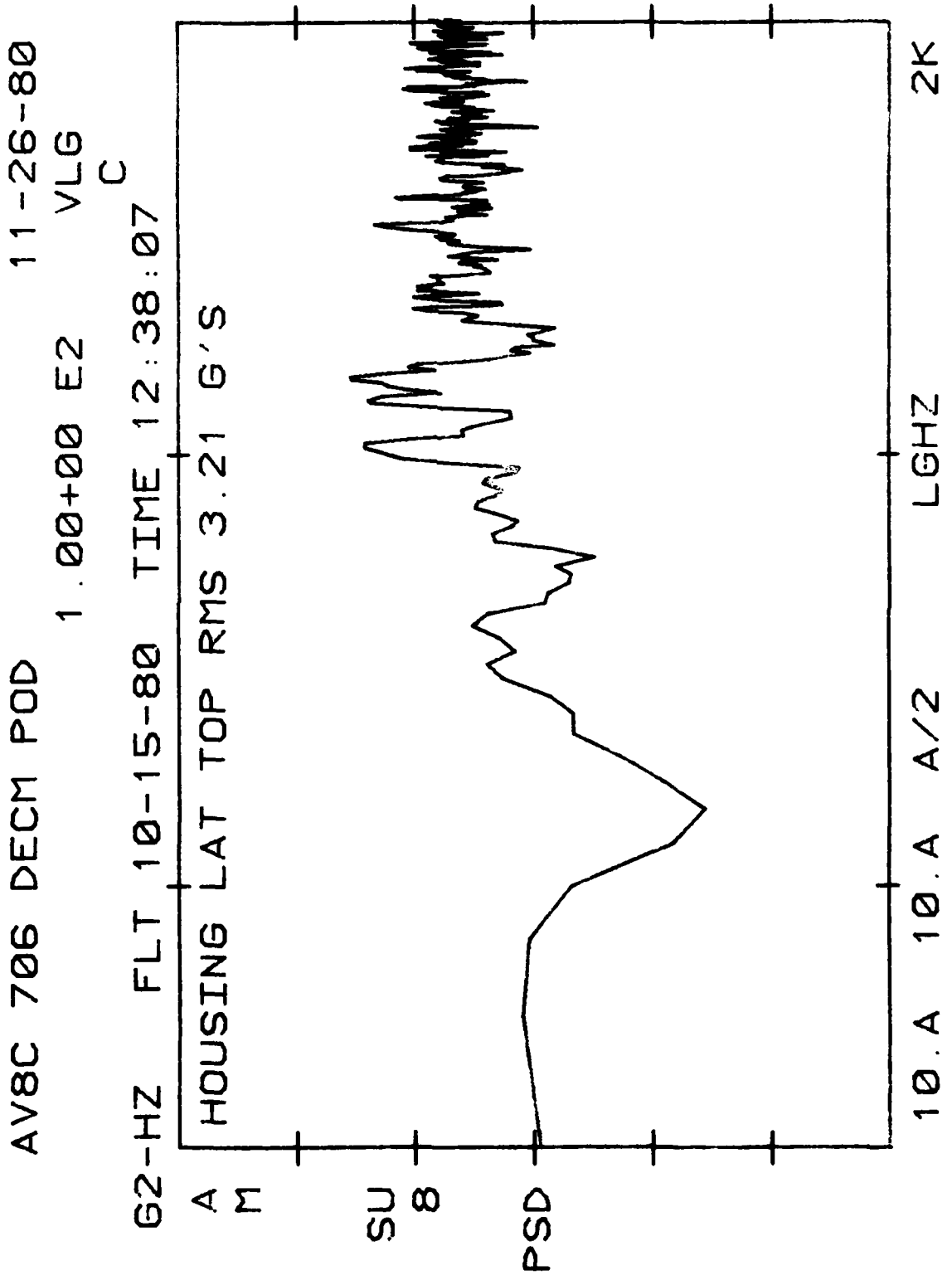

Figure 25
Short Takeoff (Wet), Initial Portion of Takeoff Roll, PSD

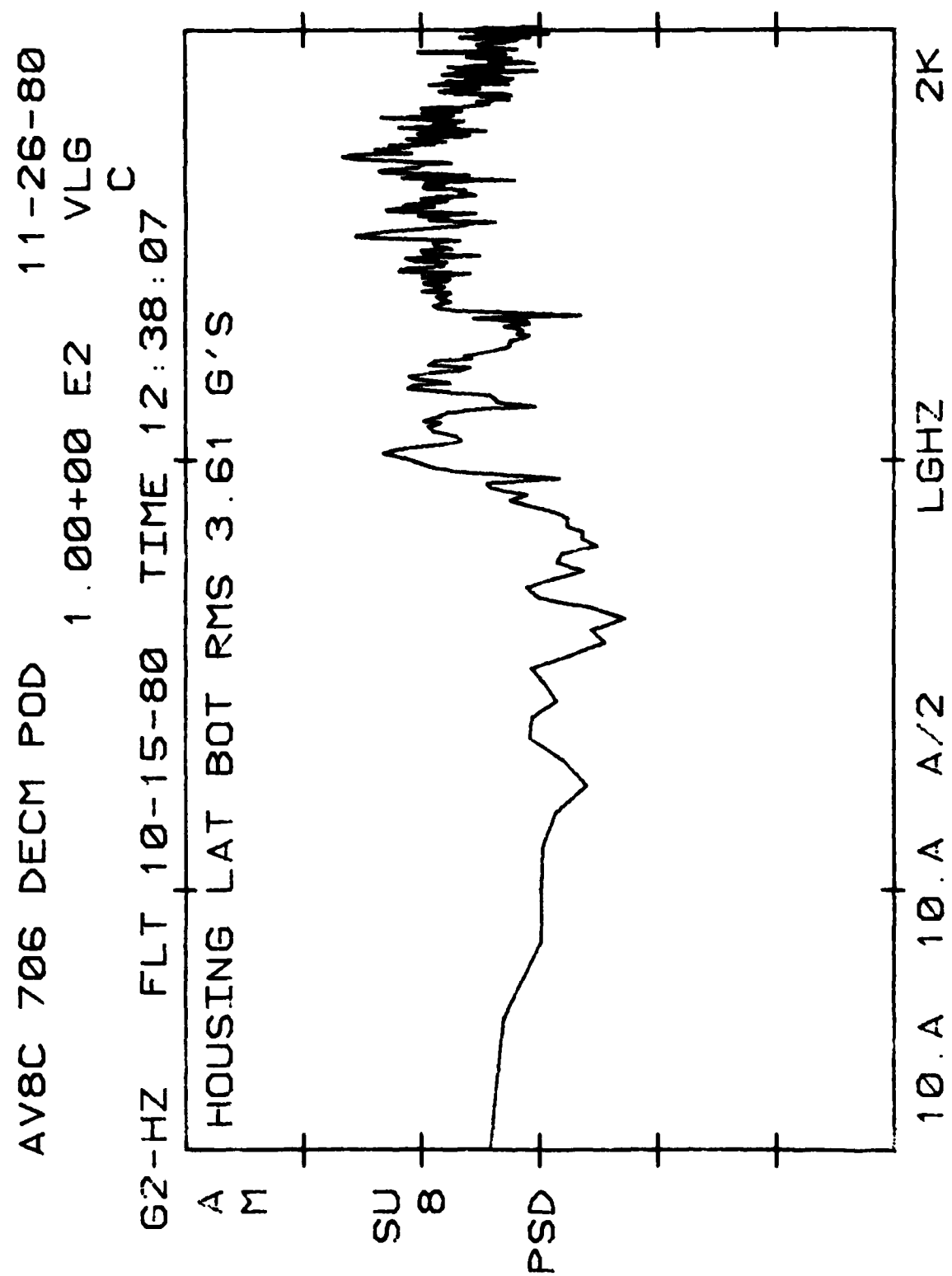

Figure 25 (Cont'd)

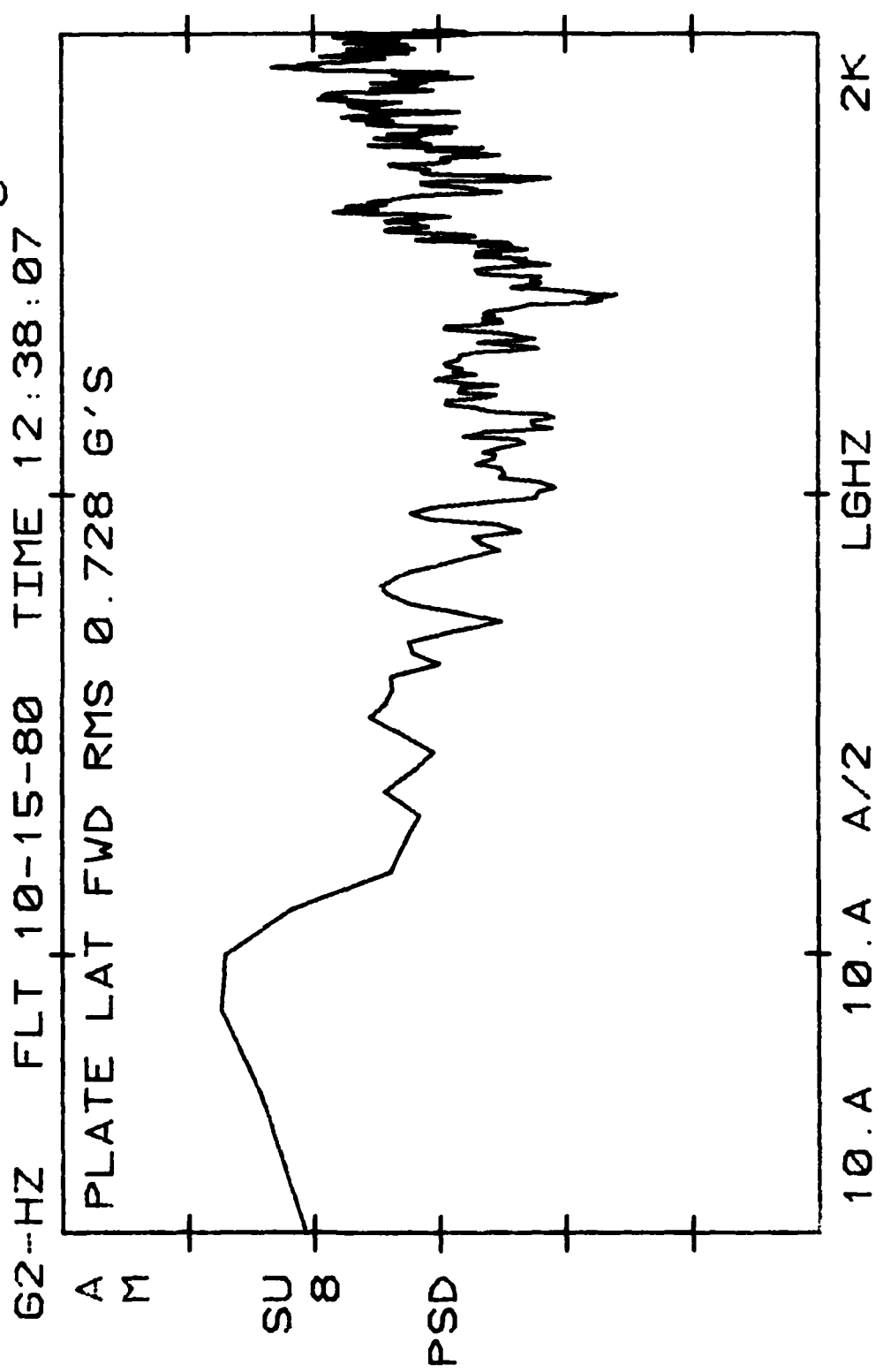

Figure 25 (Cont'd)

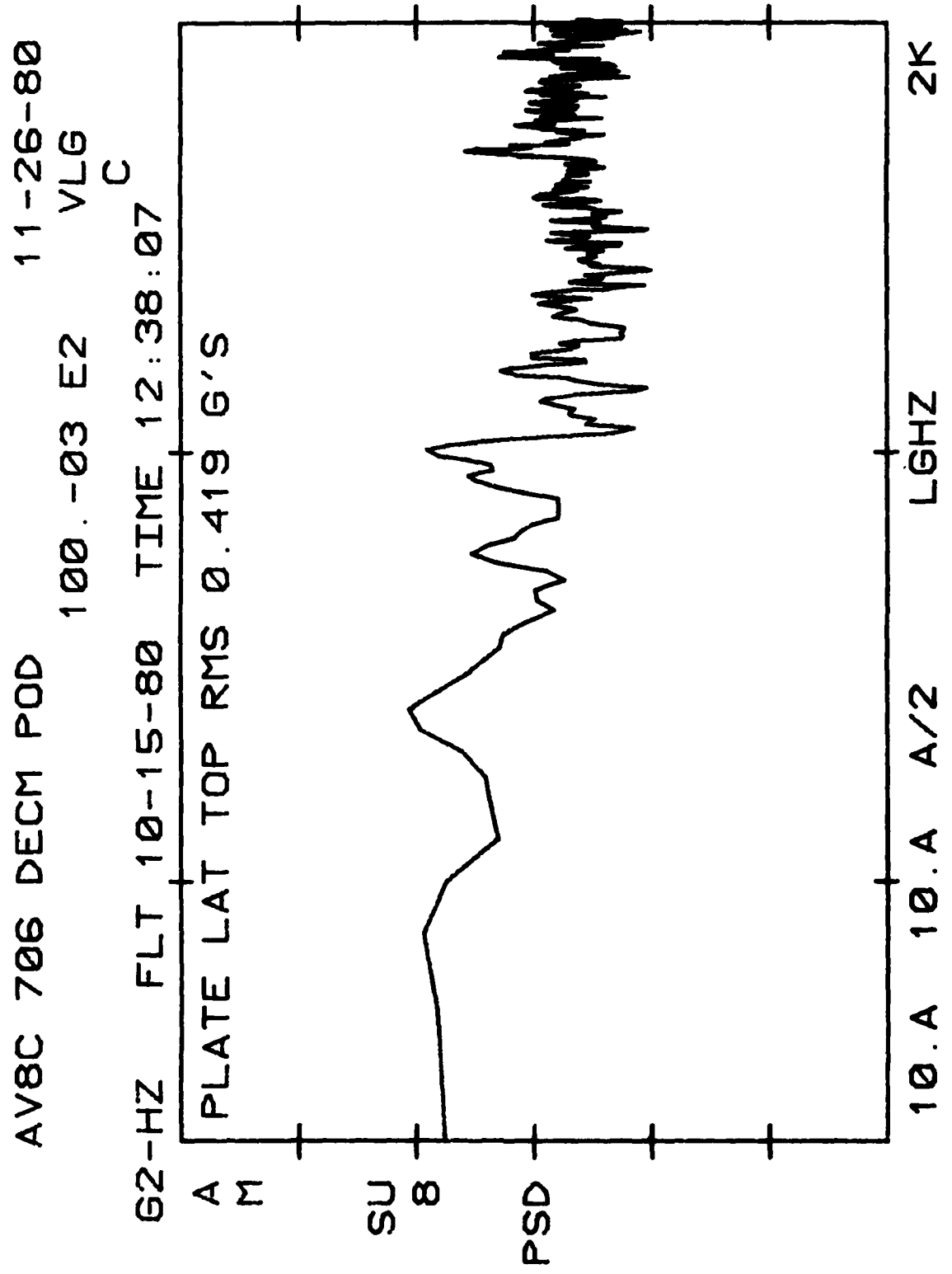

Figure 25 (Cont'd)

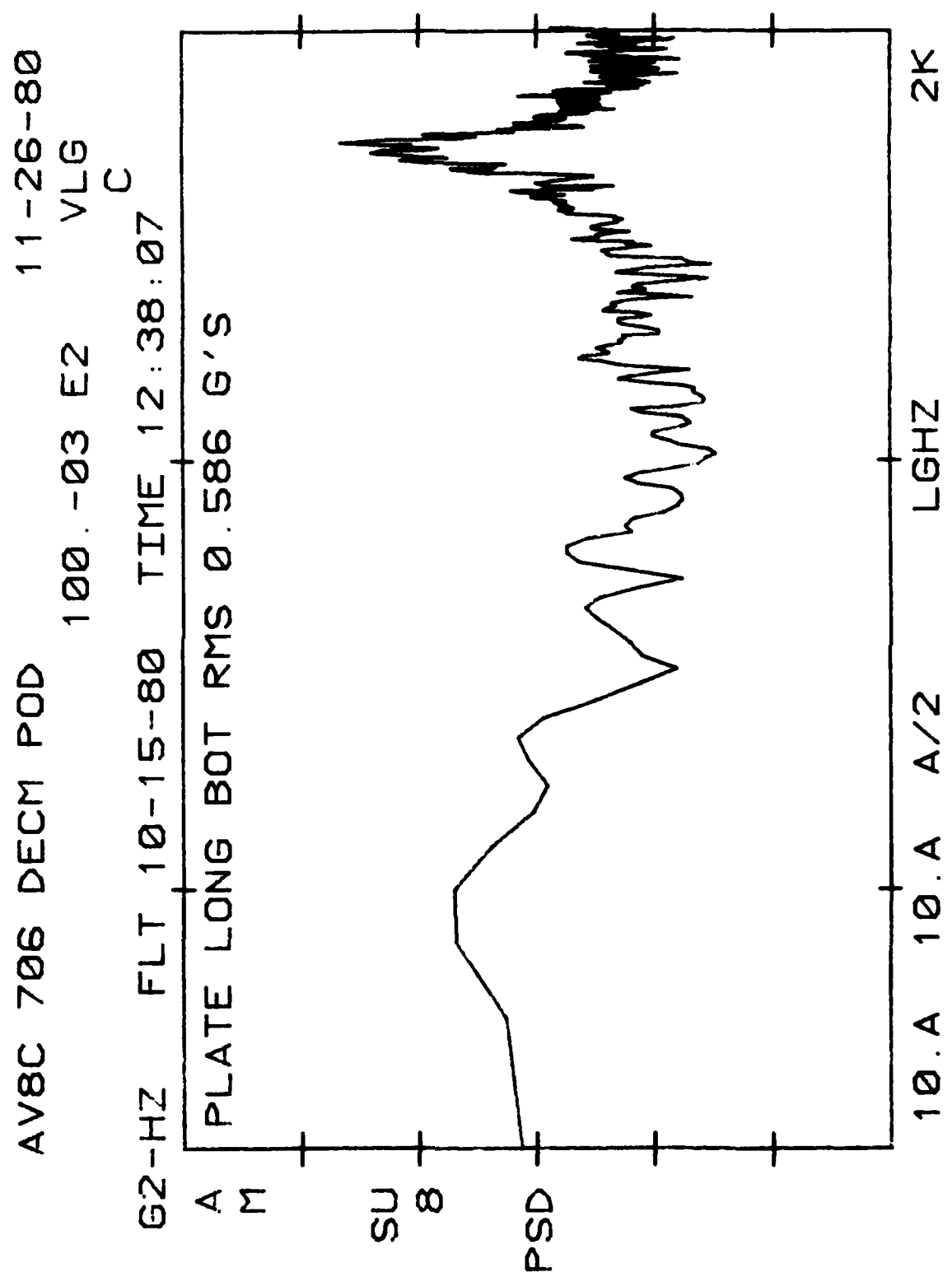

Figure 25 (Cont'd)

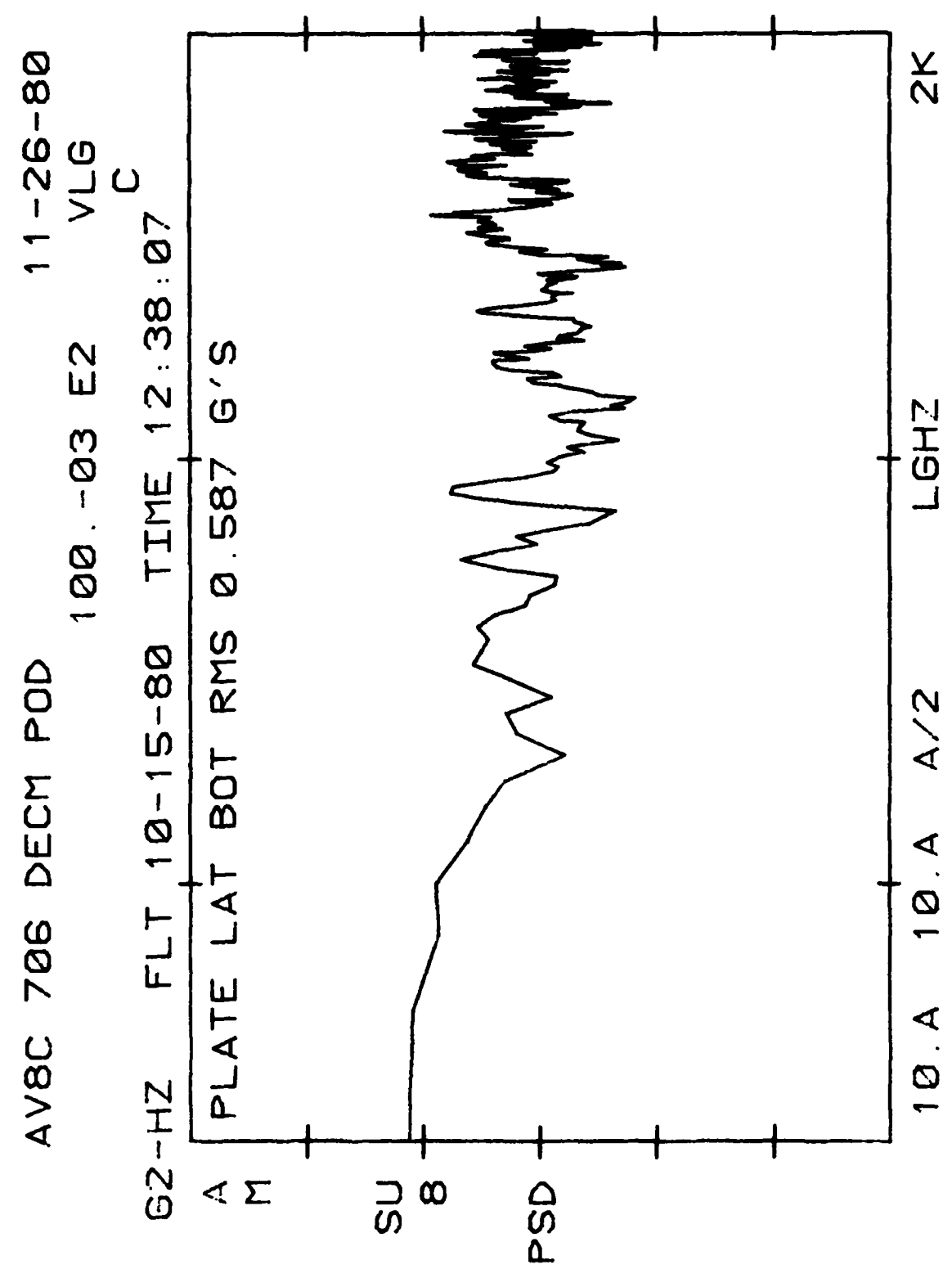

Figure 25 (Cont'd)

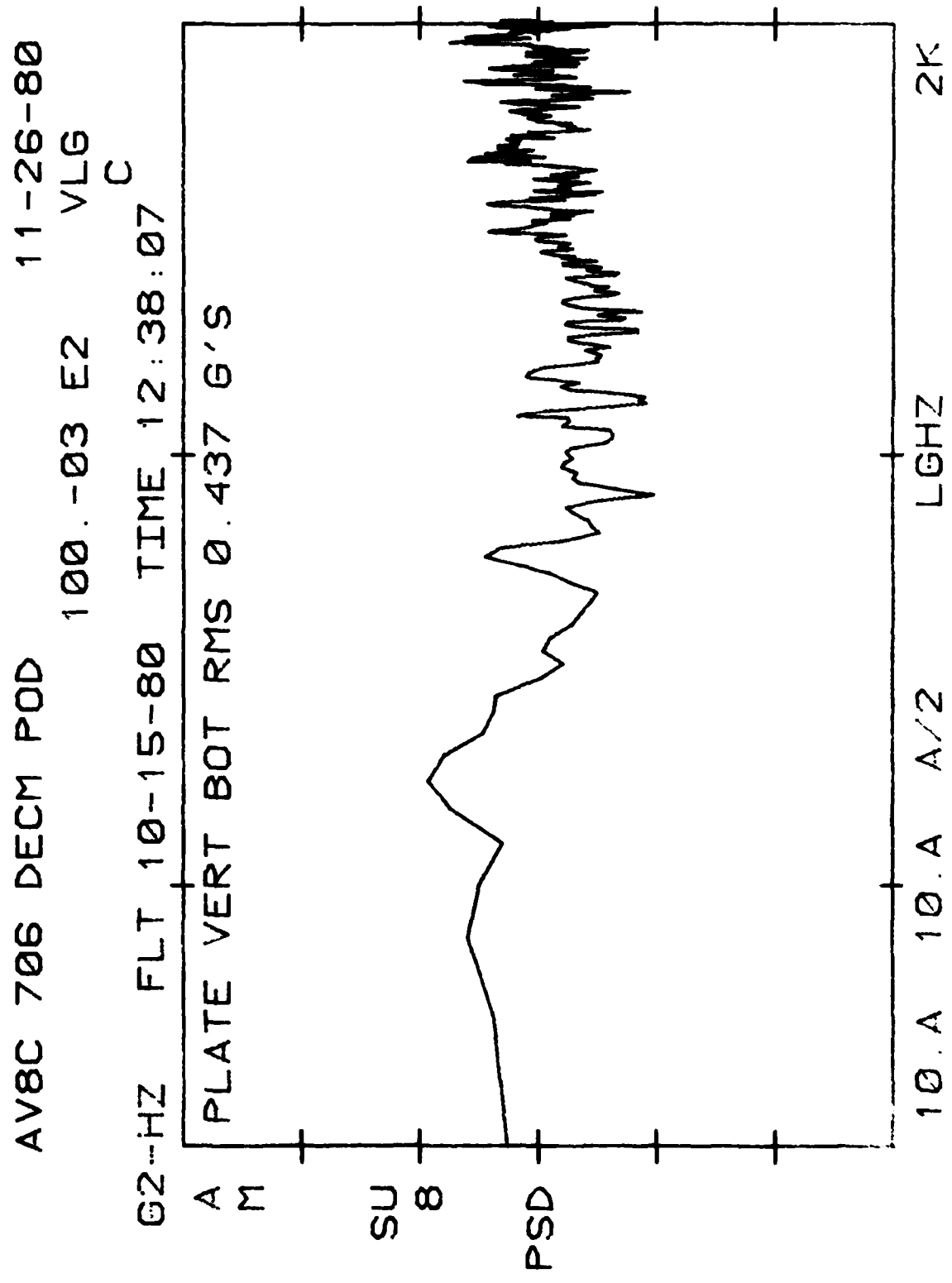

Figure 25 (Cont'd)

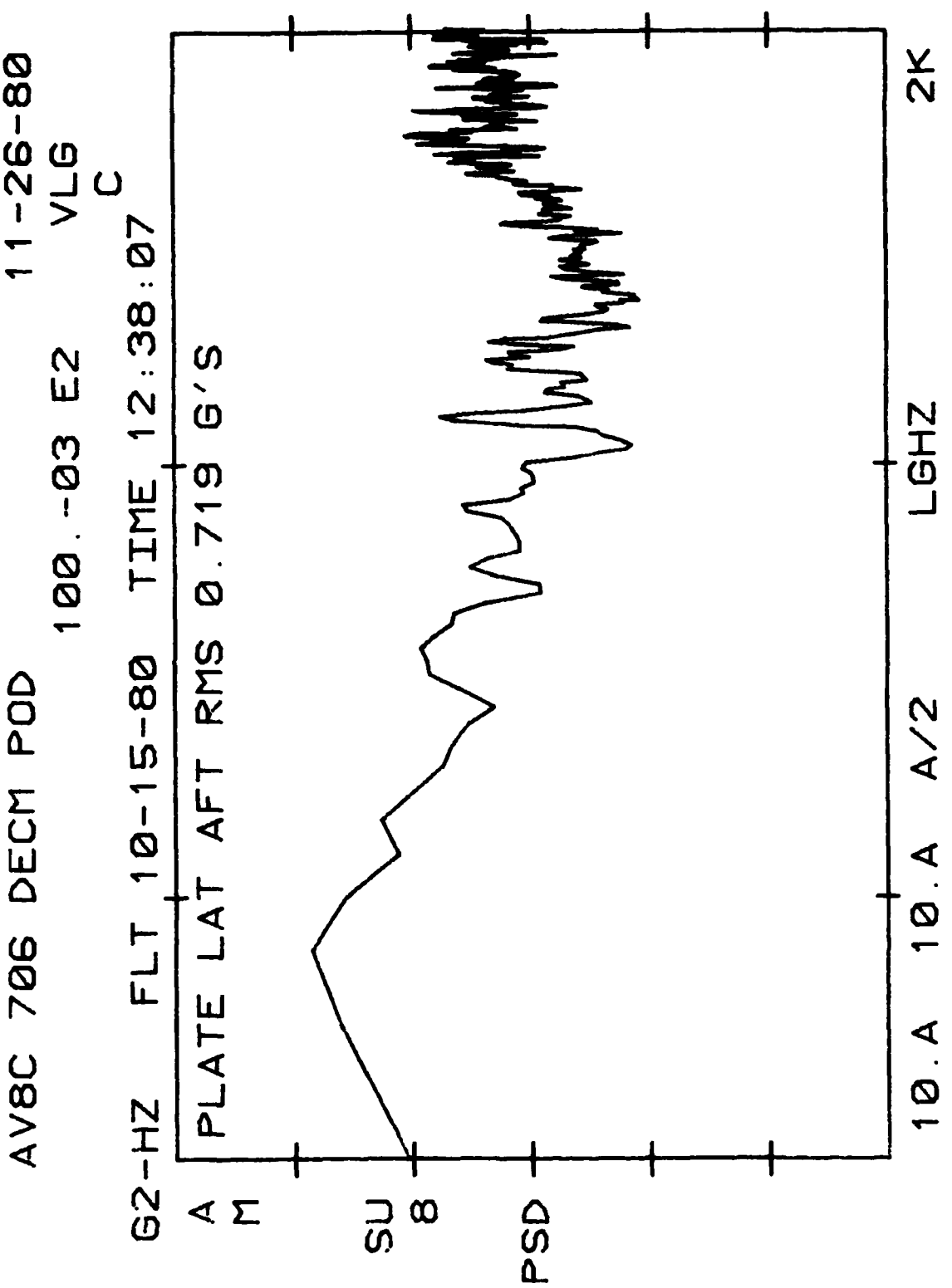

Figure 25 (Cont'd)

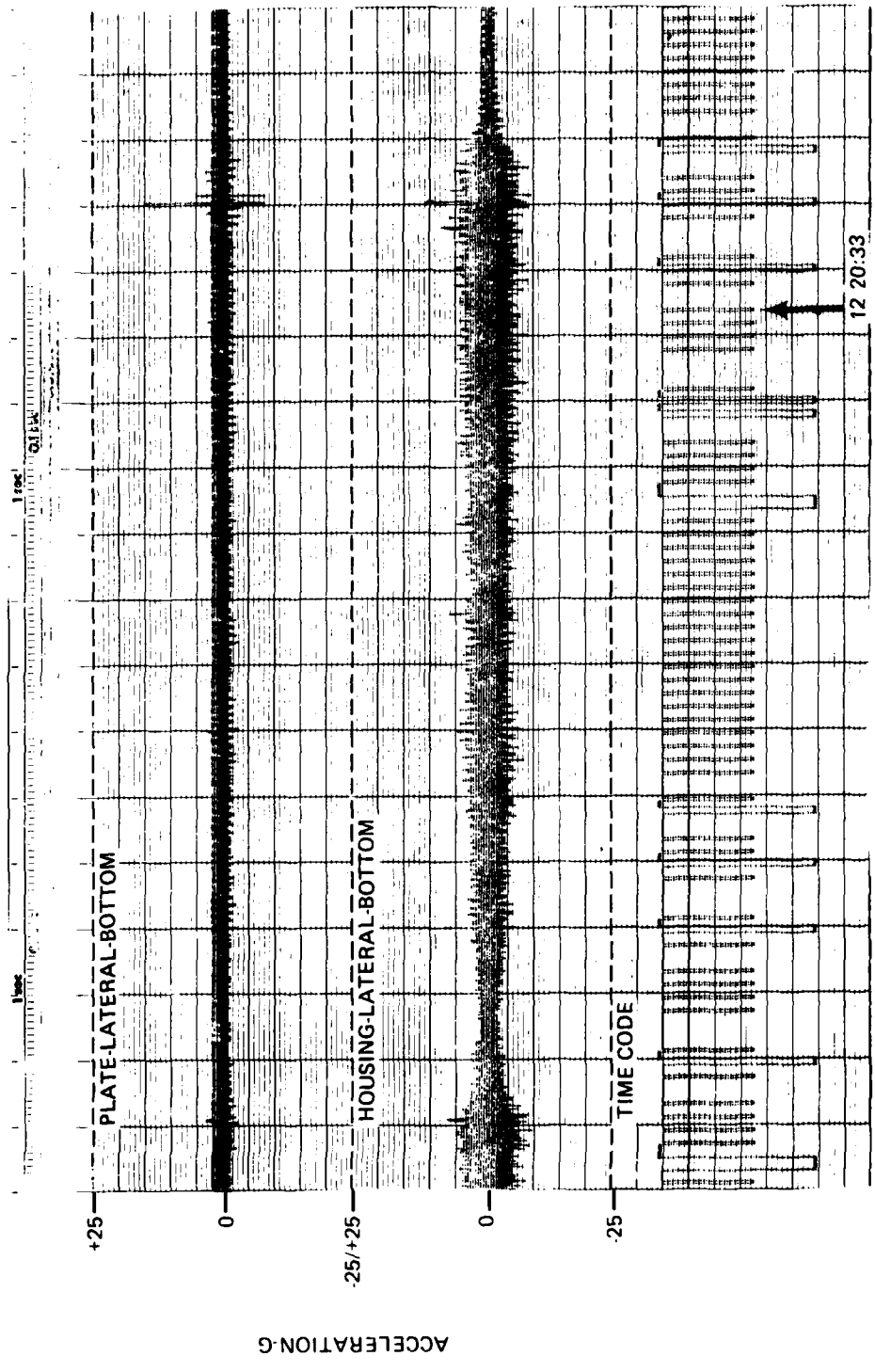

Figure 26
Short Landing (with Nozzle Braking), Time History

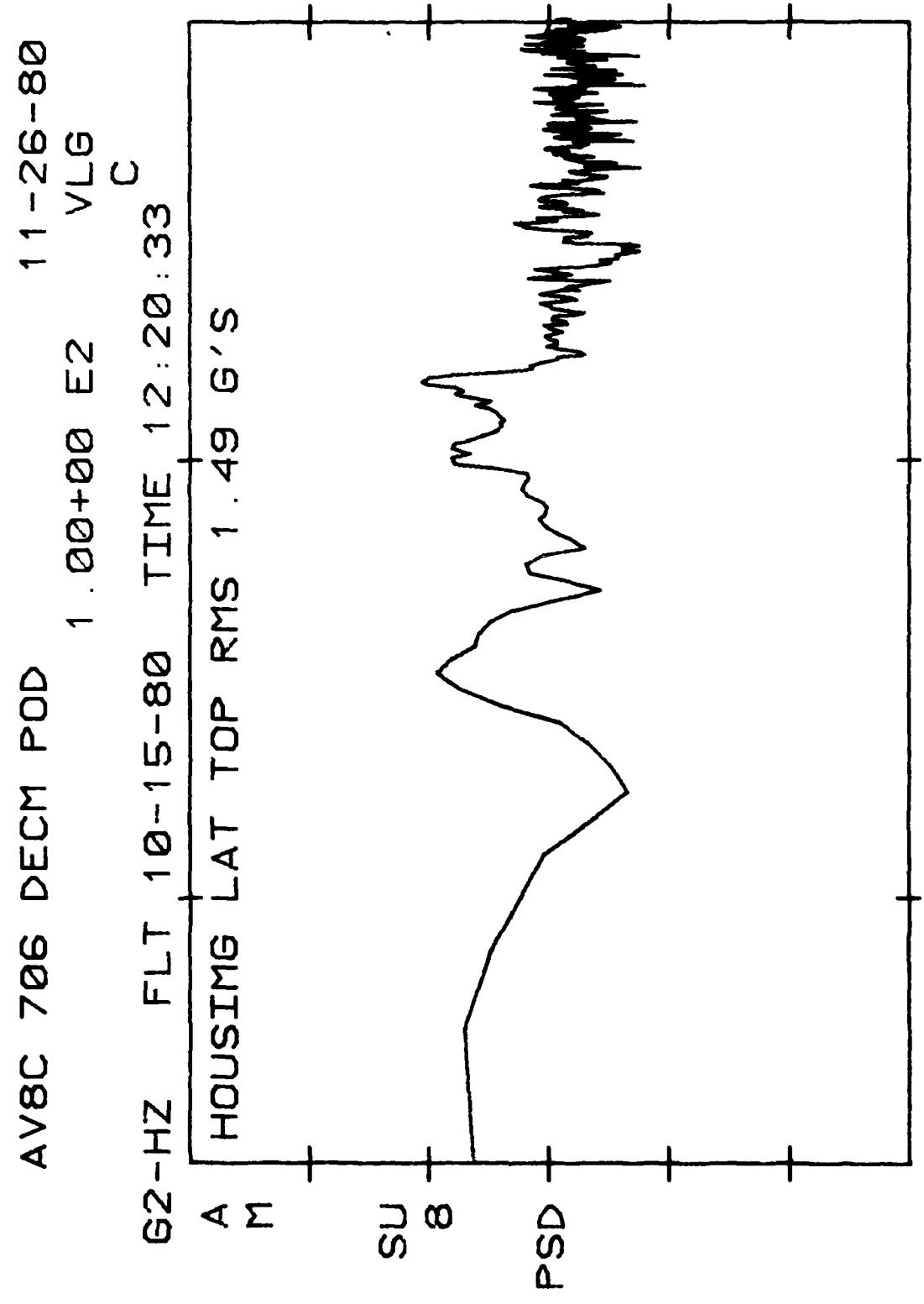

Figure 27
Short Landing (with Nozzle Braking), PSD

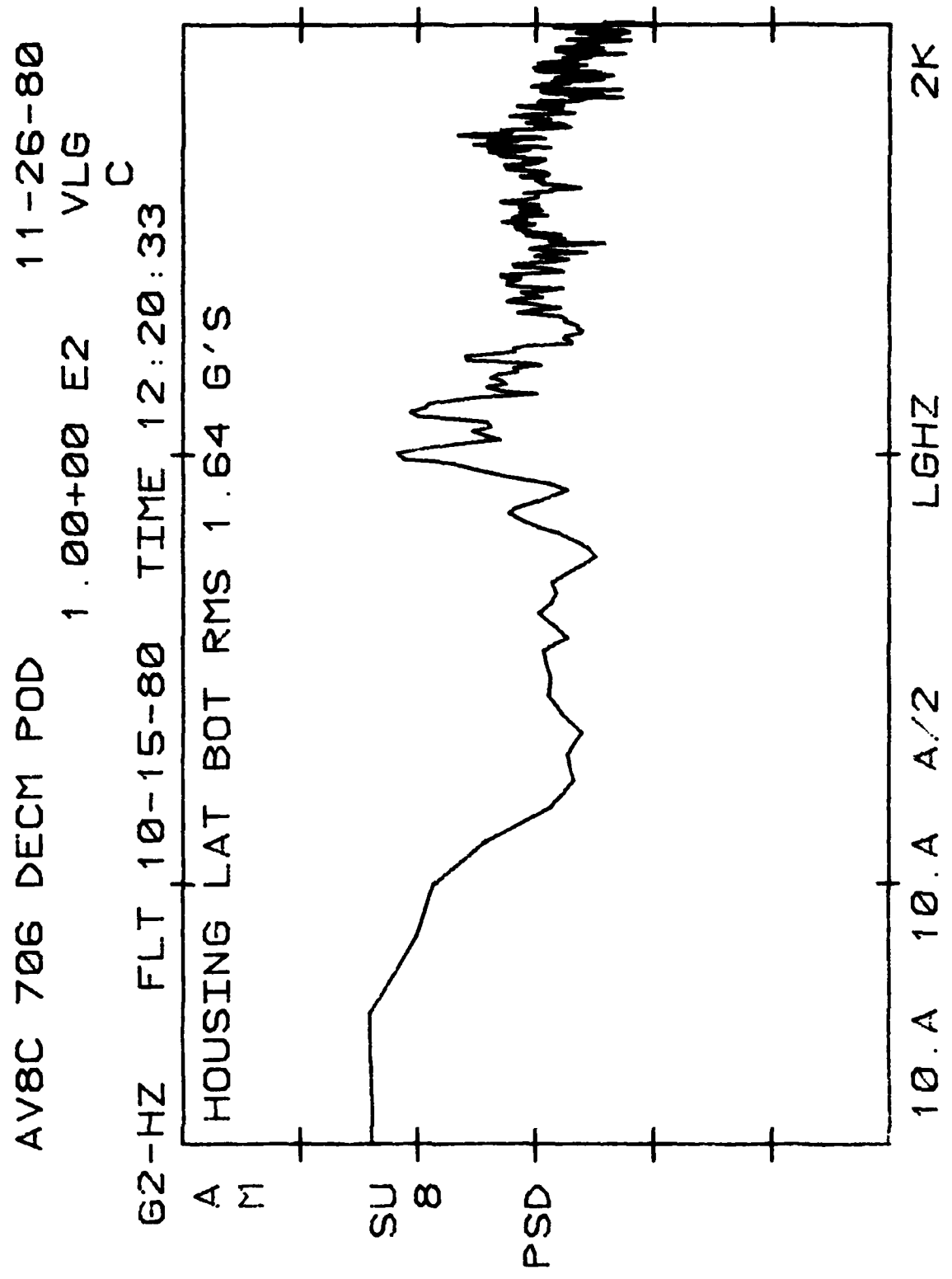

Figure 27 (Cont'd)

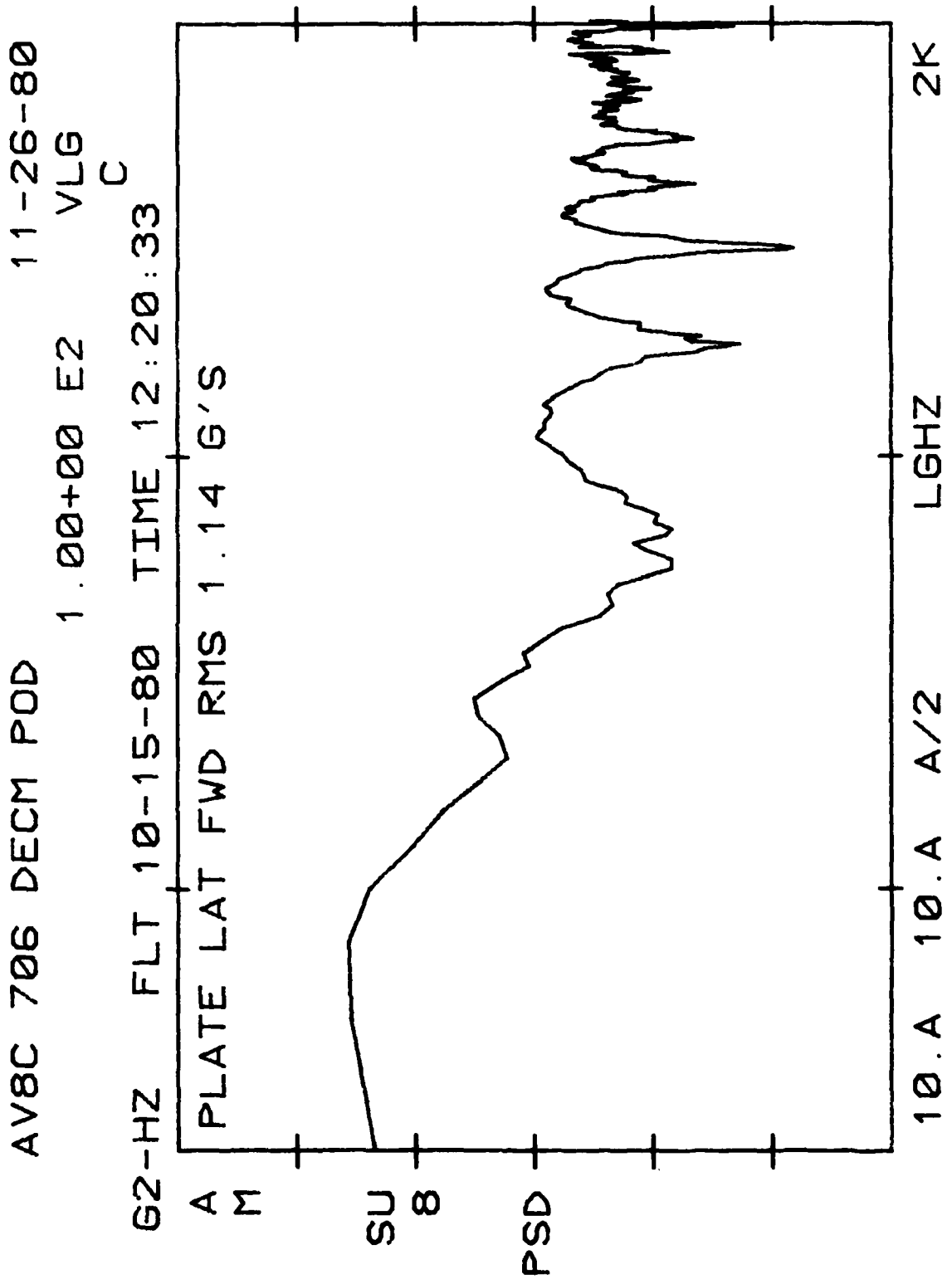

Figure 27 (Cont'd)

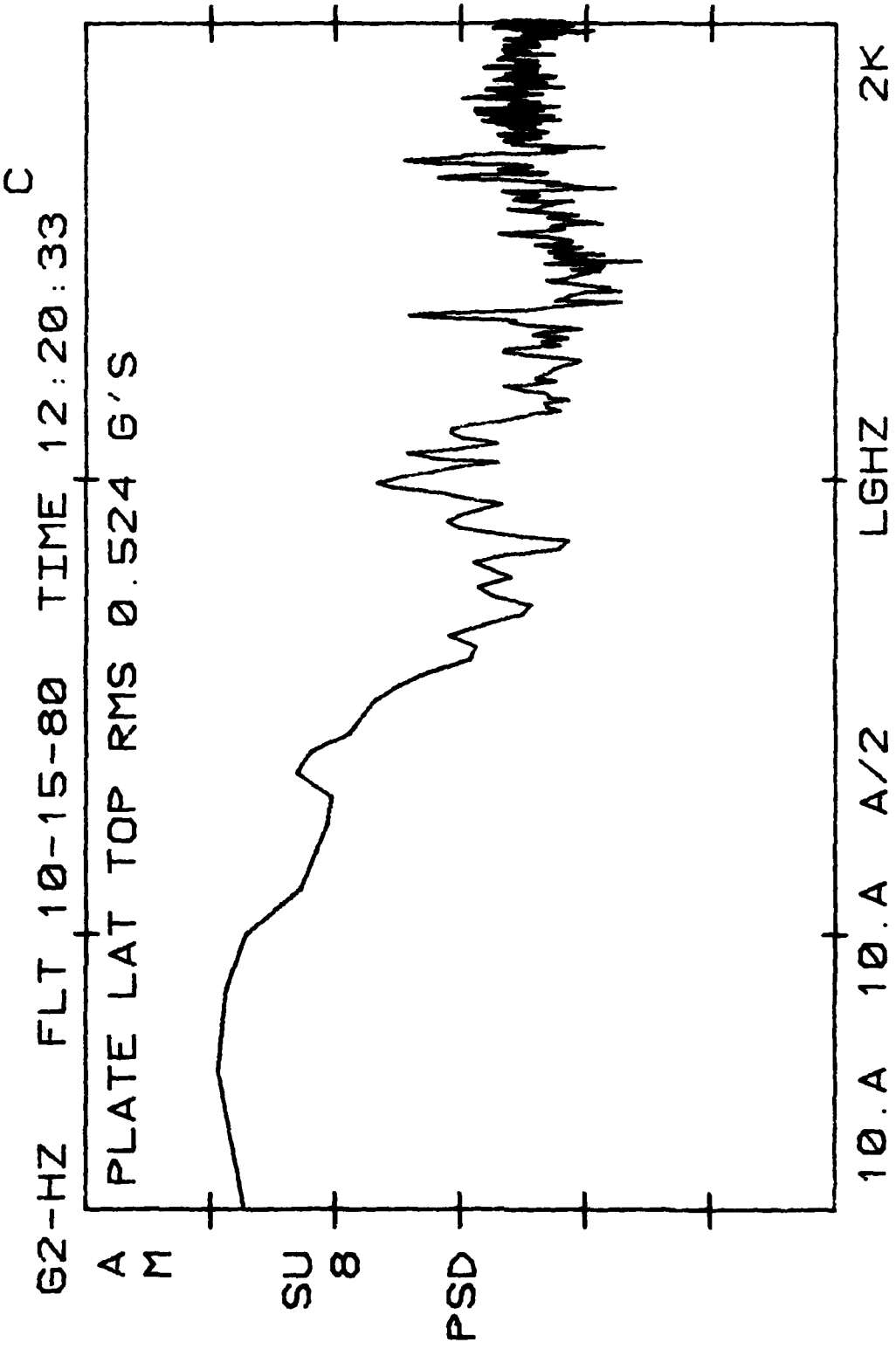

Figure 27 (Cont'd)

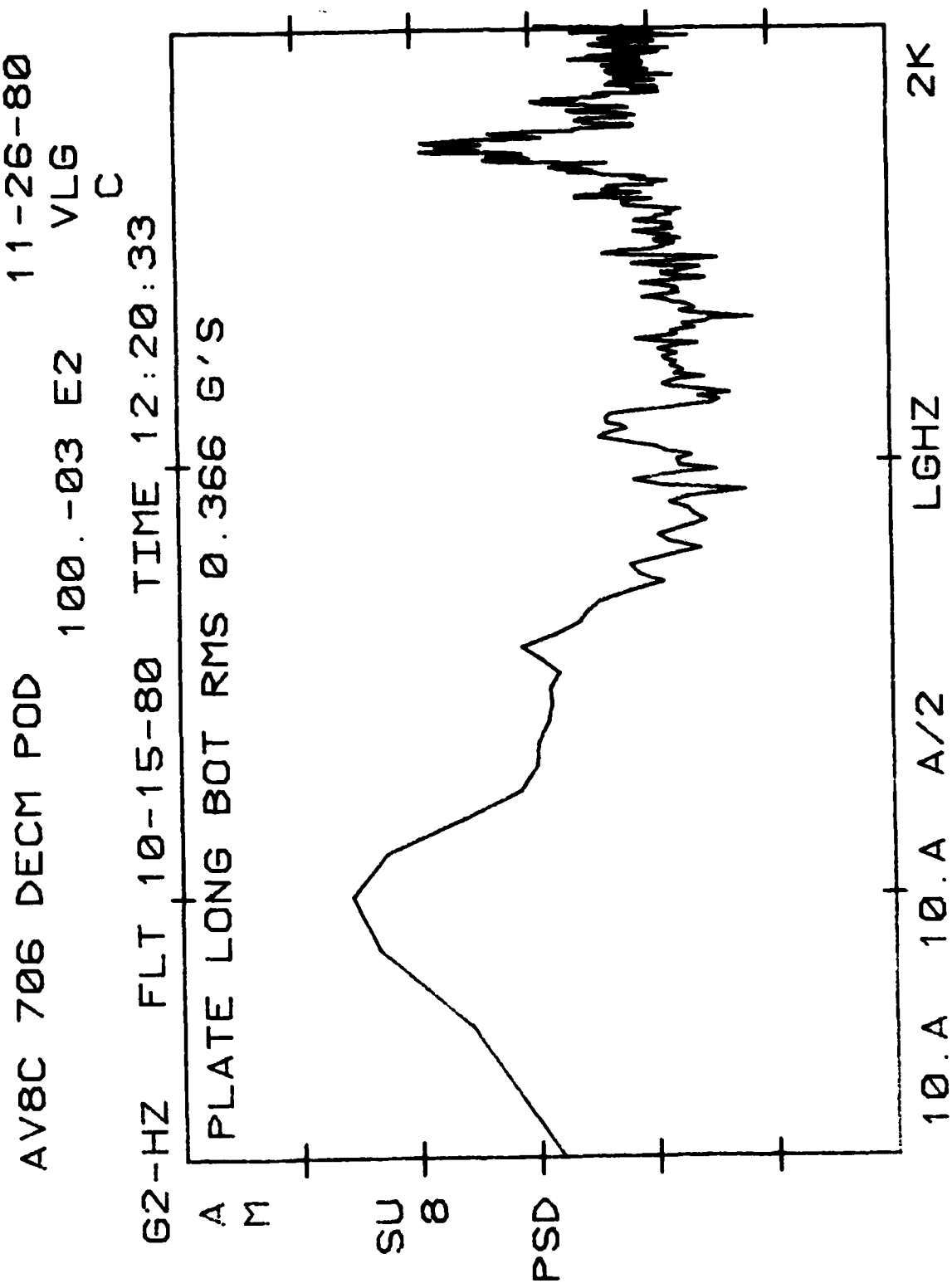

Figure 27 (Cont'd)

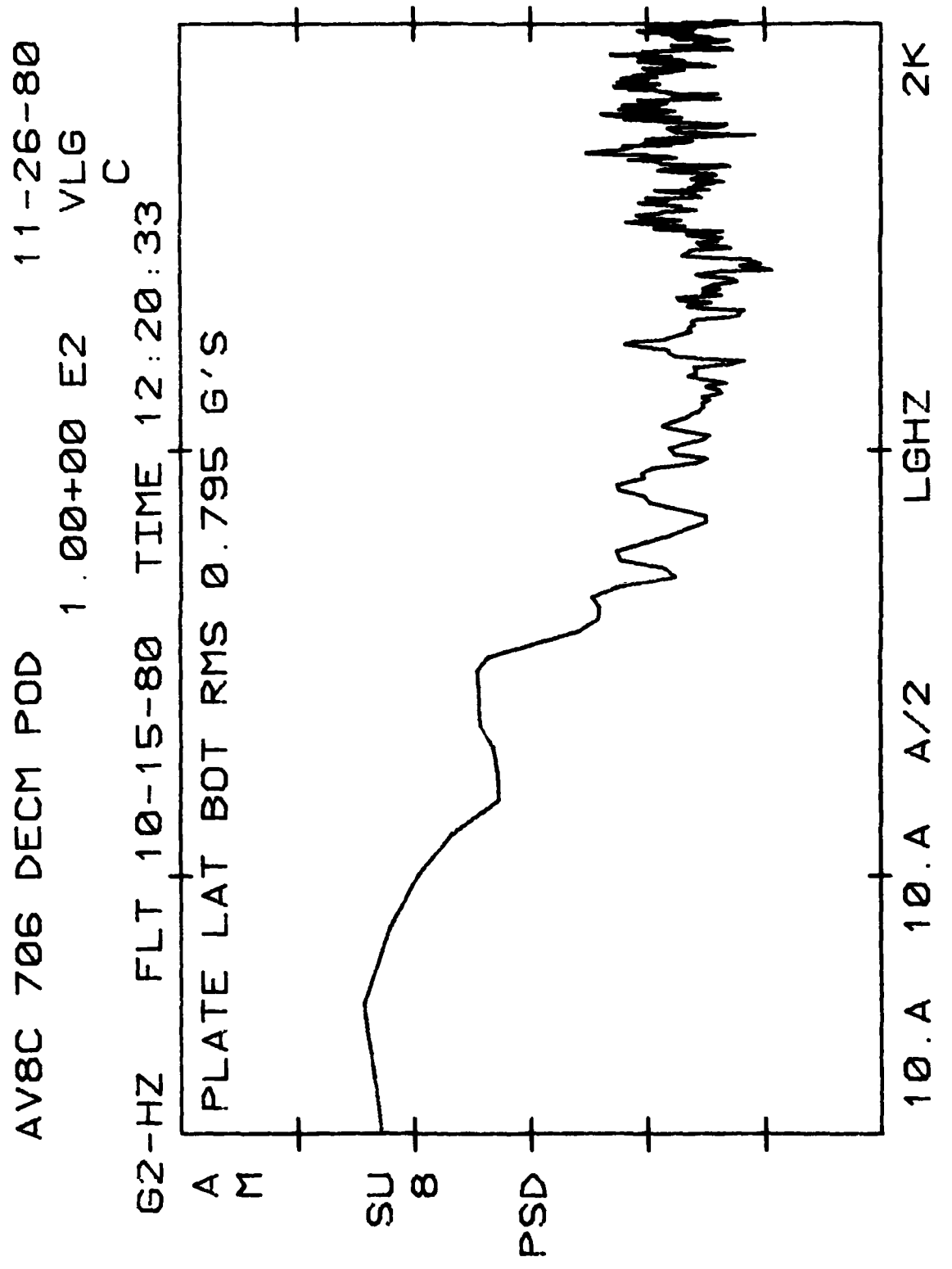

Figure 27 (Cont'd)

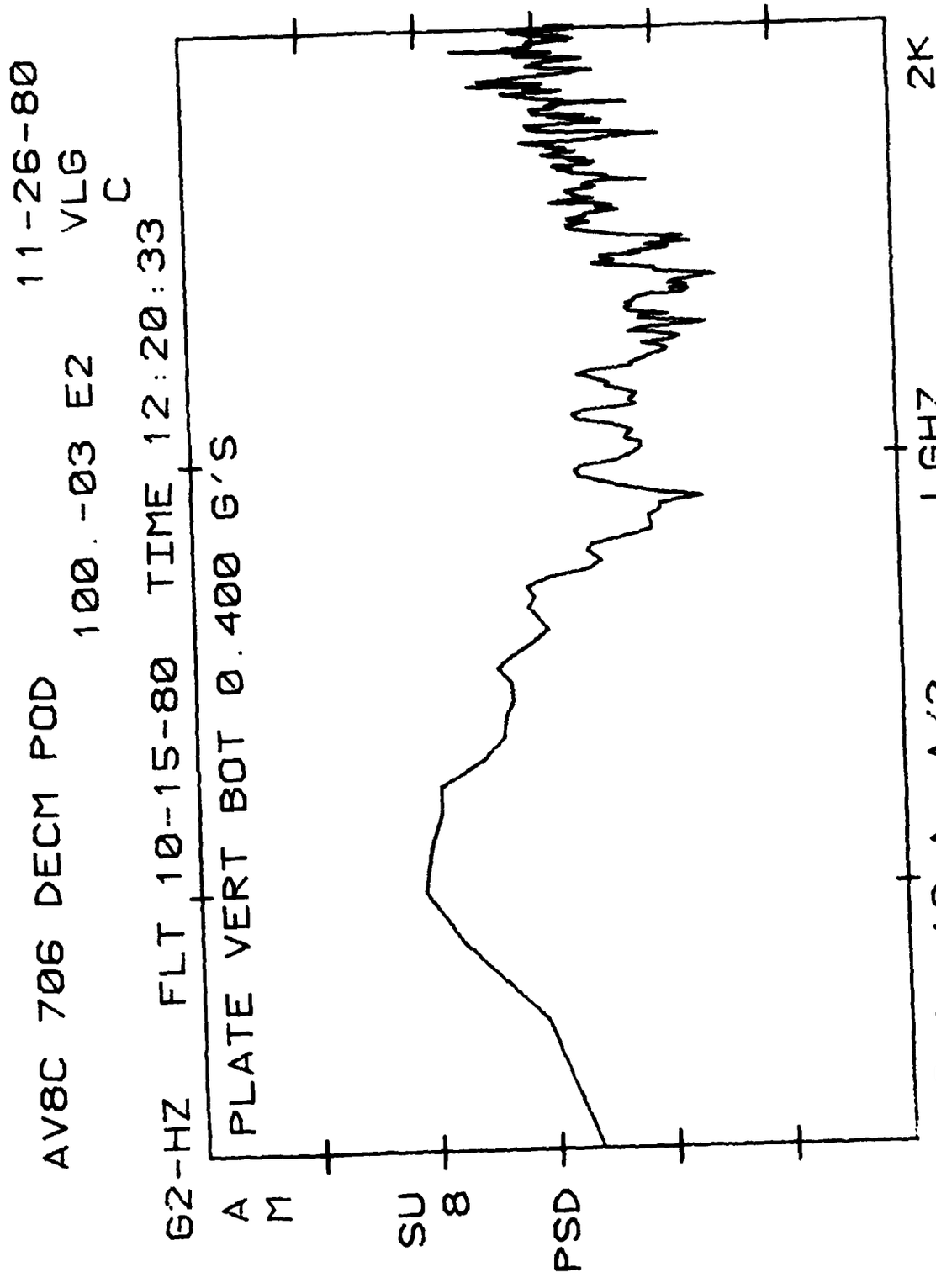

Figure 27 (Cont'd)

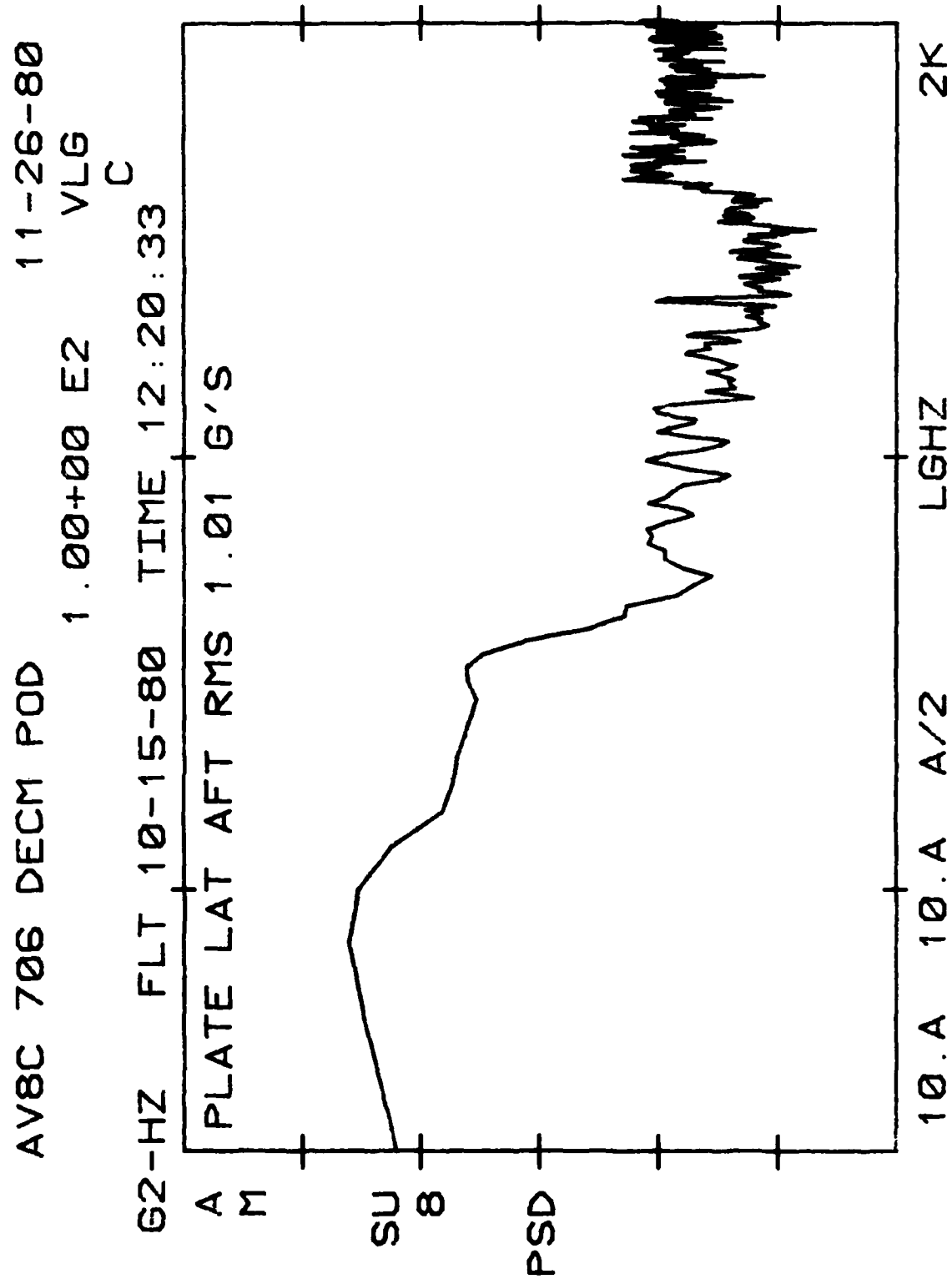

Figure 27 (Cont'd)

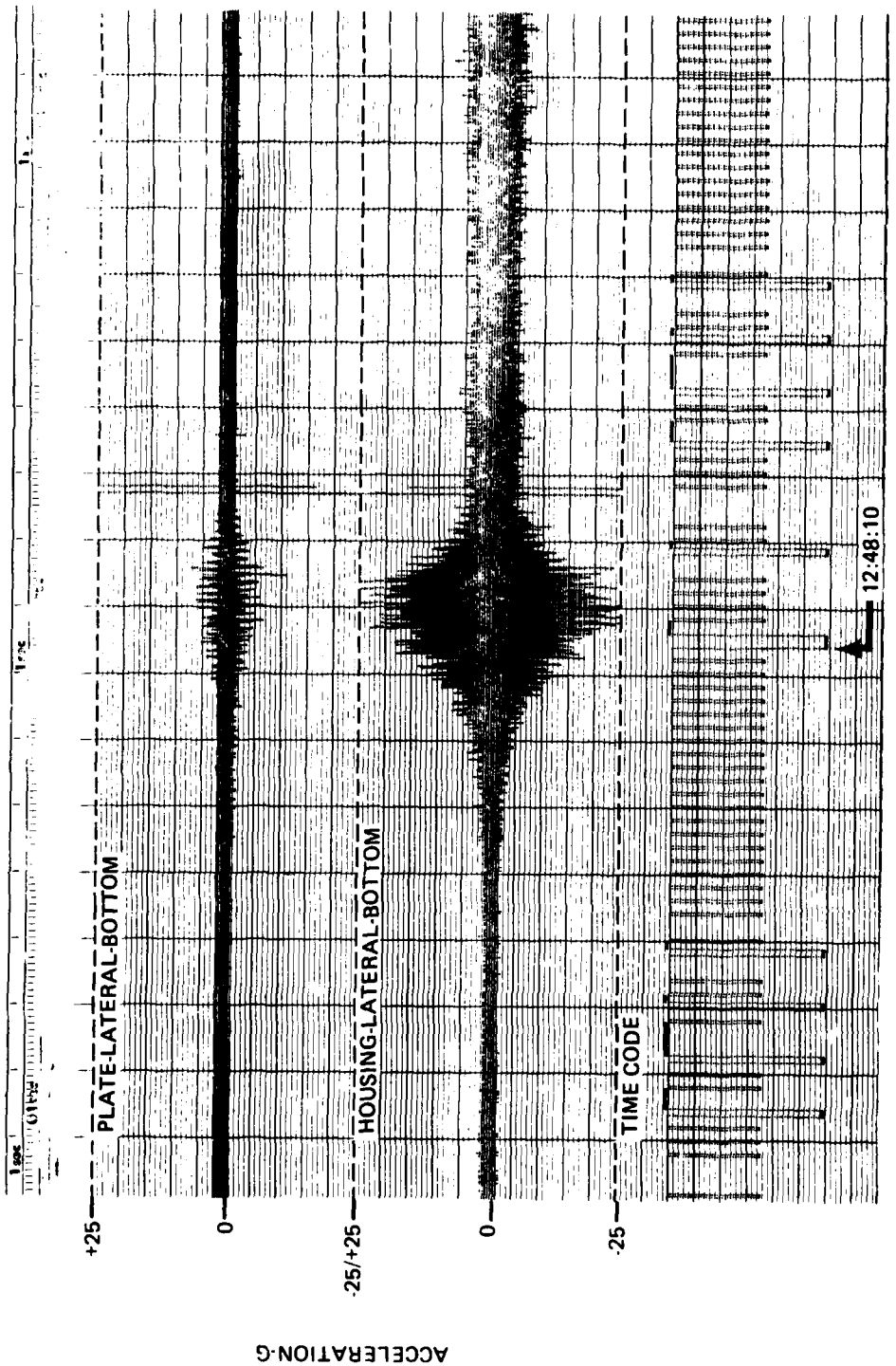

Figure 28
Vertical Takeoff, Time History

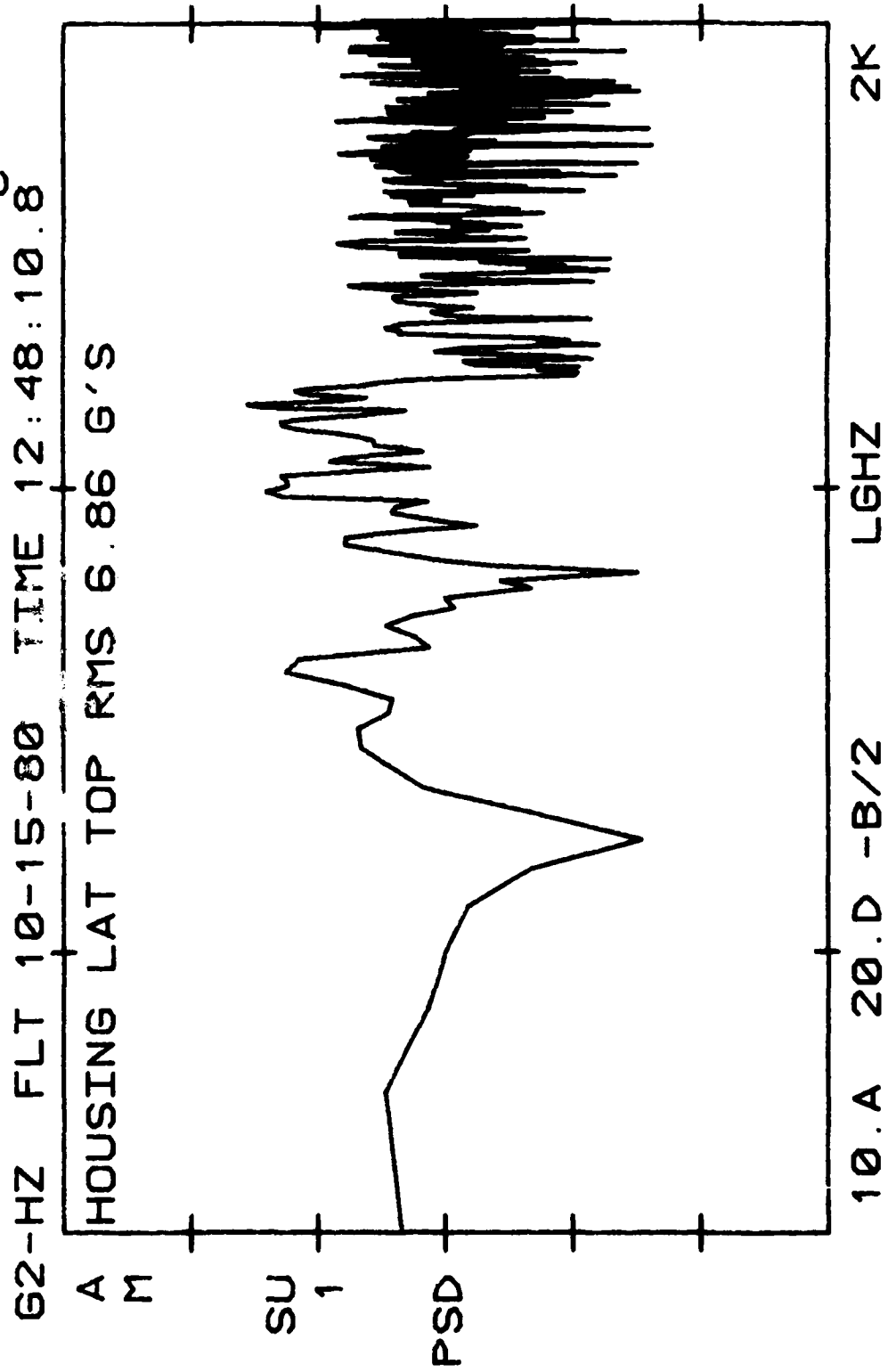

Figure 29
Vertical Takeoff, PSD

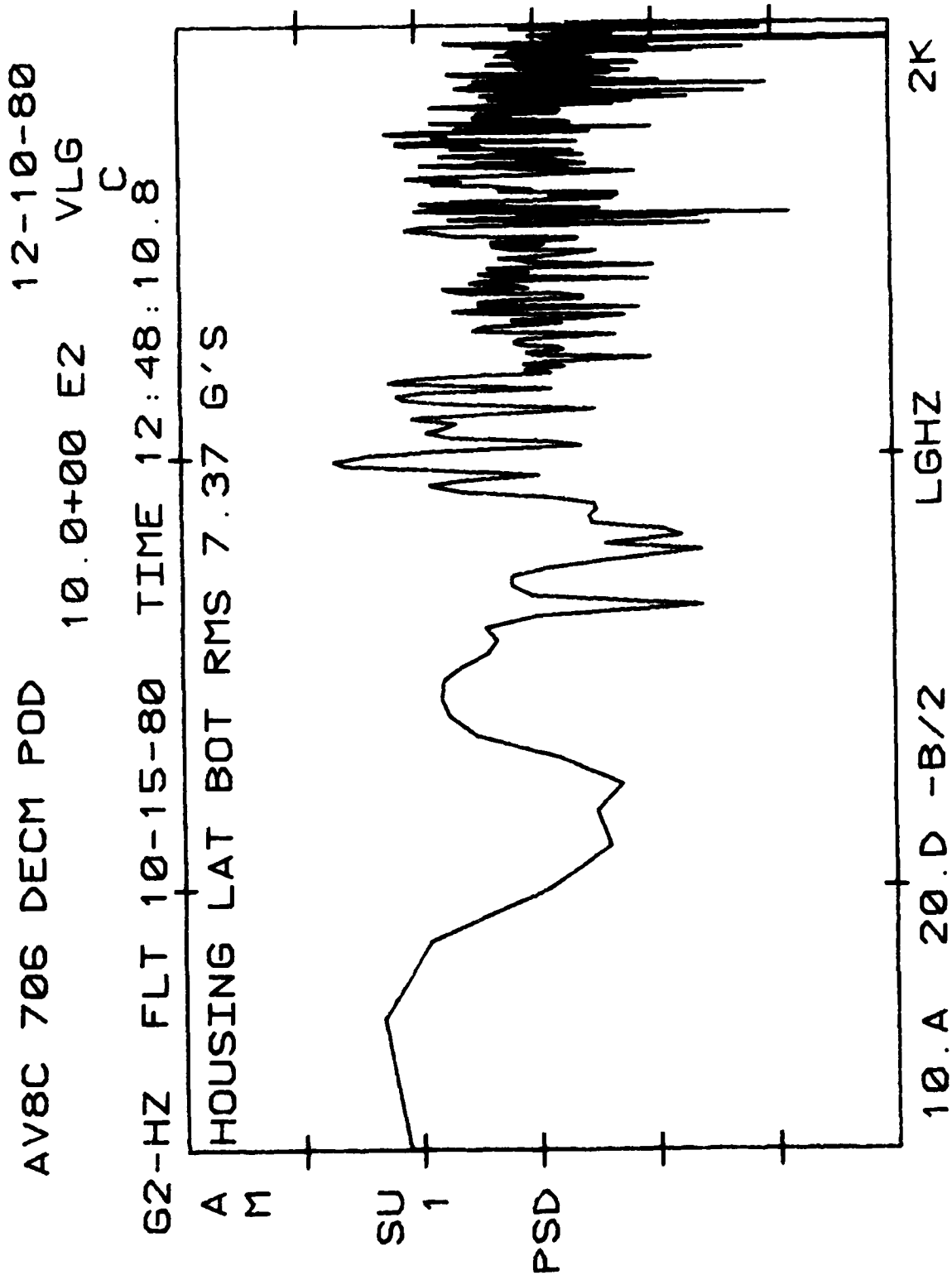

Figure 29 (Cont'd)

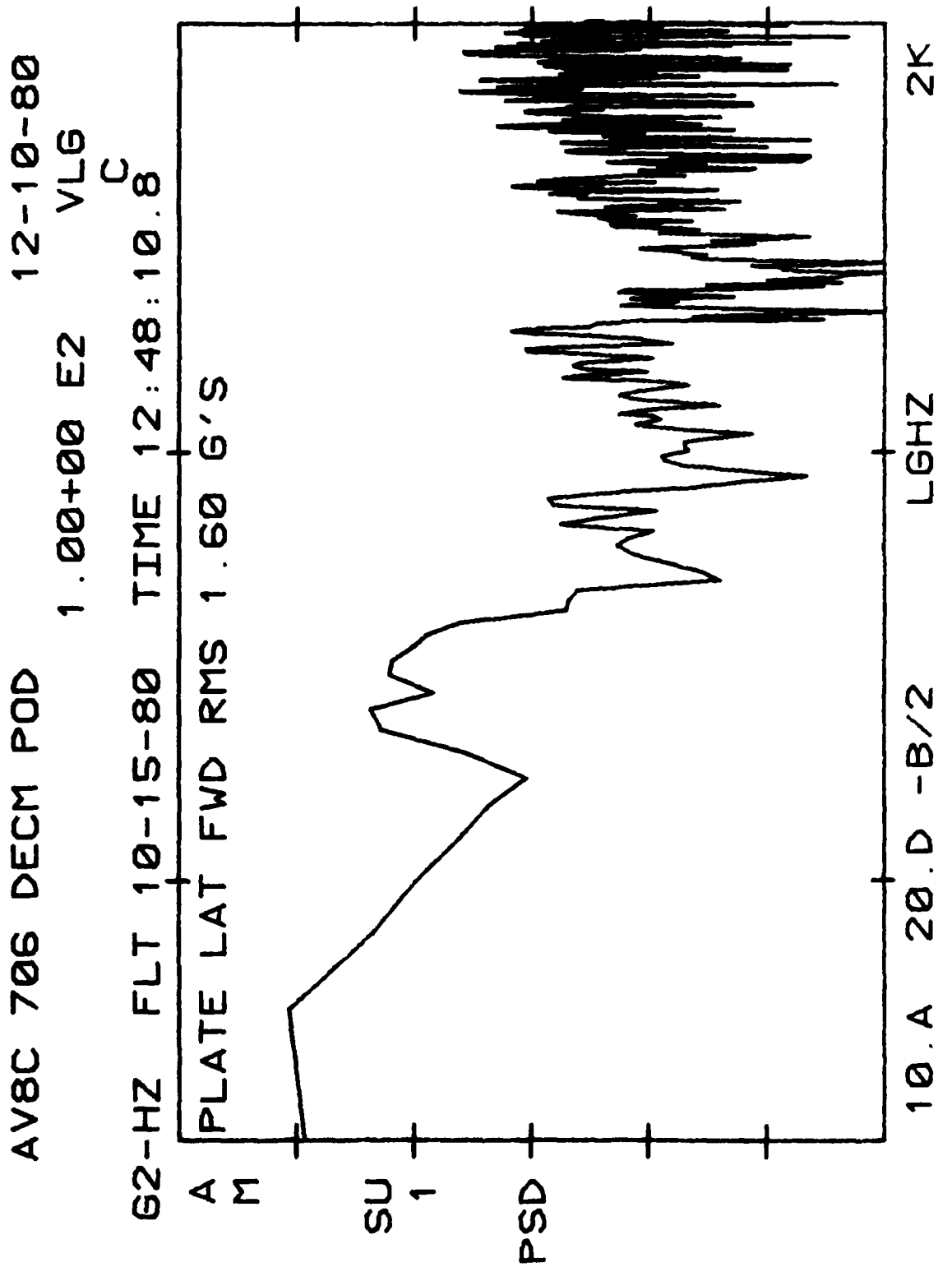

Figure 29 (Cont'd)

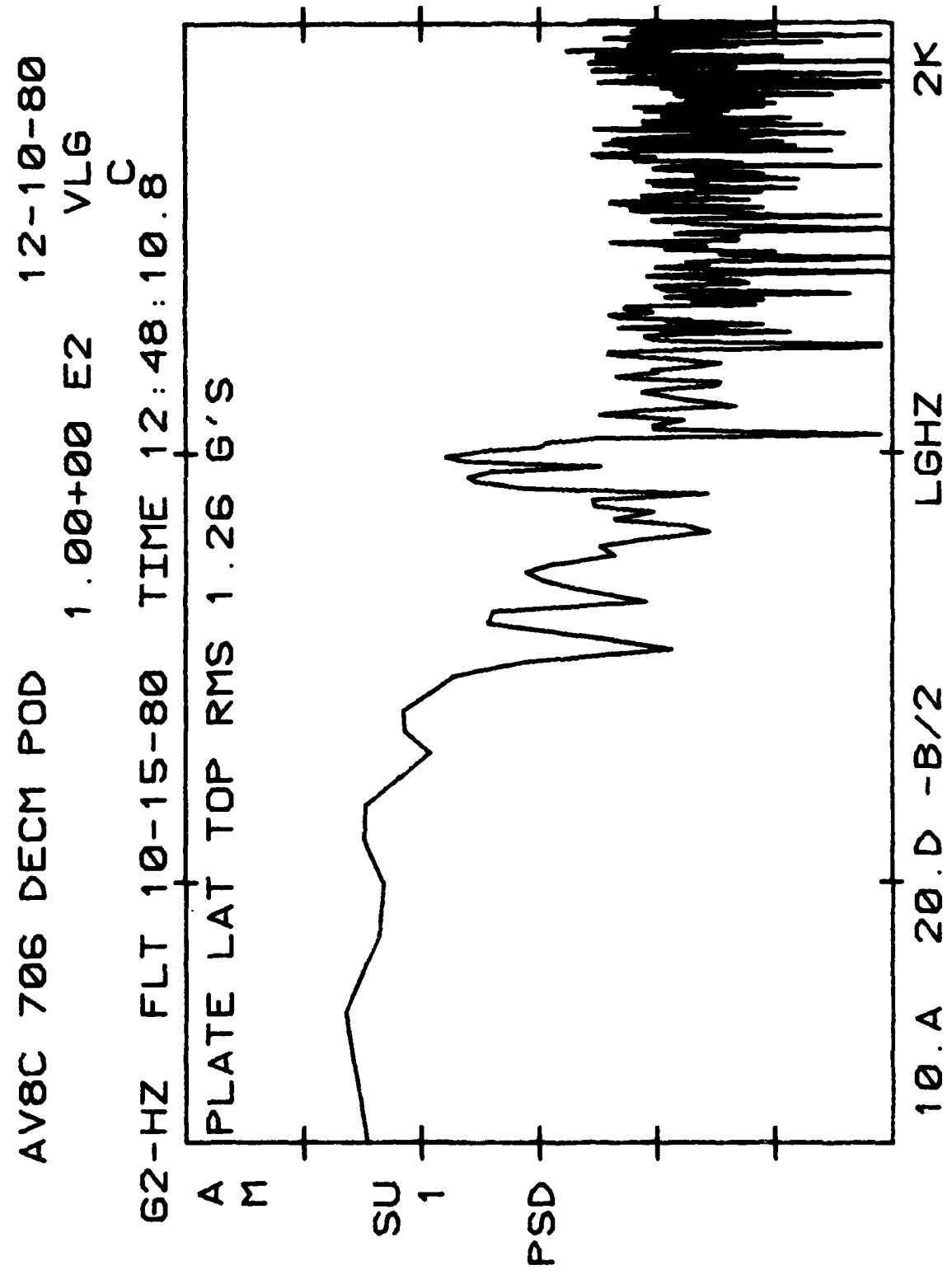

Figure 29 (Cont'd)

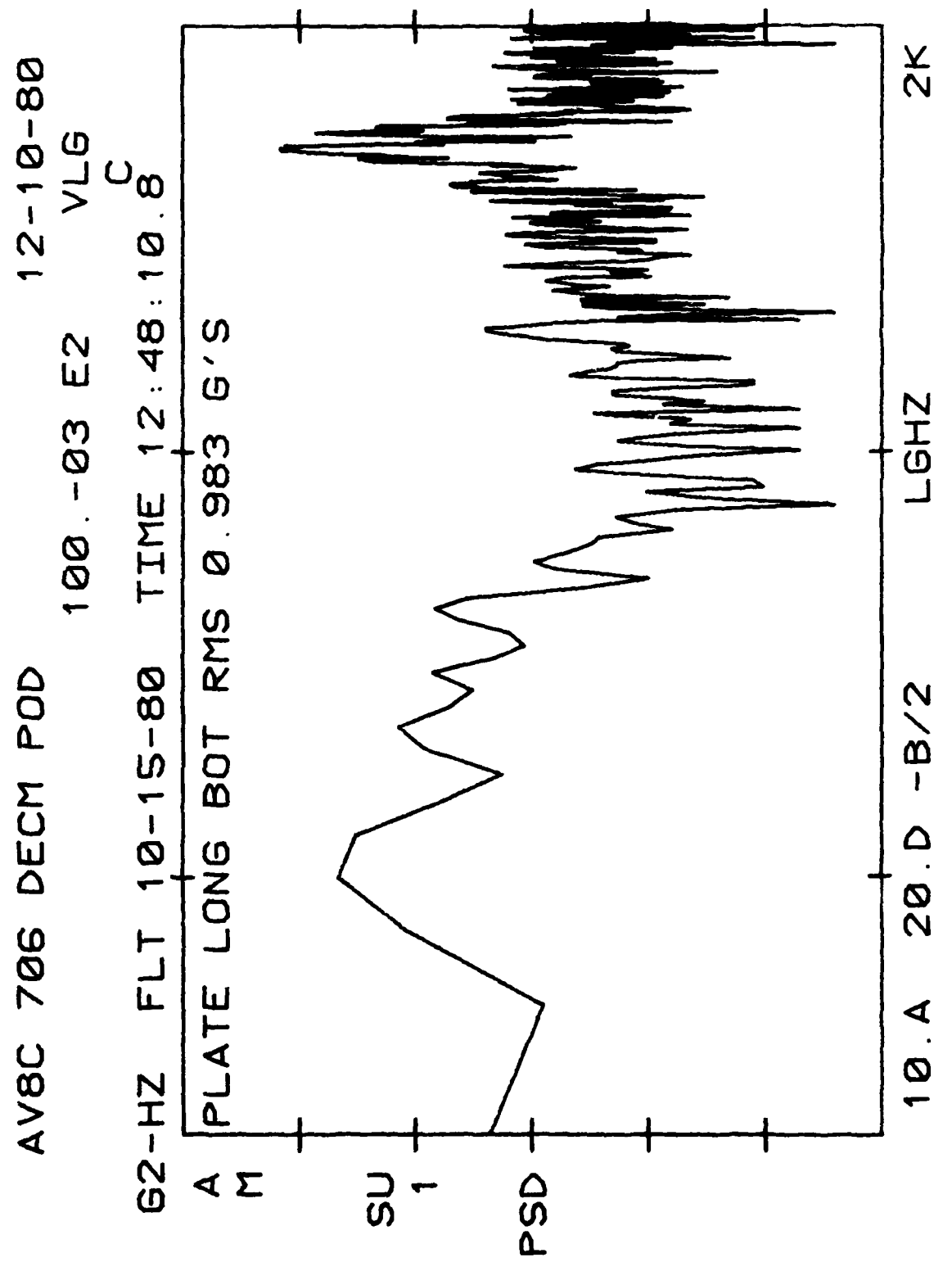

Figure 29 (Cont'd)

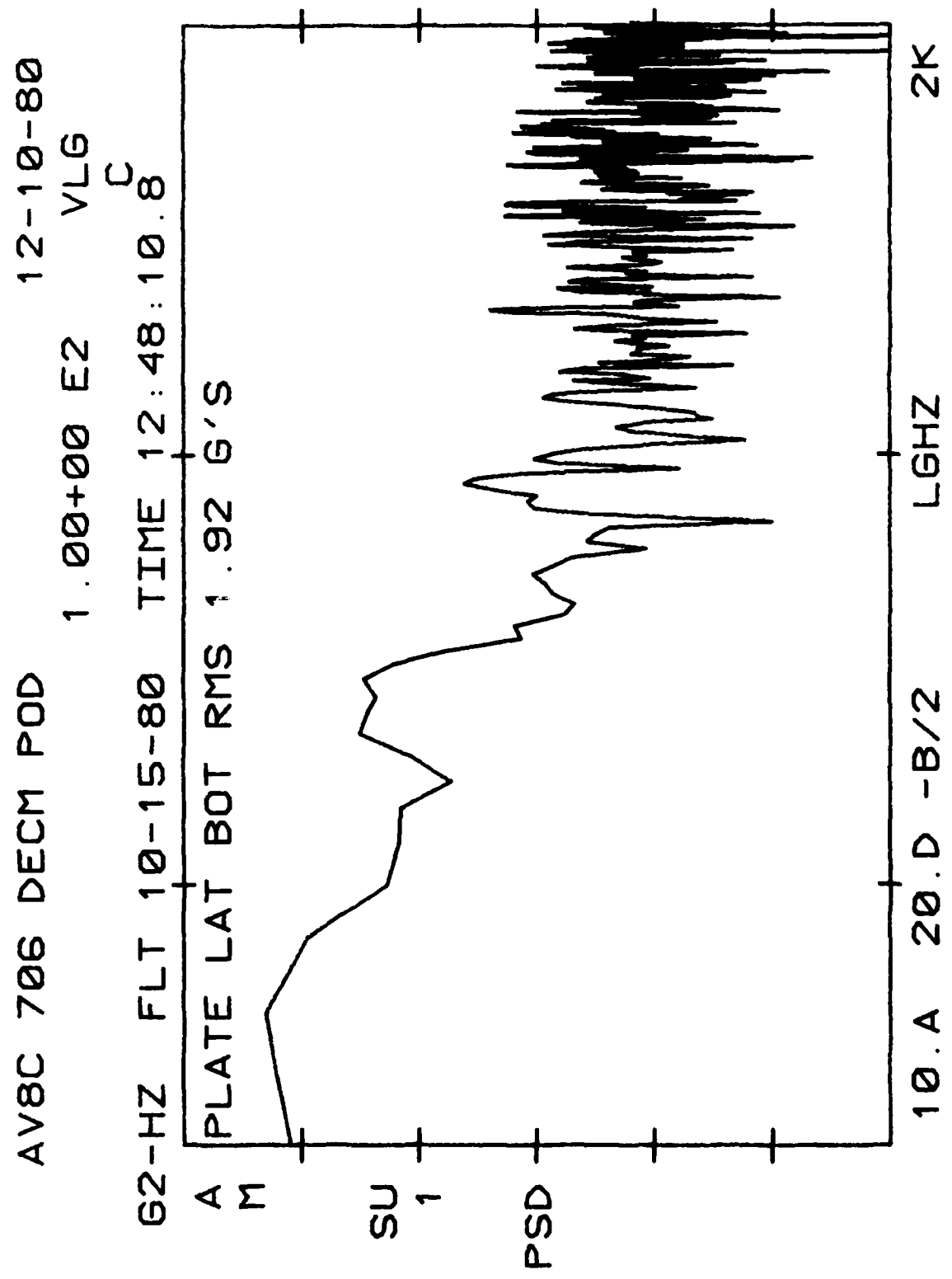

Figure 29 (Cont'd)

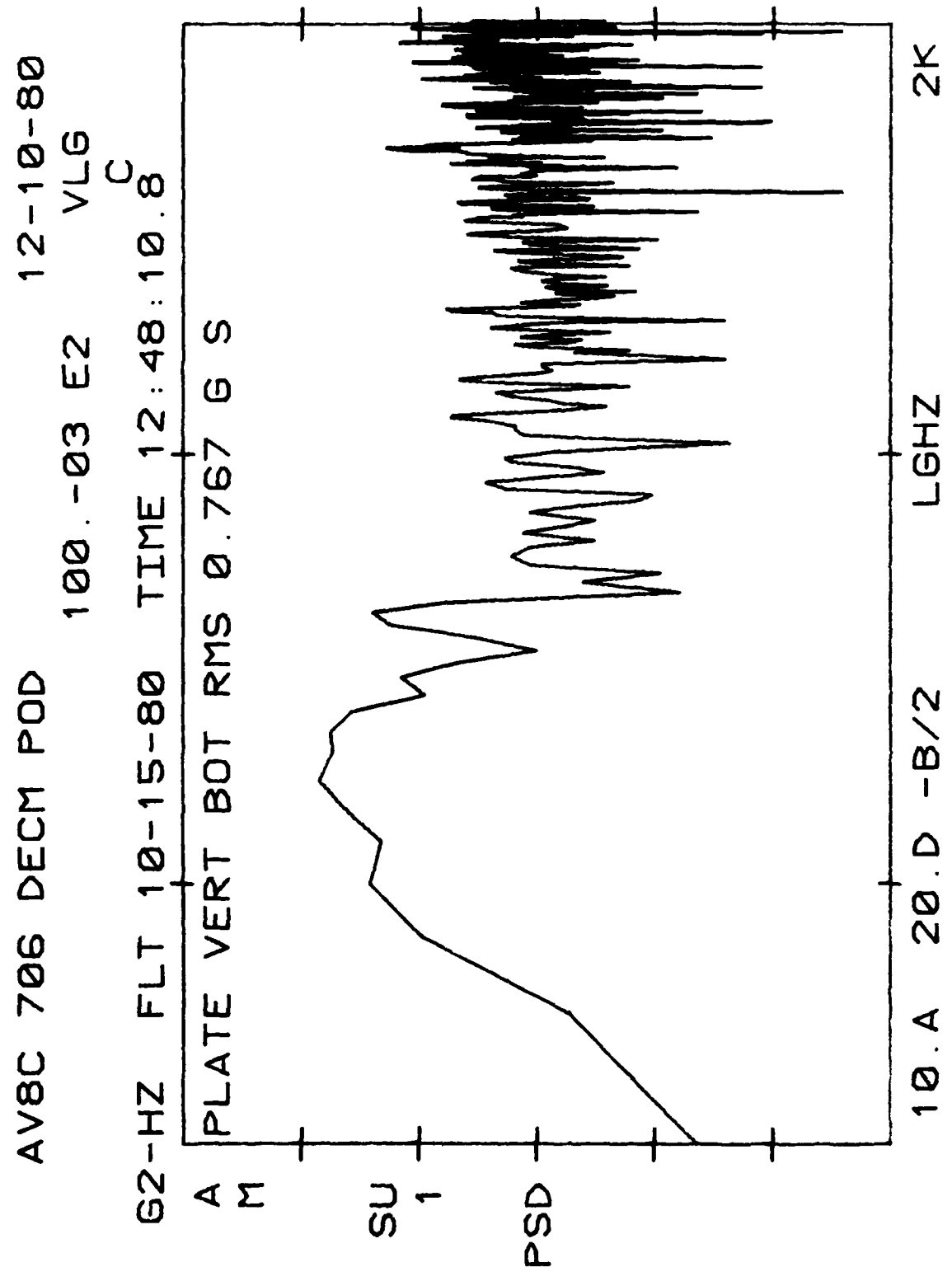

Figure 29 (Cont'd)

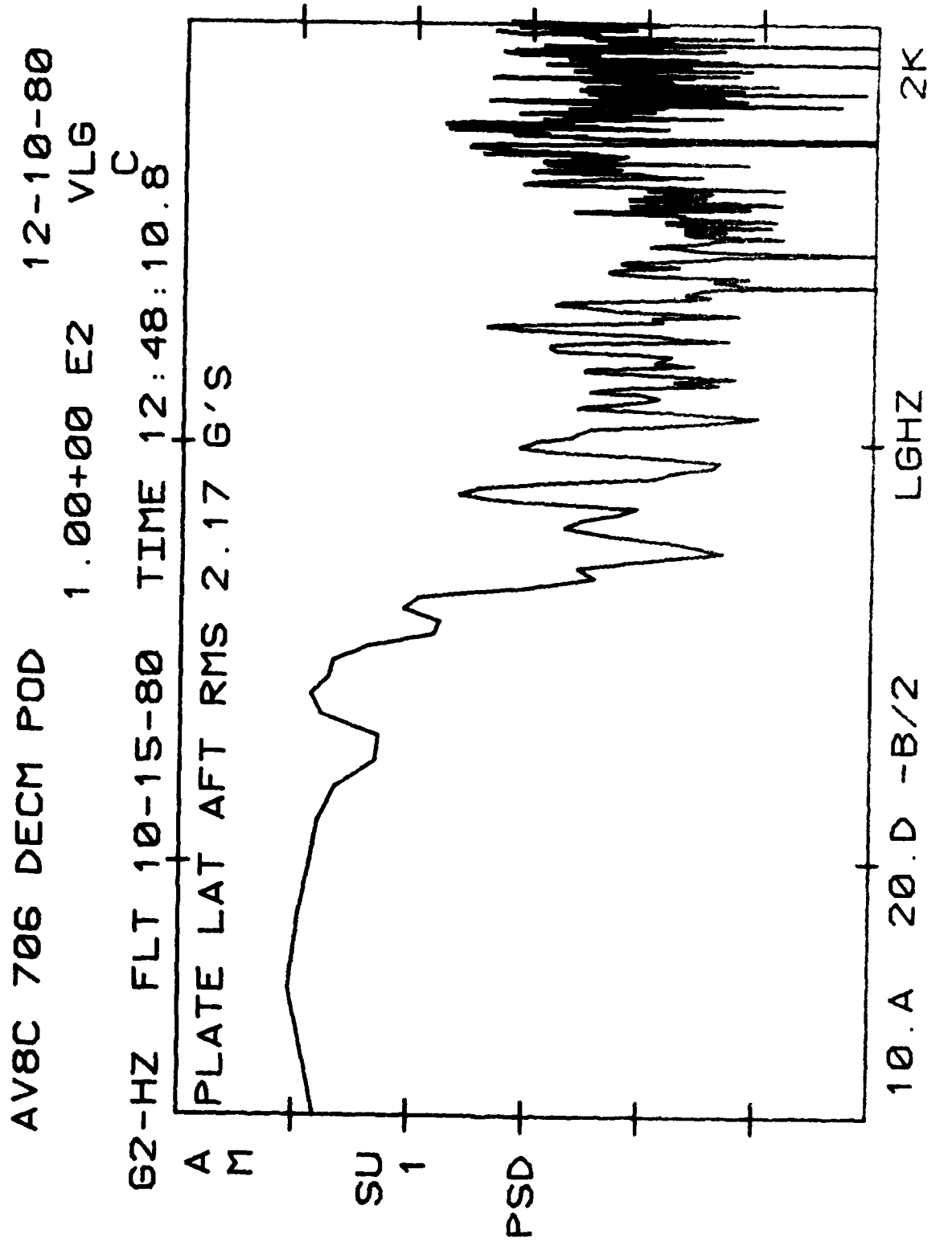

Figure 29 (Cont'd)

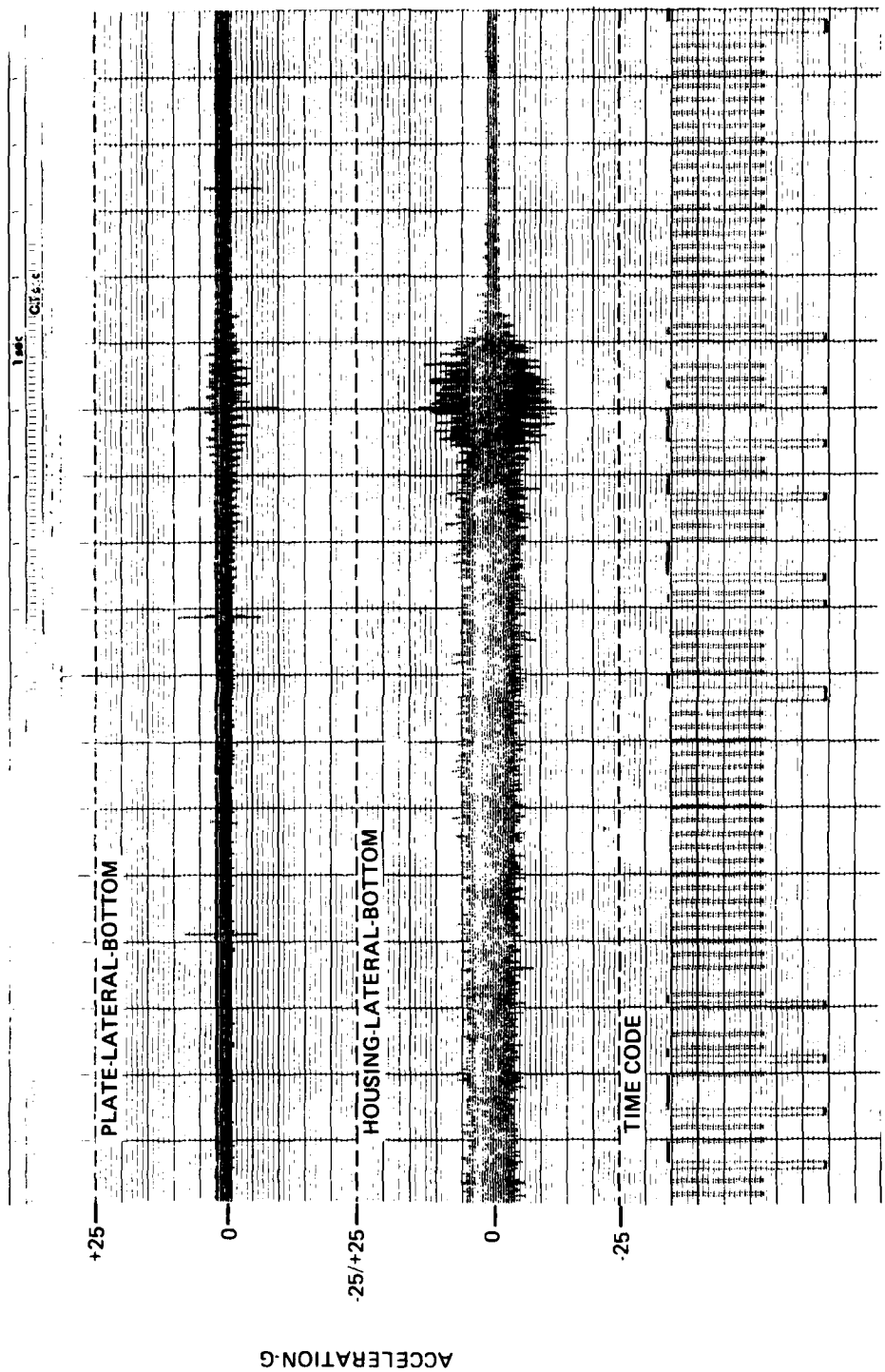

Figure 30
Vertical Landing, Time History

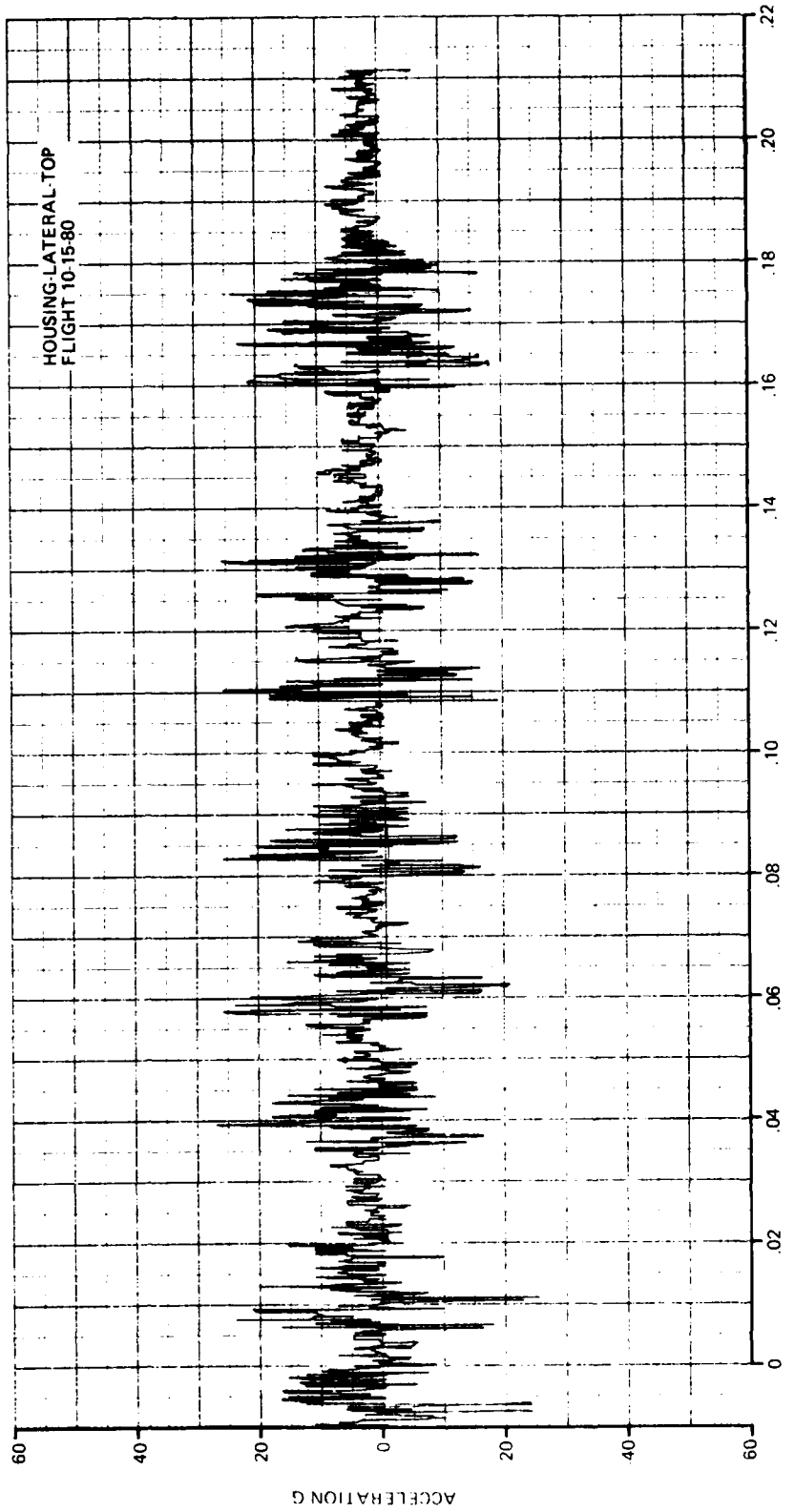

Figure 31
Gun Fire, Both Guns, about 2,000 ft Altitude, 440 KIAS, Time History

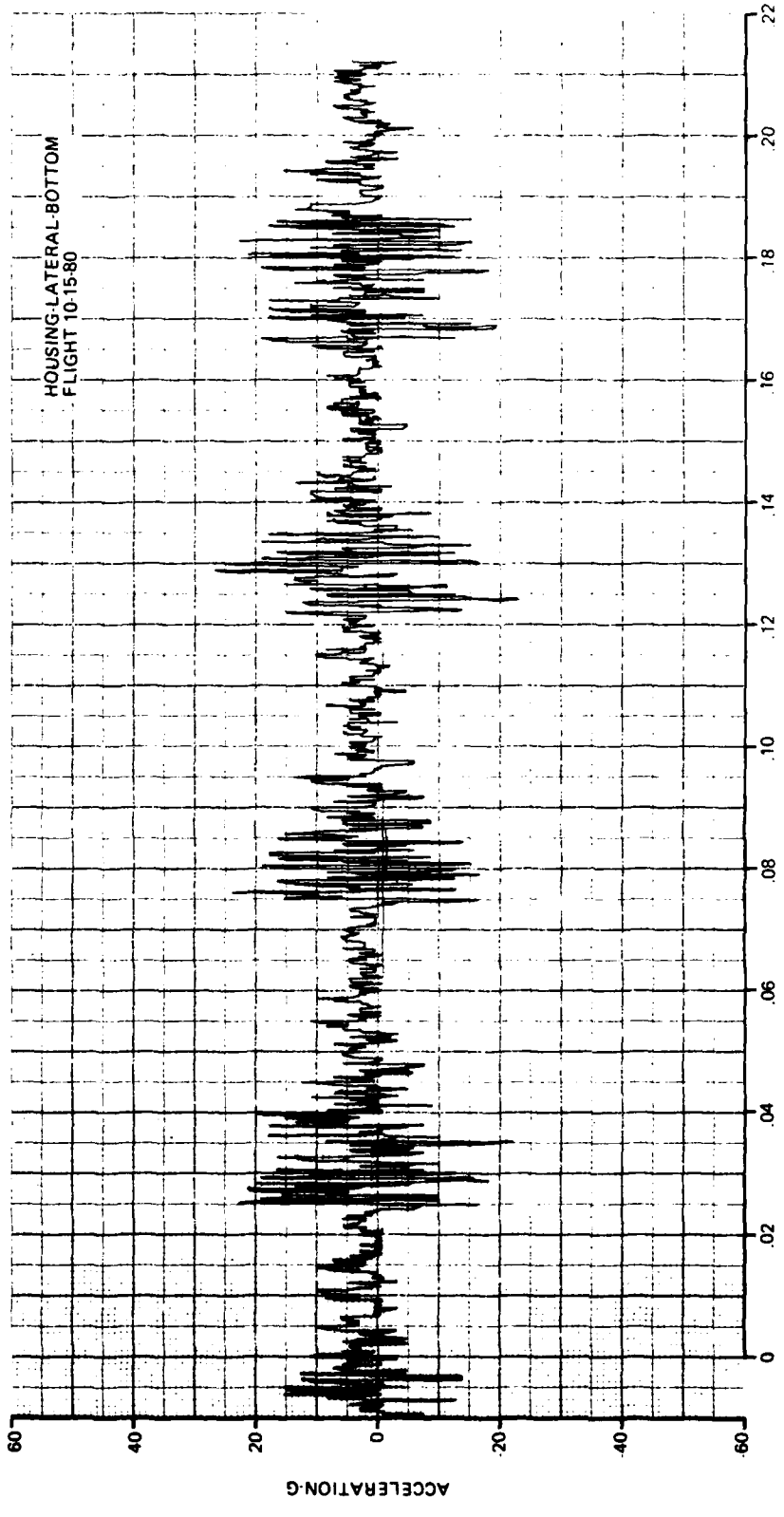

Figure 31 (Cont'd)

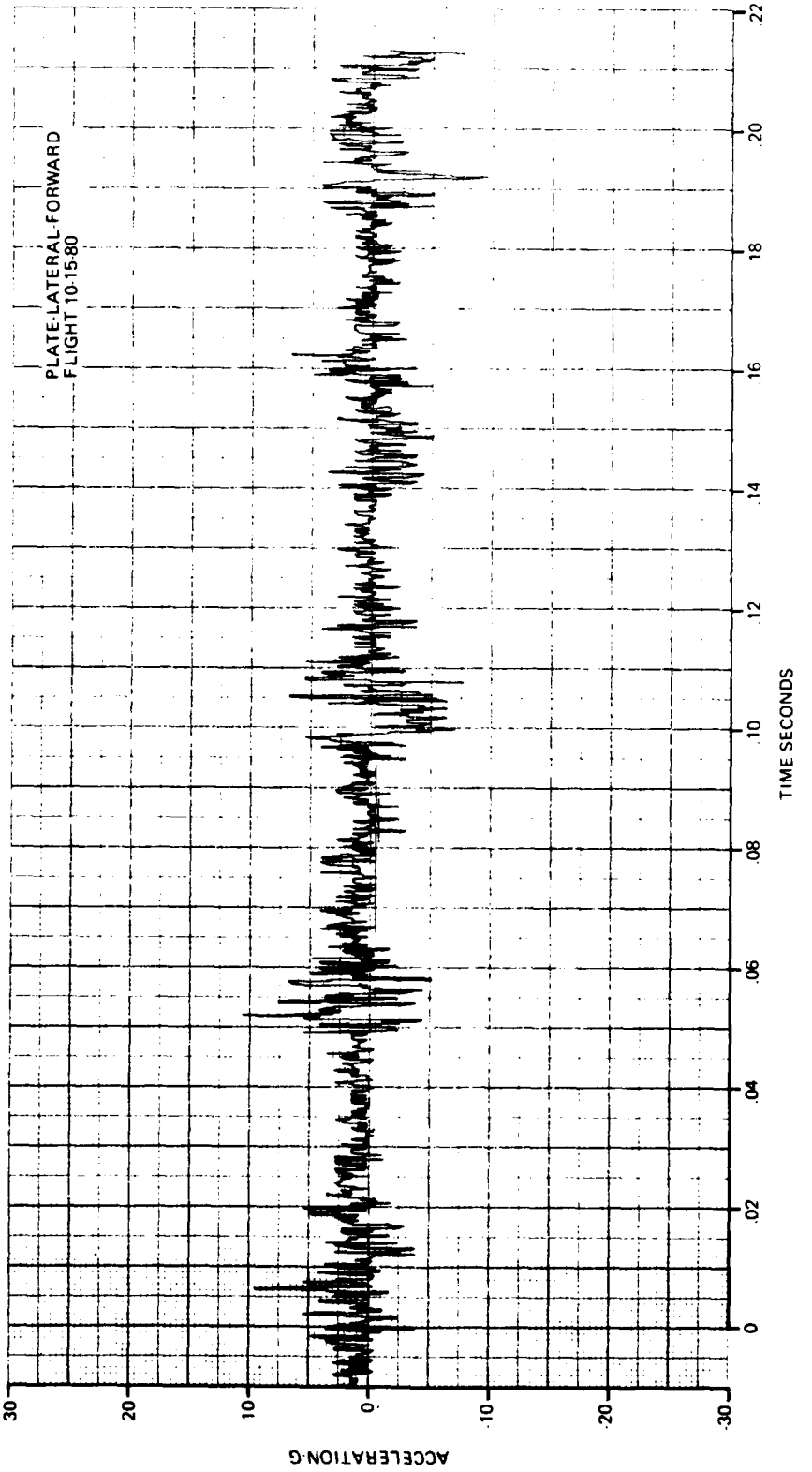

Figure 31 (Cont'd)

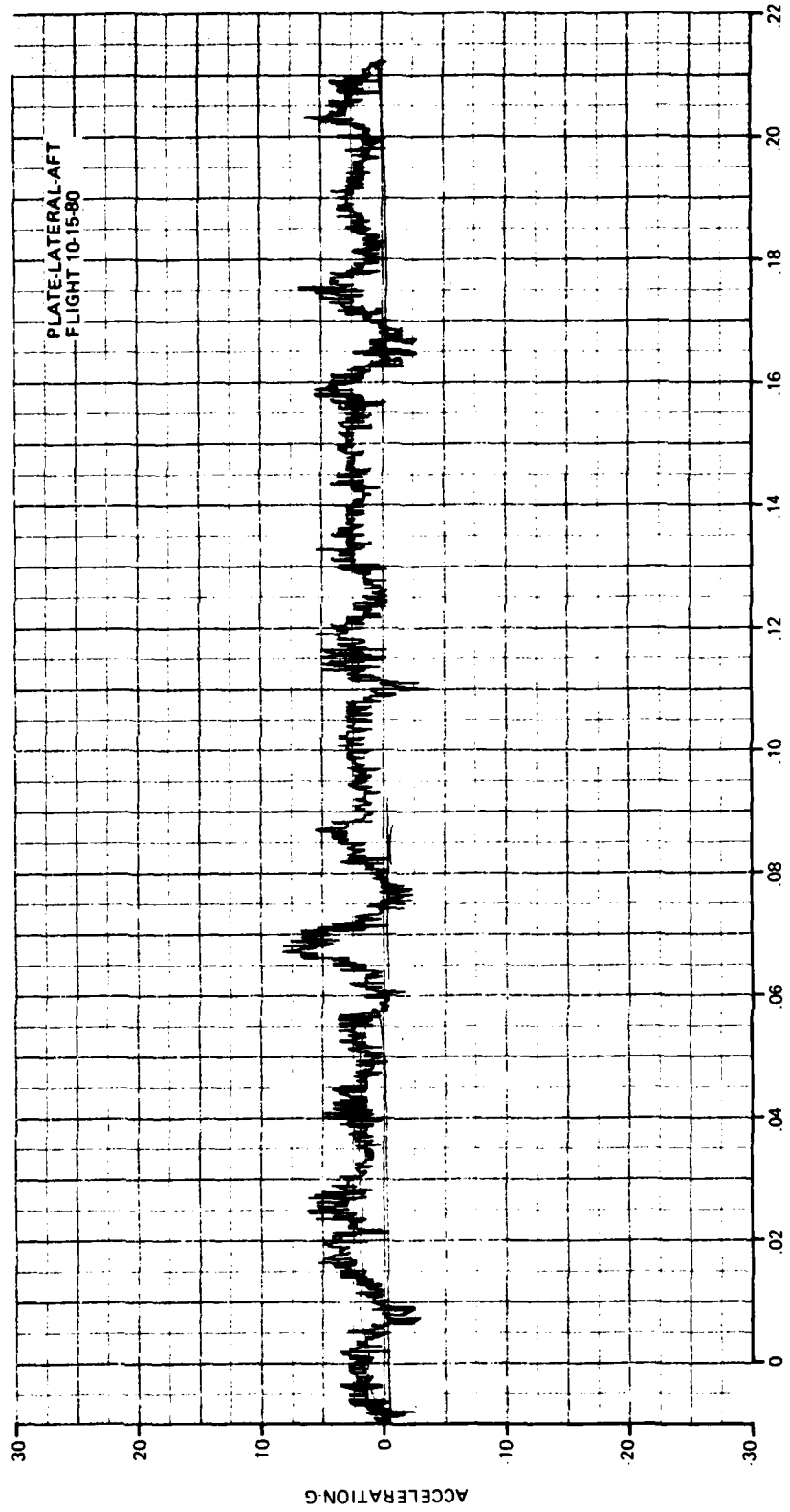

Figure 31 (Cont'd)

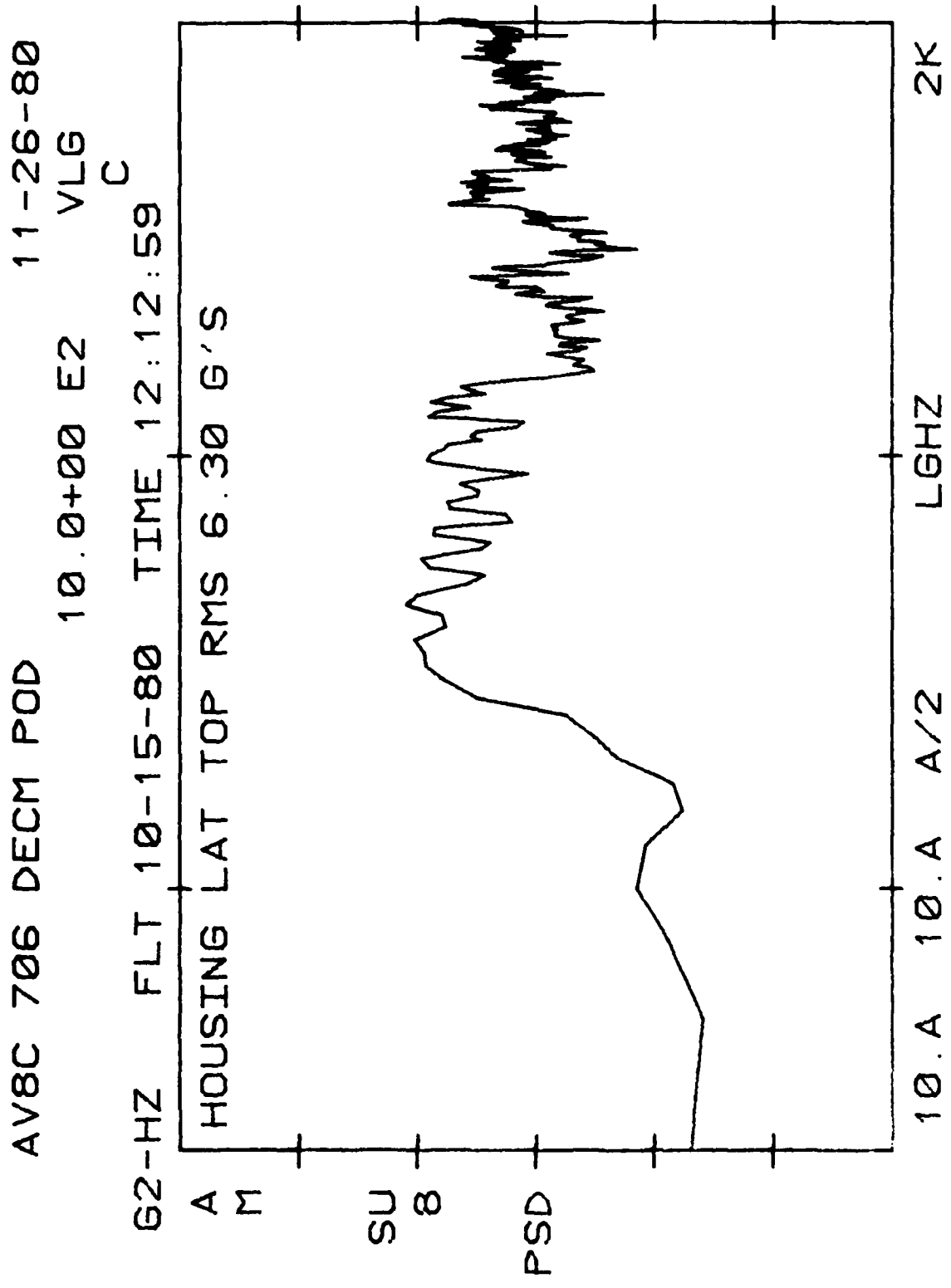

Figure 32
Gun Fire, Both Guns, about 2,000 ft Altitude,
440 KIAS, PSD

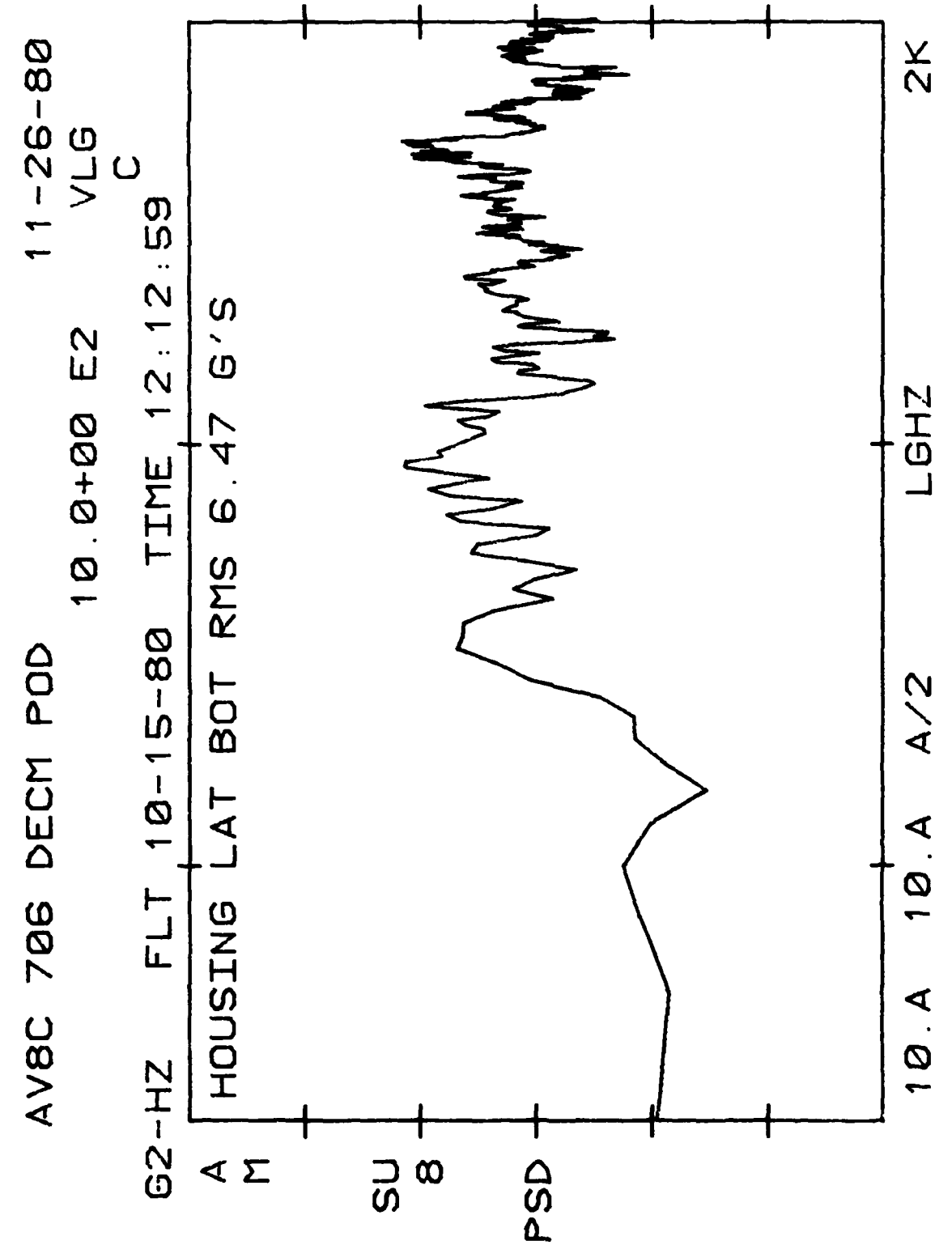

Figure 32 (Cont'd)

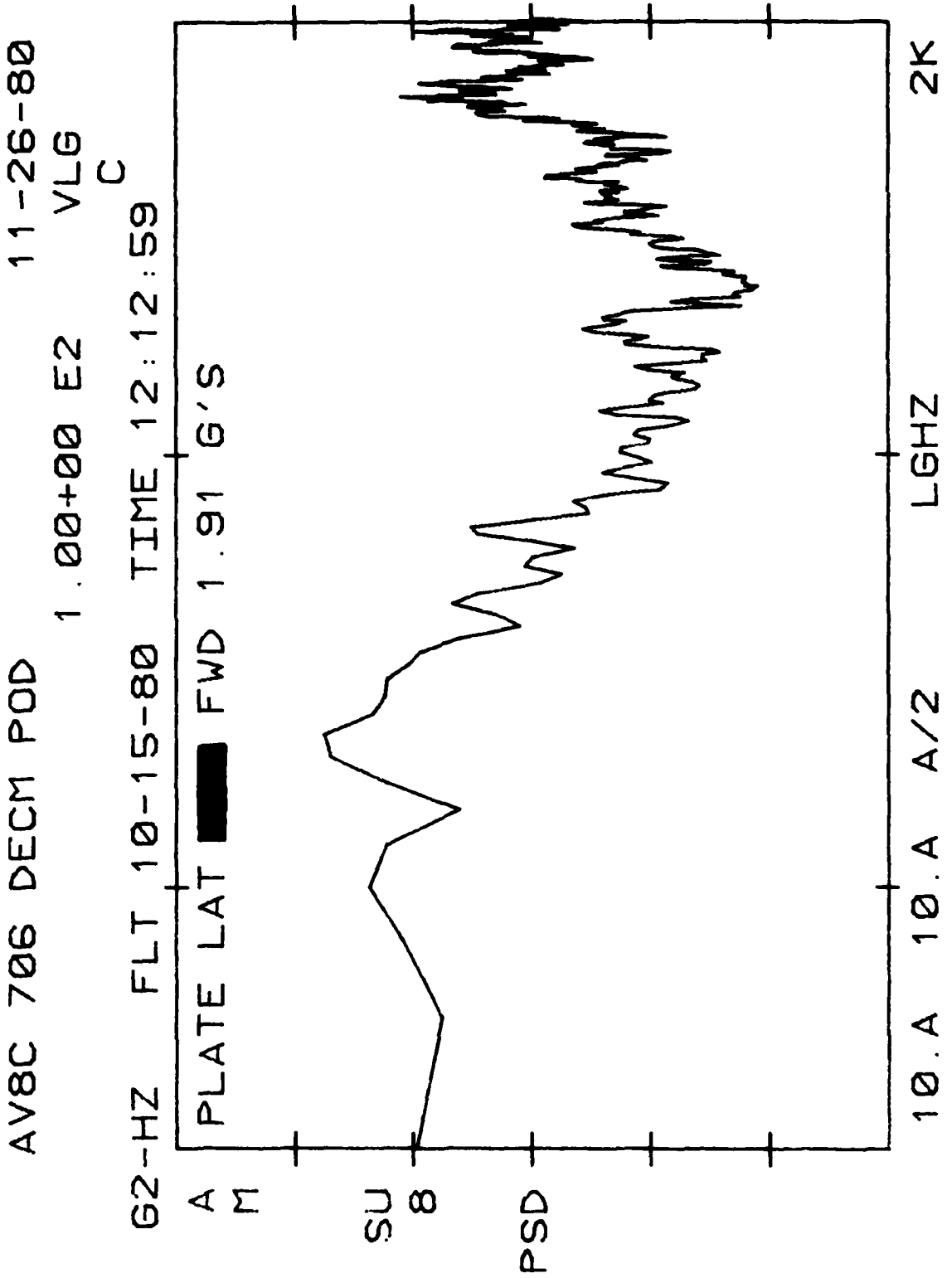

Figure 32 (Cont'd)

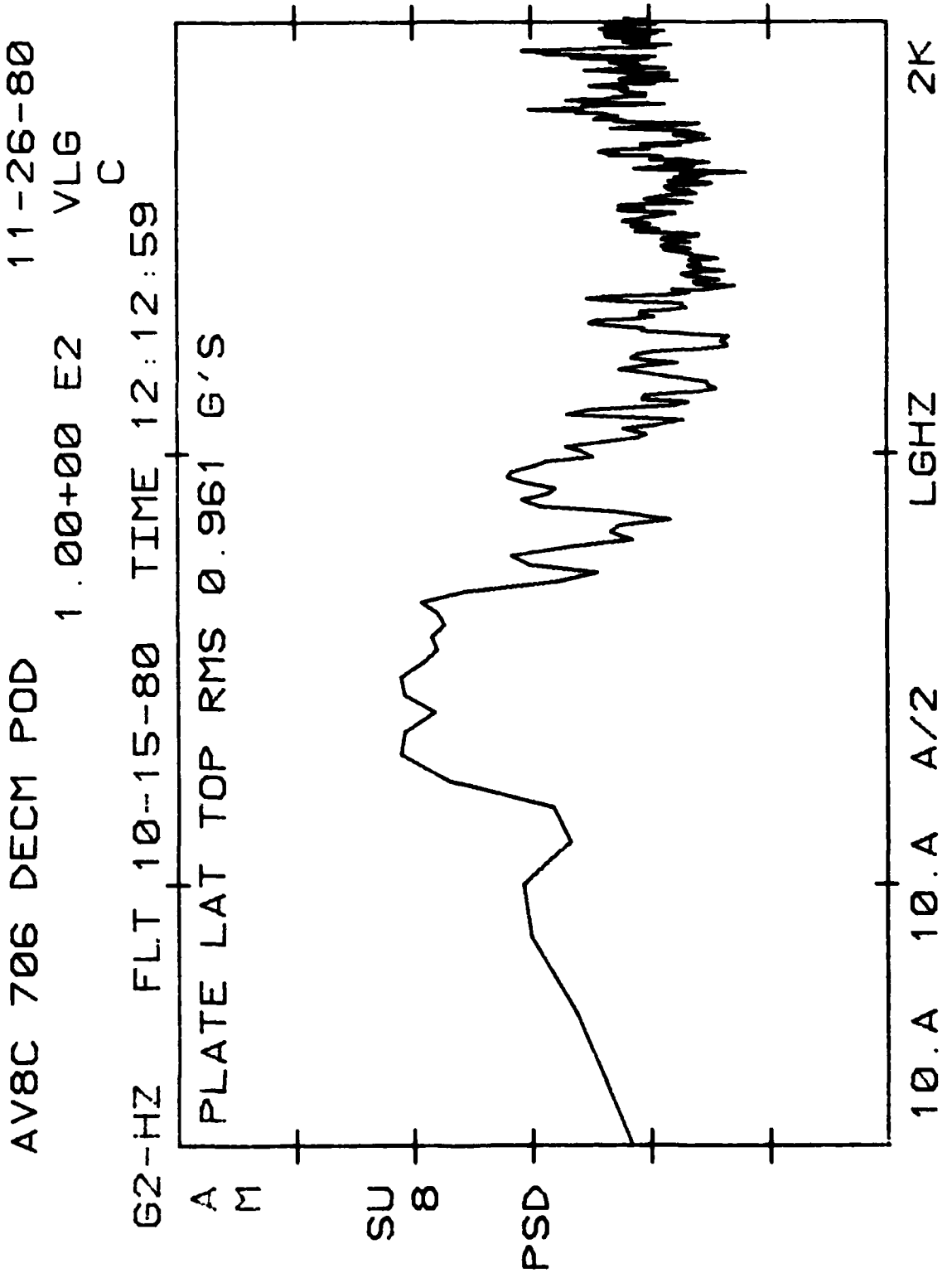

Figure 32 (Cont'd)

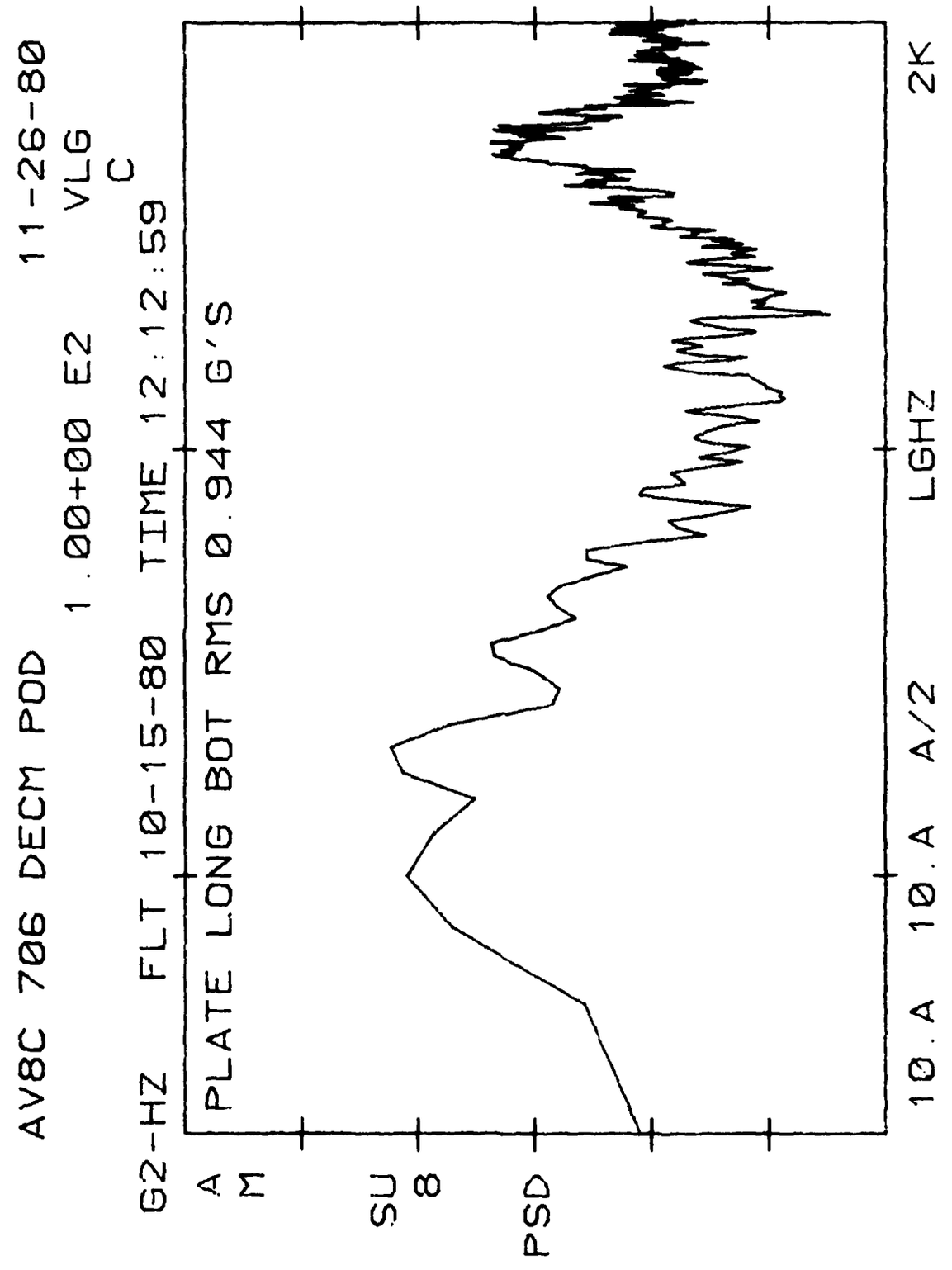

Figure 32 (Cont'd)

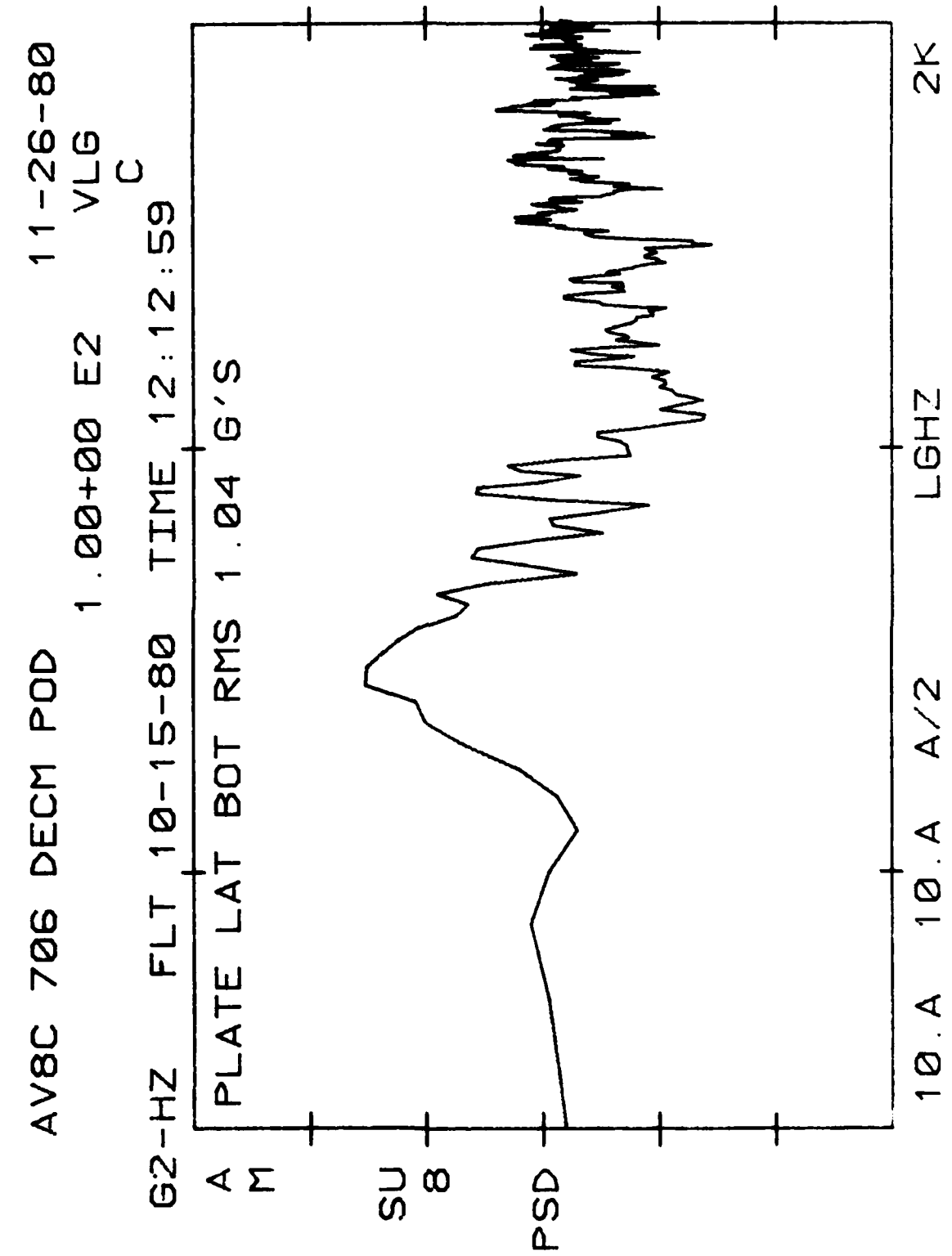

Figure 32 (Cont'd)

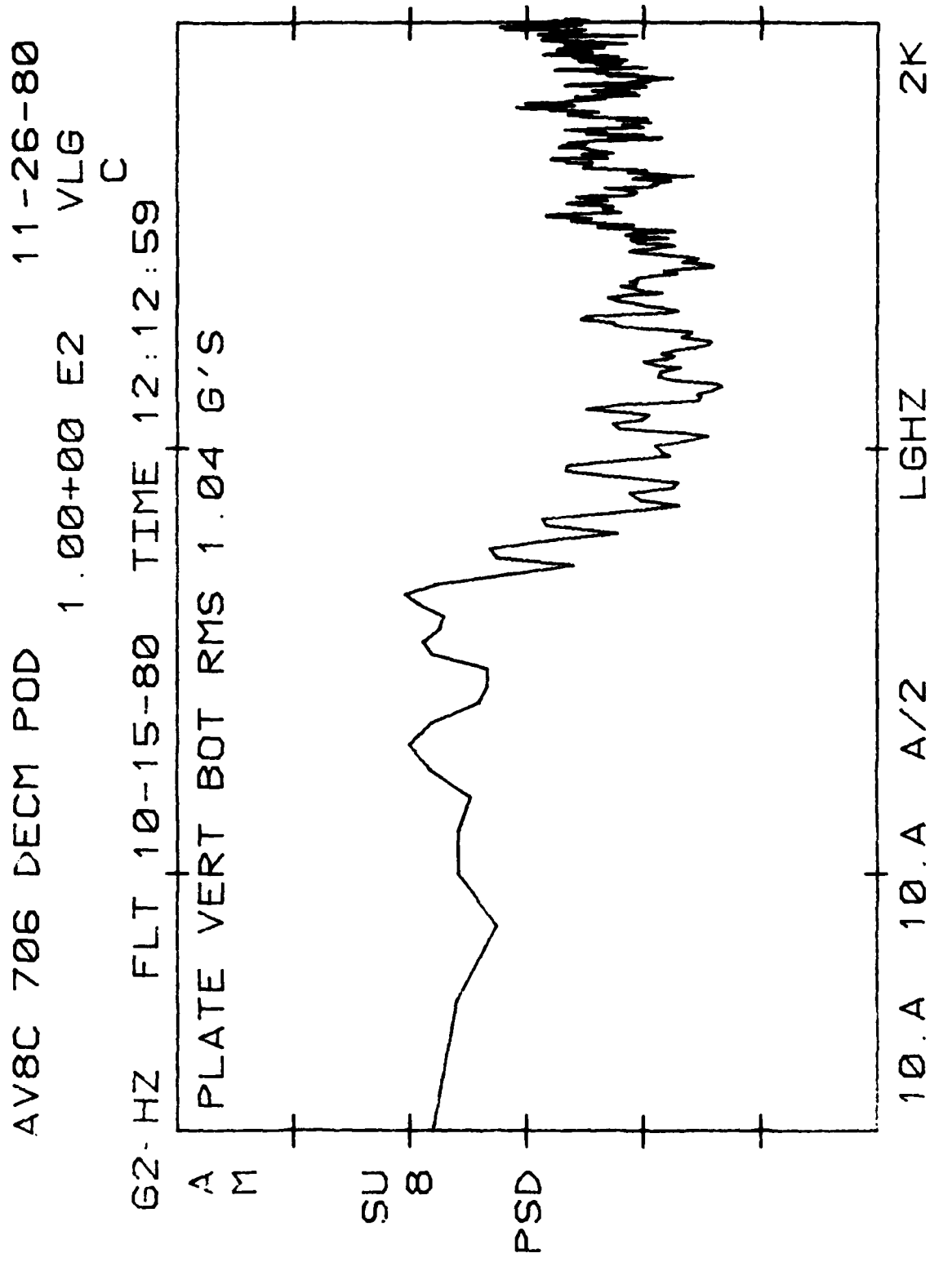

Figure 32 (Cont'd)

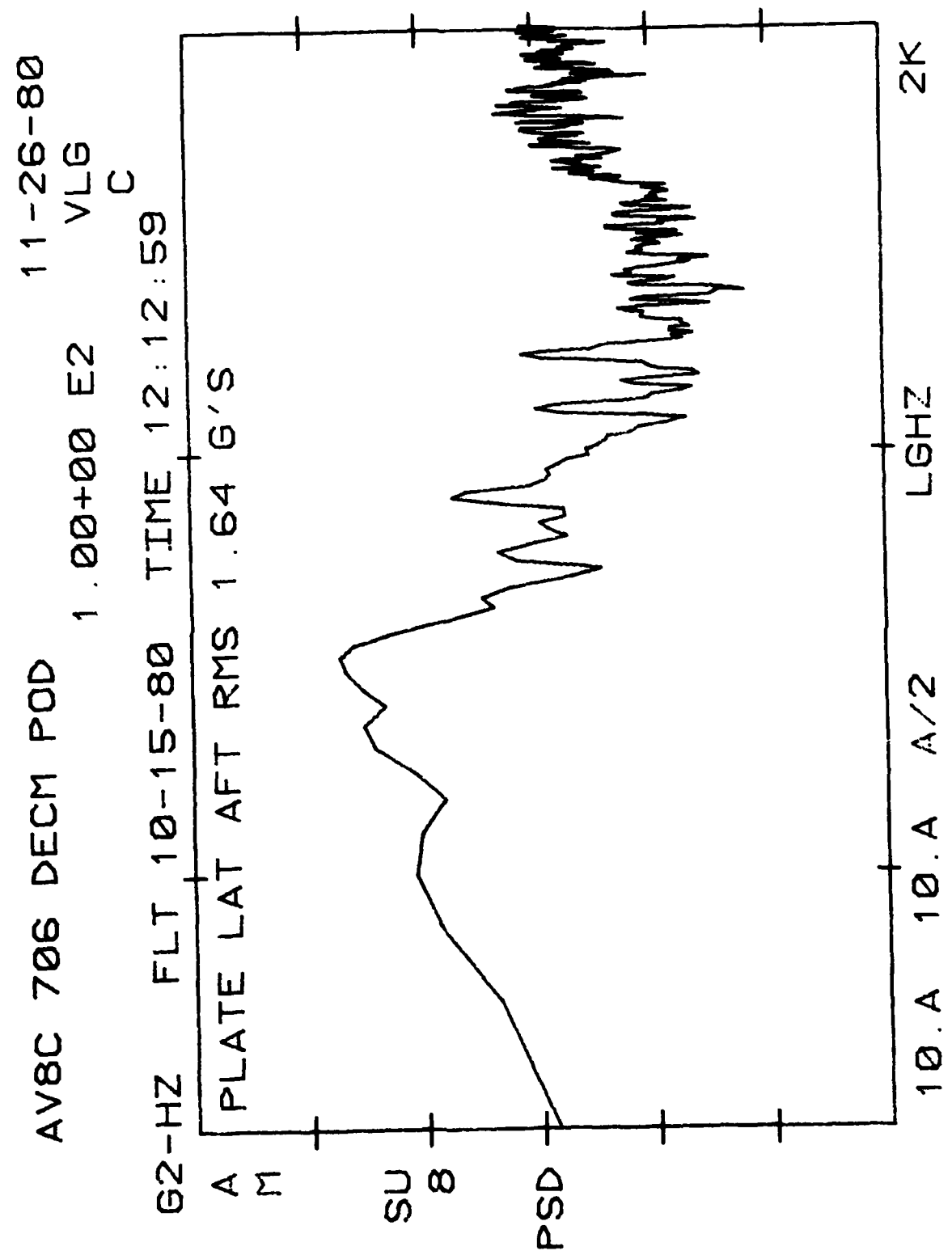

Figure 32 (Cont'd)

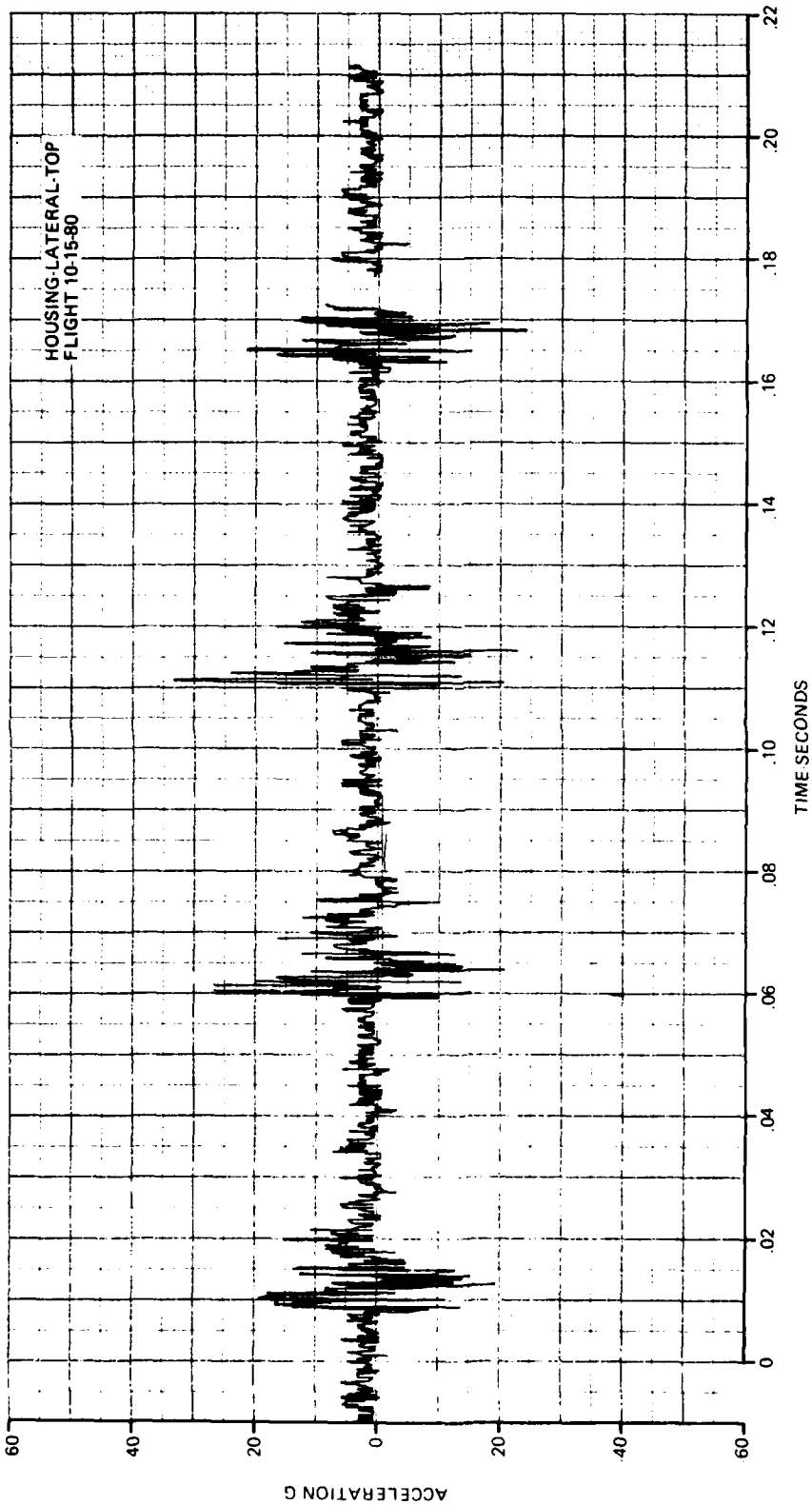

Figure 33
Gun Fire, Single Gun, about 2,000 ft Altitude,
440 KIAS, Time History

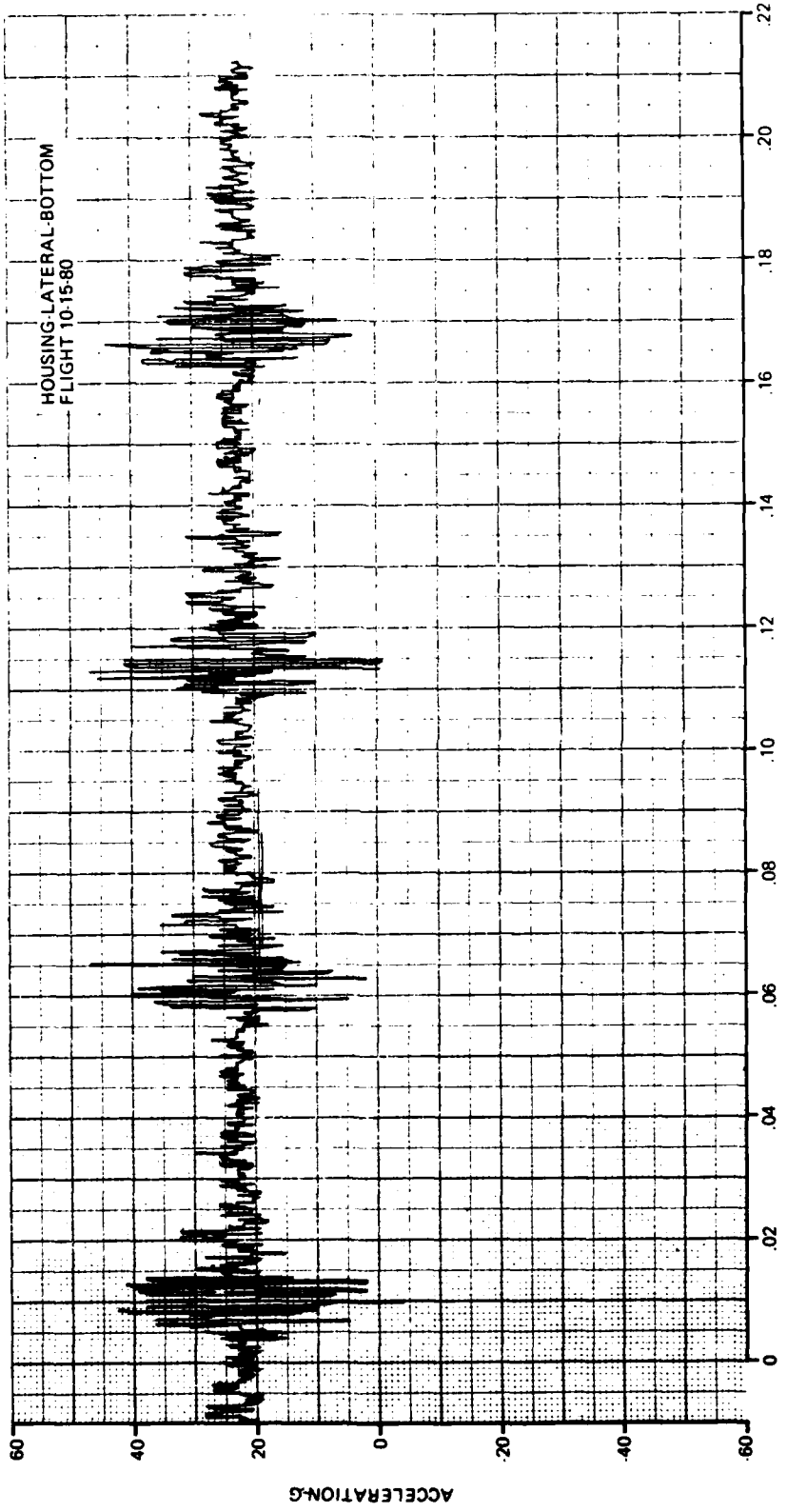

Figure 33 (Cont'd)

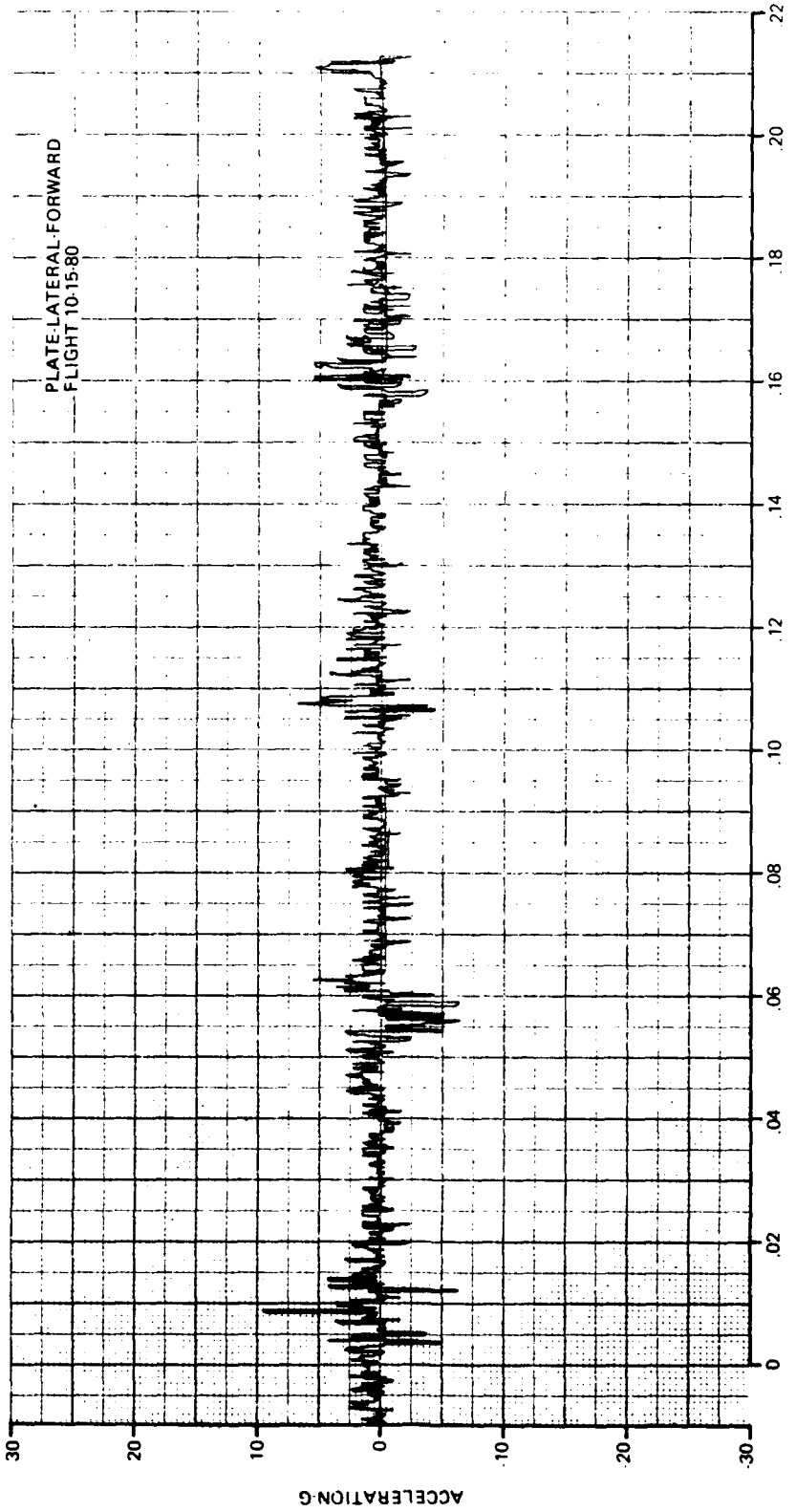

Figure 33 (Cont'd)

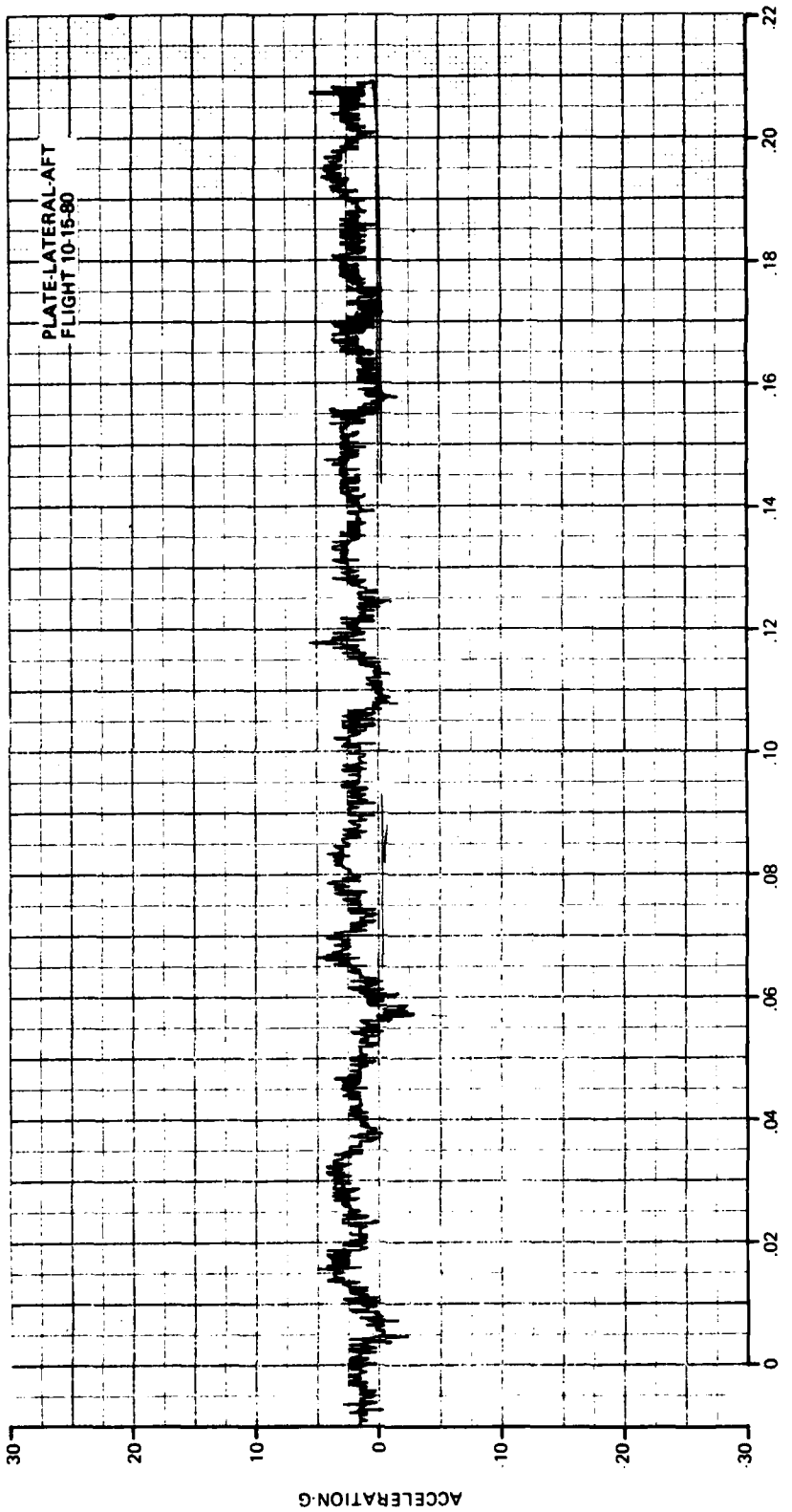

Figure 33 (Cont'd)

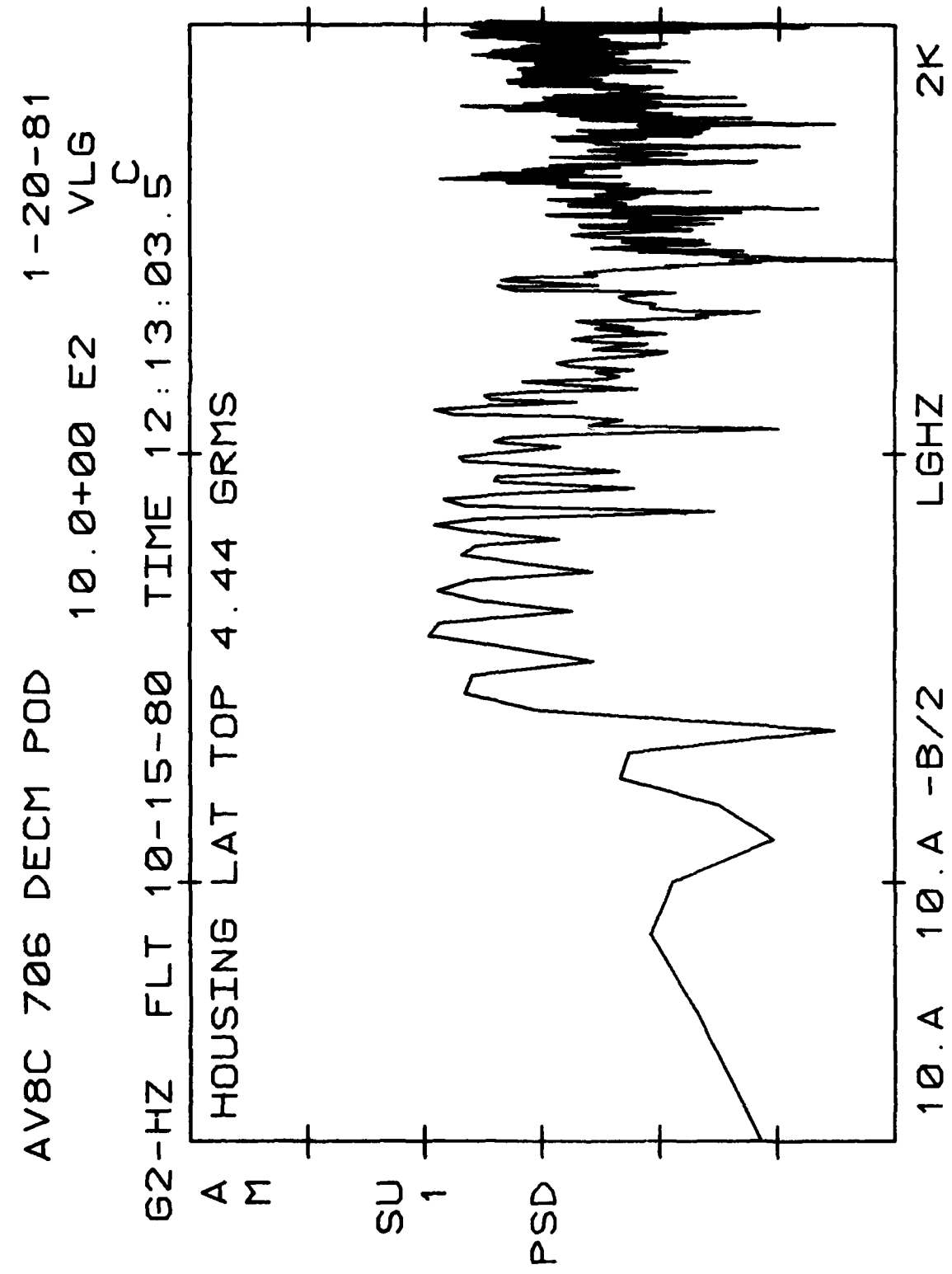

Figure 34
Gun Fire, Single Gun, about 2,000 ft Altitude, 440 KIAS, PSD

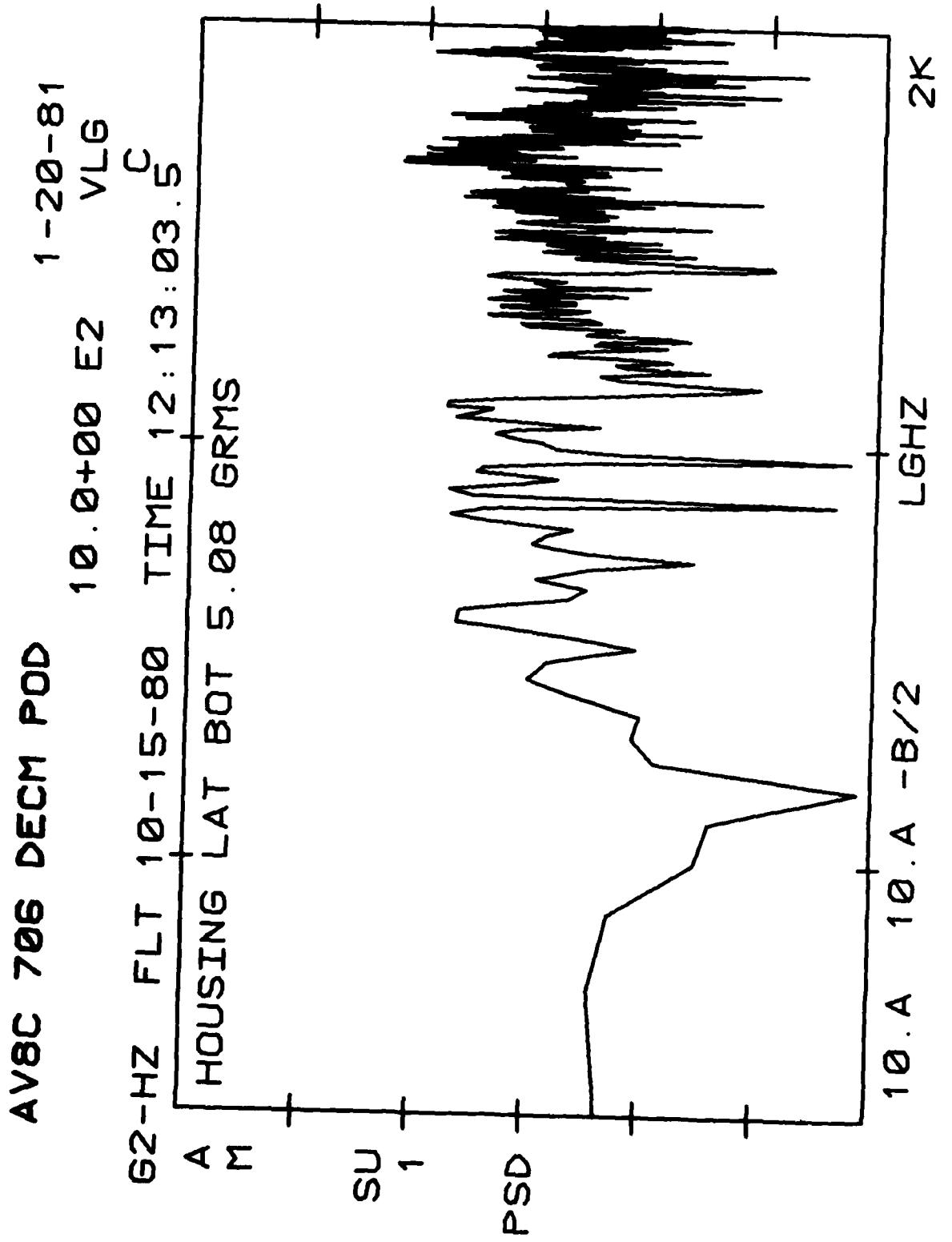

Figure 34 (Cont'd)

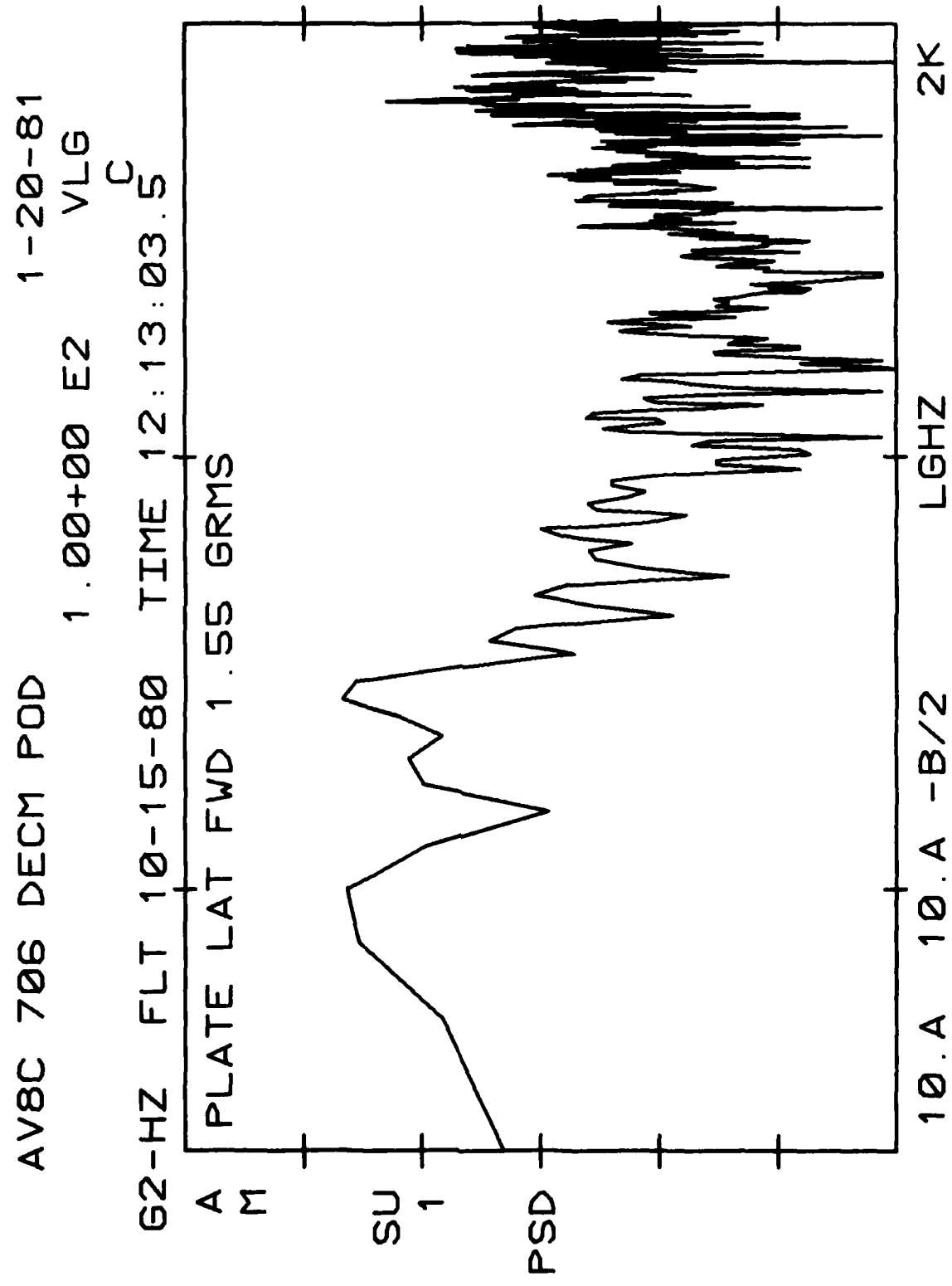

Figure 34 (Cont'd)

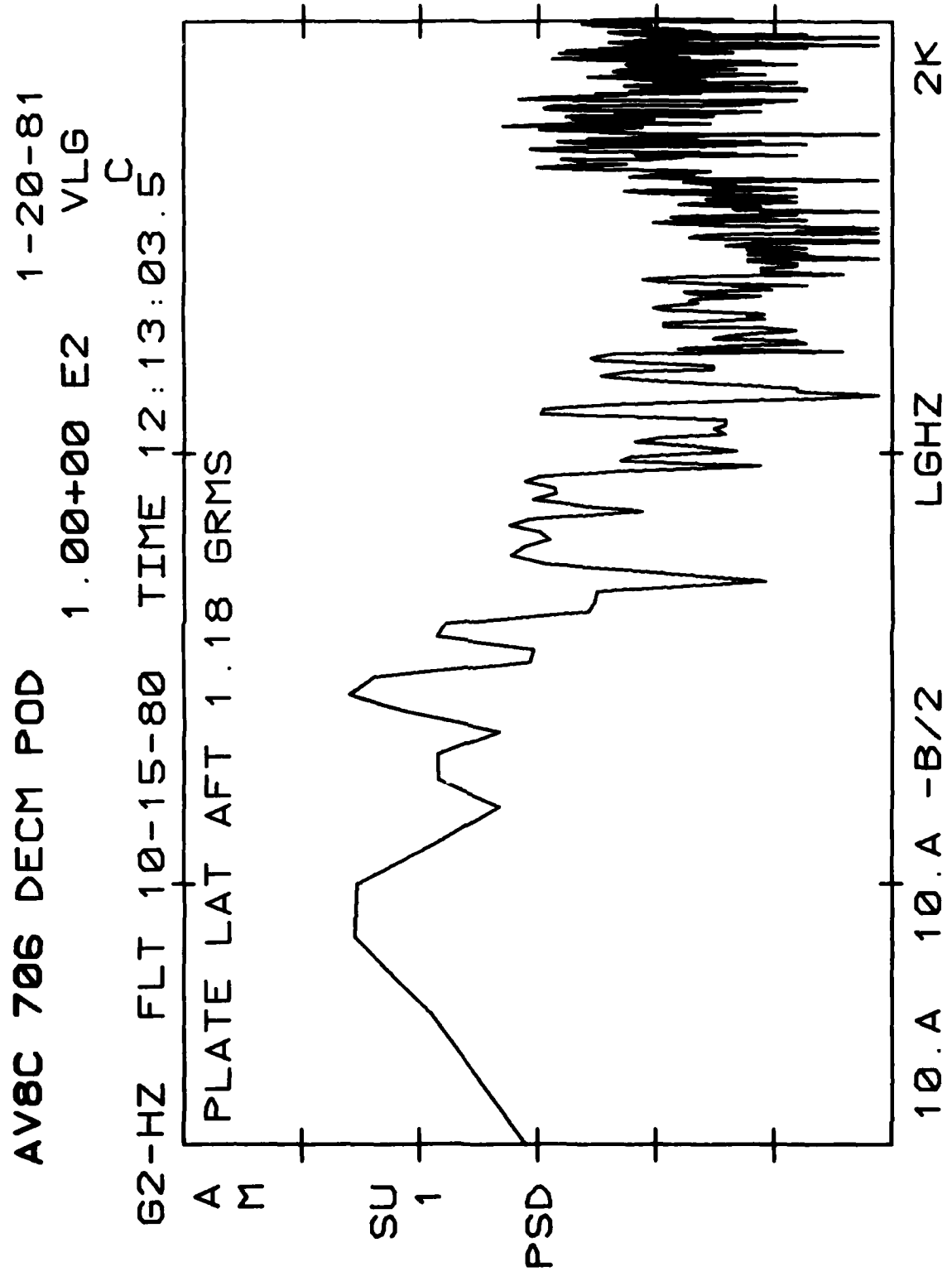

Figure 34 (Cont'd)

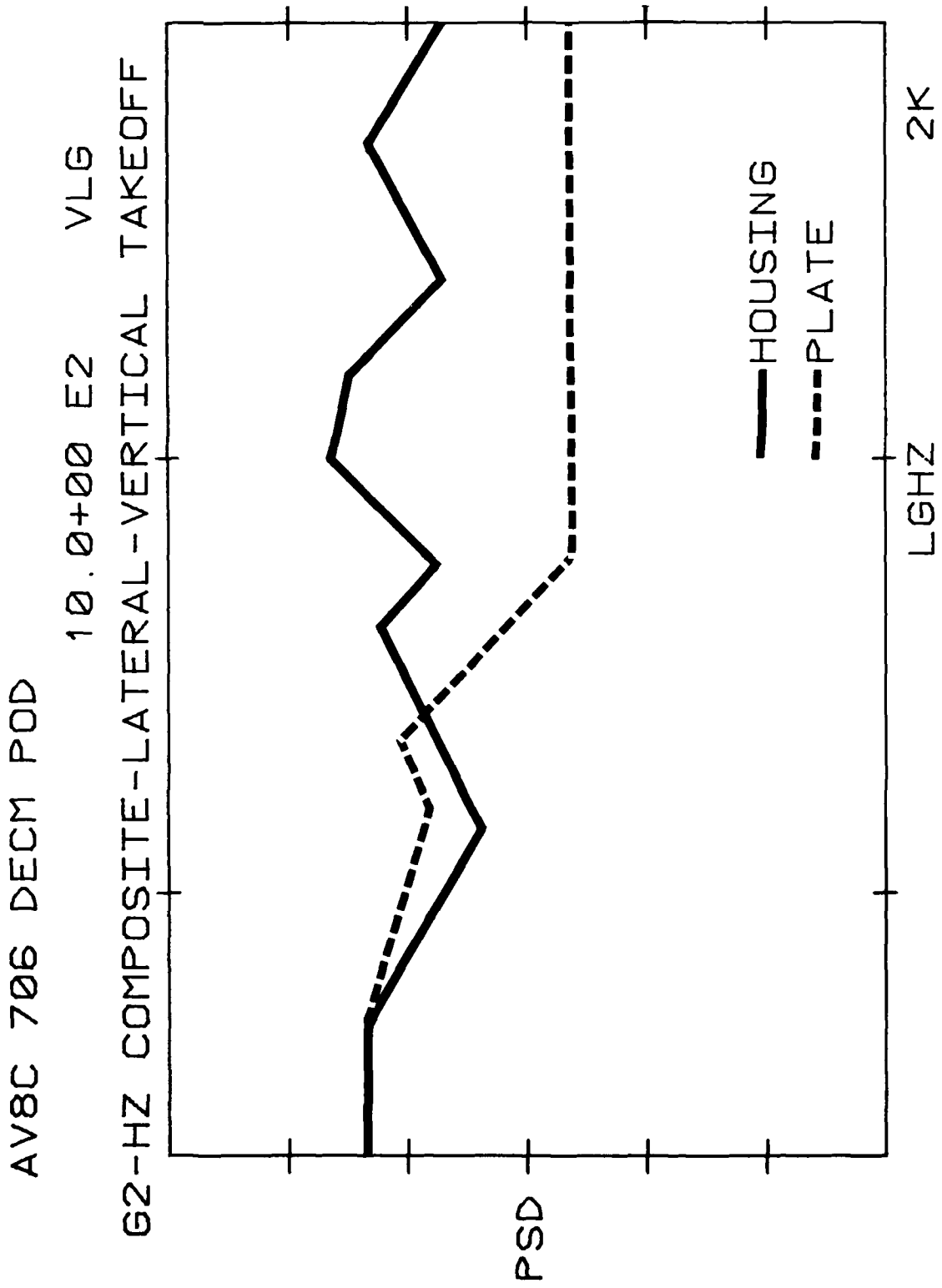

Figure 35
Summary Plots of Vibration Data, PSD

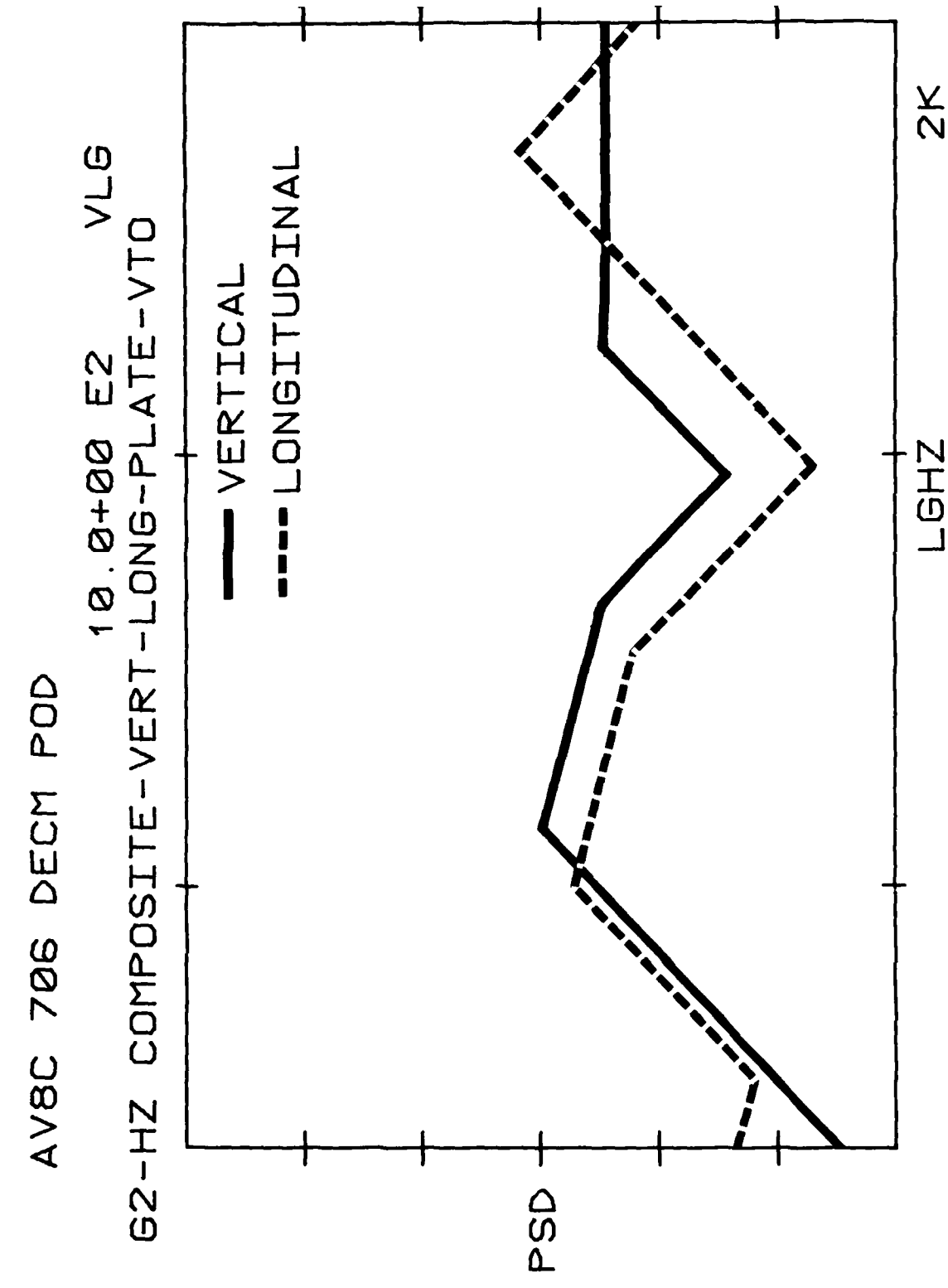

Figure 35 (Cont'd)

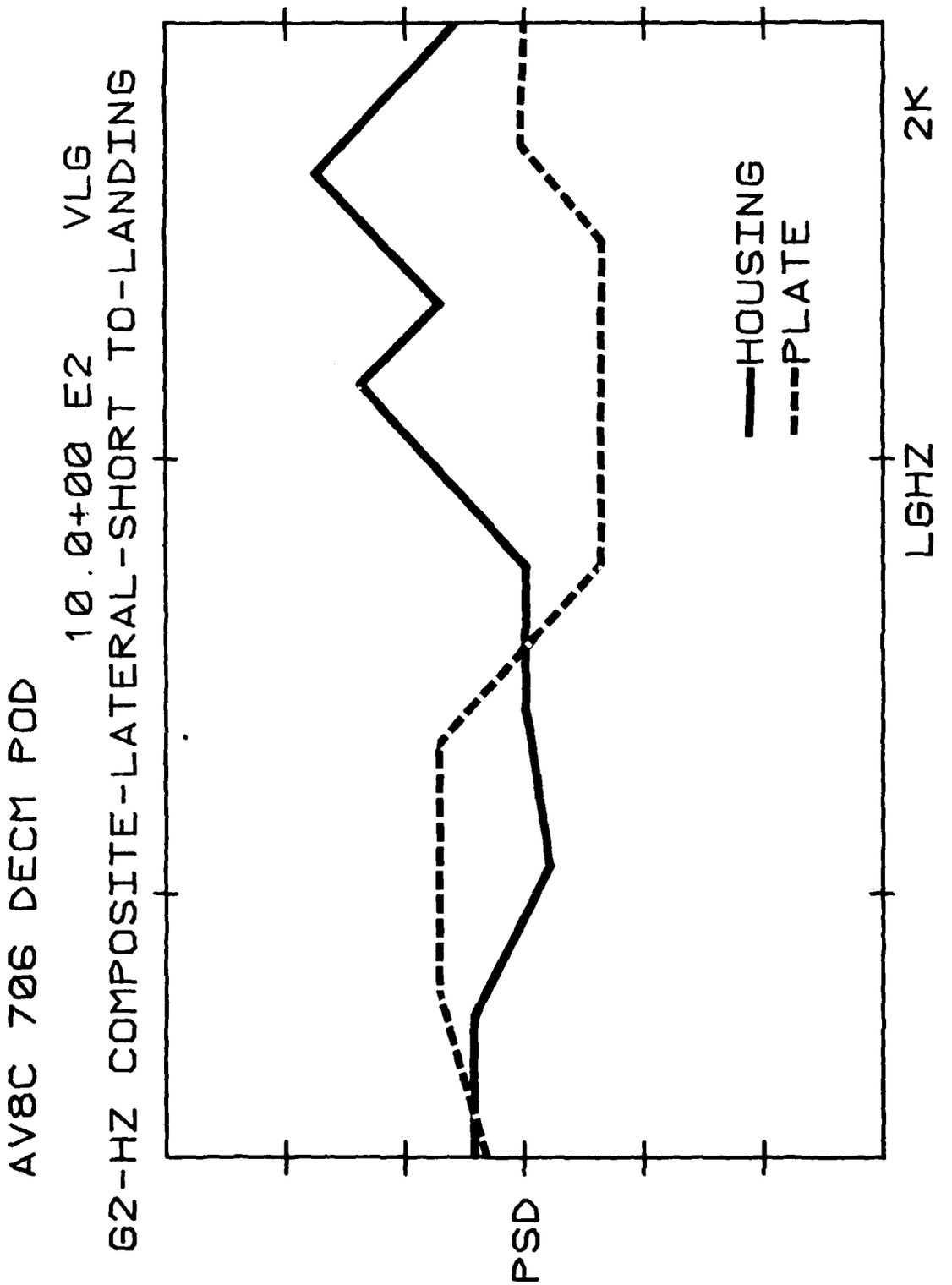

Figure 35 (Cont'd)

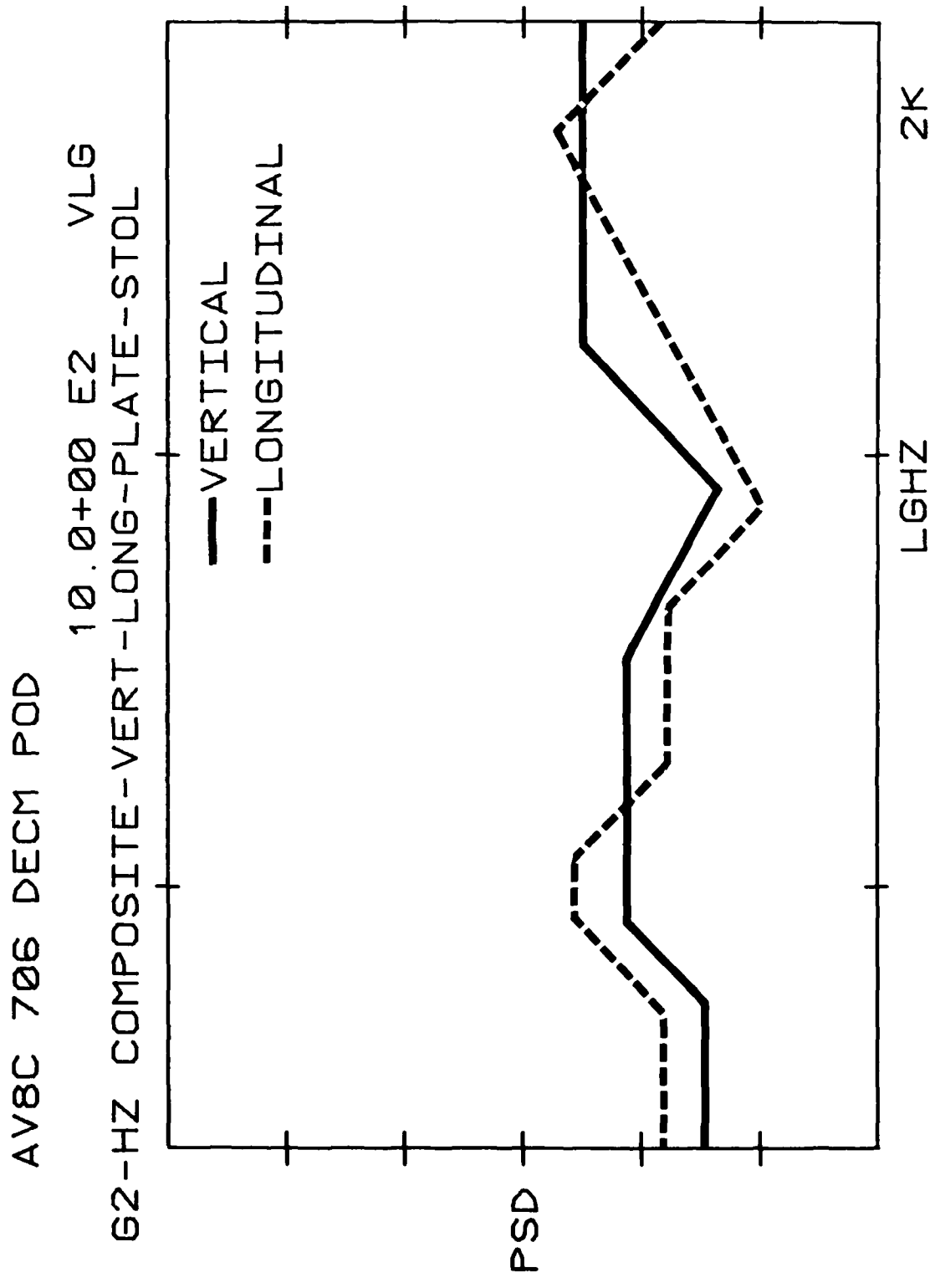

Figure 35 (Cont'd)

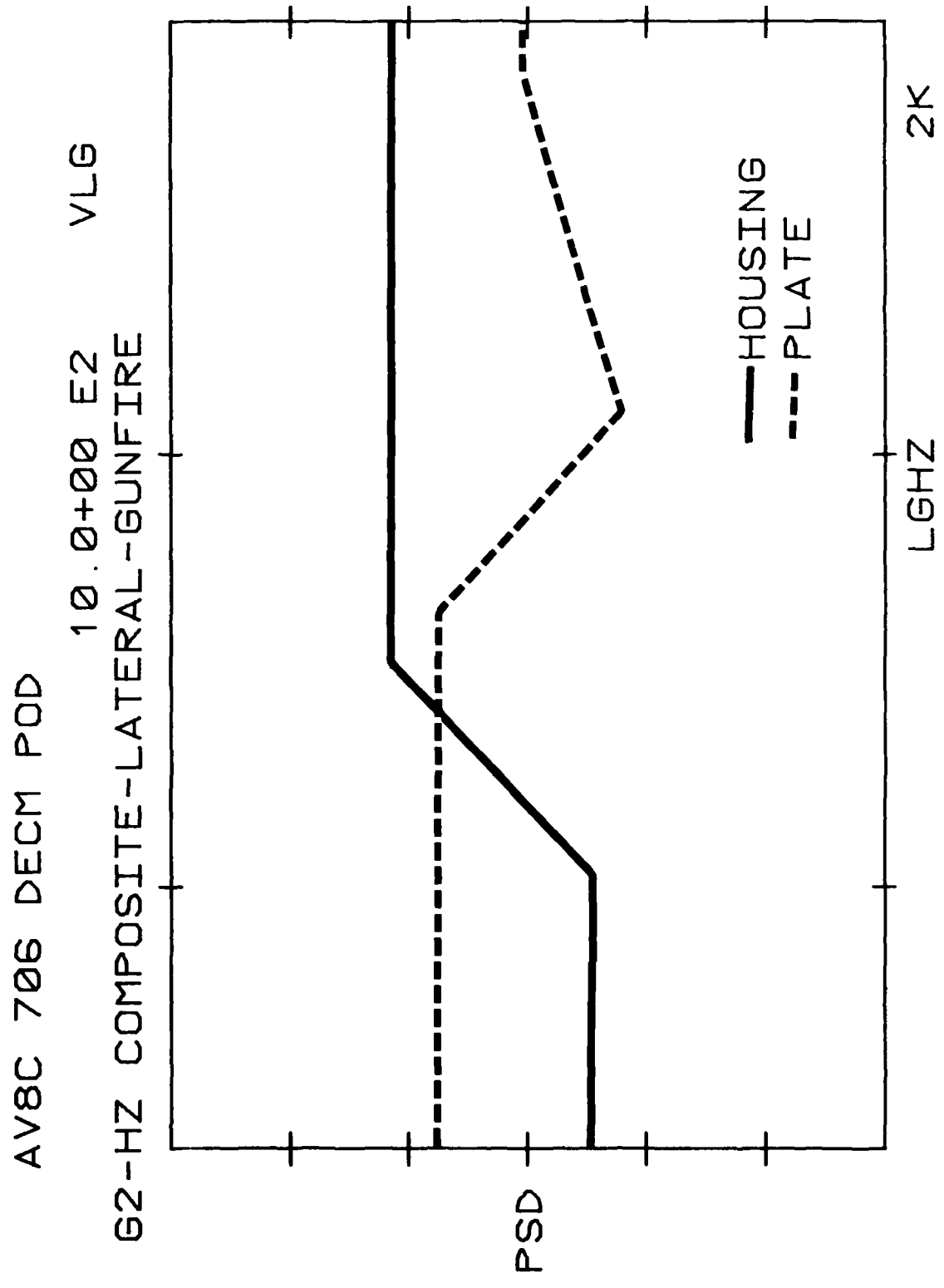

Figure 35 (Concluded)

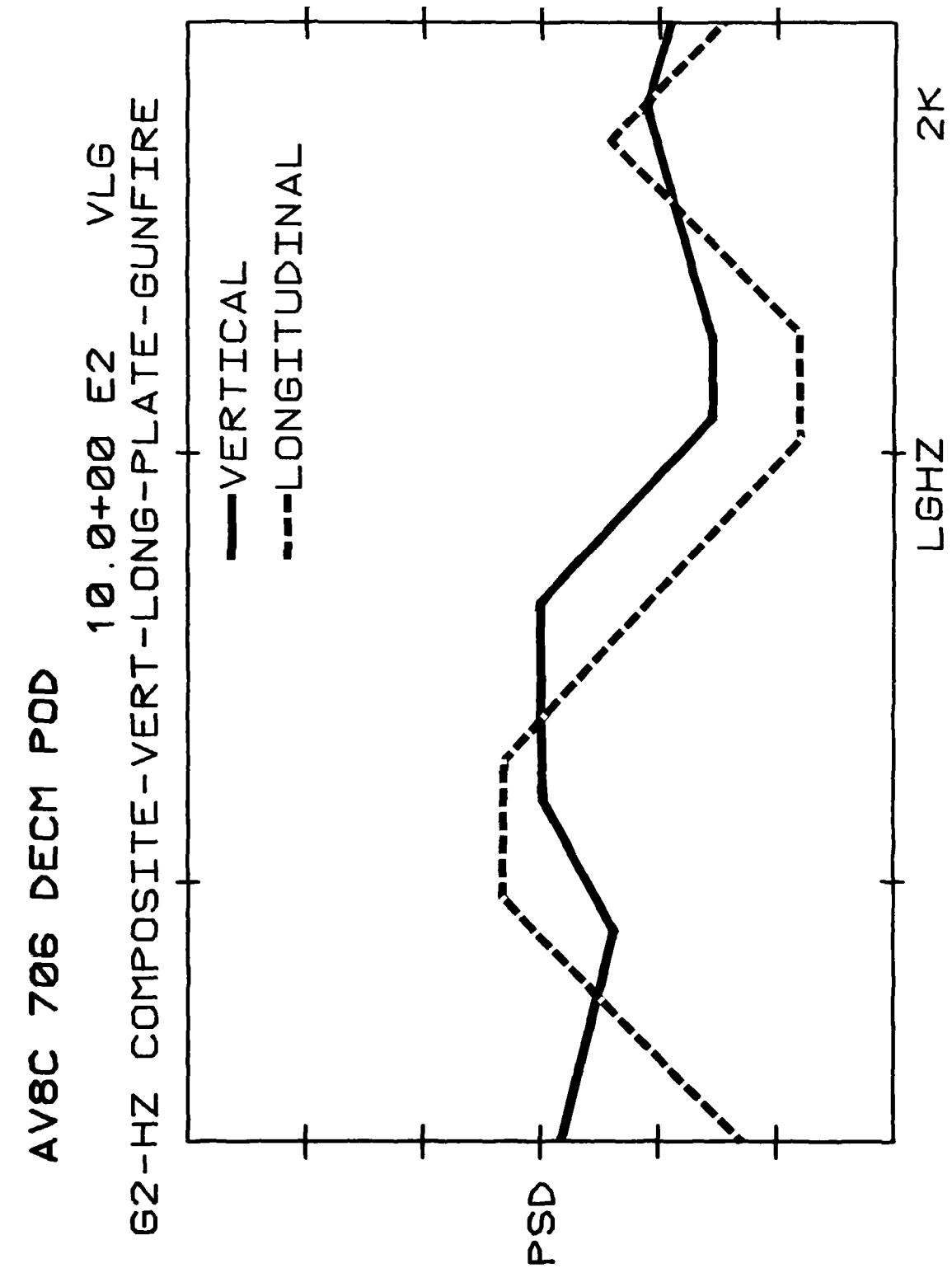

Figure 35 (Cont'd)

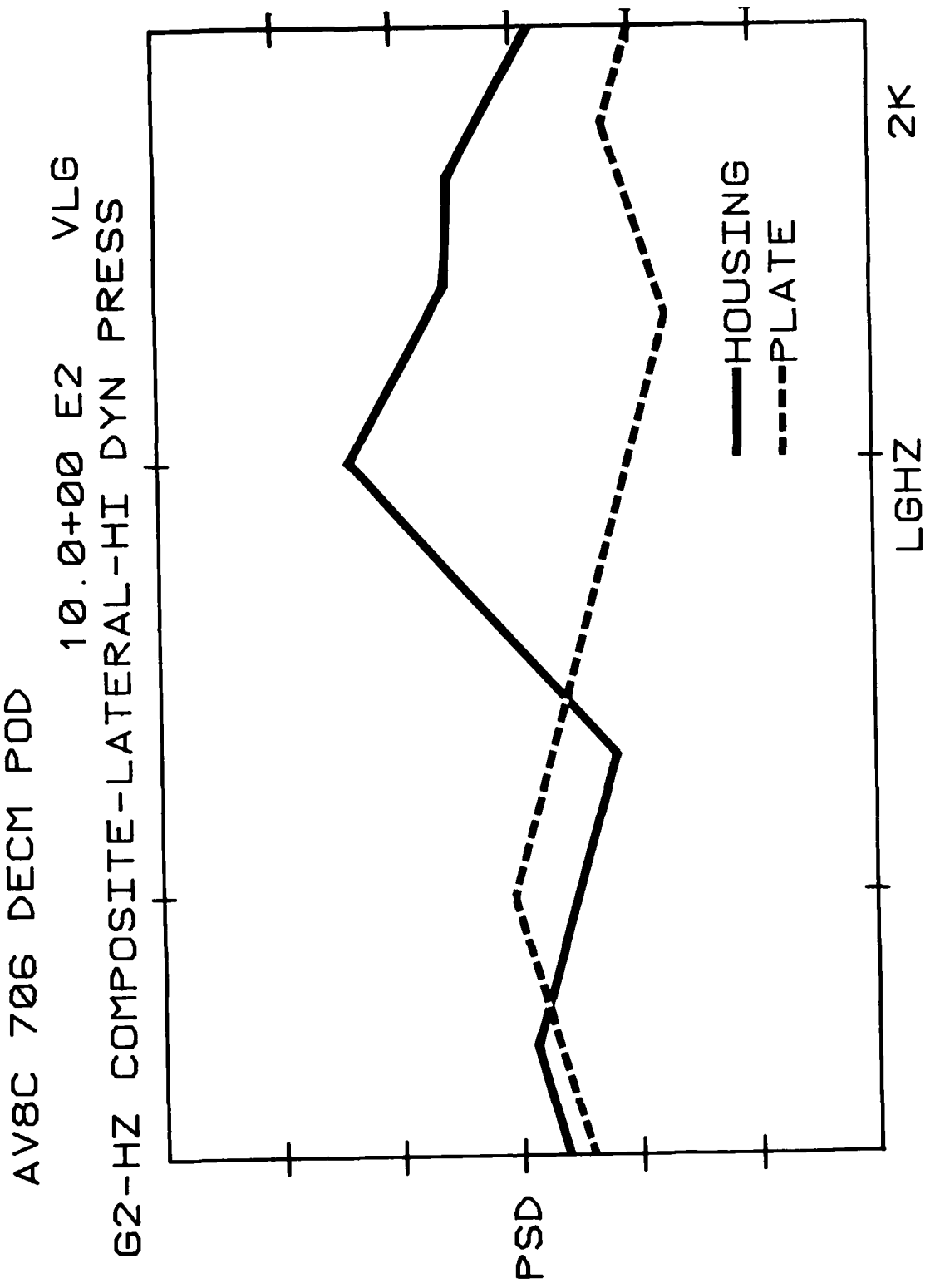

Figure 35 (Cont'd)

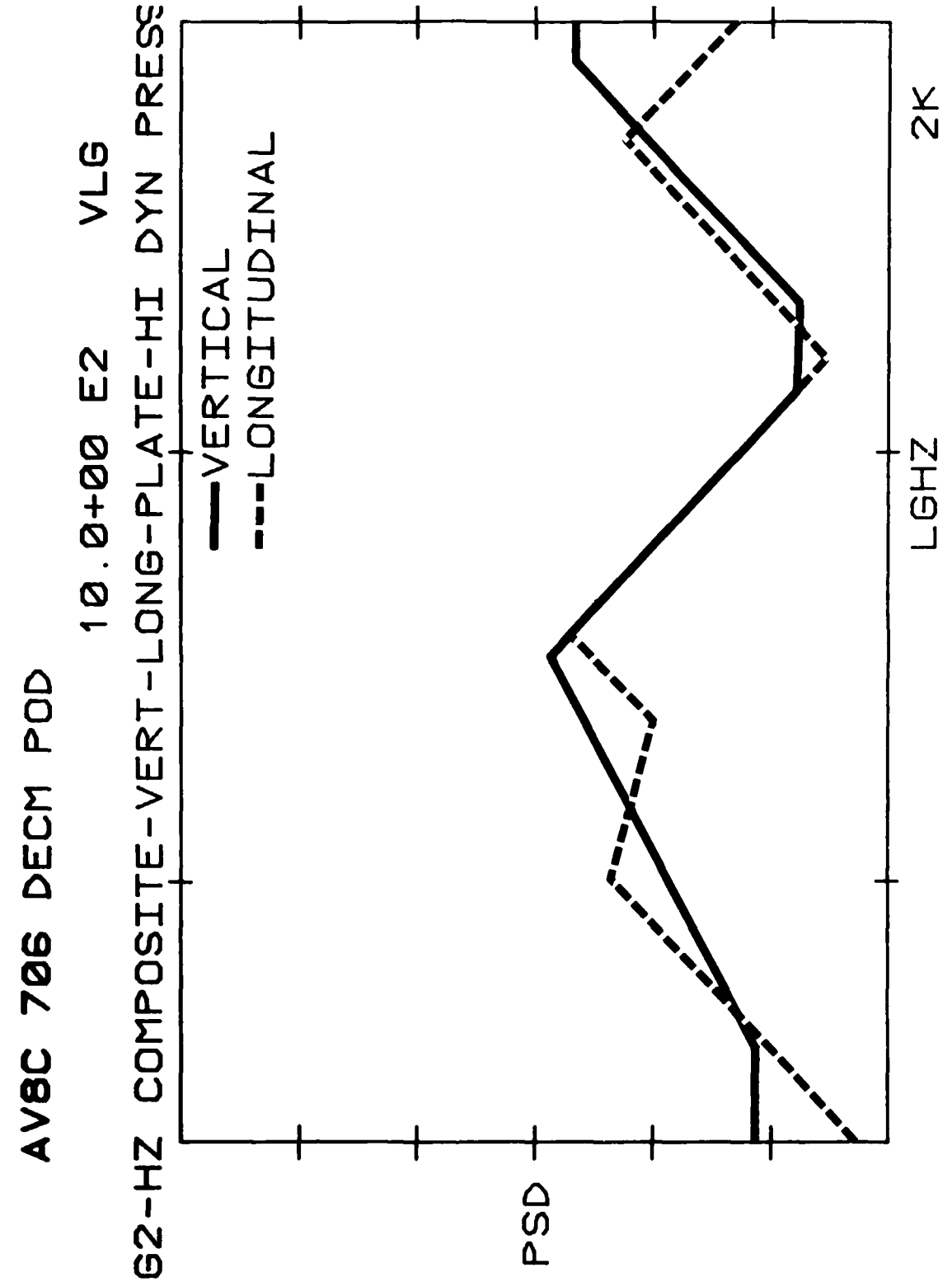

Figure 35 (Cont'd)

DISTRIBUTION:

NAVAIRSYSCOM (AIR-54921)	(8)
DCASPRO (Nashua, NH)	(2)
AFPRO (St. Louis, MO)	(1)
PMTC (CODE 1150)	(1)
NAVAIRTESTCEN (CT02)	(3)
SUBINSURV PAXRIV	(1)
NAVAIRTESTCEN (SY91B)	(6)
NAVAIRTESTCEN (SA01)	(1)
NAVAIRTESTCEN (AT01)	(1)
NAVAIRTESTCEN (RW01)	(1)
NAVAIRTESTCEN (CS01)	(1)
NAVAIRTESTCEN (TPS01)	(1)
NAVAIRTESTCEN (TS01)	(1)
NAVAIRTESTCEN (TS214)	(3)
DTIC	(12)


FILMED
8